The University Of Sheffield.

Ultrasonic Joining of Metal-Polymer Surfaces

By

Anwer J. Al-Obaidi

A thesis submitted in partial fulfilment of the requirements for the degree of Doctor of Philosophy

The University of Sheffield

Faculty of Engineering

Department of Mechanical Engineering

December 2017

Abstract

The joining of dissimilar materials is becoming increasingly important, especially for structural applications, and in transportation industries to reduce the weight and thus decrease fuel consumption and Co_2 emissions. Joining lightweight materials (metals and polymers) is commonly performed using mechanical fastenings, such as screws, bolts, and rivets, or adhesion techniques. However, disadvantages of such mechanical methods are considerable stress concentration around the fastener hole, the potential for corrosion problems, and the possibility of fatigue cracking in metallic materials.

Ultrasonic joining (USJ) is particularly suitable where rapid processing and good process reliability are demanded. Quality, strength, and energy saving capabilities also characterise ultrasonic joining. A relatively good body of work exists for polymer-polymer and metal-metal USJ, but little research has been conducted into the joining of dissimilar materials. This is therefore the focus of this thesis.

The amorphous thermoplastic polymer (ABS 750SW) and the aluminium alloy (Al6082-T6) are common engineering materials for the manufacturing of hybrid structure and components for engineering applications. These light-weight materials' applications in the transportation industries include both decorative and structural parts, such as internal and external panels, and bumpers. Additionally, metal – polymer laminates are a much more desirable and versatile option, when the replacement of a full metal construction is required.

This work presents a comprehensive study of the novel joining of these two materials through USJ and investigates the effect of joining parameters on the joint strength. The joints have been bonded without using any additional materials (fillers).

In the present work, a response surface methodology (RSM) has been used to identify the effects of joining parameters and their interactions on the lap shear strength of ABS – Al6082 joints. Moreover, analysis of variance (ANOVA) has been utilised during the statistical analysis to determine the significance of the joining parameters and their interactions.

The research has shown that is possible to achieve ultrasonically assisted joining between the ABS and Al6082-T6 material, with a maximum lap shear strength obtained of over 2.31MPa.

Bonding parameters having the greatest effect were identified as vibration amplitude, upper sample thickness (Al6082-T6), and bonding force, whilst others such as hold time and ABS thickness do not affect the strength of the bond. Neither material undergoes a change in its intrinsic characteristics during the ultrasonic process. Further work will include extension investigation to cover a wider range of material combinations.

Acknowledgments

First of all, I would like to thank Almighty Allah for everything in my life. Without his gaudiness, I would never be able to accomplish anything in my whole life.

I would like to express my sincere gratitude to my supervisors Dr. Candice Majewski and Dr. James Meredith for the continuous support of my Ph.D study and related research, especially to my first supervisor Dr. Candice Majewski for her patience, motivation, and immense knowledge. Her guidance helped me in all the time of research and writing of this thesis. I could not have imagined having a better advisor and mentor for my Ph.D study.

My sincere thanks also go to the staff of my department, mechanical workshop, especially Mr. Michael Jackson and to all in charge of laboratories in Mechanical and Material Engineering Departments at the University of Sheffield for facilitating use the devices and help me during my Ph.D study.

A special thanks to my family. Words cannot express how grateful I am to my father, my mother, brothers and sister for supporting me spiritually. I would also like to express my special thanks to my champion (my wife) for supporting me always, especially during my study, and to my heroes, lovely sons (Abdullah, and Taym), and my princess, pretty daughter (Miral) to make my life wonderful.

I would also like to thank my friend, and colleagues for their encouragement and support which made my stay and study in Sheffield more enjoyable.

A special thanks to my sponsor the Higher Committee for Education Development in Iraq (HCED) for supporting my study and give me the chance to get a Ph.D from the University of Sheffield-Mechanical Engineering Department.

Table of Contents

TABLE OF CONTENTS IV

CHAPTER 1 INTRODUCTION 1

1.1 Background and Motivation 1

1.2 Current Methods of Producing Polymer-Metal Joints 2

1.3 Aim 3

1.4 Objectives 4

1.5 Overview of the Ultrasonic Technique 4

1.6 Description of Ultrasonic Technique 5

1.6.1 Ultrasonic Welding 6

1.6.2 Ultrasonic Joining 8

1.7 Advantages of Ultrasonic Process 8

1.8 Limitations of Ultrasonic Process 9

1.9 Applications of Ultrasonic Joining 10

1.9.1 Electronic, electrical and microsystem industry 10

1.9.2 Aircraft and automotive industry 11

1.9.3 Medical industry 11

1.9.4 Packaging industry 12

1.10 Approach and Thesis Outline 12

CHAPTER 2 MATERIALS FOR ULTRASONIC JOINING 14

2.1 The Physics of Joining Materials Using Ultrasonic Technique 14

2.1.1 Metal Materials 14

2.1.2 Polymer Materials 15

2.1.3 Polymer – Metal Materials 28

2.2 Materials for Ultrasonic Process 30

2.2.1 Thermoplastic Materials 30

2.2.2 Metal Materials 38

2.2.3 Dissimilar Materials 41

2.3 Design of Experiments (DOE) 43

2.3.1 Input Variables (Parameters) 44

2.3.2 Interaction of Parameters *44*
2.3.3 Output variable (Response) *45*
2.3.4 Choice of Design *45*
2.3.5 Choice of Model *49*
2.4 DESCRIPTION OF STATISTICAL ANALYSIS 54
2.4.1 The Residual Plots *55*
2.4.2 Analysis of Variance (ANOVA) *57*
2.5 SUMMARY 63

CHAPTER 3 ULTRASONIC JOINING PARAMETERS 65

3.1 INTRODUCTION 65
3.2 MACHINE PARAMETERS 66
3.2.1 Vibration Frequency *66*
3.2.2 Effects of Bonding Time *68*
3.2.3 Effects of Bonding Force *73*
3.2.4 Effects of Vibration Amplitude *76*
3.2.5 Effects of Holding Time *78*
3.3 EFFECTS OF WORKPIECE CONDITIONS 79
3.3.1 Surface Roughness *79*
3.3.2 Sample Geometry *85*
3.4 SUMMARY 86

CHAPTER 4 METHODOLOGY AND EXPERIMENTAL WORK 87

4.1 MATERIAL SELECTION 87
4.1.1 Choice of Metal and Polymer *87*
4.1.2 Compatibility of Selected Materials *89*
4.2 DETERMINATION OF BONDING PARAMETERS 90
4.2.1 Vibration Frequency and Amplitude *90*
4.2.2 Bonding Time *91*
4.2.3 Bonding Force *91*
4.2.4 Hold Time *92*
4.2.5 Sample Position *92*

4.2.6 Sample Thickness *92*
4.2.7 Energy Director (ED) *93*
4.2.8 Surface Treatment *94*
4.3 PRODUCTION OF SAMPLES 95
4.3.1 Sample Dimensions *95*
4.3.2 Polymer Sample Preparation *96*
4.3.3 Metal Sample Preparation *99*
4.4 ULTRASONIC JOINING PROCEDURE 105
4.4.1 USW Rig Validation *108*
4.5 EXPERIMENTAL TESTING 111
4.5.1 Measurement of LSS *111*
4.5.2 Temperature Measurement *112*
4.5.3 Microscopic Analysis *115*
4.6 INITIAL EXPERIMENTATIONS 117
4.7 EXPERIMENTAL STRUCTURE 120
4.8 SUMMARY 124

CHAPTER 5 INITIAL AND DOE EXPERIMENTS RESULTS 125

5.1 INITIAL EXPERIMENTATIONS RESULTS 125
5.2 LAP SHEAR STRENGTH (LSS) 130
5.3 EFFECTS OF MAIN PARAMETERS 132
5.3.1 Vibration Amplitude *132*
5.3.2 Bonding Force *133*
5.3.3 Bonding Time *134*
5.3.4 Al6082-T6 Thickness *135*
5.3.5 Energy Director Shape (ED) *135*
5.4 EFFECTS OF PARAMETER INTERACTIONS 136
5.5 BOND CHARACTERISATION 137
5.5.1 Al6082-T6 Samples *137*
5.5.2 ABS Samples *140*
5.6 SUMMARY 156

CHAPTER 6 DISCUSSION 157

6.1 DISCUSSION OF INITIAL EXPERIMENTATIONS 157

6.2 DISCUSSION OF DOE EXPERIMENTS 162

6.2.1 Effect of Vibration Amplitude and Interactions 162

6.2.2 Effect of Bonding Time and its Interactions 169

6.2.3 Effect of Bonding Force and its Interactions 172

6.2.4 Effect of Al6082-T6 Thickness and its Interactions 174

6.2.5 Effect of Energy Director Shape 174

6.2.6 Effect of Input Energy 175

6.2.7 Effect of Bonding Temperature 177

6.3 RESULTS OF STATISTICAL ANALYSIS 186

6.3.1 Analysis of Variance (ANOVA) Results 186

6.4 SUMMARY 189

CHAPTER 7 CONCLUSIONS AND FUTURE WORK RECOMMENDATIONS 190

7.1 CONCLUSIONS 190

7.2 FUTURE WORK RECOMMENDATIONS 192

List of Figures

FIGURE 1.1 ULTRASONIC JOINING DEVICE [10]. 5

FIGURE 1.2 KINEMATIC AND COMPARISONS OF ULTRASONIC WELDING VARIANTS [15]. 7

FIGURE 1.3 FUNCTIONAL DIAGRAM OF ULTRASONIC PROCESS, ADAPTED FROM [18]. 7

FIGURE 1.4 MINIMUM ELECTRICAL POWER RELATED TO THE THICKNESS (COPPER), ADAPTED FROM [26]. 10

FIGURE 1.5 ULTRASONIC JOINING PACKAGING [28]. 12

FIGURE 2.1 AMORPHOUS AND SEMI-CRYSTALLINE POLYMERS [31]. 15

FIGURE 2.2 FORM OF POLYMER VISCOELASTICITY [32]. 16

FIGURE 2.3 ENERGY DIRECTOR SCHEME [34]. 17

FIGURE 2.4 RELATIONSHIP BETWEEN LOSS AND ELASTIC MODULUS WITH TEMPERATURE [37]. 18

FIGURE 2.5 SPECIFIC VOLUME VS. TEMPERATURE ARE SHOWN AT THE RIGHT FOR AMORPHOUS AND CRYSTALLINE POLYMERS [38]. 19

FIGURE 2.6 FOUR PHASES OF ULTRASONIC JOINING OF THERMOPLASTICS [40]. 20

FIGURE 2.7 POLYMER FLOW DURING ULTRASONIC JOINING WHERE P_O, v_O, U AND D ARE JOINING PRESSURE, PENETRATION SPEED, SQUEEZE FLOW VELOCITY AND THE HEIGHT OF MOLTEN POLYMER RESPECTIVELY[40]. 21

FIGURE 2.8 PRINCIPLE OF ULTRASONIC JOINING [25]. 24

FIGURE 2.9 DIFFERENT ORIENTATIONS (TRANSVERSE T_1, PARALLEL P_1) AND MULTI-ENERGY DIRECTORS $2P_{1/2}$ [49] 26

FIGURE 2.10 SHEAR JOINT AND ENERGY DIRECTOR ED [50]. 27

FIGURE 2.11 NOVEL ULTRASONIC JOINING PRINCIPLE SCHEMATIC DRAWING [62]. 33

FIGURE 2.12 NOMINAL STRAIN VERSUS THE NOMINAL STRESS OF PLA, PMMA AND COMPOSITE OF PLA/PMMA [62]. 34

FIGURE 2.13 FAR-FIELD AND NEAR-FIELD JOINING [66]. 35

FIGURE 2.14 WAVE AMPLITUDE INTENSITY [7] 36

FIGURE 2.15 DIFFERENT JOINT DESIGNS [39]. 37

FIGURE 2.16 BONDING ZONE OF AN (A) ULTRASONICALLY METAL BONDED AND (B) ULTRASONICALLY PLASTIC BONDED METAL/GFRP JOINT [9]. 42

FIGURE 2.17 TWO PARAMETERS WITHOUT INTERACTION (A), AND WITH INTERACTION (B) [16]. 44

FIGURE 2.18 COMPARISON BETWEEN FULL FACTORIAL AND FRACTIONAL FACTORIAL DESIGNS [82]. 46

FIGURE 2.19(A) RESPONSE SURFACE OF YIELD OF CHEMICAL PROCESS AND PROCESS PARAMETER; TIME AND TEMPERATURE, (B) A COUNTER PLOT OF THE THEORETICAL RESPONSE SURFACE [88]. 51

FIGURE 2.20 LINEAR AND QUADRATIC MODELS [81]. 52

FIGURE 2.21 CENTRAL COMPOSITE DESIGN AND BOX-BEHNKEN DESIGN. 52

FIGURE 2.22 NON-NORMAL DISTRIBUTION PLOT OF RESIDUALS [91]. 55

FIGURE 2.23 NORMALITY PLOT OF RESIDUALS [92]. 56

FIGURE 2.24 ANOVA TABLE EXAMPLE [95]. 57

FIGURE 2.25 DISTRIBUTION PLOT OF F (1, 54). 61

FIGURE 3.1 SELECTION OF THE INITIAL RANGE OF PARAMETERS' LEVELS. FOR EXAMPLE, THIS FIGURE IS TO SELECT THE ULTRASONIC TIME FOR POLYMER-METAL JOINING FROM COMBINING BETWEEN ULTRASONIC TIME FOR ABS POLYMER [30], HDPE POLYMER [39], OR PP [48] AND AL ALLOYS [97], OR [98]. 66

FIGURE 3.2 THREE DIMENSIONS OF JOINING POLYCARBONATE PARTS AT 40KHZ[25]. 67

FIGURE 3.3 RELATIONSHIP BETWEEN JOINING TIME AND SHEARING FORCE OF JOINTS BETWEEN AA6061 AND TI6AL4V UNDER 20KHZ FREQUENCY, AND DIFFERENT JOINING PRESSURE (0.3, 0.4 AND 0.5MPA) [75]. 68

FIGURE 3.4 RELATIONSHIP BETWEEN JOINING TIME AND TENSILE LOAD OF A5052-SS400 JOINTS AT 15KHZ FREQUENCY, 53µM VIBRATION AMPLITUDE, AND 588N CLAMPING FORCE [97]. 69

FIGURE 3.5 JOINING TIME AFFECTS JOINT STRENGTH BETWEEN PLA AND PMMA AT 28KHZ FREQUENCY, 30µM VIBRATION AMPLITUDE, AND AT DIFFERENT JOINING PRESSURE (0.1, 0.3 AND 0.6MPA) [62]. 71

FIGURE 3.6 RELATIONSHIP BETWEEN JOINING TIME AND SHEARING FORCE OF PC-PMMA JOINTS AT 28KHZ FREQUENCY, 30µM VIBRATION AMPLITUDE, AND DIFFERENT JOINING PRESSURE (0.3 AND 0.4MPA) [63]. 71

FIGURE 3.7 RUPTURE SURFACES OF PC BONDED INTERFACES UNDER JOINING STRESS OF 0.3 MPA. (A), (B), (C) ARE UNDER JOINING TIME OF 1.5, 3 AND 4 S, RESPECTIVELY [63]. 72

FIGURE 3.8 RELATIONSHIP BETWEEN CLAMPING FORCE AND TENSILE LOAD OF A5052-SS400 JOINTS AT 15KHZ FREQUENCY, 53µM VIBRATION AMPLITUDE, AND 1 SEC BONDING TIME [97]. 74

FIGURE 3.9 RELATIONSHIP BETWEEN JOINING PRESSURE AND JOINING STRENGTH BETWEEN PLA AND PMMA AT 28KHZ FREQUENCY, AND DIFFERENT BONDING TIME (1, 2 AND 4SEC) [62]. 75

FIGURE 3.10 ULTRASONIC JOINING CYCLE, ADAPTED FROM [108]. 78

FIGURE 3.11 VARIATION OF TEMPERATURE IN ALUMINIUM SHEET (1MM THICKNESS) WITH COEFFICIENT OF FRICTION DURING THE ULTRASONIC PROCESS AT 20KH, ADOPTED FROM [109]. 80

FIGURE 3.12 RELATIONSHIP BETWEEN TENSILE SHEAR STRENGTH OF AA5754/CFRP JOINTS (VIA THE ULTRASONIC JOINING) AND PRE-TREATED TYPE OF AA5754 SHEETS: A) INITIAL STATE, AS ROLLED (R), B) CORUNDUM BLASTING (CB), C) ACID PICKLED (AP), D) COMBINED PRE-TREATED, CB AND AP [9]. 82

FIGURE 3.13 EFFECT OF SURFACE ROUGHNESS ON THE BOND STRENGTH (VIA ADHESION TECHNIQUE) OF STEEL AND DIFFERENT TYPES OF POLYMERS [111]. 83

FIGURE 3.14 RELATIONSHIP BETWEEN THE JOINT STRENGTH (BY ADHESION PROCESS) AND SURFACE ROUGHNESS OF AL6061 JOINTS [112]. 84

FIGURE 4.1 THE INITIAL RANGE OF VIBRATION AMPLITUDE FOR ABS/AL6082 JOINTS. 90

FIGURE 4.2 THE INITIAL RANGE OF BONDING TIME FOR ABS/AL6082 JOINTS. 91

FIGURE 4.3 THE INITIAL RANGE OF ULTRASONIC FORCE FOR ABS/AL6082 JOINTS. 91

FIGURE 4.4 SCHEMATIC OF LAP JOINT. 92

FIGURE 4.5 THE INITIAL RANGE OF SAMPLE THICKNESS. 93

FIGURE 4.6 GEOMETRY OF ED. 94

FIGURE 4.7 LAP JOINT OF DISSIMILAR MATERIALS A) SIDE VEIW, B) TOP VEIW. 96

FIGURE 4.8 INJECTION MOULDING DEVICE. 97

FIGURE 4.9 MOULD WITH CHANGEABLE CAVITIES OF ED. 97

FIGURE 4.10 ABS 750SW SPECIMENS (DIFFERENT ED SHAPE). 98

FIGURE 4.11 THE OXIDE LAYER AFTER ANODISING [110]. 100

FIGURE 4.12 PHOSPHORIC ANODISING OF AL6082. 100

FIGURE 4.13 MICROSTRUCTURE IMAGES OF AL6082-T6 SURFACE, A) BEFORE PRE-TREATMENT (TOP VIEW), B) AFTER PRE-TREATMENT (TOP VIEW), C) BEFORE PRE-TREATMENT (SIDE VIEW), D) AFTER PRE-TREATMENT (SIDE VIEW). 102

FIGURE 4.14 THE VEECO DEKTAK 150 INSTRUMENT. 103

FIGURE 4.15 SCAN SURFACE ROUGHNESS PROFILE [12]. 103

FIGURE 4.16 SCAN SURFACE PROFILE OF THE MEAN ROUGHNESS DEPTH [124] 104

FIGURE 4.17 SIDE PROFILE OF ROUGHNESS BEFORE AND AFTER PRE-TREATMENT. 104

FIGURE 4.18 THE ULTRASONIC JOINING DEVICE. 107

FIGURE 4.19 FIXING TOOL SYSTEM A) DIMENSIONS OF THE TOOLS, THICKNESS OF BLOCK IS 6 MM, B) INSTALLATION OF THE TOOLS. 108
FIGURE 4.20 EFFECT OF CROSSHEAD SPEED ON BREAKING FORCE. 111
FIGURE 4.21 MOTILITY GRIPS FOR LAP JOINT. 112
FIGURE 4.22 DATA ACQUISITION SYSTEM. 113
FIGURE 4.23 EXPERIMENTAL SETUP OF TEMPERATURE MEASUREMENT SYSTEM. 114
FIGURE 4.24 THERMOCOUPLE POSITION ON FLAT SURFACE. 115
FIGURE 4.25 SELECTION OF THE LEVEL OF ULTRASONIC FORCE. 121
FIGURE 4.26 SHAPES OF ENERGY DIRECTORS. 122
FIGURE 5.1 OVER-BONDED JOINT. 126
FIGURE 5.2 COMPARISON BETWEEN WELL BONDED AND OVER-BONDED JOINTS. 126
FIGURE 5.3 UNDER-BONDED JOINT. 127
FIGURE 5.4 THE INITIAL RESULTS OF THE QUALITY OF ABS/AL6082 JOINTS VS. THE VIBRATION AMPLITUDE. 127
FIGURE 5.5 THE INITIAL RESULTS OF THE QUALITY OF ABS/AL6082 JOINTS VS. THE ULTRASONIC TIME. 128
FIGURE 5.6 THE INITIAL RESULTS OF THE QUALITY OF ABS/AL6082 JOINTS VS. THE ULTRASONIC FORCE. 128
FIGURE 5.7 THE INITIAL RESULTS OF THE QUALITY OF ABS/AL6082 JOINTS VS. HOLD TIME. 128
FIGURE 5.8 THE INITIAL RESULTS OF THE QUALITY OF ABS/AL6082 JOINTS VS. AL6082 THICKNESS. 129
FIGURE 5.9 THE INITIAL RESULTS OF THE QUALITY OF ABS/AL6082 JOINTS VS. ABS THICKNESS. 129
FIGURE 5.10 THE IRREGULAR SHAPE OF THE JOINT AREA. 130
FIGURE 5.11 THE SET SCALE OF DISTANCE IN IMAGEJ SOFTWARE. 130
FIGURE 5.12 THE ADJUSTMENT OF IMAGES. 131
FIGURE 5.13 THE JOINT AREA USING THE MANUAL METHOD. 131
FIGURE 5.14 COMPARISON BETWEEN MANUAL AND IMAGEJ METHODS FOR FINDING THE JOINT AREA. 132
FIGURE 5.15 RELATIONSHIP BETWEEN VIBRATION AMPLITUDE AND MEAN OF LSS. THE ALL DATA POINTS OF DOE EXPERIMENTS ARE DISTRIBUTED AT THREE LEVELS OF VIBRATION AMPLITUDE. EACH EXPERIMENTAL RUN WAS REPEATED THREE TIMES. 133

FIGURE 5.16 RELATIONSHIP BETWEEN BONDING FORCE AND MEAN OF LSS. THE ALL DATA POINTS OF DOE EXPERIMENTS ARE DISTRIBUTED AT THREE LEVELS OF BONDING FORCE. EACH EXPERIMENTAL RUN WAS REPEATED THREE TIMES. 134

FIGURE 5.17 RELATIONSHIP BETWEEN BONDING TIME AND MEAN OF LSS. THE ALL DATA POINTS OF DOE EXPERIMENTS ARE DISTRIBUTED AT THREE LEVELS OF BONDING TIME. EACH EXPERIMENTAL RUN WAS REPEATED THREE TIMES. 134

FIGURE 5.18 RELATIONSHIP BETWEEN AL6082 THICKNESS AND MEAN OF LSS. THE ALL DATA POINTS OF DOE EXPERIMENTS ARE DISTRIBUTED AT THREE LEVELS OF AL6082 THICKNESS. EACH EXPERIMENTAL RUNS WAS REPEATED THREE TIMES. 135

FIGURE 5.19 RELATIONSHIP BETWEEN ED SHAPE AND MEAN OF LSS. THE ALL DATA POINTS OF DOE EXPERIMENTS ARE DISTRIBUTED AT THREE LEVELS OF ED SHAPE. EACH EXPERIMENTAL RUN WAS REPEATED THREE TIMES. 136

FIGURE 5.20 HARDNESS TEST SAMPLE. 139

FIGURE 5.21 MICRO HARDNESS DISTRIBUTION ALONG THE CROSS SECTION OF AL6082. 140

FIGURE 5.22 ED COLLAPSE DURING ULTRASONIC JOINING PROCESS. 141

FIGURE 5.23 ED COLLAPSE OF ABS SAMPLE. 141

FIGURE 5.24 RELATIONSHIP BETWEEN ED COLLAPSE AND LSS. 142

FIGURE 5.25 ED COLLAPSE FOR SERIAL NUMBER 1 IN TABLE 5.3 (21μM VIBRATION AMPLITUDE, 1.5SEC BONDING TIME, 950N BONDING FORCE, 1MM AL6082 THICKNESS, AND TRIANGULAR SHAPE OF ED). 143

FIGURE 5.26 ED COLLAPSE AT 18.9 μM, 950N, 1.5 SEC, AND 1.5MM THICKNESS OF AL6082. 144

FIGURE 5.27 CHARACTERISTIC CURVES OF BONDED AND UN-BONDED ABS. 146

FIGURE 5.28 TGA COMPARISON BETWEEN BEFORE AND AFTER BONDING FOR ABS SAMPLES. 148

FIGURE 5.29 AIR BUBBLES ON ABS SURFACE AFTER BONDING. 148

FIGURE 5.30 SIDE-VIEW OF AL6082 SAMPLE AFTER PRE-TREATMENT. 150

FIGURE 5.31 PITS ON THE ABS SAMPLES. 151

FIGURE 5.32 SCANNING ELECTRON MICROGRAPHS OF PROFILE OF ABS PIT ON AL6082 SURFACE. 152

FIGURE 5.33 SCANNING ELECTRON MICROGRAPHS OF THE SURFACE OF ABS PATCH DUE TO THE SHEAR FORCE. 152

FIGURE 5.34 RELATIONSHIP BETWEEN PIT SIZE AND LSS 154

FIGURE 5.35 FORM OF PORES ON AL6082 SURFACE. 155

FIGURE 5.36 SCANNING ELECTRON MICROGRAPHS OF ABS-AL6082 INTERFACE. 155

LIST OF FIGURES

FIGURE 6.1 EFFECT OF THE PRESENCE OF ENERGY DIRECTOR OF ABS. 158

FIGURE 6.2 RELATIONSHIP BETWEEN ABS THICKNESS AND LSS AT CONSTANT OTHER PARAMETERS. EACH TEST REPEATED THREE TIMES. 159

FIGURE 6.3 RELATIONSHIP BETWEEN HOLD TIME AND THE JOINT STRENGTH AT CONSTANT OTHER PARAMETERS. EACH TEST REPEATED THREE TIMES. 160

FIGURE 6.4 OVER-BONDED JOINT. 162

FIGURE 6.5 EFFECT OF VIBRATION AMPLITUDE- BONDING TIME INTERACTION ON LSS. 164

FIGURE 6.6 CONTOUR PLOT OF LSS VS. BONDING TIME, VIBRATION AMPLITUDE. 164

FIGURE 6.7 EFFECT OF VIBRATION AMPLITUDE- BONDING FORCE INTERACTION ON LSS. 165

FIGURE 6.8 CONTOUR PLOT OF LSS VS. BONDING FORCE, VIBRATION AMPLITUDE. 166

FIGURE 6.9 DIRECTION OF MOLTEN POLYMER. 167

FIGURE 6.10 EFFECT OF VIBRATION AMPLITUDE- AL6082-T6 THICKNESS INTERACTION ON LSS. 167

FIGURE 6.11 CONTOUR PLOT OF LSS VS. AL6082-T6 THICKNESS, VIBRATION AMPLITUDE. 168

FIGURE 6.12 EFFECT OF VIBRATION AMPLITUDE- ED SHAPE INTERACTION ON LSS. 169

FIGURE 6.13 COMPARISON BETWEEN TWO DIFFERENT BONDING TIMES WHEN OTHER PARAMETERS ARE CONSTANT. 170

FIGURE 6.14 EFFECT OF BONDING TIME- BONDING FORCE INTERACTION ON LSS. 171

FIGURE 6.15 EFFECT OF BONDING TIME- AL6082-T6 THICKNESS INTERACTION ON LSS. 172

FIGURE 6.16 EFFECT OF BONDING FORCE- AL6082-T6 THICKNESS INTERACTION ON LSS. 173

FIGURE 6.17 RELATIONSHIP BETWEEN INPUT ENERGY AND MEAN OF LSS. 176

FIGURE 6.18 EFFECT OF BONDING TEMPERATURE ON LSS. 178

FIGURE 6.19 RELATIONSHIP BETWEEN BONDING TEMPERATURE AND BONDING FORCE. 179

FIGURE 6.20 COMPARISON BETWEEN SERIAL NO. 5 IN TABLE 6.2(16.8μM AMPLITUDE, 2SEC BONDING TIME, 850N BONDING FORCE AND 2MM AL6082 THICKNESS), AND SERIAL NO. 6 (16.8μM AMPLITUDE, 1SEC BONDING TIME, 1050N BONDING FORCE AND 2MM AL6082 THICKNESS). 180

FIGURE 6.21 RELATIONSHIP BETWEEN BONDING TEMPERATURE AND BONDING TIME. 181

FIGURE 6.22 COMPARISON BETWEEN SERIAL NO. 13 IN TABLE 6.2 (21μM AMPLITUDE, 1SEC BONDING TIME, 1050N BONDING FORCE AND 1MM AL6082 THICKNESS), AND SERIAL NO. 14 (21μM AMPLITUDE, 2SEC BONDING TIME, 1050N BONDING FORCE AND 1MM AL6082 THICKNESS). 181

FIGURE 6.23 RELATIONSHIP BETWEEN BONDING TEMPERATURE AND AL6082 THICKNESS. 182

FIGURE 6.24 COMPARISON BETWEEN SERIAL NO. 13 IN TABLE 6.2 (21μM AMPLITUDE, 1SEC BONDING TIME, 1050N BONDING FORCE AND 1MM AL6082 THICKNESS), AND SERIAL NO. 17 (21μM AMPLITUDE, 1SEC BONDING TIME, 1050N BONDING FORCE AND 2MM AL6082 THICKNESS). 182

FIGURE 6.25 RELATIONSHIP BETWEEN BONDING TEMPERATURE AND VIBRATION AMPLITUDE. 183

FIGURE 6.26 COMPARISON BETWEEN SERIAL NO. 1 IN TABLE 6.2 (16.8μM AMPLITUDE, 1SEC BONDING TIME, 850N BONDING FORCE AND 1MM AL6082 THICKNESS), AND SERIAL NO. 11 (21μM AMPLITUDE, 1SEC BONDING TIME, 850N BONDING FORCE AND 1MM AL6082 THICKNESS). 183

FIGURE 6.27 JOINING AREA AT DIFFERENT BONDING TEMPERATURE. 184

FIGURE 6.28 RELATIONSHIP BETWEEN THE INPUT ENERGY AND INTERFACE TEMPERATURE. 185

List of Table

TABLE 1.1 ADVANTAGES AND DISADVANTAGES OF THE ADHESION METHOD AND MECHANICAL FASTENERS 3

TABLE 2.1 DIFFERENCES BETWEEN AMORPHOUS AND SEMI-CRYSTALLINE THERMOPLASTIC POLYMERS. 15

TABLE 2.2 COMPARISON BETWEEN EXPERIMENTAL DESIGNS. 48

TABLE 2.3 COMPARISON BETWEEN CCD AND BBD. 53

TABLE 2.4 EXAMPLE TO UNDERSTAND SUMS OF SQUARES. 59

TABLE 4.1 THE COMPOSITION OF AL6082. 87

TABLE 4.2 THE PROPERTIES OF A6082-T6. 88

TABLE 4.3 THE PROPERTIES OF ABS 750SW 89

TABLE 4.4 THE SAMPLE DIMENSIONS. 95

TABLE 4.5 THE INJECTION MOULDING PARAMETERS. 99

TABLE 4.6 THE SURFACE ROUGHNESS OF AL6082-T6. 105

TABLE 4.7 THE ACCURACY OF THE PARAMETERS' MEASUREMENTS. 109

TABLE 4.8 BONDING PARAMETERS OF CALIBRATION. 110

TABLE 4.9 THE CALIBRATION RESULTS. 110

TABLE 4.10 BONDING PARAMETERS OF INITIAL EXPERIMENTATIONS. 117

TABLE 4.11 THE STRUCTURE OF INITIAL EXPERIMENTATIONS 118

TABLE 4.12 PARAMETER LEVELS FOR THE DOE EXPERIMENTS. 123

TABLE 4.13 THE DOE EXPERIMENTAL STRUCTURE. 123

TABLE 5.1 THE OPTIMUM LEVELS OF PARAMETERS. 136

TABLE 5.2 HARDNESS TEST SAMPLES. 139

TABLE 5.3 ED COLLAPSE FOR DIFFERENT PARAMETERS. 142

TABLE 5.4 DSC PROGRAM FOR ABS 145

TABLE 5.5 DSC SAMPLE. 145

TABLE 5.6 TGA PROGRAM FOR ABS. 147

TABLE 5.7 MOISTURE ANALYSER PROGRAM FOR ABS. 149

TABLE 5.8 BOND PARAMETERS AND PIT SIZE. 153

TABLE 6.1 THE EFFECT OF PARAMETERS ON INPUT ENERGY AND LSS. 176

TABLE 6.2 THE EFFECT OF BONDING TEMPERATURE ON THE JOINT STRENGTH. 177

TABLE 6.3 ANOVA RESULTS. 186

TABLE 6.4 BONDING PARAMETERS INTERACTIONS. 188

ABBREVIATIONS LIST

Abbreviations	Meaning
USW	Ultrasonic Welding
USMW	Ultrasonic Metal Welding
USPW	Ultrasonic Plastic Welding
ABS	Acrylonitrile Butadiene Styrene
Al6082	Aluminium alloy 6xxx Series
T6	Tempered grades, Artificially aged
LSS	Lap Shear strength
Sqrt of LSS	Square root of LSS
DSC	Differential Scanning Calorimeter
TGA	Thermogravimetric Analysis
T_g	Glass Transition Temperature
T_m	Melting Temperature
ED	Energy Director
Tri	Triangular
Semi-C	Semi-Circular
Rect	Rectangular
°C	Unit of Temperature, Degree Centigrade
Hz	Unit of Frequency, Hertz
sec	Unit of Time, Second
N	Unit of Force, Newton
m	Unit of length, Meter
Pa	Unit of Pressure, Pascal
Bar	Unit of Pressure
J	Unit of Energy, Joule
W	Unit of Power, Watt
μ	Micro, 10^{-6}
M	Mega, 10^{6}
VA	Vibration Amplitude
BF	Bonding Force

ABBREVIATIONS LIST

BT	Bonding Time
t	Sample (Al6082-T6) Thickness
Q	Dissipated Energy
OM	Optical Microscope
SEM	Scanning Electron Microscope
HAZ	Heat affected Zone
DOE	Design of Experiments
FFd	Full Factorial Design
RSM	Response Surface Methodology
CCD	Central Composite Design
ANOVA	Analysis of Variance

Chapter 1 INTRODUCTION

1.1 Background and Motivation

Polymers and metals are both important types of engineering materials. Metal materials can be characterised by being generally ductile, having a high melting temperature, good thermal and electrical conductivity and being corrosive. Additionally, the atoms of metal materials are typically formed in structures as crystalline solids and bonded through metallic bonding. Whilst, polymer materials are made up of large molecules consisting of many repeated subunits. Secondary bonding, such as van der Waals and hydrogen bonds hold the polymer chains together and these bonds are weaker than the primary bonds in metal materials. Polymers are cheap materials, which can be often recycled, have a low melting temperature, and poor electrical and thermal conductivity.

Polymers and metals are widely used as structural materials. Much research goes into one or the other, but there is an increasing need for combinations of the two. Practically the use of light-weight polymers and metals (e.g. aluminium alloys) offers great potential importance across many industries, especially in transportation. In addition, these two material types can both provide the desired properties for a given application, such as reducing weight, increasing strength, and lowering cost. Hence, the issues of combining these dissimilar light-weight materials in engineering applications, or hybrid structures has become unavoidable. Moreover, metal-polymer laminates are a much more desirable and versatile option, when the replacement of a full metal construction is required. In addition, all transportation industries can benefit from mass reduction enabling them to produce vehicles that are more fuel-efficient and thus reducing Co_2 emissions. This reduction in the total mass depends on the selected materials that should have higher strength, be less dense, and well-engineered materials.

These materials (polymers and metals) have considerably different properties in their behaviour during in-service, and manufacturing processes, but they are used together frequently within a single load carrying structure. For example, with polymer-metal applications, the use of light-weight metals in the automotive industry has grown by more than 80% during the last five years, especially the outer panel applications which prefer Al 6xxx alloys [1]. While, the use of polymers has risen to become 10-15% of the total car weight, and the most frequently used polymers in the automotive industry are ABS, PS, PVC, and PC [2].

There is, therefore, a clear need for new methods to join them (polymers and metals) together, and an increased understanding of how to do so.

1.2 Current Methods of Producing Polymer-Metal Joints

Joining methods between metals and polymers almost exclusively depend on the mechanical fastenings and adhesion techniques. These current traditional methods for joining metals to thermoplastic polymers are feasible. However, the mechanical fastening has a number of limitations: stress concentration is considerable in metallic part, delamination during drilling, different thermal expansion of the fasteners relative to the polymer, water intrusion into the joint, possible galvanic corrosion, higher weight than other methods and extensive labour and time required [3]. Adhesion method, although more favourable than mechanical fastening because the stress concentrations are avoided, still presents some difficulties when applied on the thermoplastic polymers during the joining of dissimilar materials, such as it requires extensive surface preparation [4]. In addition, the adhesion method is generally difficult to control in an industrial environment, and adhesives used (usually epoxies) have long curing period. It has also problems in terms of environmental restrictions on the emission of volatile organic compounds. Table 1.1 shows the summary of advantages and disadvantages of using the traditional methods (adhesion techniques and mechanical fasteners) to join dissimilar materials [5] and [6].

Table 1.1 Advantages and disadvantages of the adhesion method and mechanical fasteners

	Adhesion Method	Mechanical Fastener
Advantages	Stress concentration in adherents is small	Ability to disassemble
	It is relatively lightweight	Thickness is not limited
	Connections are stiff	It is not environmentally sensitive
	No deformation in the substrate	Joint configuration is simple
	Fatigue resistance	No chemical changes
	Reduction in other components such as screw, nuts, etc.	Ease of manufacturing process
Disadvantages	Difficulty of inspection procedure	Stress concentration is considerable in metallic part
	High degree of quality control is required	Materials damage due to hole formation
	Environmental concern	Prone to metal corrosion
	Costly tooling and facilities may be required	Metallic components may be subject to fatigue cracking
	May be subject to environmental degradation	Higher weight than other methods
	Long curing period required	Extensive labour and time required

It can, therefore, be seen that there is a demonstrable need for improved methods of joining metals and polymers. This research will focus on the use of an ultrasonic technique commonly used to join similar materials and will attempt to apply this technique to the problem of joining dissimilar materials.

1.3 Aim

This thesis aims to investigate the feasibility of joining a polymer and a metal surface using an ultrasonic technique, and to develop a comprehensive and in-depth understanding of the parameter space in which optimisation of the joint strength can occur.

1.4 Objectives

In order to achieve this aim, there are several objectives in the present work, as follows:

1- Preliminary trials to demonstrate feasibility of the approach.
2- Identifying the parameter space to achieve the joining.
3- Investigating the effects of ultrasonic bonding parameters and the interactions on the polymer–metal joints.
4- Evaluating the optimum values of parameters leading to the strongest joint.
5- Determining the correlation between bond characteristics and the bond strength.

To achieve these objectives, Appendix (A) represents the current work flow diagram that will be applied in the following chapters.

1.5 Overview of the Ultrasonic Technique

One of the most popular industrial techniques for joining materials is ultrasonic method. This technique was invented in the 1950s and has been used to bond metallic and non-metallic components for various applications [7]. This method uses high-frequency at relatively low temperatures and low energy consumptions [8].

The ultrasonic method can be used for welding (chemical and physical bond) similar materials, such as metals-metals, or polymers-polymers. In addition, it was used to joint (physical bond) dissimilar materials, such as metals-fibre reinforced polymers joints [9].

The ultrasonic technique is promising and may offer an alternative technique compared to traditional methods for the realisation of metal/polymer hybrid joints. This joining technique is considered one of the fastest joining methods where an effective joint can be formed in seconds. In addition, the ultrasonic technique is a connecting method that can be used without any additional or foreign substances such as a resin (adhesive) or solvent.

This technique has the potential to reduce bonding time within an assembly line whilst maintaining high joint strengths. However, as there has been very little investigation into its ability for dissimilar materials, there is a need for investigation in this area.

1.6 Description of Ultrasonic Technique

Ultrasonic method is a process that uses high-frequency sound waves in order to create a bond. The process of ultrasonic technique is outlined briefly as follows:

The generator of ultrasonic device generally transfers the input power (50-60 Hz) into a high-frequency (commonly 20 KHz), then this electrical energy is converted into mechanical oscillations at a particular amplitude by a piezoelectric transducer. A booster can achieve a suitable vibration amplitude in the joining field. This vibration amplitude is transferred to the bonding zone by a sonotrode (horn) that is in contact with the workpieces to be bonded, and the workpieces are held by the anvil, as shown in Figure 1.1.

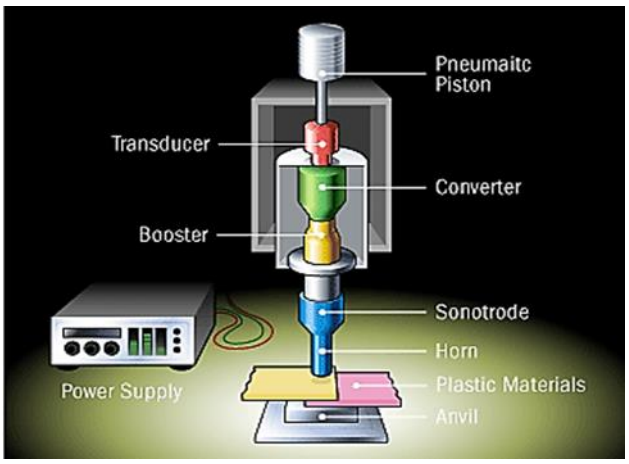

Figure 1.1 Ultrasonic Joining Device [10].

The ultrasonic technique can be used for welding similar materials or joining dissimilar materials using the same above procedure. The difference is only on the mechanism of bonding. The welding process is the result of combined chemical and physical bonds, while the joining process depends on the physical bond only. The following is explained briefly the welding and joining of materials using the ultrasonic technique:

1.6.1 Ultrasonic Welding

There are two base variants of ultrasonic welding methods that are related to the direction of oscillation with respect to the surface of the workpiece, and bonding nature: ultrasonic metal welding (USMW) and ultrasonic plastic welding (USPW).

- **Ultrasonic Metal Welding (USMW)**

USW of metals is technique whereby high-frequency vibrations are applied to specimens to hold them together. This technique happens when pressure on workpieces is applied to create a solid-state weld. Ultrasonic metal welding (USMW) uses the oscillation to act parallel to the welding interface. This parallel movement will increase the area contact and disperse contaminants and an oxide layer due to the scrubbing motion [11], and [12], as shown in Figure 1.2. This type of joining can be used for similar and dissimilar metal materials. The bonding nature of USW in metals is solid-state welding, meaning no fusion or melt is required between workpieces. USMW is used in different fields, such as automotive, electronic components, manufacture and shipbuilding [13].

- **Ultrasonic Plastic Welding (USPW)**

For polymers, the bonding nature of USW depends on the melting of polymers [14]. High-frequency mechanical vibrations generate heat in the joining zone thereby starting the melting of the thermoplastic polymers, and the weld is created after cooling. Ultrasonic plastic welding (USPW) and its oscillation is perpendicular to the welding zone [9]. Both types of USW are shown schematically in Figure 1.2 [15].

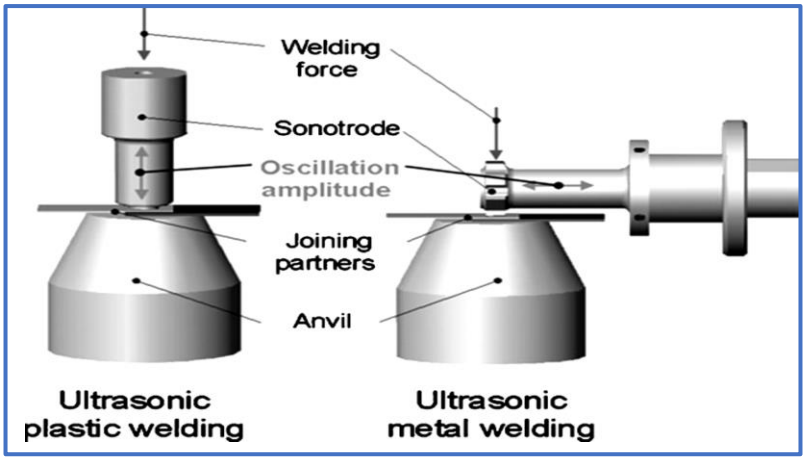

Figure 1.2 Kinematic and comparisons of ultrasonic welding variants [15].

The bonding zone in plastic depends on melting; the absorption of mechanical oscillations can produce an increase of temperature due to friction between the contact surfaces and within the molecular chains that generate the heat [16]. Therefore, USW is suitable for thermoplastic polymers only because the chemical reaction will be initiated in the thermoset polymers when the temperature rises, thereby forming the cross-linked molecular chains [17]. The welded samples are concurrently pressed together under static force (P_{st}) and this force is very important for reliable contact between the sonotrode (horn) and the welded workpieces. This force increases the mechanical energy concentration in the welding region [18]. The concurrent action of the dynamic force (F) that develops, due to the mechanical vibration and static force, causes a fusion of the workpieces, as shown in Figure 1.3.

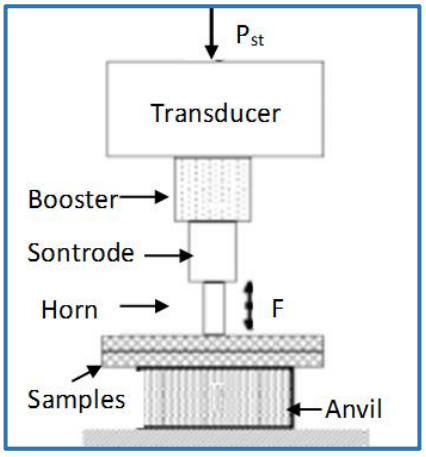

Figure 1.3 Functional diagram of ultrasonic process, adapted from [18].

1.6.2 Ultrasonic Joining

The ultrasonic joining of dissimilar materials depends on creating mechanical bonding (physical) between the surfaces of the dissimilar materials (metals-polymers). The heat generates at the bonding zone due to the high-frequency mechanical vibrations which leads to melt the polymer at the bonding zone. The melted polymer flows inside the microstructural cavernous on the metal surface to create the mechanical interlocking [9].

Therefore, the procedure to generate the heat at the bonding zone is the same for both ultrasonic plastic welding and joining. The type of bonding creation is the difference between ultrasonic welding of similar material (chemical and physical bonds) and ultrasonic joining of dissimilar materials (physical bonds).

Whilst some literature refers to the ultrasonic process as 'ultrasonic welding' in some cases, this thesis will use term 'ultrasonic joining' to cover all categories.

1.7 Advantages of Ultrasonic Process

There are many benefits of using ultrasonic technique, either welding or joining, as follows:

- Ultrasonic method is considered one of the fastest bonding methods compared with other techniques such as arc welding, roll welding, and friction welding, as the joining takes place very quickly (around 1 sec.) [19].
- It is a high mass production process, usable for applications such as casings for mobile telephones, electronic components, and hermetic sealing [20].
- This process can weld without any additional materials (filler), such as resin or solvent [21].
- It can be used for spot or seam bonding of different materials, such as polymers, metals, and composite materials.

- The ultrasonic device is compact and the process easily automated, it can also weld through contaminants and oxides that result from the friction [22].
- The ultrasonic energy is generated at the interface zone rather than the top surface as in other welding processes, such as friction stir welding. Hence, the surface deformation or damage is minimal [13], and [23].
- It does not generate fumes, flames, or sparks and, thus, is considered environmentally friendly and a clean joining process [24].
- The ultrasonic process has a variety of applications in many fields, including automotive, electrical components and medical devices [14].

1.8 Limitations of Ultrasonic Process

Although the ultrasonic process has many benefits, it also has the following limitations of use:

- One of these limitations is restricted to the lap joints and the thickness of workpieces is currently limited to 3 mm due to the power of equipment being specified [24], but the ultrasonic method succeeds in joining plastic microparts of approximately 300 μm thickness [25]. The relationship between the thickness of workpieces and ultrasonic power for metals is a direct one, as shown in Figure 1.4 [26]. In addition, the thicker parts absorb high energy in the upper sample (where the vibration is applied), and thus the oscillation in the bonding zone is not sufficient to produce a joint [3]. On the other hand, the surface of the upper workpiece cannot endure the increasing driving force pressure. Thus, the thickness of workpieces should be limited.

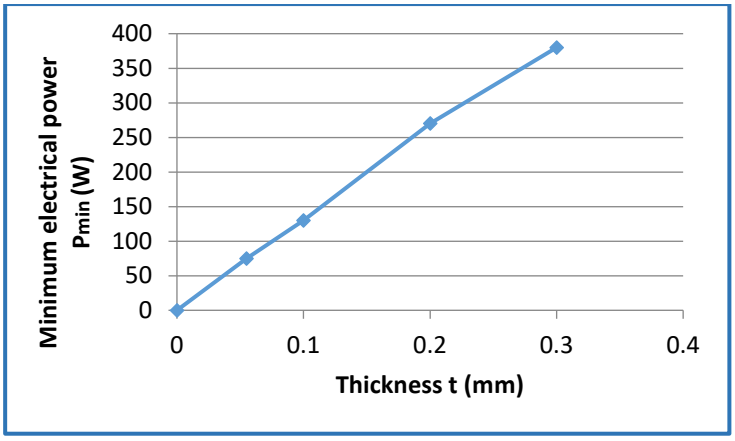

Figure 1.4 Minimum electrical power related to the thickness (copper), adapted from [26].

- Some properties of materials are considered as a challenge when using ultrasonic process, for example, high hardness, high stiffness and high damping factor, because the basis of working ultrasonic technique converts the vibration (mechanical energy) into thermal energy and these properties decrease the amount of mechanical energy that is delivered to the bonding region [18].
- Since vibration is the main factor in the ultrasonic process working, audible noise may be produced from the resonance state.
- The workpieces and components of the device may be fatigued due to the cyclic loading that is created by ultrasonic oscillation [13].

1.9 Applications of Ultrasonic Joining

Ultrasonic joining process has a large number of applications and these can be found in many industries, in particular the electronic and electrical, aircraft and automotive, medical and packaging fields [27].

1.9.1 Electronic, electrical and microsystem industry

The applications of microsystems technology are increasing because of the continuous miniaturisation in industrial branch plastics. As such, the joining processes must be suitable to merit a warranty of the functionality of the system. Hence, ultrasonic joining is suitable for joining plastics in microtechnology applications rather than the traditional methods

(mechanical fastening and adhesion process) because it uses low thermal and mechanical loads and has high positioning accuracy [25].
Furthermore, the electronic parts, such as diodes and semiconductors, can be assembled with substrates using the ultrasonic joining. Additionally, electrical connection between current device parts, such as motors, field coils and capacitors are also assembled using the ultrasonic joining. Since a small or insignificant temperature increase is produced during the ultrasonic joining process, it does not cause any damage to the parts [14]. In contrast to this, the mechanical fastening can damage the small parts due to increase the temperature by the drilling forming.

1.9.2 Aircraft and automotive industry

The aircraft and automotive industry and engineering in general require weight reduction in order to reduce energy consumption. This reduction can be achieved by using lightweight metals such as titanium, magnesium and aluminium alloys as well as FRP (fibre-reinforced polymers) composites in engineering structures [9]. The traditional methods, such as the mechanical fastening is unsuitable due to increase the weight. Whilst, the environmental concern is the obstacle of using the adhesion method. Thus, the ultrasonic joining is very important of bonding these dissimilar materials (metals-FRP).

1.9.3 Medical industry

One property of the ultrasonic joining is that it is an environmentally friendly and clean joining process because the ultrasonic process does not introduce contaminants or degradation and the devices can be specialised for use in clean rooms. Based on this and as explained in Section 1.2, the mechanical fastening and adhesion method might not be preferred to use in clean rooms, or medical chips. Hence, the ultrasonic joining technique can be applied to many medical items, such as hospital wear (gowns), medical chip tests, sterile clothing, masks and textiles that are used in clean rooms [27].

1.9.4 Packaging industry

Nowadays, the ultrasonic joining technique is used to package many common items in the food industries, such as milk and juice containers. These containers were made from glass and sealed by aluminium foil using the ultrasonic joining because it is quick, healthy and capable of producing hermetic seals [27], as shown in Figure 1.5. Thus, it is difficult to join these containers with foil by the mechanical fastening. Furthermore, it is not preferred to used filler, such as epoxies during the adhesion process in the food industries.

Figure 1.5 Ultrasonic joining packaging [28].

1.10 Approach and Thesis Outline

The overall focus of this thesis is to determine the potential for using this USJ technique for joining dissimilar materials. Although it is not possible to 'weld' a polymer to a metal due to the mismatch between the chemical and physical properties of the materials, the hypothesis is that some of the same principles/parameters can provide a useful starting point in how to go about using the same approach to join dissimilar materials (polymers and metals).

The current research is structured in brief as follows:

In Chapter 2, an extensive literature review on the type of materials used during ultrasonic process is presented. This chapter illustrates the physics of joining materials using the ultrasonic technique. In addition, the design of experiments that used to collect the data and analyse it is explained.

Chapter 3 describes the parameters (machine parameters and workpiece property parameters) that are known to influence the joint strength and that have been studied in previous research.

In Chapter 4, the materials to be used in the current research are explained and justified. Additionally, the chapter illustrates the initial investigations of the ultrasonic process between polymer (ABS) and metal (Al6082-T6) materials, to identify the relevant parameter space. Furthermore, the main topics of this chapter include the procedures of ultrasonic joining for dissimilar materials and a joint strength measurement.

In Chapter 5, the initial and DOE results are presented in detail. In addition, the influence of bonding parameters and their interactions on LSS are determined. Furthermore, the influence of various bond features is investigated. The optimum values of parameters' levels that achieved the best LSS are determined.

In Chapter 6, the results of initial and DOE experiments are discussed in detail. Furthermore, the results of an experimental design are analysed statistically to deduce meaningful information using the analysis of variance (ANOVA).

Finally, Chapter 7 concludes the current research and offers recommendations for future work.

Chapter 2 MATERIALS FOR ULTRASONIC JOINING

This chapter presents an extensive review of the materials which can be ultrasonically bonded and the mechanism and physics of the process. This chapter is divided into three main parts: 1) the physics of joining materials, 2) materials for ultrasonic joining, and 3) design of experiments (DOE), and description of statistical analysis.

2.1 The Physics of Joining Materials Using Ultrasonic Technique

According to Section 1.6 the ultrasonic technique can be used to join similar materials (metal-metal), or (polymer-polymer) through creating chemical and physical bonds at the interface region. Additionally, this technique was conducted to join the dissimilar materials (metal-FRP) by creating physical bond at the interface. This section illustrated the physics of bonding similar and dissimilar materials using the ultrasonic method.

2.1.1 Metal Materials

According to Section 1.6.1, ultrasonic metal joining depends on the horizontal vibrations that act parallel to the joining interface, leading to an increase of the friction between the surfaces. This friction leads to increased heat, which leads to an increase in the contact area. The friction at the interface causes shearing and plastic deformation.

Therefore, the physics of joining similar metals may not appropriate for joining dissimilar materials (metal-polymer). This is because the mechanism of joining similar metals depends on the friction which leads to displace the polymer out of the bonding region by the transversal vibration. The transversal vibration leads to decrease the thickness of polymer. Therefore, the mechanism of joining metals to non-metals materials needs a different

mechanism to create a strong joint and thus the current thesis will focus on this area.

2.1.2 Polymer Materials

Whereas the ultrasonic process of metals does not melt the material, ultrasonic joining of polymers depends on melting it. The mechanical oscillations are transmitted through the thermoplastic polymers to reach the joint area. These vibrations cause intermolecular friction which leads to frictional heat (dissipated energy) [29]. This energy causes the polymer to melt and forms the joint by joining molecular chains across the interface. Thermoplastic polymers can be classified into two main groups depending on molecular structure [30], as shown in Figure 2.1.

- **Semi-crystalline thermoplastics**
- **Amorphous thermoplastics**

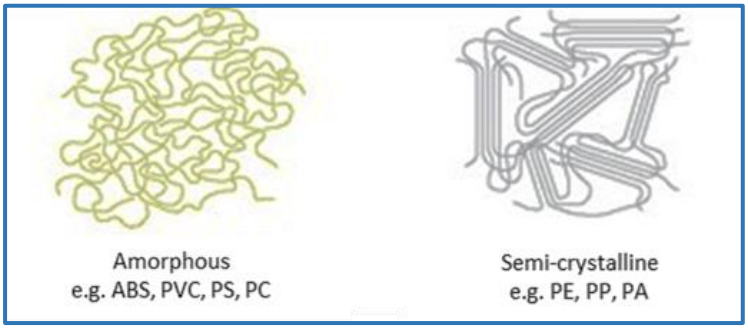

Figure 2.1 Amorphous and semi-crystalline polymers [31].

Key differences between amorphous and semi-crystalline thermoplastic polymers are summarised in Table 2.1.

Table 2.1 Differences between amorphous and semi-crystalline thermoplastic polymers.

Amorphous Polymers	Semi-crystalline Polymers
No melting point, it has a glass transition temperature (T_g).	It has a sharp melting point (T_m).
The molecular structure is random	It has an orderly molecular structure
It is easy to thermoform	It is difficult to thermoform
Creep, rigid, and chemical resistance	Its chemical resistance is excellent

e.g. ABS, PS, PVC, PC, and PMMA	e.g. PP, HDPE, Nylon, and PEEK
Rigid polymers	Soft polymers

The main requirement for high-quality joint in polymer components is heating polymers to reach the viscous flow state in the contact area [18]. Thermoplastic polymers have viscoelastic behaviour, meaning they are neither perfectly elastic or viscous but it exhibits both elastic and viscous qualities. The model for elastic materials can be described as a spring and performed under Hook's law.

$$\sigma = E\epsilon \tag{2.1}$$

Where "σ", "ε" and "E" are the applied stress, the strain and Young's modulus respectively, whilst the viscous materials can be identified as a damper or dashpot and performed under Newton's law.

$$\tau = \mu\gamma^{o} \tag{2.2}$$

Where "τ", "μ" and "γ^{o}" are the shear stress, viscosity and shear strain rate respectively. Therefore, the viscoelasticity of the polymer can be represented basically in Figure 2.2.

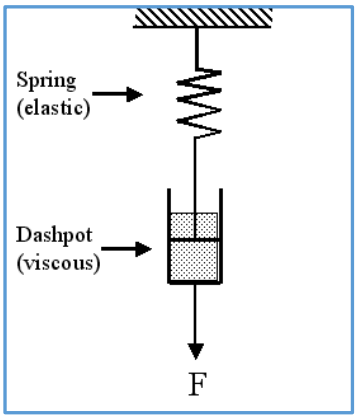

Figure 2.2 Form of polymer viscoelasticity [32].

The heat generated during the ultrasonic joining of polymers results from the viscoelasticity phenomenon. To form a good bond rapidly, the ultrasonic energy should be concentrated at the joining zone. Therefore, it is necessary to form a protrusion on the polymer surface. An energy director (ED) is a

protrusion on one side of the polymer surface, as shown in Figure 2.3 (further details about ED in Section 2.1.2.1). The energy of ultrasonic polymer joining is concentrated and focused to a smaller region on the surface of the polymer using this energy director increasing the quality and speed of the joining [33].

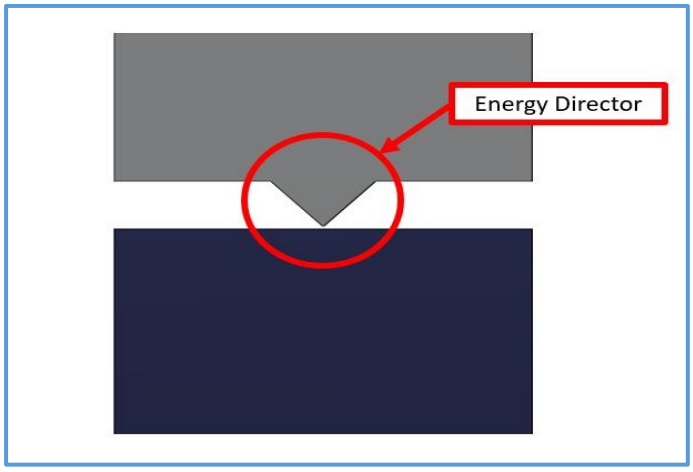

Figure 2.3 Energy director scheme [34].

Benatar [35] predicted the energy required to melt the energy director and form the joint, and defined the complex modulus that comes from sinusoidally varying stress and strain.

$$\sigma^* = \sigma e^{i\omega t} \tag{2.3}$$

$$\epsilon^* = \epsilon e^{i\omega t} \tag{2.4}$$

Where $\sigma^*, \epsilon^*, \omega$ and i are sinusoidal stress, sinusoidal strain, frequency and $\sqrt{-1}$ respectively. Hence, the complex modulus is described as:

$$E^* = \frac{\sigma^*}{\epsilon^*} = E' + E'' \tag{2.5}$$

Therefore, the complex modulus of viscoelasticity materials includes the storage modulus (E') which relates to the ability of materials to store elastic energy, and the loss energy (E'') which relates to the ability of materials to dissipate energy through intermolecular friction mechanisms.

The behaviour of polymers by determining their properties through ultrasonic wave propagation was investigated by Lionetto and Maffezzoli [36]. These authors have found that the sound velocity is relevant to the storage

modulus and density of the polymer, whilst the loss modulus is relevant to absorption of the ultrasonic waves. The viscoelasticity behaviour of polymer can be understood by using UDMA (Ultrasonic Dynamic Mechanical Analysis).

During the ultrasonic technique, the polymers are subjected to sinusoidal oscillations, which increases the temperature at the interface. At the beginning, the temperature is low and thus the polymer's molecular structure remains stiff because its molecular segments are immobile. This state is called the glass state or energy elastic state, as shown in Figure 2.4.

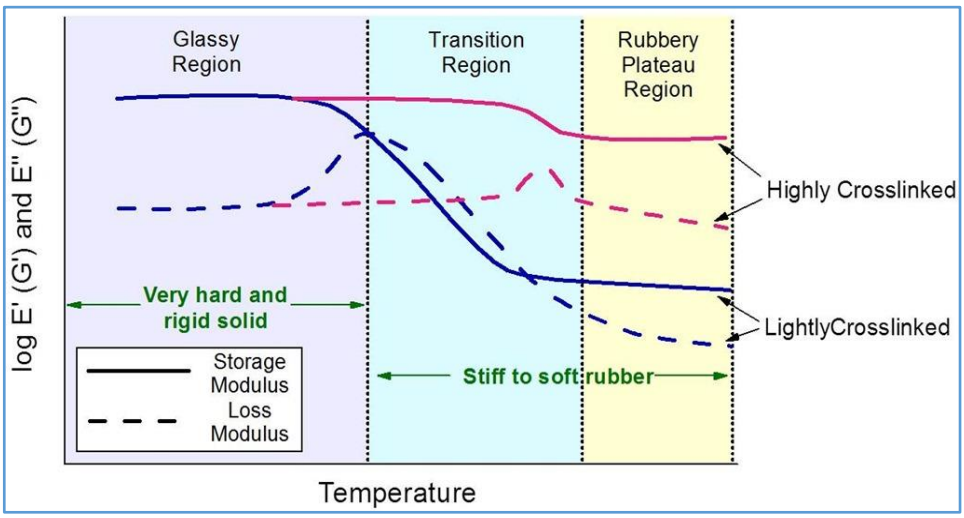

Figure 2.4 Relationship between loss and elastic modulus with temperature [37].

The figure (Figure 2.4) clearly shows that the elastic modulus is decreased with complex modulus when the temperature is increased until it reaches glass transition temperature (Tg) due to decreasing the required force for deformation. In the glass transition region, polymers are changed from glassy into rubber state where the molecular segments become activated, but these motions occur with difficulty due to molecular friction. Therefore, the volume of polymers expands through increasing the temperature due to decrease strength of molecular bonds in the molten state, as shown in Figure 2.5.

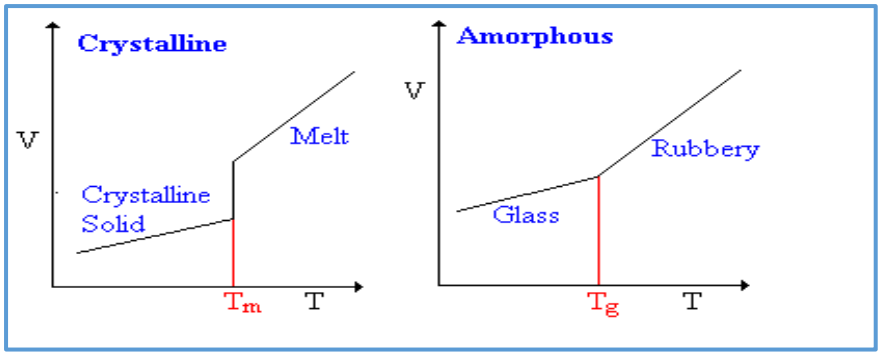

Figure 2.5 Specific volume vs. temperature are shown at the right for amorphous and crystalline polymers [38].

Continuously increasing the temperatures above T_g leads to a fall in the elastic modulus and complex modulus, as well as a decrease in loss modulus due to the drop-in viscosity. At this point, amorphous polymers (lightly crosslinked) flow more easily, whilst the loss modulus of semi-crystalline polymers (highly crosslinked) becomes maximum around its melting temperature (T_m).

In case of joining polymer to metals, the best range of temperature that achieves the highest joint strength has been not investigated. Therefore, the current thesis will discuss this issue to understand the mechanism of joining dissimilar materials. This is because appropriate temperature at the interface is important for obtaining the best results due to melt the polymer (ED collapse) and flow it inside the pores of metal without drop-in the viscosity.

The joinability of thermoplastics has been affected by these differences between amorphous and semi-crystalline thermoplastics. The joinability of amorphous thermoplastics is better than semi-crystalline thermoplastics because the semi-crystalline thermoplastics are soft polymers and their molecular structures are ordered. These characteristics act as springs and, thus, absorb a large amount of the ultrasonic vibrations instead of transmitting them into the joint region at the interface [39]. Whilst this might suggest that amorphous polymers are the better choice for ultrasonic joining, amorphous materials tend to be softer and have lower melting points, and solvents can penetrate them more than semi-crystalline polymers.

The average heating rate in ultrasonic joining of polymers which leads to melting the energy director depends on the loss modulus as shown in Equation (2.6) [14].

$$Q_{avg} = \frac{\omega \varepsilon^2 E''}{2} \tag{2.6}$$

Where Q_{avg}, ω and ε are average heating rate, frequency (rad) and applied strain. Therefore, the best state to join polymers ultrasonically is in the glass transition region for thermoplastic polymer.

The phases of joining thermoplastics polymers are divided into four phases depending on the penetrations of polymers, as demonstrated by Nonhof and Luiten [40] and shown in Figure 2.6.

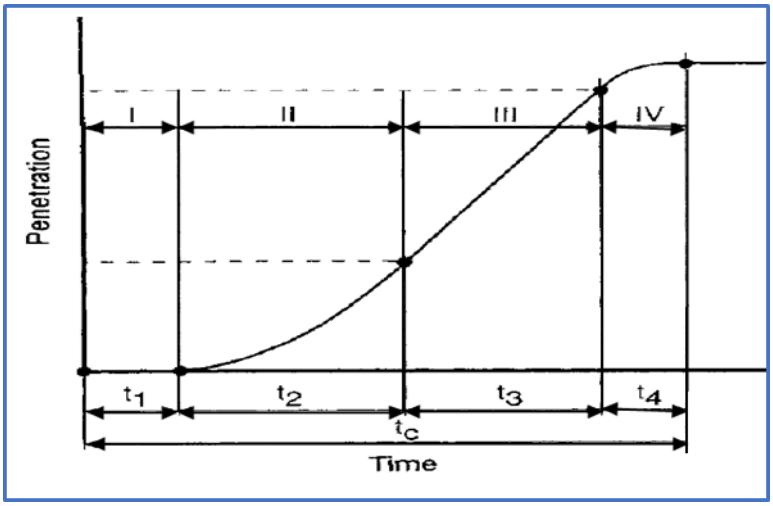

Figure 2.6 Four phases of ultrasonic joining of thermoplastics [40].

In the first phase (I), the polymer (solid) is heated to start the softening of the material. Then, the joining zone is developed, and the material begins to flow in the second phase (II) due to the energy dissipated. The third phase (III) leads to a steady state of the molten plastic flowing, while the last phase (IV) begins when the ultrasonic generator is off. A weld is made after solidification of the joint zone. This joint is produced because of the interdiffusion of the molecules across the bond region. These authors (Nonhof and Luiten) described the flow of the polymers out of the joining zone by using the Navier-Stokes formula for a viscous flow, as shown in Figure 2.7. This formula neglects external forces, such as gravity.

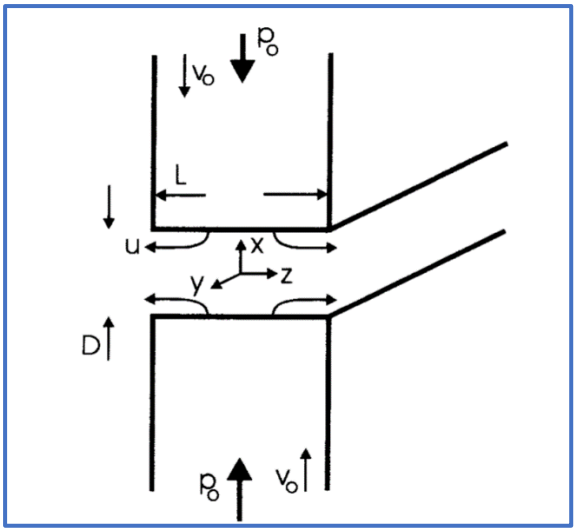

Figure 2.7 Polymer flow during ultrasonic joining where P_o, v_o, u and D are joining pressure, penetration speed, squeeze flow velocity and the height of molten polymer respectively[40].

$$\rho\left(\frac{\partial v}{\partial t} + (v.\nabla)v\right) = -\nabla P + \mu\nabla^2 v \qquad (2.7)$$

Where ρ, v, t, P and μ are density, velocity, time, pressure and viscosity respectively. Hence, according to equations (2.6) and (2.7) the viscoelastic heating depends on the ultrasonic frequency, the amplitude and loss modulus while compressive flow of molten polymers is related to joining force, joining time, density, viscosity and velocity. Figure 2.7 explained the mechanism of flowing the molten polymer (the energy director (ED)) during the ultrasonic joining of similar polymers (polymer-polymer) at the interface.

The collapse of energy director that is produced due to the polymer melting may have a relationship with the joint strength. The joint area increased when the collapse of ED is increased and thus increasing the joint strength [30]. Chuah et al. [33] observed that the joint width was increased due to increase the ED collapse height when semi-circular and triangular shape were used. While the rectangular shape had the same width of the joint interface with variation of the melted height (collapse).

This formula (Equation (2.7)) was developed to calculate the velocity in the steady state of Phase III (Figure 2.6) by assuming the viscosity is constant in the joint zone, and neglecting the inertia, as follows [40]:

$$v_x(x,z) = \frac{v_o}{D^3}(4x^3 - 3D^2x) \quad (2.8)$$

$$v_z(x,z) = \frac{12v_o}{D^3}z(0.25D^2 - x^3) \quad (2.9)$$

The driving force for flowing the molten polymer (ED) at the interface is providing by the ultrasonic pressure in the z-direction.

Although these formulae are related to polymer-polymer joints, they provide valuable indications of the expected behaviour of a polymer when joining to a dissimilar material. In the case of polymer-polymer joining, an amount of the molten polymer (from the ED collapse) penetrates the surface of the sample, whilst the remainder is squeezed out of the joint zone. Since the metal is a rigid material, the expected amount of molten polymer that is squeezed out of the joint region is bigger than in the polymer-polymer joining at the same ultrasonic pressure (P). Therefore, it can be concluded that the required ultrasonic pressure to join polymer-metal will be lower than for the polymer-polymer joining, in order to avoided pushing the molten polymer out the joint region. The current thesis will take this into consideration when selecting the relevant range of ultrasonic parameters to consider.

Therefore, the effect of input energy on the joint strength is very relevant. This is because the input ultrasonic energy is correlated with ultrasonic force, time, amplitude and ultrasonic frequency. The input energy was governed by physical principles of ultrasonic technology, as shown in Equation (2.10) [30] and [41].

$$E = F * f * A * t \quad (2.10)$$

Where,

E Input Energy (J)

F Ultrasonic Force (N)

f Frequency (Hz)

A Vibration Amplitude (μm)

t Ultrasonic Time (sec)

Few studies have considered the effect of input energy on the joint strength. The results of these studies observed that the joint strength increased with input energy increasing until it reaches its highest point and then starts decreasing. This decrease in the joint strength at the higher energies was produced because the plastic deformation regions spread and expanded to the whole bond zone, rather than only at the joint line [42], and [43]. In addition, it was also a result of material degradation due to increase in temperature. Too much input energy can be generated due to extreme levels of ultrasonic force, time and vibration amplitude.

The current thesis will therefore discuss the effect of input energy on the strength of polymer-metal joints to understand the mechanisms of dissimilar joining. This discussion will be used to help define a suitable range of ultrasonic energy for use in producing a polymer-metal joint, and therefore to select the appropriate range of the ultrasonic parameters' levels.

Beside the ultrasonic joining, there are many techniques used for joining thermoplastics. The chosen process is affected by the material to be bonded, the joint configuration, the required joint strength, the level of seal required, the process cost and speed, and the production quantity. Although there are many different processes of welding polymers, such as hot plate welding, extrusion welding, vibration welding, spin welding, and laser welding, these processes depend on heat at the joint to melt the adjacent polymer and pressure to form the joint. The importance of applying pressure is related to delivering intimate contact between the two contacting surfaces. However, the excessive increase of pressure can cause a decrease in the molten-layer thickness and thus reduce the joint strength [44]. Based on this, the welding processes of polymers are governed by the factors; temperature, time, and pressure [45]. Therefore, careful optimisation of these parameters is required to achieve high quality joints.

More details about the influence of ultrasonic parameters can be found in the next chapter (Chapter 3).

2.1.2.1 Energy Directors

In the ultrasonic process, the longitudinal waveforms are a standing ultrasound wave within the workpiece between the horn and the base of the sample by the wave reflection. With this wave, there are some areas that have maximum acoustic cyclic stresses and at these locations the heat will be maximised. The area of the polymer that need to be bonded should be designed to be in these areas (the areas of maximum heating), as shown in Figure 2.8 [25]. Therefore, the selection of areas that have maximum heating is important, but it is not always possible to do this in practice because it will significantly limit the part design. Narrowing the cross section of workpieces can increase the mechanical cyclic stress, such as using an energy director (ED) and, thus, the position of the joining area can be located without restrictions.

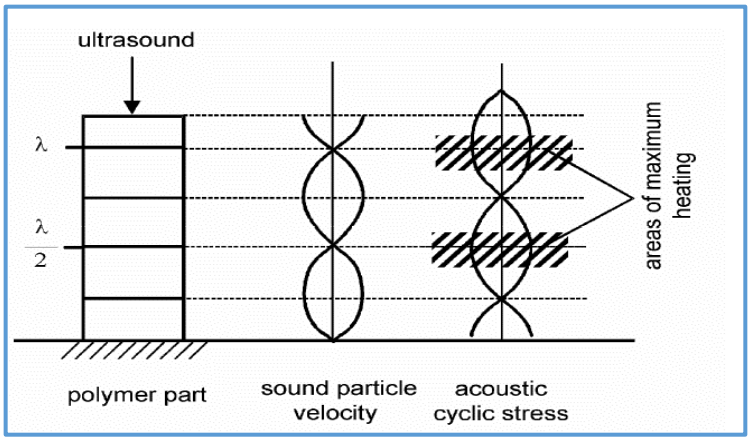

Figure 2.8 Principle of ultrasonic joining [25].

One of the most significant joining parameters for ultrasonic polymer joining is the energy director. This is a protrusion on one side of the polymer surface and it is considered a very important joining parameter because it allows focusing and direction of the energy concentration during the joining of thermoplastic polymers, thereby increasing the quality of the joint strength [33], and [46].

Different shapes of energy directors have been used in previous studies, as triangular, semi-circular, and rectangular shapes [33], [30], and [47].

Liu and Chang [48] investigated the effect of the ED's geometry on the joint strength of polypropylene plastics. Three different shapes (triangular, rectangular, and semi-circular) were used. Mathematical techniques (design of experiments) were employed to find the best and significant parameters. The experimental results indicated that the energy director factor has a significant effect on the joint strength and the triangular shape was the best due to the quicker deformation of the energy director (ED collapse). Other researchers also studied the effect of ED geometry on the joint strength. Chuah et al. [33] investigated the effect of ED geometry on the joining efficiency by using three different shapes (triangular, semi-circular, and rectangular) of the joints between thermoplastic polymers amorphous (Acrylonitrile butadiene styrene, ABS) and semi-crystalline (Polyethylene, PE). The results concluded that the semi-circular shaped energy director (ED) had the largest joining efficiency compared with rectangular and triangular shapes under the same joining parameters. This was because the semi-circular shape had produced the greatest contact area, whereas, a triangular shape had the lowest joining efficiency. Additionally, the results showed the ABS bonded samples absorbed a large amount of the joining energy by the energy director compared with the absorbed energy in PE. The different energy absorption in this work was due to the differences between amorphous (ABS) and semi-crystalline (PE) polymers in viscosity and elasticity properties. Where the ABS sample is a better conductor for the ultrasonic energy, the ultrasonic energy is able to transmit more easily through it. However, less joining energy can transmit to the energy director of semi-crystalline (PE) plastic because it is a more viscous polymer.

The energy directors (semi-circular, triangular and rectangular) also had different dimensions for example, the high of ED was 1.732 mm for the triangular shape while it was 1 mm for the semi-circular shape, and 2mm width for triangular while 1 mm for rectangular. These differences in dimensions may also affect the results.

The effect of the configuration of the ED on the joint strength was investigated by Villegas and Berse [49]. Three types of ED (triangular shape) configurations

were tested in this research, as shown in Figure 2.9. Carbon fibre reinforced–polyetherimide (CF-PEI) composite joints were used in this study. The results showed that the lap shear strength (LSS) of the transverse ED joints was the highest compared with other configurations because the transverse joints had the largest joining area, about 90% of the total overlap area; parallel joints covered 80% of the overlap area. Furthermore, use of multiple EDs showed a significant effect on reducing the disturbance of fibres due to decreasing the joining pressure.

Whilst this study (Villegas and Berse [49]) provided a good understanding of the effects of Energy Directors, the effect of ultrasonic parameters were not investigated as part of this study. It is highly possible that these findings might be expected to be affected when using varying ultrasonic parameters, meaning there is a strong case for examining the effects of EDs and ultrasonic parameters simultaneously. These investigations will form part of the current thesis.

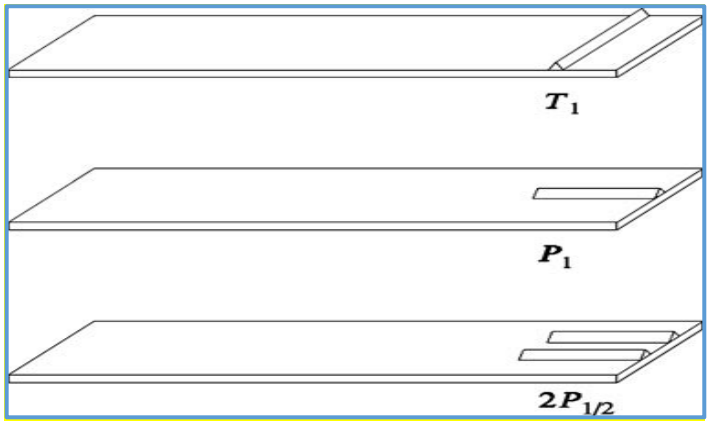

Figure 2.9 Different orientations (transverse T_1, parallel P_1) and multi-energy directors $2P_{1/2}$ [49]

Shear joint (SJ) is another joint design of polymers that was compared with the energy director (ED) type. Rani et al. [50] investigated the effect of different joint designs on the bond strength of polymers amorphous polymer ABS and semi-crystalline polymer HDPE (High-Density Polyethylene), as shown in Figure 2.10. The findings showed that ED joints absorb less energy than shear joints because the contact area is bigger in shear joints. The shear joint is recommended for joining semi-crystalline because semi-crystalline polymers

have a sharp melting point meaning that they melt and solidify rapidly. Therefore, shear joints give semi-crystalline a chance to melt the small initial contact area. Then, the controlled interface continues melting along the vertical walls and this allows a strong joint to be obtained. A fractional factorial design was adopted as the experimental design to determine the optimum values of joining parameters. These findings have also been confirmed by Devine [51], and in a technical report by Branson [52].

Although the previous study [50] clarified the importance of joint design on the bond strength of polymers (amorphous and semi-crystalline), this previous study was limited to constant other ultrasonic parameters, such as vibration amplitude. In addition, the relationship between the ultrasonic parameters (joining force, joining time, hold time) and the joint strength was not investigated. Therefore, the current thesis will discuss the effects of a variety of the ultrasonic parameters on the joint strength of dissimilar materials. In addition, and from this previous study [48], the current thesis will use an ED if the chosen polymer is amorphous.

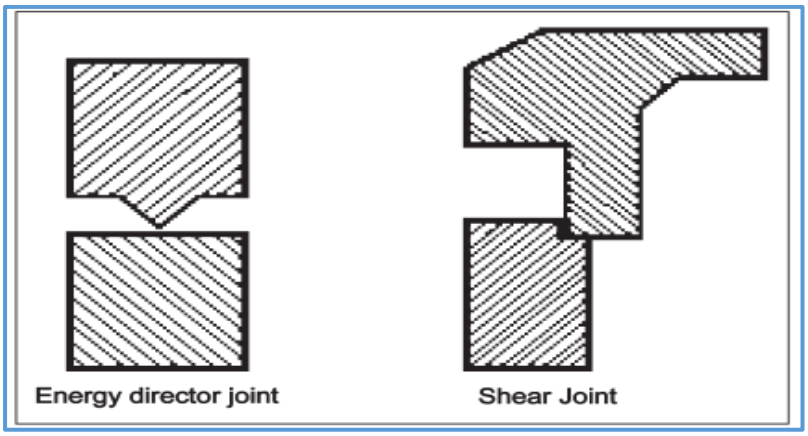

Figure 2.10 Shear joint and energy director ED [50].

Relatively few researchers have used new techniques to join thermoplastics ultrasonically instead of with an energy director. Luo et al.[53] investigated using a preheating technique to joining a thermoplastic polymer (Polymethylmethacrylate PMMA) without using an ED. The reason for using this technique was to avoid the problem of controlling the flow of the molten material in the microstructure during the joining process, so this method can be described as non-molten joining. This technique depends on heating PMMA

to $75C^0$ (below T_g $105C^0$), and the amplitude must be chosen cautiously. The reason for choosing this temperature and amplitude is to retain the joining process in the interfacial friction state. If the temperature reaches glass transition temperature (T_g), the polymer changes to the viscoelastic stage, thus the heat generated in the viscoelastic state by ultrasonic oscillation is much faster compared with the glassy state. Therefore, some regions of the bonding zone reaches the T_g quicker than other regions because the heating field is non-uniform thus making the molten material non-uniform. The results showed that the critical amplitude for PMMA was 6.6μm and the time of joining was longer than common ultrasonic joining (with ED) at approximately 25s.

Therefore, although there are other ways to potentially join polymers, it is clear that the use of energy directors is currently the most appropriate as it is possible to concentrate and focus the energy on a specific area, consuming less time for joining. Despite the importance of energy directors there is some confusion about the best ED geometry, so the current thesis will consider several of these. This will be the first time the use of an ED will be reported for polymer-metal ultrasonic joining.

2.1.3 Polymer – Metal Materials

From the above (Section 2.1.1), the mechanism of joining for metals is not appropriate for joining metals to polymers because it depends on the parallel motion and this motion would displaces the polymer out of the bonding region by the transversal vibration.

As discussed in Section 1.2, common methods of joining a polymer to a metal include adhesion and mechanical fastening. Whilst these are distinctly different techniques, they all rely on both an external method of transmitting energy, and a rough surface in order to all mechanical interlocking. Adhesion depends on creating a rough surface of metal samples and employing a polymer adhesive on it to create mechanical interlocking and chemical bonding [54]. Therefore, no chain entanglement occurs in metal/polymer joining. The joining between metals and polymers is important where it is

possible to use as a hybrid structure, i.e. two layers of Al alloys and between them a layer of polymer. This hybrid structure can be used in railways, automobile, and aircraft industries to prevent vibration and to reduce noise emission [55], and [56]. The hybrid structure was obtained by using adhesion technique to join the metal faces with polymer core by thermoplastics resins, or using blank-holder method [57]. Although these hybrid structures are necessary, there has been limited use of these hybrid material structures in the mass production industries, such as automotive, and railways due to the long production times [57]. Therefore, new methods, such as ultrasonic technique are required to produce products in high volume.

Hopmann et al. [58] used laser radiation for joining hybrid structure metal/plastics. This approach also depends on creating microstructures cavities on the metal surface and using laser radiation to melt the polymers. Mechanical interlocking occurred when the molten polymers flow inside the pores of metal. Balle et al. [59] ultrasonically joined aluminium alloys with composite fibre thermoplastics and the mechanism of joining depends on creating microstructural pores on the metal surface using chemical pre-treatment to allow the melted polymer to flow inside it and create mechanical interlocking.

The main point of joining dissimilar materials in previous examples in [58] and [59] depends on increasing the temperature at the interface which makes the polymer melt, reducing its viscosity and allowing it to fill in the rough bits and increase the effective surface area of the bond.

The focus of the current thesis will therefore benefit most from the literature relating to joining polymers, as the best results can be expected when the polymer flows into the other surface without being squeezed out of the joint. Combining the polymer with a rough surface will be considered, in order to provide a large area of interlocking.

2.2 Materials for Ultrasonic Process

After explanation of the physics of joining materials (polymer, metals and dissimilar) using ultrasonic technique in Section 2.1, the materials that were used in the ultrasonic technique are discussed in this section.

2.2.1 Thermoplastic Materials

As discussed in Section 2.1.2, amorphous thermoplastics, such as ABS or PS (Polystyrene) are easier to join ultrasonically than semi-crystalline polymers, and more energy efficient thereby being preferred for ultrasonic joining [17]. These properties of amorphous thermoplastics result from random molecular arrangements of the amorphous polymers and their wide softening temperature range. These characteristics allow polymer materials to flow easily and gradually, as such premature solidifications are avoided [14]. Whereas, semi-crystalline polymers are difficult to join ultrasonically because they tend to absorb the oscillation energy before passing through the joining zone and they have a sharper fusing temperature. Thus, semi-crystalline materials need more power to join them [7].

Raza [30] bonded ABS (amorphous polymer), and PP (semi-crystalline polymer) ultrasonically. This author adopted GLM (General Linear Model) statistical analysis to find the effect of using joining parameters on the lap shear joint strength. The findings of this work (Lap Shear Strength LSS) were 17MPa (about 34 % of the base material), and 6MPa (about 14.6 %) for ABS and PP respectively. This work observed that the LSS of ABS was higher than the LSS of PP at the same joining parameters because the softening temperature of ABS (103 °C) is lower than the melting point of PP (170 °C) and that meant ABS material began melting and flowing quicker than PP material. Thus, a stronger joint strength was achieved. Additionally, Raza observed that pits were formed at the interface by-product of fracture, and measured the pit depth. These pits were performed due to the penetration of ED into the sample during the joining. Furthermore, the author showed that higher ED collapse leads to increase the joint strength through increasing the joint area.

Although the findings of this study by Raza [30], such as the pits observation, and the correlation between ED collapse and LSS were important, the effect of bonding temperature on the joint strength which may help to select the optimum conditions to obtain the strongest bond was not investigated. In addition, the influence of sample thickness, which may have an effect on the values of joint strength was not studied. Furthermore, the relationship between pits size and the joint strength was not investigated. Therefore, further studies on these missed investigations will may have a substantial impact on the main findings of this thesis.

A further comparison between the amorphous polymer ABS and semi-crystalline polymer HDPE (High-Density Polyethylene) during ultrasonic joining was studied by Rani et al. [50]. Under the same joining conditions, it was observed that the HDPE required more energy than ABS to break its crystalline structure. In addition, the author observed that the interface temperature of ED was higher than of non-ED due to the focussing of ultrasonic energy at small area. The increase of temperature led to the ED collapsing and creating the joint. From this it can conclude that measurement of temperatures within the process may be used to assist in understanding and predicting the behaviour of the ultrasonic joining process under a larger range of conditions.

Khmelev et al. [60] studied the maximum strength of joints that have properties close to the base material of thermoplastic polymer materials (polyvinylchloride (PVC) and polypropylene (PP)). PVC and PP were joined separately using the ultrasonic joining and their storage coefficient was calculated. The storage coefficient is useful because it gives indicate the quality of joints and is obtained by dividing the stress of the joined connection by the main material stress. The results showed the storage coefficient of PVC and PP were 81% and 76% respectively. Any energy deficiency during ultrasonic joining leads to incomplete melting of polymer materials in the joining area or hyper energy that causes the destruction of the thermoplastic polymer.

Liu et al. [61] investigated the optimal joint strength of ultrasonically joined amorphous polymer general purpose polystyrene GPPS and semi-crystalline polypropylene PP. These authors adopted an experimental matrix design that

depended on the statistical approach (Taguchi method) to optimise the joint strength and its parameters. This approach is a type of the experimental design methods that used fewer testing trials to give the same information as a full factorial experimental design (further details on the design of experiments in Section 2.3). The results found that GPPS polymers (amorphous) can be successfully joined using low energy compared with PP (semi-crystalline) polymers because the crystals in semi-crystalline polymers required extra energy to break and allow to flow and, therefore, the intermolecular diffusion between the surfaces at the interface can happen.

Although these authors used a good range of key parameters, such as joining force, time, vibration amplitude and energy director shape, the effects of the interaction between these parameters on the joint strength was not studied. These missing investigations may give a clear vision about achieving the best bond and optimum levels of parameters during polymer- metal joining.

Thus, the thermoplastic polymers, either amorphous or semi-crystalline, show their ability to join effectively using the ultrasonic technique. Amorphous polymers are easier to join than semi-crystalline plastics, and more energy efficient thereby being preferred for ultrasonic joining. This finding can be useful when choosing materials in the current research. Furthermore, there are many ways to find the correlation between parameters and the joint strength, and determine the optimum values of parameters levels, but design of experiments is still the best way currently because it saves time consumption and cost through using a few experiments. The best design choice will be taken into consideration in the current research.

Zhang et al. [62] presented a new ultrasonic method to join heterogeneous polymers. This new method works by inserting an interposed sheet (IPS) between the plastic samples and this interposed sheet is fixed in a sonotrode (the vibrating body). The IPS material depends on workpiece materials. If workpieces are metals, IPS are commonly made from aluminium, whereas, if the material of workpieces is a polymer, IPS will be produced from a composite of the workpiece materials. These authors used this technique to

join different polymers such as polylactide (PLA) (this type of polymer is a crystalline polymer and has been used in biomedical applications because it is non-toxic and biocompatible) with an amorphous polymer as poly (methyl methacrylate) PMMA (this type of polymer has been widely used due to its good engineering properties) by inserting an IPS (interposed sheet) between them, which can be joined to the workpieces due to the heat from friction, as shown in Figure 2.11. This method produced a joint (PLA/PMMA) with a yield strength enhanced to 73 MPa that is 18% higher than that of PLA.

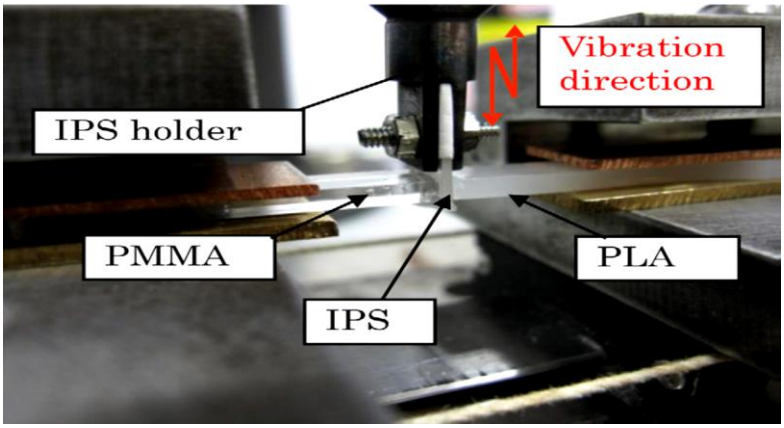

Figure 2.11 Novel Ultrasonic joining principle schematic drawing [62].

Figure 2.12 shows the comparison of nominal strain and stress in the three materials (PLA, PMMA, and a composite of PLA/PMA). These authors also used this technique to join poly methyl-methacrylate (PMMA (brittle)) and polycarbonate (PC (ductile)) [63]. The results showed that air bubbles appear at the interface because of the IPS cracking due to the excessive joining time. Additionally, both the enlargement of the joining area and reduction of the air bubbles are important to enhance the join strength. Furthermore, both a shorter joining time and higher joining pressure were the effective joining situations, because the excessive temperature produces air bubbles due to decomposing the polymers, thus rupturing the specimens during the tensile test and creating a weak join area. The decomposition temperature of PMMA and PC is 300 and 450 °C respectively.

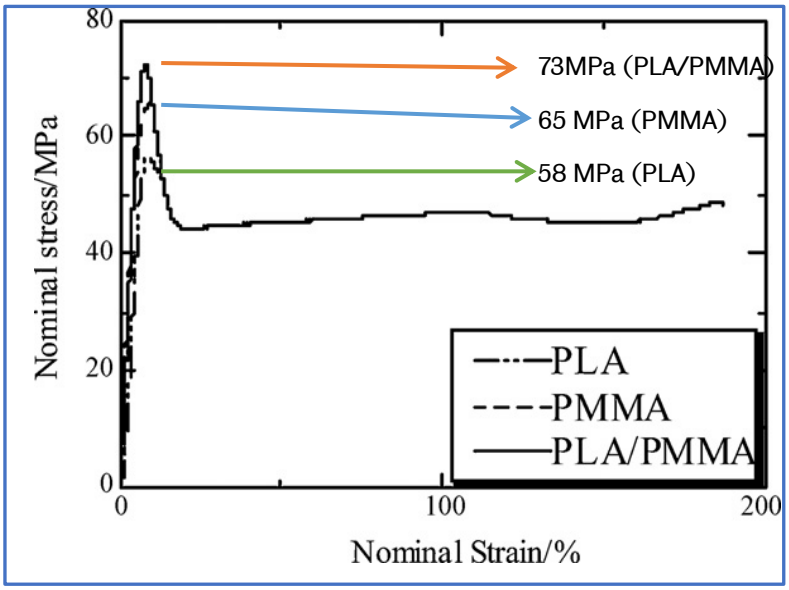

Figure 2.12 Nominal strain versus the nominal stress of PLA, PMMA and composite of PLA/PMMA [62].

This research (Zhang et al. [62]) investigated the influence of excessive joining time on the joint strength and also explained the effect of air bubbles. Although this provides useful information regarding the effects of excessive energy input into a joint, the work did not include the effect of excessive levels of other significant parameters, such as joining force and vibration amplitude, where a subsequent decrease might also be expected. The current thesis will extend this type of work to cover a broader range of information on these parameters.

One of the primary challenges facing structure applications when using fibre reinforced polymer composite materials is repairing matrix cracks. These cracks are produced due to increasing the load, impact damages, degradation of the environment, or other consequences of damaging. Hargou et al.[64] investigated using an ultrasonic joining technique to repair cracks in composite laminates. A mesh of an effective adhesive repair agent [poly (ethylene–methacrylic acid) (EMAA)] was added between the layers of the composite before the curing process. In this work, ultrasonic joining was adopted to rapidly heat up the composite material to reach the required temperature of 150 ^{0}C within 4 seconds; less than oven heating which needs 30 minutes. The results exhibited that the fracture toughness was raised around 30% compared with the original toughness (undamaged).

Hargou shows the speed of increasing the temperature using the ultrasonic technique compared with other methods, such as the oven, demonstrating that the ultrasonic technique is one of the fastest techniques for joining similar and dissimilar materials compared with other techniques, such as other joining types, mechanical fastening and adhesion technique.

2.2.1.1 Types of Polymer Joining

Depending on the distance between the sonotrode (ultrasonic horn) and the bonding interface, there are two types of ultrasonic joining of thermoplastics [7]:

- **Near-Field Joining**
- **Far- Field Joining**

Near-field joining occurs when the join joint is within 6.3 mm of the sonotrode contact. Far-field joining occurs when the joint is further away from the sonotrode; both types of joining are shown in Figure 2.13.

The selection of this critical value (6.3mm (0.25in)) depends on the acoustic intensity [7]. The intensity of the wave amplitude that is transmitted in the sound field from the source may change based on the travelled distance, as shown in Figure 2.14. In the near-field (within 6.3mm (0.25in)), the vibration amplitude at the interface zone is close to the amplitude at the sonotrode tip during 20kHz frequency, whilst the amplitude at the joint zone is lower than the amplitude at the sonotrode when the interface is further away [65].

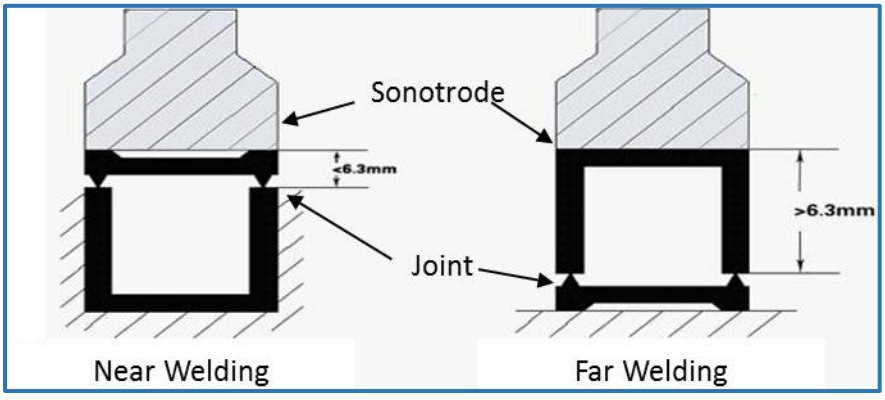

Figure 2.13 Far-field and near-field joining [66].

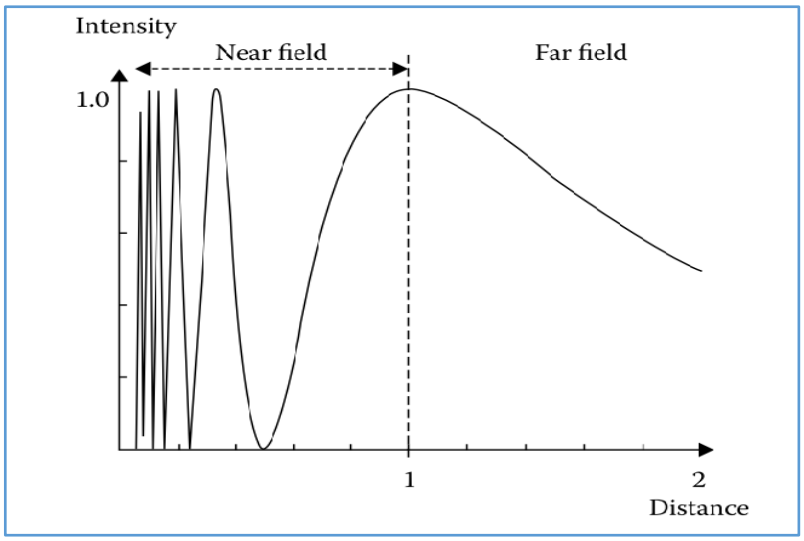

Figure 2.14 Wave amplitude intensity [7]

Rani et al. [50] investigated the effect of far and near joining field on the joints of ABS, and HDPE polymers. The findings of this research were that far-field joining requires more energy than near-field joining because the transfer of ultrasonic energy is better through a short distance. Furthermore, amorphous thermoplastics or rigid plastics can achieve an adequate bond through either near-field or far-field joining because amorphous polymer ABS absorbs less energy than HDPE under the same conditions for breaking its structure. Whereas, for soft polymers or semi-crystalline thermoplastics use of a near joining type is suggested due to the difficulty of breaking its crystalline structure; this concurs with Gutinek et al. [18]. Rani et al. [39] performed other research about joining semi-crystalline polymers in far-field with different designs of the energy director. High-density Polyethylene (HDPE) was used during this study and it was concluded that the most appropriate joint of far-field joining for HDPE was the texture joint (see Figure 2.15) because it contains many surface asperities. These asperities prevent the molten polymer from flowing out of the joining zone, acting as a natural barrier. Furthermore, the asperities create a larger surface area for joining and, thus, the joint strength is increased. The temperature at the interface area of energy director joints is higher than non-energy director joints due to focusing the joining energy that leads to rapid melting of the polymer.

Although Rani measured and observed the effect of the bonding temperature on the collapse of the energy director, the ultrasonic parameters used, such as vibration amplitude, joining force, joining time and hold time were constant; variations in these are likely to have an effect on the bonding temperature that affects the joint strength.

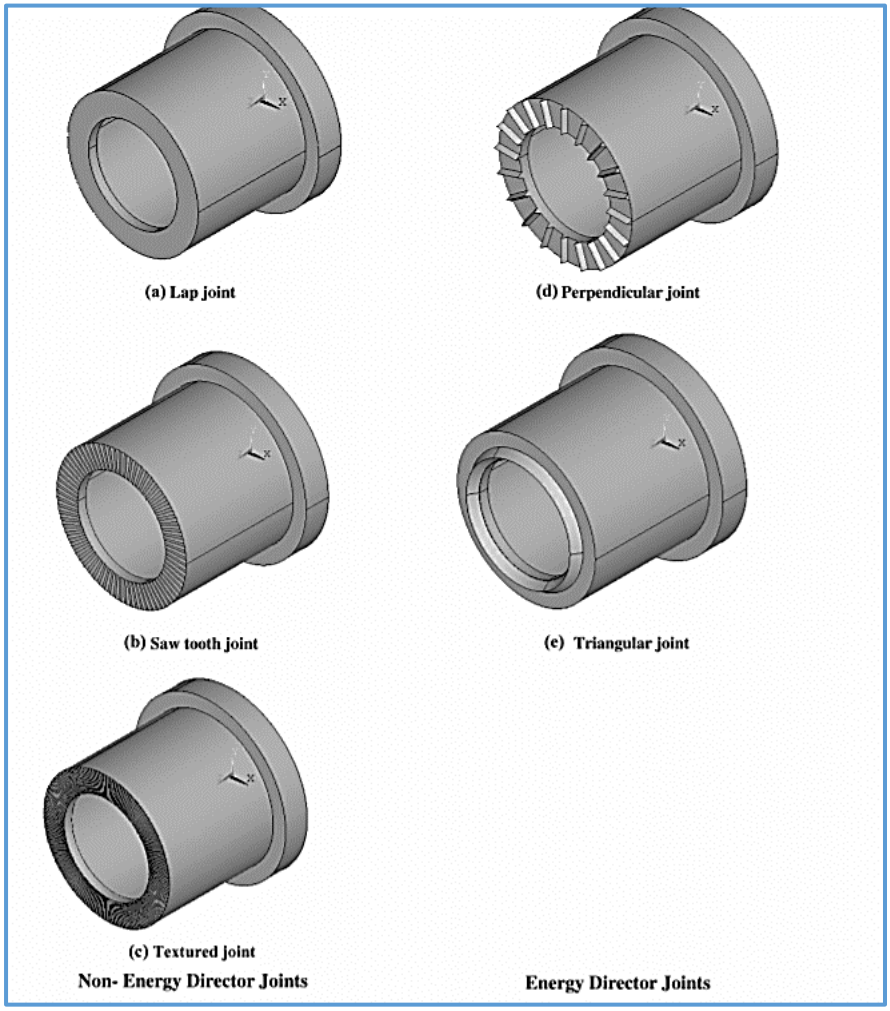

Figure 2.15 Different joint designs [39].

In addition, Benatar investigated the effect of near-field [67] and far-field [68] on amorphous and semi-crystalline thermoplastics joints. This author observed that the far-field are more successful for amorphous than semi-crystalline polymers because the loss modulus of amorphous polymers is bigger than in semi-crystalline and therefore the energy that is dissipated to the heat at the interface is bigger than in semi-crystalline. The joint strength was improved when the joining energy was increased by raising the vibration

amplitude because the dissipated energy is related with the square of amplitude.

The main conclusion of research in this area is therefore that semi-crystalline polymers should use near field and amorphous polymers can use either near or far field, but that in practice near-field would be most likely be used as it is less energy intensive. Therefore, the near-field type will be used in the current research.

2.2.2 Metal Materials

The ultrasonic joining of metals is a solid state type, meaning metals do not reach the melting point, and its energy is proportional to the shear force that results from the horizontal oscillations [69], and [70]. Hence, the diffusion process in the joining area is the basis of the joining process in metals [71].

Ultrasonic metal joining was invented by accident during efforts to improve the grain structure of traditional spot welds using ultrasonic waves. It was discovered that welds could sometimes occurr through the vibration of the electrode without the joining current flowing [70].

The primary keys of metals' weldability are Young's modulus, hardness, yield strength and thermal conductivity that improve the atoms' diffusions between the contact surfaces. Therefore, soft metals, such as aluminium and copper are easier to weld than hard metals like nickel [72]. Due to these variances of properties between the metals, the joinability between them is different.

The mechanism of joining metals is different from the mechanism of polymer joining because it depends on the horizontal vibration that leads to surface friction between the sample and therefore heat generation. The temperature at the interface is below the melting temperature of metals. The ultrasonic joining of metals depends on the interatomic diffusion process which diffuses the atoms from high a concentration region (heat) to a low concentration region by the force presence [69].

Watanabe et al. [73] studied the effects of hardness and surface roughness on the joint strength of Al-Cu and also Al- austenitic steel joints. The results

showed that the surface roughness had a low effect on the strength of Al-Cu joints when the surface roughness of Al at the faying surface was increased by emery paper compared with electrolytic polishing. However, the joint strength was decreased when the surface roughness of Cu increased because Cu is harder than Al. Thus, the formed peaks on Cu surface caused surface fractures on the Al side. Therfore, the surface roughness of harder metal strongly affects the joint strength and requires more energy to allow the diffusion. The position of samples during ultrasonic joining and the comparison between Al-Al joints and the Cu-Cu joint was also investigated by Alsarraf [12]. This study found that the joint strength of Al-Al was more than 15% higher than the joint strength of Cu-Cu at the same joining parameters. The reason for these findings is that the aluminium materials can be easily deformed plastically during the USW process because aluminium has lower hardness than copper. Hence, there are a lot of dislocations produced at the interface of softer material, causing a metallic bonding by electron exchange between both surfaces. Additionally, this author studied the effect the location of the metal during the lap joints, such as Al-Cu, and Cu-Al joints. The results showed that the joint strength becomes stronger when Al is placed on the top rather than when Cu is placed on the top because copper materials are harder than aluminium.

Althougth Alsaraaf investigated the effect of joining force, amplitude and position of samples during the lap joint by ultrasonic technique, the effect of other significant joining parameters, such as joining time and the parameters interaction were missed.

The ultrasonic joining of advanced alloys was evaluated by Bloss and Graff [74]. The alloys that were bonded in this study, were titanium, stainless steel, and nickel-based. The results emphasise that the yield strength and the hardness of the oxide layer had a significant effect on the joinability. Hence, the joining process of titanium alloys presents excellent weldability because the oxide layer of titanium is thin and can be removed easily by ultrasonic vibration, whereas the oxide layer of a nickel-based alloy is hard and needs more energy to remove it, thus the joining process was very difficult.

Bloss and Graff did not investigate the hardness around the joint area that may be affected during the ultrasonic process, which is expected to affect the joint quality through changing the microstructure of this area.

Zhu et al. [75] studied this hardness around the joints between Ti6Al4V sheet and aluminium alloy sheet (AA6061) which was increased after the joining process, compared with the original material hardness. The reason for the hardness increasing was plastic deformation that causes dislocation movement. In addition, the movement of other dislocations was hindered by the existence of one dislocation. The percentage of hardness increase varied from 20-50%. Therefore, microhardness investigation of the area around the joining zone is important to study the change of hardness on the joint strength. The increase of hardness around the joint area leads to decrease the ductility of metal and this area becomes exposed to cracks in the base material and it can be considered as an indicator of joint properties and LSS quality [76].

Bakavos [42] studied the mechanism of joint and microstructure formation of aluminium sheet. The author reported that the created joints by ultrasonic technique have good mechanical performance and no heat affected zone damage due to shorter weld cycle (typically <0.5 s). This damage in the joint resulted from the excessive energy above 500J that generated high bonding temperature. Therefore, the microstructure of the zone around the joint could be affected due to the high temperature. In addition, Patel [77] studied the effect of ultrasonic technique on the microhardness of the joint. Patel observed that the hardness values of the area around the joint varied within 10% of the base metal and the heat affected zone was very small due to poor conductivity of the sonotrode material (steel) compared to the thermal conductivity of the samples. In addition, Shakil et al. [43] investigated the hardness distribution of metal joints. The author found that the hardness value of joined samples was higher than of the received samples at the interface. The increase of ultrasonic energy leads to increase the hardness near the joint zone due to take place the recrystallisation at the surface by the plastic deformation.

It can be concluded that the variation of hardness around the joint depends on the ultrasonic energy, type of metals, and ultrasonic parameters. It may therefore be possible to use hardness measurements of the joint area in order to comment on the quality of the joint itself. In the current thesis, dissimilar materials will be used and therefore the joining process between these materials will also lead to collapse of the energy director. The existing literature, such as [30], and [78] describes this ED collapse as a heat affected zone (HAZ). Therefore, the ED collapse in the polymer side and hardness in the metal side will be examined. These examinations will give clear information about the effect of these features on the joint strength.

2.2.3 Dissimilar Materials

There are very few studies that use the ultrasonic joining technique to join dissimilar materials compared with polymer-polymer, and metal-metal joints. Furthermore, the studies that have been undertaken have only focused on a metal-fibre composite material joint.

The ultrasonic technique has been used to join dissimilar materials between metals and composites. One study reviewed using ultrasonic bonding between Al6061 and Polypropylene (PP) by Ramarathnam et al. [54]. These authors used amorphous Polypropylene (APP) as a tie layer between PP and Al6061 samples. This tie layer was joined with Al6061 surface by using hot pressing technique. Then, the ultrasonic bonding was employed to bond PP with the tie layer (APP) and therefore these authors used the ultrasonic process to join a polymer sample (PP) to a polymer layer (APP). Therefore, the ultrasonic technique was not used to directly bond polymer with metal. In addition, this previous study did not investigate any ultrasonic parameters.

Balle et al. [9] investigated the joining between aluminium alloy (AA2024) and CFRP (carbon fibre reinforced polymer). This investigation was applied using ultrasonic metal joining (USMW) meaning the vibration direction was parallel to the joining surface. The reason for using USMW was the polymer matrix of the CFRP, which plasticised and displaced out of the joining region by the transversal vibration, thus, contact between AA2024 and the fibres of the CFRP

was formed. Therefore, the load was transmitted directly from the metal into the fibres. Whereas, ultrasonic plastic joining (USPW) forms a joint between the polymer matrix and metal, thus the mechanical load cannot be transmitted directly from the metal into the fibre. Furthermore, the USPW method caused damage to the fibres because the direction of oscillation was perpendicular to the bonding surface, as shown in Figure 2.16.

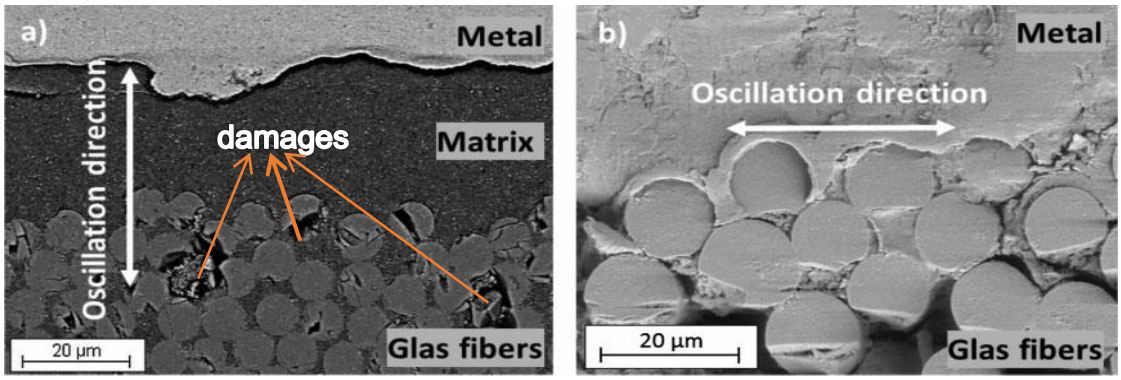

Figure 2.16 Bonding zone of an (a) ultrasonically metal bonded and (b) ultrasonically plastic bonded metal/GFRP joint [9].

These authors (Balle et al.) conducted further research to compare between AA5754 and AA1050 alloys when they were bonded ultrasonically with carbon fibre reinforced thermoplastic composite (CF-PA66) [79]. A statistical planning (central composite design) was adopted to evaluate the joining parameters. The results concluded that the tensile shear strength of the AA5754 – CF-PA66 joint (about 32.5 Mpa) was stronger than the AA1050 – CF-PA66 joint (about 24.2 Mpa). That happened because the mechanical properties differ between AA5754 and pure aluminium AA1050 and therefore the failure of AA1050-CF-PA66 took place at the base material of AA1050 with ultimate strain, 7%. In contrast, the failure of AA5754-CF-PA66 joints took place at the interface region with higher strain, 13%. Many small cracks were observed on the AA1050 surface when the vibration amplitude was higher than 34µm, due to high cyclic loading. While, the best joint strength of AA5754 was achieved at an amplitude of 40µm.

These authors (Balle et al.) show the importance of pre-treatment of the aluminium alloys when joining them with composite polymers due to the creation of a rough surface which allows effective interlocking from the melted

polymer. Although these are important findings, the investigations depend on the two joining parameters; oscillation amplitude and ultrasonic force. There are other factors that may significantly affect the joint strength, such as joining time, thickness of samples and using energy director, but these factors were missed. Therefore, these factors will be investigated in the current research.

Bolt [3] presented a discussion of surface fracture during the ultrasonic joining between aluminium and carbon fibre reinforced polyamide 6 (PA6). The author observed that different size pieces, referred to as patches, of PA6 stayed adhered on the pre-treated aluminium surface. In addition, less polymer could be found left on the aluminium surface and these residuals PA5 shown as white areas. Although the author presented the fractography of hybrid joints between aluminium and CF-PA6, the relationship between the size of the patches and the joint strength was not investigated. Therefore, the current study will investigate the relationship between existence and the size of patches and any correlation with joint strength.

It can be concluded that there is lots of useful literature regarding polymer-polymer joining, but that there is a lack of dissimilar material joining information, and that no existing studies combine investigations of all the relevant parameters at once.

2.3 Design of Experiments (DOE)

Design of Experiment is a mathematical technique for analysing any case that involves a response that changes as a function of one or more independent variables [80]. DOE was adopted to collect and analyse experimental data, and can be used in many branches of scientific study, especially in manufacturing, engineering, economics, biology and marketing [81]. The answer to particular questions about the behaviour of a system can be provided by DOE if it is used correctly by applying the optimum number of experimental runs (observations) [81]. Any process model has input variables, which may be called parameters, that determine how the process runs. There are also one or more outputs, which may be called the responses, generated by the process.

Therefore, determining the effects of inputs on the outputs is the purpose of an experiment.

2.3.1 Input Variables (Parameters)

The input variables are the values that change and provide an output. There are two main types of input variables in the DOE: quantitative and qualitative variables [81]. The former is any variable or data that can be measured or written down as numbers such as height, length or age. The latter cannot be measured, and includes, for example, colour and shape. In the current study, all input variables are quantitative, except for the energy director shape that is qualitative.

2.3.2 Interaction of Parameters

An interaction occurs when the response of one variable differs at different levels of another variable. Interactions can occur between two or more parameters, but higher-order interactions such as three-parameters or more are usually safely assumed to be insignificant [81]. For example, Figure 2.17 shows the two-way parameter interactions.

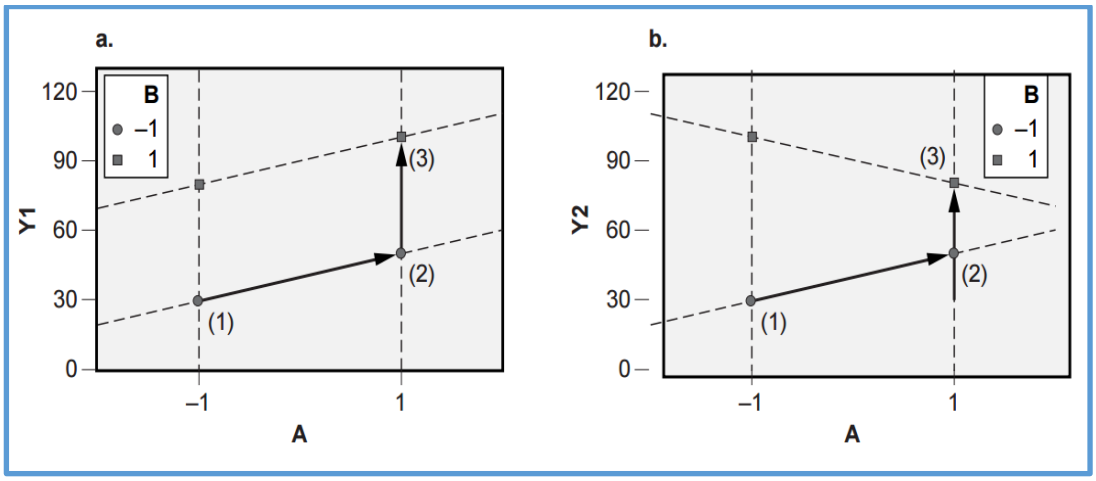

Figure 2.17 Two parameters without interaction (a), and with interaction (b) [16].

According to Figure 2.17a, the parameters (A and B) are not interacting because the line segment (between points 2 and 3) that connect two different levels of parameter (B) is substantially parallel. Thus, the levels of parameter (B) do not cause a change in how parameter (A) affects the output (the response); this implies the interaction between (A) and (B) is insignificant or there is no interaction. Conversely, Figure 2.17b shows that the connected line (between points 2 and 3) diverges, thus the chosen level of parameter (B)

determines how the response is affected by parameter (A), so there is an interaction (significant) between A and B. The interaction of parameters becomes practically significant when the lines (the relationship between input and output variables) meet at a point within, or close to the given range of levels [81].

The two-way interaction effects of bonding parameters on the LSS were deemed to be important for this research in order to establish whether effect of one bonding parameter may depend on the level of the other parameter.

2.3.3 Output variable (Response)

The output variable of an experiment should be quantitative in order to provide a clear indication of the effects. The response of this study is the lap shear strength (LSS) and it is a quantitative variable.

2.3.4 Choice of Design

There are many types of experimental designs and the most common DOE types are full factorial design (FFd), fractional factorial, the Taguchi approach and response surface methodology (RSM).

- **Full Factorial Design**

The full factorial design is applied when the experiment has two parameters or more and each parameter has several levels. The experiment will undertake all combinations of these levels across all parameters. Therefore, this type of DOE investigates the effects of all the main factors and their interactions on the response. In addition, FFd is well-known and easier, compared with other experimental designs such as RSM and the Taguchi approach. However, the FFd is not feasible for large numbers of factors and levels because it will produce a huge number of runs. The number of full factorial experiments is referred as (L^k), where L and K are number of levels and factors respectively, for example five factors at five levels (5^5) = 5*5*5*5*5=3125 runs. Thus, the main disadvantages of using full factorial design are that it can be expensive and time consuming. Hence, this design is mainly appropriate for applications that have a low number of factors and levels.

- **Fractional Factorial Design**

As the FFd may become very onerous when the number of parameters and their levels are increasing, the fractional factorial design is used to perform only a subset of the full factorial experiments. The number of fractional factorial experiments compared with the number of full factorial experiments can be one-half, or one-quarter, and so on. The fractional factorial design is based on -1 and +1 levels of each parameter of interest and presented as 2^{k-1}, 2^{k-2}, or 2^{k-3} for half, quarter, and eighth-fractional design [81]. Two-level fractional factorial design is used when only the response of the main parameters and low order interaction is required. Therefore, it is an economic design as it saves cost and time compared with the FFd. However, one of the big disadvantages of fractional design is the ability to miss important interactions. Figure 2.18 shows the comparison between full factorial and fractional factorial designs.

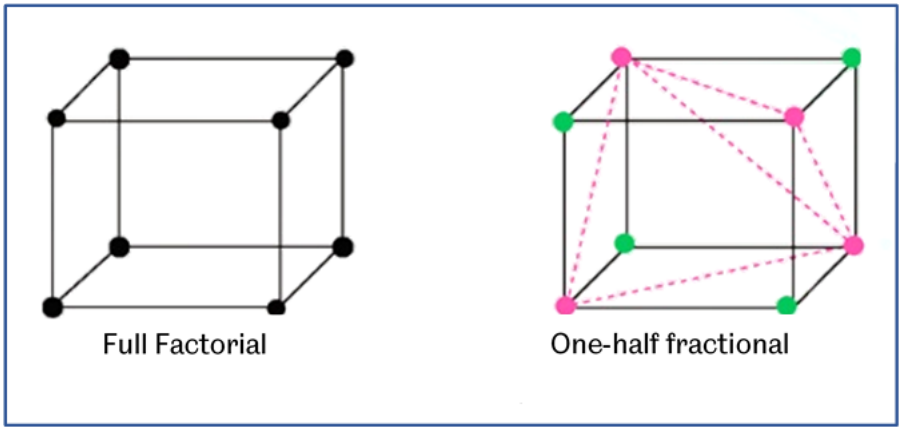

Figure 2.18 comparison between full factorial and fractional factorial designs [82].

There are other types of fractional factorial design that use more than 2 levels at each factor such as Taguchi design.

- **Taguchi Approach**

The Taguchi approach is an experimental design that uses a few numbers of experimental runs and has used fractional factorials for orthogonal array design to estimate the mean values of the response. These orthogonal arrays provide a set of balanced experiments and meaning each level of parameter

has the same number of samples. This method can use two, three or mixed levels of parameters. The optimum values of the parameters' levels are found by calculating the signal to noise ratio (the larger the better) type as shown in Equation (2.11). This ratio measures the deviation of the output value from the target value [83].

$$\frac{S}{N} = -10 \log \left(\frac{1}{n}\sum\left(\frac{1}{y^2}\right)\right) \quad (2.11)$$

Where "n" and "y" are the number of replications and the observation respectively. Despite the fact that the Taguchi method is a powerful design of DOE, the main disadvantage of using it is that the parameter interactions cannot be identified because it does not test the combinations of input parameters [84]. In addition, it provides only the optimum value of the response at any levels provided by the experimenter. Therefore, using this approach should be avoided when the relations between all the parameters are being tested.

- **Response Surface Methodology**

Response surface methodology (RSM) is a collection of statistical and mathematical methods to build an experimental model. The block design of RSM is a combination of two-level factorial design and points at the centre of provided levels. The objective of using the RSM is to optimise the output variable (response) that is affected by many input variables (parameters) (up to 10 input variables) [85]. In addition, the smoothing functions of RSM can reduce the associated numerical noise, thereby improving the convergence of the optimisation process [86]. Furthermore, it can identify the optimum value of parameter's levels at any point within the provided range of the levels. It can also efficiently with the effect of parameter interaction on the response and it is considered a suitable method when the response expected is a curve [85].

For instance, in the case of a plant's growth (Y), the plant growth is affected by any combination of the sunshine (x_1) and amount of water (x_2). Thus, both

parameters x_1 and x_2 can vary continuously and the response (y) is a function of parameters x_1 and x_2, as expressed in Equation (2.12).

$$Y = f(x_1, x_2) + e \quad (2.12)$$

Where "e" represents the error or noise on the response and it is a statistical error. RSM is an important technique to develop, improve, and optimise the response variable when the input variables are a continuous range of values [85]. Although RSM observes the parameter interaction, this property should be applied with caution in some applications, such as chemical applications because in some cases the interactions become unusable. The comparison between these designs can be tabulated, as shown in Table 2.2.

Table 2.2 Comparison between Experimental designs.

	Full Factorial	Fractional Factorial	Taguchi Approach	Response Surface Methodology
How it works	Employing all combinations of all levels across all parameters. The number of experiments is (L^k), where L and K are the number of levels and parameters respectively.	Performing only a subset of the full factorial design based on 2 levels.	Using fractional factorial for orthogonal array design. The orthogonal array provides a set of balanced experiments (i.e. each level has the same number of samples.	The block design of it depends on using two levels factorial design and points at the centre of provided levels.
Advantages	Investigating the effects of all main parameters and their interactions.	It is an economic design as it saves the cost and time.	Selecting the optimum values of levels by calculating the signal to noise ratio. Saving time and cost by using fewer number of runs	Estimating the optimum values of levels in any point between the provided levels. Saving time and cost by using fewer number of runs. Observing the main parameters

				and their interactions.
Limitations	It is expensive and time consuming because it produces huge numbers of experimental runs	Indicating interactions among some parameters but not all. Adopting only two levels per factor.	Cannot identify the parameter interaction. Providing only the optimum value at any levels provided by experimenter.	Although RSM evaluates the interactions of parameters, some applications, such as chemical are unusable.

From this section, the response surface methodology was selected for the current work because this design is used to optimise the variables and investigate the main parameters and their interactions. In addition, it used fewer experimental runs compared to the classical method, such as factorial designs. The response surface methodology has many types of designs and depends on a polynomial model to explain the relationship between the input variables (parameters) and out variable (the joint strength). Selection of a suitable model and design are illustrated in the next section (Section 2.3.5).

2.3.5 Choice of Model

The word model indicates the mathematical description of the response behaviour as a function of the input parameters [81]. Generally, there is a relationship between the data, the selection model, and the error (residuals), expressed as follows:

$$\text{Data} \longrightarrow \text{Model + Error (Residuals)}$$

The error statement or the residual is reported as a standard deviation. Generally, the model used to describe the response surface is the polynomial model and it is a sufficient approximation for the unknown relationship between the response and parameter [85]. There are two important polynomial models commonly used in RSM, first order model and second order model as shown in Equations (2.13), and (2.14) respectively [87].

$$y = \beta_o + \sum_{i=1}^{k} \beta_i x_i + e \tag{2.13}$$

$$y = \beta_o + \sum_{i=1}^{k} \beta_i x_i + \sum \sum_{i<j}^{k} \beta_{ij} x_i x_j + \sum_{i=1}^{k} \beta_{ii} x_i^2 + e \tag{2.14}$$

Where, y represents the response (the output variable), while β_*, β_{**} are regression coefficients and x_* represents the input parameters where the * is used to indicate the ordinal numbers from i or j to k. The purpose of selecting a model is:

1. Finding the relationship between the output variable (y) and the parameters (x_1, x_2, ..., x_k) to predict the values of response for the given setting of the parameters.
2. Determining the optimum settings of parameters (x_1, x_2, ..., x_k) that result in the maximum or minimum response over the region where the optimal response occurs.

The difference between using either the first order or second order model depends on the position of the required response. This means the first order model becomes appropriate if the approximation of true response is over a small region that has a little curvature or a flat surface, such as the small region around point *A* in Figure 2.19(b). Often, the curvature in the true response is very strong and thus the first order equation is not enough as an approximation to the true response [88]. Thus, the second order model is likely to be required in these positions, as shown at point B in Figure 2.19(b).

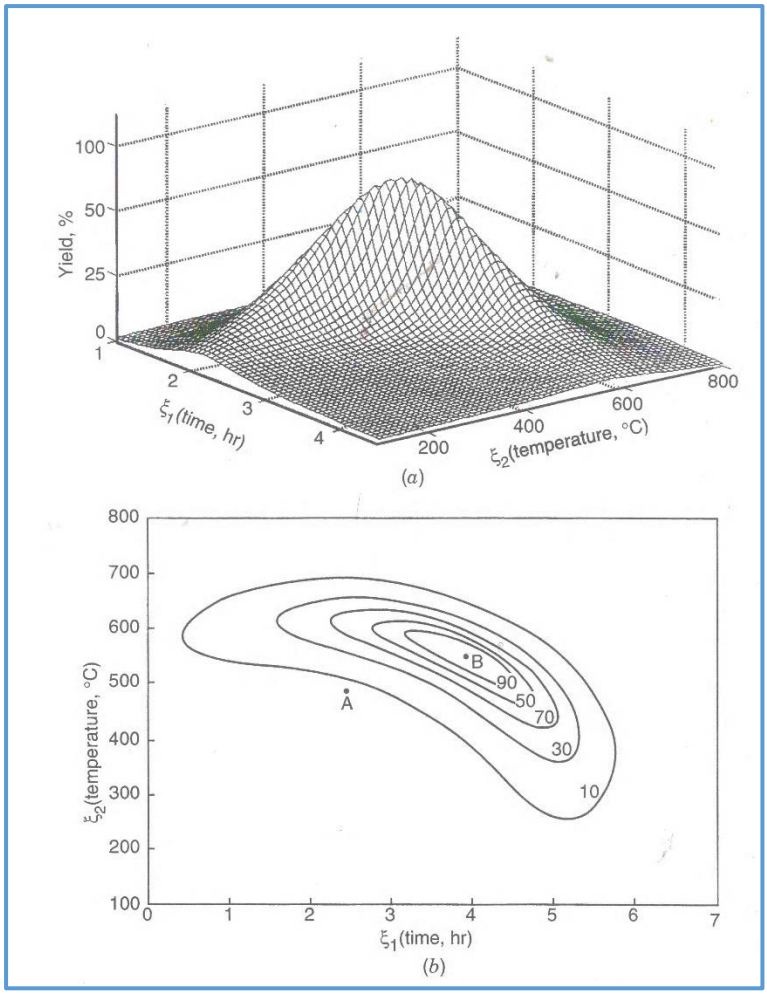

Figure 2.19(a) Response surface of yield of chemical process and process parameter; time and temperature, (b) A counter plot of the theoretical response surface [88].

As expressed in Equation (2.14), the second order model involves all the terms of the first order model, all quadratic terms, and all two-way interaction terms. Since the second order model, also called the quadratic model, includes a variety of functional terms, it is considered a flexible model and a good estimation of the true response surface. For example, Figure 2.20 shows the importance of using the second order model fit compared with the first order model or a linear fit. The second order model fit passes exactly through the means of response at each level of x_1.

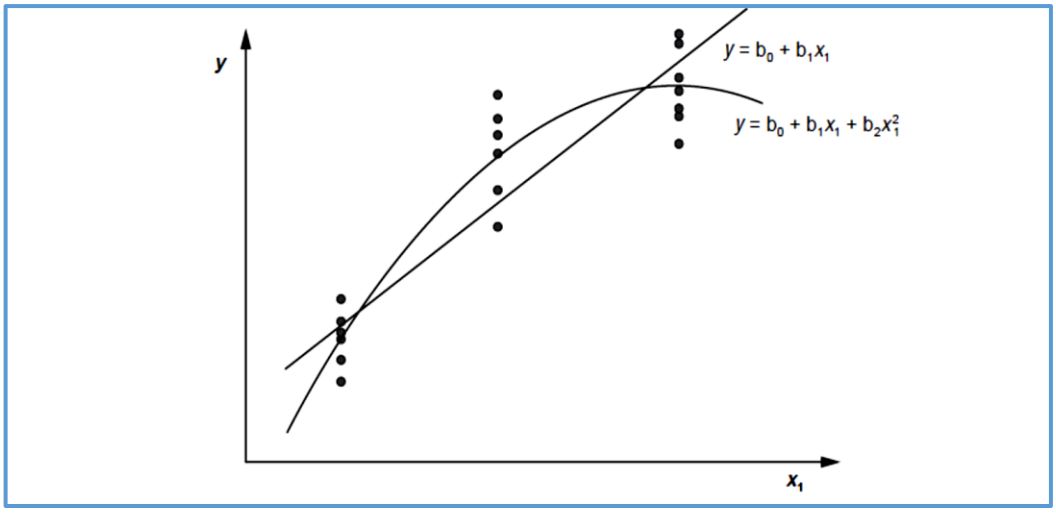

Figure 2.20 Linear and quadratic models [81].

In this study, and based on this section, the quadratic model (second order model) was adopted to indicate the accurate and reliable values about the maximum or optimum values of bonding parameters.

There are two most popular families of designs for fitting a second order model: Central Composite Design (CCD) and Box-Behnken Design (BBD), as shown in Figure 2.21. The block represents the relationship between the input variables (parameters) and output variable (the response). The length of block depends on the values of parameter levels.

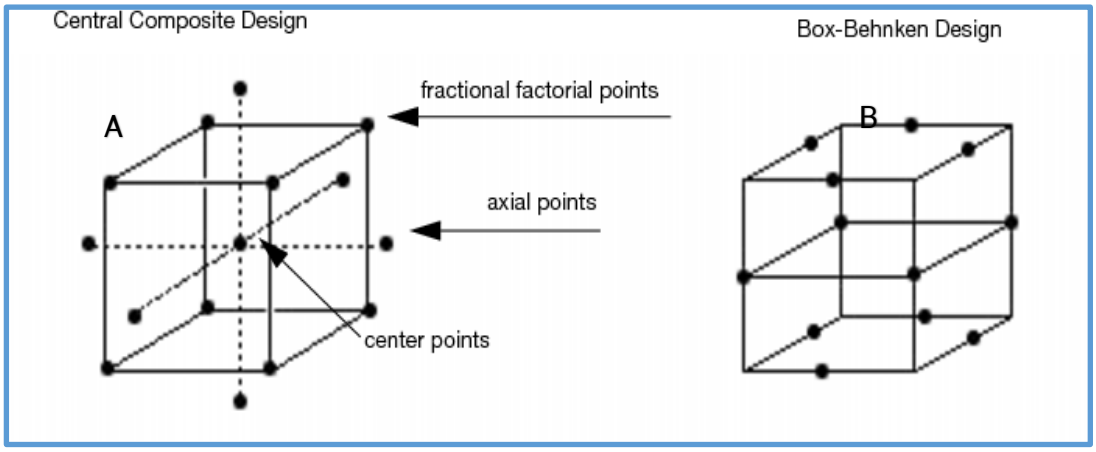

Figure 2.21 Central Composite Design and Box-Behnken Design.

Both CCD and BBD are much more useful in studying the quadratic model (second order model) and 2-way interactions between the parameters. The differences between the CCD and BBD are tabulated in Table 2.3.

Table 2.3 Comparison between CCD and BBD.

Central Composite Design (CCD)	Box-Behnken Design (BBD)
The total number of design points is [81]: $N = 2^k + 2k + C_o$ Where, N is the total number of points 2^k is two-level factorial design (K is the number of parameters) 2k is star points or called axial points C_o is the centre point	The total number of design points is [81]: $N = 2k(K-1) + C_o$ N is the total number of points K is the number of parameters C_o is the centre point
It includes star points.	It does not include star points.
The number of centre points is greater than in BBD.	The number of centre points is less than in CCD.
It includes corner points.	It does not include corner points.
The total number of points (experimental runs) is slightly more than in BBD.	The total number of points (experimental runs) is slightly less than in CCD.
For example, 4 factors, 3 levels for each factor $N = 2^4 + 2(4) + 7$ N = 31 runs (points) C_o is 7 when the number of factors is 4 [81]	For example, 4 factors, 3 levels for each factor $N = 2(4)(4-1) + 3$ N = 27 runs (points) C_o is 3 when the number of factors is 4 [81]
CCD cube is shown in Figure 2.21(a).	BBD cube is shown in Figure 2.21(b).

In the experimental design, the purpose of the centre point replications is to provide a measure of stability to the process, and give information about the curvature of the system [81], and [86]. The axial points generate the quadratic terms, thus giving the ability of curvature description [86]. BBD does not contain star points and corner points; thus, it does not involve combinations

made from the highest or lowest levels of parameters at the same time. Therefore, BBD is a useful design to avoid tests that perform under extreme conditions, for which unsatisfactory results might occur such as electro-analytical test, and chemical reactions [89]. Conversely, this cannot be indicated for other situations or applications that need to know the responses at extreme conditions. Therefore, CCD shows a better prediction of response and an efficient estimation compared with BBD in a comparative study [90].

Based on Section 2.3.5, this research has adopted the central composite design (CCD) to create a statistical model to collect the data. Although the number of experimental runs in CCD is slightly more than in BBD (as illustrated in Table 2.3), CCD is advantageous in fitting the second order model in this study. Based on the CCD description, the number of levels for all parameters should be an odd number and equal for all used parameters.

2.4 Description of Statistical Analysis

The results of an experimental design can be analysed to deduce meaningful information and achieve the following goals:

- To establish the best conditions in the process.
- To estimate the contribution and significance of individual parameters and their interactions.
- To estimate the response under the best conditions.
- To estimate the fit theoretical model to the response.

The purpose of using statistical analysis is to describe and interpret the response data. In addition, a suitable statistical analysis is important to determine the effect of bond parameters on the joint strength, and the bond parameters that have more effect. This type of analysis is specific for the data collected by using a response surface experimental design.

To achieve the goals and objectives of the statistical analysis, the following steps should be undertaken:

1- Identifying the important parameters depending on the results of the analysis of variance (ANOVA) of response surface design.

2- Examining the statistical results and plots such as the fitted model plot, interaction plots, and ANOVA statistics (R-square, adjusted R-square, standard error) to find out whether the model fit is acceptable or satisfactory.
3- Exploring the effect of changing the parameter levels on the response results by using the contour plots of the response surface.
4- Determining the optimal parameter settings.

There are statistical terms and tests that were used throughout this analysis, which require the following explanation:

2.4.1 The Residual Plots

In the current analysis, the residual plots investigated the goodness of fit in ANOVA. The residual is the difference between the observed value of the response (the output variable) and the predicted value [81]. Minitab 17 provides the residual plots for the lap shear strength results. The importance of using these plots is to investigate the normality and equality of variance of the data as assumptions to use in the statistical analysis. The normality assumptions mean the residuals have a normal distribution. This data checking should be tested before using ANOVA to confirm the reliability of data to use statistical tests such as ANOVA and regression because these tests depend on the residuals during the analysis. Figure 2.22 shows an example of non-normal distribution [91].

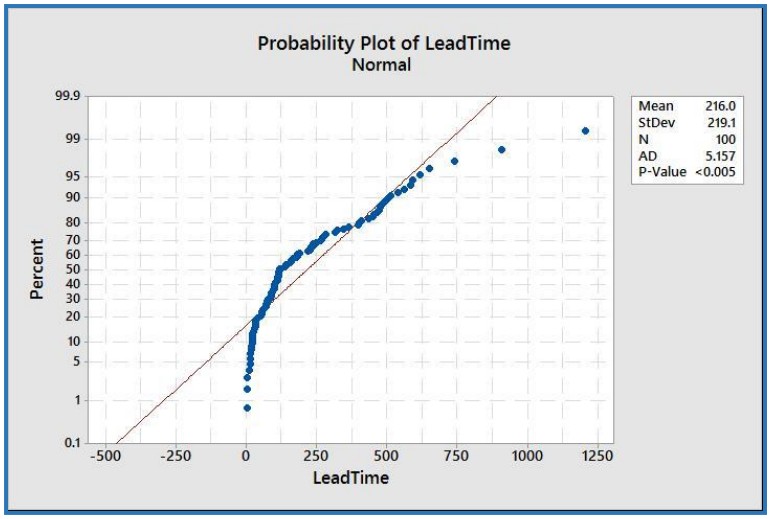

Figure 2.22 Non-Normal distribution plot of residuals [91].

To recognise the normal and non-normal distribution, the normal residuals plot should approximately follow a straight line and not skew around the fit line. Figure 2.23 represents the normality plot. Therefore, the statistical tests, such as ANOVA and regression can be used after the normality.

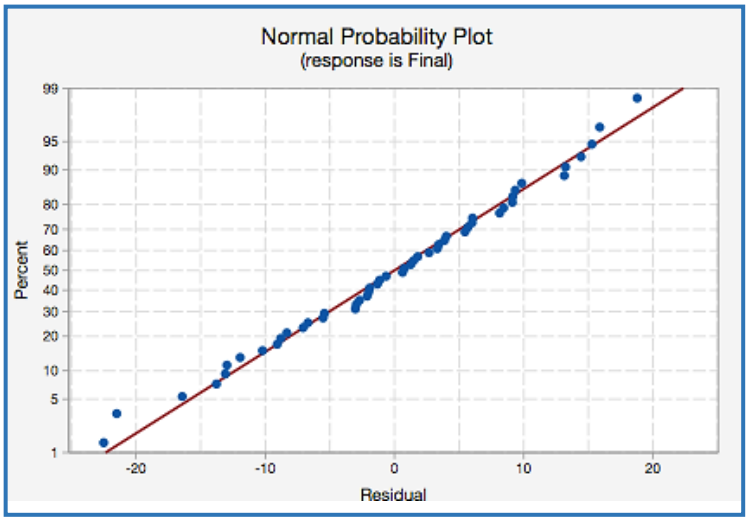

Figure 2.23 Normality plot of residuals [92].

If the data observed is a non-normal distribution, there are many options to transfer the data to meet the normality condition, which are called data transformations.

2.4.1.1 Data Transformation

The data transformation is a mathematical application used to modify all points in the data set. Thus, each point (x_i) in the data will be replaced with the transformed value $y_i = f(x_i)$, where f is a function.

Generally, the data transformation is applied to make the data more closely meet the assumptions of the statistical tests. Using statistical tests, such as ANOVA or regression with non-normal distribution of the residuals, may give a misleading impression about the results [93].

Examples of data transformation options are square root transformation, logarithm transformation and Box-Cox transformation [81].

Sometimes, the non-normality of residuals happens for reasons such as extreme values that means extreme deviation from the fit values, missing data

values, or data entry error [81]. In other words, the normality is a means to an end; it is not the goal itself.

2.4.2 Analysis of Variance (ANOVA)

Analysis of variance (ANOVA) is a statistical method used to interpret and explain the experimental results. In addition, the ANOVA technique is applied to find out the impact that independent factors have on the dependent factor in a regression analysis [94].

In the present research, ANOVA was used to determine the significance and influence of bonding parameters on the lap shear joint strength results. In an effort to understand the ANOVA table for current analysis, Figure 2.24 represents an example of an ANOVA table [95].

Analysis of Variance

Source	DF	Adj SS	Adj MS	F-Value	P-Value
Gender	1	29.40	29.40	1.63	0.207
Educational Level	2	5328.10	2664.05	147.52	0.000
Gender*Educational Level	2	167.70	83.85	4.64	0.014
Error	54	975.20	18.06		
Total	59	6500.40			

Figure 2.24 ANOVA table example [95].

The ANOVA table has terms that are shown as column headings in the table (six columns), and these columns are now explained:

2.4.2.1 The Source (1st column)

This column represents the main parameters (independent variables) and the interactions that have effects on the response (dependent variable). According to the example in Figure 2.24, the source column includes a linear mean effect of parameters (gender and educational level) because each of these parameters is expected to have an effect on the results. The interaction between the parameters has an effect on the response if present. The presence of the main parameters' interaction effects (gender*educational level) means the effects of the main parameters on the response are not independent.

2.4.2.2 Degree of Freedom (DF) (2nd column)

The statistical term degree of freedom is the number of values that are free to vary in the final statistical calculation. Thus, the degree of freedom 'DF' can be calculated by deducting the number of parameter levels from one, i.e. DF = n – 1, n is the number of parameter levels. For the parameters' interaction, the degree of freedom is counted by multiplying the degree of freedom of individual parameters.

2.4.2.3 Adjusted Sum of Squares (Adj SS) (3rd column)

In the analysis of variance of response surface design, the adjusted sum of squares (Adj SS) is adopted. The sum of squares is a measure of deviation or variation from the mean. In other words, the sum of squares can be computed as a summation of the squares of the differences from the mean. The total sum of squares (TSS) in the data set can be calculated from the treatment sum of squares (SS_T), and the sum of squares randomness or error (SS_E) [81], as shown in Equation (2.15).

$$TSS = SS_T + SS_E \tag{2.15}$$

The sum of squares is important in the analysis of variance because it helps to determine the dispersion of data points. The sum of squared error (SS_E), also called the residual sum of squares, is the sum of squares of residuals and implies that the SS_E measures the discrepancy between the output data and an estimation model (fitted line). In other words, when the SS_E becomes small, the data have a tight fit to the model. The SS_E formula is:

$$SS_E = \sum_{i=1}^{n}(X_i - \bar{X}_i)^2 \tag{2.16}$$

Where (n) is the number of observations and X_i and $\bar{X}_i$ are the value of the ith observation and the mean of all observations respectively. The treatment sum of squares (SS_T) is the differences between the fitted line and the grand mean, as shown in Equation (2.17).

$$SS_T = \sum_{i=1}^{n}(\bar{X}_i - \hat{X})^2 \tag{2.17}$$

The symbol $\hat{X}$ represents the mean of all observations mean (grand mean). For example, there are three groups and each group has three numbers, as shown in Table 2.4. All sums of squares are calculated to understand it.

Table 2.4 Example to understand sums of squares.

Group One (G1)	Group Two (G2)	Group Three (G3)
3	5	5
2	3	6
1	4	7

$\bar{X}$ of group one = (3+2+1)/3 = **2** , $\bar{X}$ of G2 = **4** and $\bar{X}$ of G3 = **6**.

$SS_E = \underline{(3-\mathbf{2})^2+ (2-\mathbf{2})^2+ (1-\mathbf{2})^2} + \underline{(5-\mathbf{4})^2+ (3-\mathbf{4})^2+ (4-\mathbf{4})^2} + \underline{(5-\mathbf{6})^2+ (6-\mathbf{6})^2+ (7-\mathbf{6})^2}$

$SS_E = 6$

According to Equation (2.17), the SS_T equal:

$\hat{X}$ = (2+4+6)/3 = **4** (this is the mean of the observation mean or the grand mean).

$SS_T = \underline{(2-\mathbf{4})^2+ (2-\mathbf{4})^2+ (2-\mathbf{4})^2}+ \underline{(4-\mathbf{4})^2+ (4-\mathbf{4})^2+ (4-\mathbf{4})^2}+ \underline{(6-\mathbf{4})^2+ (6-\mathbf{4})^2+ (6-\mathbf{4})^2}$

$SS_T = 24$

TSS = 6 +24 = 30 (the total sum of squares of data).

Adjusted sum of squares (Adj SS) is the variance of the sum of squares between the full model and the model obtained when omitting the variable. It does not depend on the parameter order that is entered into the model. For instance, the Adj SS of group one (G1) in Table 2.4 equals:

Adj SS (G1) = SS (G1, G2 and G3) – SS (G2 and G3) or

Adj SS (G1) = SS (G2 and G3) - SS (G1, G2 and G3)

The Adj SS is used to calculate the percentage contribution of parameters that affect the response, and it is equal the division of Adj SS of parameter on the total Adj SS [96]. Furthermore, the Adj SS is used to measure F-value for a parameter and this value is very important in selecting the significance of parameters. This is explained in detail in Section 2.4.2.6.

2.4.2.4 Adjusted Mean Squares (Adj MS) (4th column)

Adjusted mean squares represent the variation of a parameter or the model. The Adj MS of a parameter can be calculated by dividing the adjusted sum of squares for this parameter by the degree of freedom of the parameter. In the analysis of variance, the Adj MS is essential to calculate both the F-value and adjusted R-square statics of parameters.

2.4.2.5 F-value (5th column)

F-value is a statistical test used to find out how close the parameter is with the data set. In the analysis of variance table, the F-value appears for each parameter and its interactions. It can be calculated by using Equation (2.18)[80]:

$$F - value = \frac{Adj\ SS/_{DF}}{Adj\ SS_{error}/_{DF_{error}}} \quad (2.18)$$

Thus, each parameter, or the parameter interactions, has its F critical value and these F-values have (x, y) degree of freedom (DF), i.e. x represents numerator DF (degree of freedom of the factor or the interaction), while y represents the denominator DF (error degree of freedom). The selection of F critical value depends on the standard statistical tables of F distribution where the F critical value is taken from the corresponding values of x and y on the standard statistical table. In addition, statistical software such as Minitab can select the critical value of F by inserting x and y values.

For example, the gender (factor) in Figure 2.24 has 1 degree of freedom and this is x. While the degree of freedom of error is 54 and this represents y. The F critical value using Minitab Software is 4.02, as shown in Figure 2.25.

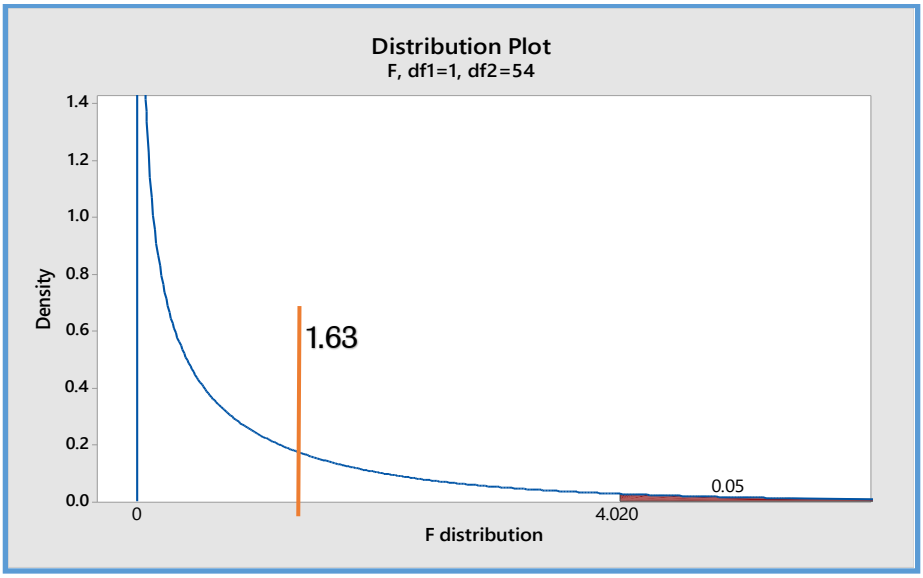

Figure 2.25 Distribution plot of F (1, 54).

F- value of gender based on Figure 2.24 is 1.63, thus it is smaller than 4.02. Therefore, the gender is an insignificant factor because it does not fall in the shaded region (the significance level of the test α = 0.05, further details in this in the next section). The high value of F-value (F-value > F critical value), for the parameters or the interactions, indicates a significant effect [81].

2.4.2.6 P-value (6th column)

The last column in the ANOVA table is a P-value and it indicates whether the results are statistically significant. In addition, it can be defined as the probability of obtaining a result equal to or "more extreme" than what was actually observed [80]. Therefore, it provides a clear and concise summary of the significance of the experimental results. The range of P-value is from 0 to 1 and it is compared directly to the significance level. The confidence level, also called the significance level, in good scientific practice, is often set to 0.05 (5%), and it means the results have a 95% level of confidence [80], and [81]. Thus, the parameter or its interaction is a significant factor when the P-value is less than the confidence level (0.05). For example, Gender (factor) from Figure 2.24 and Figure 2.25 is an insignificant parameter because its P-value (0.207) is bigger than 0.05.

2.4.2.7 R-squared, Adjusted R-squared and Predicted R-squared tests

In statistical analysis, there are other tests needed to explain and understand the results, such as R-squared and adjusted R-squared. These tests are necessary when the model fits the data and thus the goodness of the fit is required [81] .

R-squared, also known as the coefficient of determination, is a number between 0 and 100% that indicates the goodness of the data fit in the model. In other words, the R-squared test measures how much the data deviates from the fitted line. Thus, the model fit of the data becomes better when the R-squared is high. The term 'data' represents the lap shear strength in the current research.

The adjusted R-squared, also known as the adjusted correlation coefficient or adjusted coefficient of determination, is also an indicator of the data fitting. When the model has many independent variables and the interaction term is possible, the measure of data goodness by R-squared only is unfair because of the model complexity. The R-squared value will be increased when more terms are carried in the complex model. Therefore, adjusted R-squared is used with R-squared when evaluating a complex model and is always less than R-squared.

Predicated R-squared refers to acceptance of a fit model that predicts responses for new observations. It can be calculated by systematically removing each experimental run (observation) from the data and estimating the fit model, then finding out how well the model predicts the removed run (observation).

2.4.2.8 The Standard Deviation

The standard deviation (S) provides a measure of the goodness of the fit and is calculated in the units of the response. It can be calculated from Equation (2.19) [81].

$$S = \sqrt{\frac{1}{N}\sum_{=1}^{N}(x_i - \mu)^2} \qquad (2.19)$$

Where, N represents the total number of observations (runs), x_i represents sample data, and μ is the mean of all observations. The standard error represents the average distance from which the observed values fall from the fitted line. Thus, it is better if the standard error has a small value because that means the observations are closer to the fitted line.

2.5 Summary

The literature has provided several key points to take forward in the current investigation into joining of a metal to a polymer using the ultrasonic technique. In the existing literature, the majority of research was conducted into metal-metal or polymer–polymer joints, and there have been very limited attempts with metal–thermoplastic composites using ultrasonic joining. It can therefore be concluded that this investigation into metal-polymer bonding will provide a novel contribution.

A polymer can be bonded when it starts to flow during the ultrasonic process. The polymer flows when it reaches its glass transition temperature (if amorphous), or melting temperature (if semi-crystalline). The viscosity of polymers dropped at high temperatures and therefore the melted polymer can be forced out of the bonding zone. The choice of polymer is therefore important when joining with a metal ultrasonically, as the level of bonding will depend on the ability of the polymer to flow across the surface of the metal whilst not being forced away from the joint area.

Amorphous polymers can be joined together more effectively and efficiently than semi-crystalline polymers using the ultrasonic technique as their molecular chains can be more easily broken.

The energy director is the best technique to concentrate and focus the ultrasonic energy on a specific area, to improve strength and to reduce joining time. The literature does not provide a solid consensus regarding ED size and shape, and this will therefore be investigated in this thesis.

The type of joining (near- or far-field) can have an influence on the joining process, but it has been established that near-field is suitable for both semi-crystalline and amorphous.

Roughness of the metal surface will be important in order to provide a larger surface area through filling these cavities.

Design of experiments have been adopted in the literature to investigate the relationships between the joint strength and the parameters. The current research uses the design of experiments to analyse the influence of parameters and their interactions statistically and evaluating the optimum values of parameters leading to the strongest joint. A central composite design was adopted as the experimental design after making comparison with other types of designs such as full factorial, Taguchi approach, and Box-Behnken design.

Chapter 3 ULTRASONIC JOINING PARAMETERS

The relationship between an ultrasonic joining process and its parameters are complex and difficult to control, because the strength and quality of the joints can be affected by changing any of the parameters.

The joining parameters can be divided into two groups. The first group is called machine or process parameters such as joining time (vibration time), vibration amplitude, joining force, and holding time, whereas the second group can be called materials' parameters such as the type of material, joint design, sample thickness, and pretreatment of samples.

3.1 Introduction

So far in the existing literature, the metals have rarely been joined with polymers using the ultrasonic technique. It has been bonded with metals and few studies showed the possibility to join them with fibre reinforced composites, whilst polymers have been bonded only with polymers ultrasonically.

The mechanism of joining polymers and metals depends on melting polymers and allowing them to flow inside pores of metallic substrate. Therefore, the approach of finding key variables of joining metals with polymers using the ultrasonic method depends on reviewing the variables that have an effect on polymers reaching the melting state. Moreover, this chapter reviews the ultrasonic variables of metals that contribute to generating the necessary heat into the interface for melting the energy director of a polymer. In addition, the relationship between ultrasonic variables and joint strength is described in this chapter.

Logically, the range of levels of ultrasonic variables of polymers are less than the variables of metals due to the significant differences of the mechanical and thermal properties between them. There is no information in the existing literature or in the standard about the range of levels for joining metals and

polymers ultrasonically, therefore, it is not logical to use the ultrasonic variables of polymer-polymer or metal-metal joints that are shown in the existing literature directly to join polymer-metal. Hence, this chapter looks at the variables during similar joining ultrasonically (polymer or metals) to identify the initial range of variables (minimum and maximum) that have the possibility to achieve the necessary heat at the interface without damaging the samples, as shown in Figure 3.1. This figure is example to select the ultrasonic time for polymer-metal joining from combining between ultrasonic time for ABS polymer [30], HDPE polymer [39], or PP [48] and Al alloys [97], or [98]. This initial range of parameters is used in the pre-investigation tests to identify the suitable range of levels for joining metals and polymers (Chapter 4). Additionally, the chapter investigates the effects of theses variables on the joint strength.

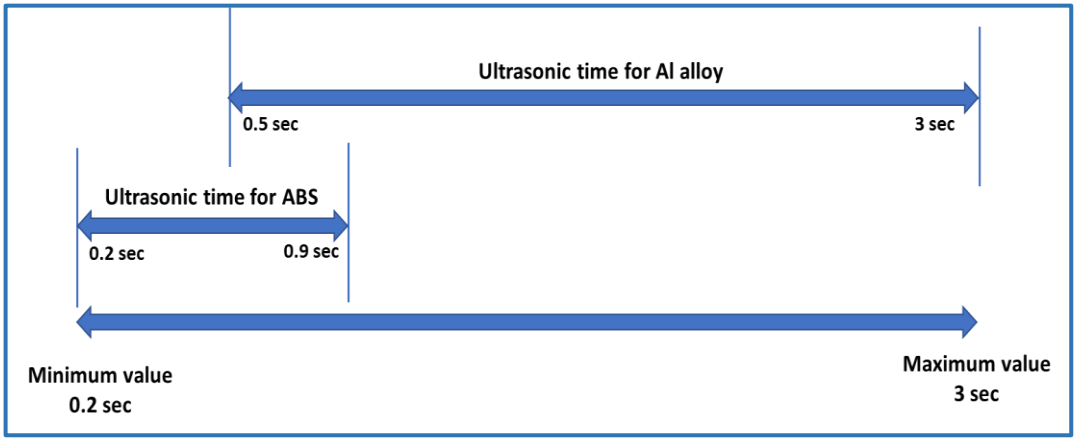

Figure 3.1 Selection of the initial range of parameters' levels. For example, this figure is to select the ultrasonic time for polymer-metal joining from combining between ultrasonic time for ABS polymer [30], HDPE polymer [39], or PP [48] and Al alloys [97], or [98].

3.2 Machine Parameters

3.2.1 Vibration Frequency

The frequency that is used in the ultrasonic process is produced by the ultrasonic generator. Tsujino et al. [99] investigated the joining characteristics and temperature rises of thermoplastics polymers (propylene PP, and Polymethyl methacrylate PMMA) over different frequency ranges (27, 40, 67, 94, 150, and 180 KHz). This study observed that the joint strength was higher at the high frequency (from 67 to 180 KHz) than the lower frequencies (27 and

40 kHz) due to increasing the vibration velocity and thereby increasing the temperature and joint strength/joint area. Additionally, the results showed that the temperature at the interface (joining area) was the highest compared with the upper and lower surfaces of the lap joint because the intermolecular friction was as great as possible at the interface and therefore the temperature rises. Meanwhile, the temperature at the upper sample was higher than the lower sample and it appeared that the vibrations are reflected and lost at the interface. One of the applications of using a higher range of ultrasonic frequencies is micro polymer parts joining. The ultrasonic seam joining of the three dimensions of micro polymer parts was investigated by Michaeli et al. [25], as shown in Figure 3.2. The specimens bonded in this study, were made from Polycarbonate (PC) and were bonded using a modified ultrasound device at 40KHz. The study showed that the use of high amplitudes (28 µm) can produce too high and an inhomogeneous input energy, which leads to an irregular plasticising of the joint region and decomposes the polymer. The best results were achieved when the amplitude was decreased to 16.5 µm. Hence, the microparts can be bonded ultrasonically at the extreme frequency (40KHz) when low amplitude is used.

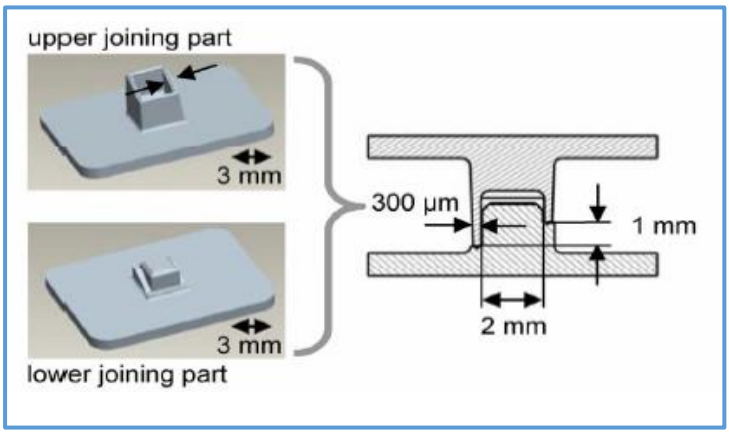

Figure 3.2 Three dimensions of joining polycarbonate parts at 40KHz[25].

The available ultrasonic generator in the current thesis has certain restrictions and produces frequency 20KHz, but that the frequency 20KHz has been used previously and shown to be a good compromise. This value of frequency is not coincidental but it is considered the best compromise in the

size and cost of equipment beside the performance, as explained by Shoh [100].

Therefore, this value of frequency (20KHz) is commonly used during the ultrasonic technique either for joining polymers or metals in the literature [30], [15] and [13].

3.2.2 Effects of Bonding Time

The period when the ultrasonic vibration is applied is called the joining time. The duration of joining is one of the most significant factors that impacts on the joint strength.

- **Metal - Metal**

The relationship between the joining time and the shearing force of the joint between titanium alloy (Ti6Al4V) and aluminium alloy (A6061) was investigated by Zhu et al. [75], as shown in Figure 3.3. In this work, there were some regions from which atomic bonds disappeared due to the short joining time. Thus, increasing the joining time caused an increase in the joint strength to produce the maximum joint strength at 170 ms. However, the joining strength decreased when the joining time was increased for too long because fatigue cracks appeared on the surface and internally. The reason for this reduction was the expansion of plastic zone due to the friction between surfaces at the interface that led to weakening the cross section and cracks appearing, thereby reducing the joint strength.

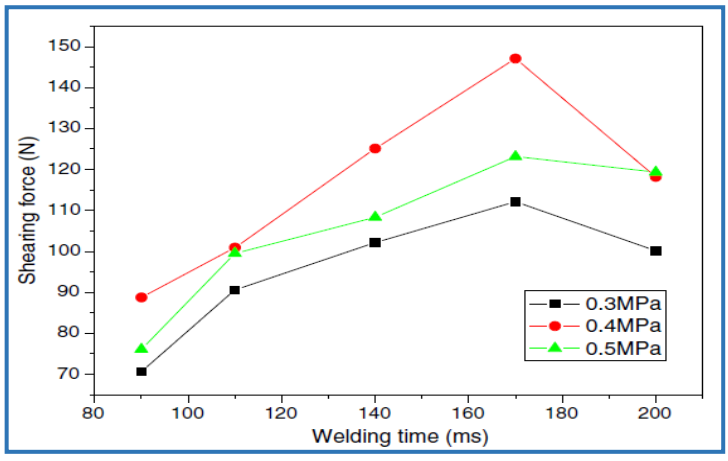

Figure 3.3 Relationship between joining time and shearing force of joints between AA6061 and Ti6Al4V under 20KHz frequency, and different joining pressure (0.3, 0.4 and 0.5MPa) [75].

The importance of joining time on the joint strength between mild steel (SS400) and aluminium alloy (A5052) was also observed by Watanabe et al. [97]. As shown in Figure 3.4, the tensile load increased around 300% when the joining time was increased from 0.5 to 2.5 sec; after that the tensile load was decreased. The reason for this tendency is an intermetallic compound of Fe_2Al_5 that was formed at the joining interface during a hyperthermal temperature. This relationship between joining time and tensile load took place under a constant clamping force. This investigation by Watanabe missed the effects of vibration amplitude and sample thickness on the joint quality which may have a significant effect on the findings.

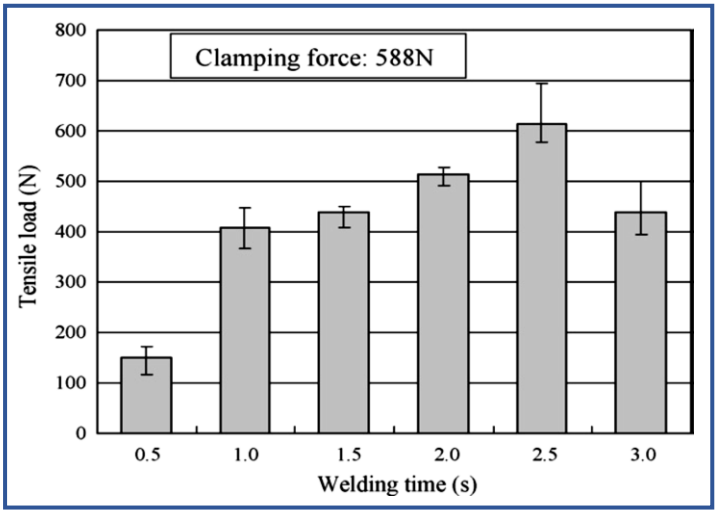

Figure 3.4 Relationship between joining time and tensile load of A5052-SS400 joints at 15KHz frequency, 53μm vibration amplitude, and 588N clamping force [97].

Additionally, the possibility of obtaining higher joint strength, through moderate increase of joining time when joining Al-Al, was achieved by Elangovan et al. [101] where the joint strength increased about 66% to reach 2.26MPa when the joining time increased from 2 to 3 sec. Elangovan et al. [94] determined that the increase of joining time from 2 to 2.25 sec led to increasing the strength of a Cu-Cu joint by about 51% to reach 1.6MPa. The reasons for this increase was the expansion of area for rubbing action at the interface which increases the joint strength and achieves a better bond. Elangovan only investigated three main parameters: joining time, joining force and vibration amplitude, but the effects of these parameters' interactions were not investigated. The parameter interaction may change the effect of one

parameter on the output (the joint strength) by changing another parameter. Therefore, it is necessary to study the parameters' interactions on the joint strength in the current thesis.

- **Polymer - Polymer**

Raza [30] found a linear relationship between the lap joint strength and the join time for thermoplastic polymer (polypropylene) joints. The joint strength increased around 133% when the join time was increased from 0.8 to 1.4 sec. The increase of joining time was shown to increase the cycle of vibrations on the samples and thus a large amount of energy director melted when the ultrasonic energy dissipation was increased at the interface, therefore producing a strong joint.

Moreover, the effect of joining time on the joint strength for thermoplastic polymer joints between PMMA and PLA was described by Zhang et al. [62]. The joining strength was increased when the joining time increased, as shown in Figure 3.5. There were some non-joint areas that appeared with short joining times and the joint strength was enhanced by increasing the joining time. After the optimum joining time, the joint strength decreased with the continuous increase of the joining time because ruptures occurred in the interface joining area at an excessive temperature. Whereas, the joint strength generally increased when the joining time was extended under a 0.1 MPa joining press because the joining pressure was too low. Thus, the joining time should be increased to enhance the rise of frictional heat in order to obtain an increase of the joint strength. When the joining time was 4 sec, the joint strength was increased slightly, compared with 1 and 2 sec. This behaviour occurred because the bubbles that were produced by excessive joining pressure and overheating temperature mixed with melted polymers and were compressed out of the interfaces.

This shows the importance of parameter interactions. The same behaviour in this study was also found in ultrasonic bonded carbon/nylon composites by Liu et al. [102].

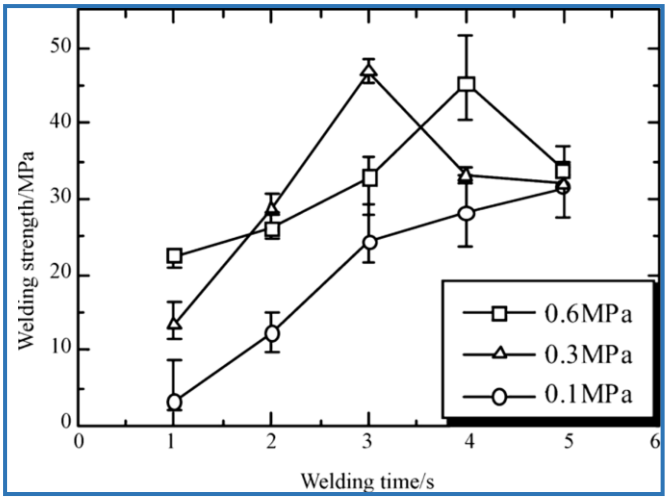

Figure 3.5 Joining time affects joint strength between PLA and PMMA at 28KHZ frequency, 30μm vibration amplitude, and at different joining pressure (0.1, 0.3 and 0.6MPa) [62].

Qiu et al. [63] also observed a non-linear effect of the joining time on the joint strength took place in the bond between poly methyl-methacrylate (PMMA) and polycarbonate (PC), as shown in Figure 3.6.

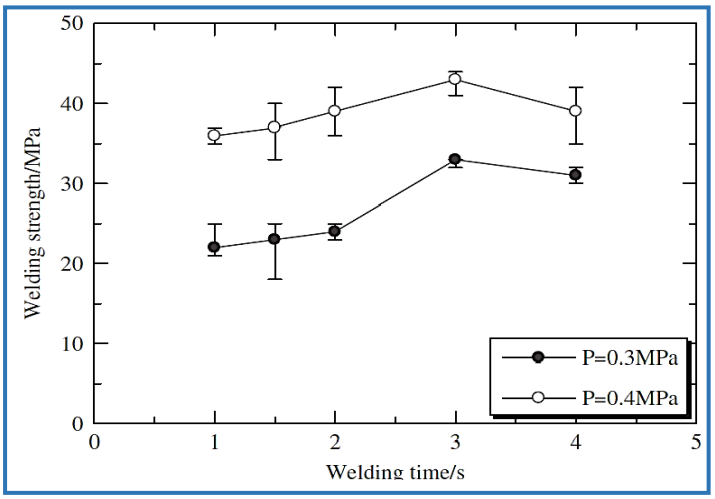

Figure 3.6 Relationship between joining time and shearing force of PC-PMMA joints at 28KHz frequency, 30μm vibration amplitude, and different joining pressure (0.3 and 0.4MPa) [63].

In the above case, the joint strength decreased because of the air bubbles that exist on rupture surfaces when the joining time was longer than 3 seconds, as shown in Figure 3.7. These bubbles are produced when the polymers are decomposed, and gas is released because the ultrasonic oscillation and heat were excessive. Therefore, the properties of polymers in the current thesis

should be investigated and examined to see if there are any air bubbles on the joint strength that may decrease the joint.

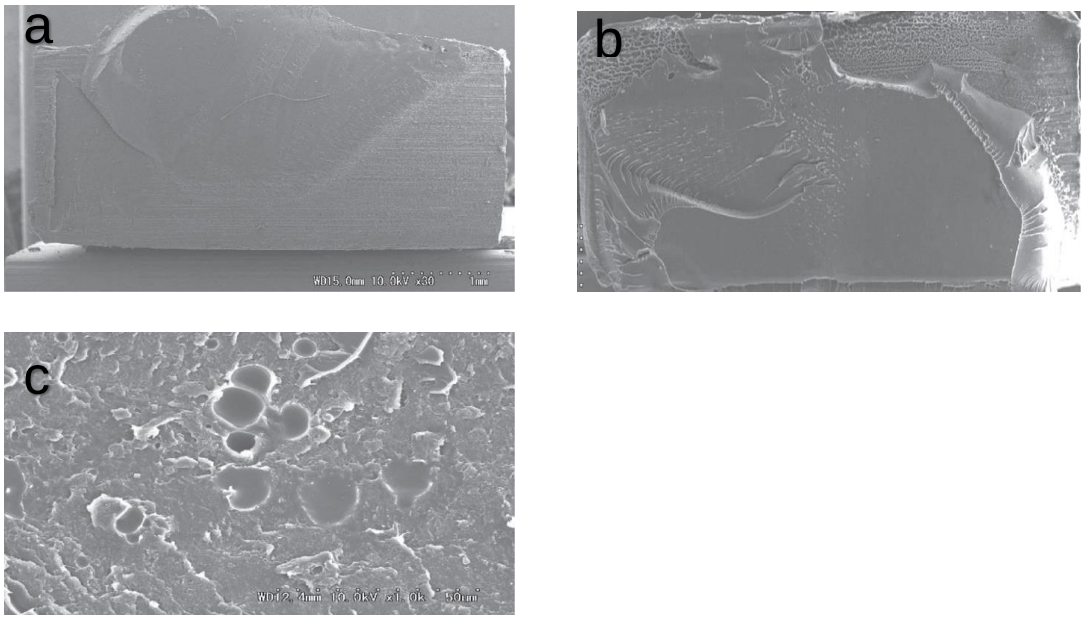

Figure 3.7 Rupture surfaces of PC bonded interfaces under joining stress of 0.3 MPa. (a), (b), (c) are under joining time of 1.5, 3 and 4 s, respectively [63].

Similarly, the above trend between joining time and the joint strength can be seen through the bond that was made of Acrylonitrile butadiene styrene (ABS) and Polyethylene (PE) thermoplastics by Chuah et al. [33]. These authors showed that the semi-crystalline polymers (PP) require a longer joining time than amorphous polymers (ABS) to break its ordered structure and start to flow. The efficiency of joining was increased when the joining time increased because more ultrasonic energy was dissipated at the joining interface. However, the extensive join time produced extensive flash of the melted polymer that leads the molecular chain to be aligned perpendicular to the acting force, which decreases the joint strength.

It can be concluded from this section (Section 3.2.2) that the relationship between joining time and joint strength, during the ultrasonic joining process, is a direct one. However, the joining time should not be excessively long because this increase leads to a reduction in the joint strength. This behaviour can be seen in metal or polymer joining. Therefore, it is important for the current research to investigate the effects of joining time on ultrasonic assisted joining of polymers with metal.

3.2.3 Effects of Bonding Force

Joining force is a static force and it is necessary to connect the joining horn to the surface of the top sample, so the vibration may be introduced into samples. A high-quality joint strength cannot be produced without real contact [103].

- **Metal - Metal**

A linear relationship between the joining pressure and the joint strength of Al-Al joints was observed by Elangovan et al. [104]. The increase of joining pressure led to an increase in the interface friction and thus increased the interface temperature that was required to create the joint. Hence, the average joint strength increased around 20% by increasing the pressure from 2 to 2.5 bar when the range of vibration amplitude was between 40 to 50 μm. Elangovan [101] observed that the strength of aluminium joints had an inverse linear relationship with joining pressure. The joint strength of thin sheet aluminium joints decreased around 127% when the pressure was increased from 2 to 2.5 bar at a constant vibration amplitude of 28μm. This behaviour happened when the maximum displacement (sliding motion at the interface between surfaces) was reduced and therefore the joining action that decreases the joint area was also reduced.

Watanabe et al. [97] studied the effect of joining pressure on the bond between the mild steel (SS400) sheet and the Al-Mg alloy (A5052) sheet. The joint strength was increased by increasing the clamping force until the strength reached the optimum value at force 588 N. Then, the tensile load of the bond was decreased with the continued increase of joining pressure, as shown in Figure 3.8. The reason for this is because the excessive clamping seemed to generate huge friction and arrest the relative motion at the interface surface of joining, thus decreasing the joining strength. This relationship between joining pressure and tensile load took place under a constant joining time.

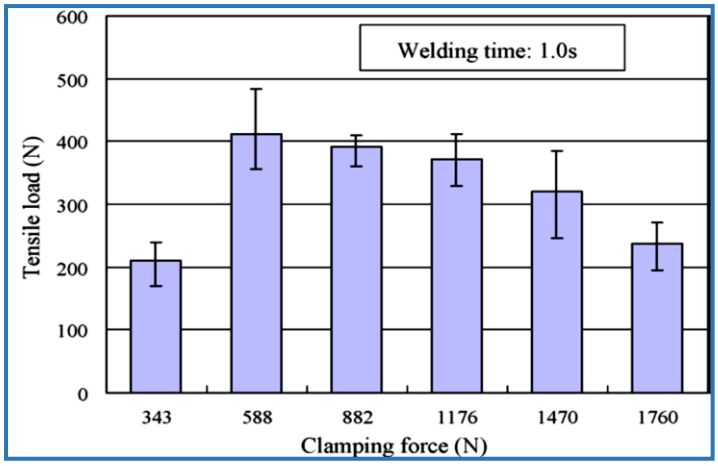

Figure 3.8 Relationship between clamping force and tensile load of A5052-SS400 joints at 15KHz frequency, 53µm vibration amplitude, and 1 sec bonding time [97].

Furthermore, the influence of joining pressure during the ultrasonic metal joining process, between aluminium alloy (Al6061) and the titanium alloy (Ti6Al4V) sheet, was studied by Zhu et al. [75]. In this study, the joint strength increased when the joining pressure (clamping force) was increased due to enhancing the ultrasonic energy and therefore increasing the joint strength. However, the joint strength decreased when the increase of clamping force was too large, due to reducing the efficient amplitude. Additionally, huge friction was created that produced a crash on the contact surface and weakness in the joint strength at the excessive joining pressure.

- **Polymer - Polymer**

When considering polymers, Zhang et al. [62] studied the influence of the joining pressure on the joint strength between polylactide (PLA) and poly (methyl meth acrylate) PMMA. The increase of pressure on specimens by the sonotrode tip produced an increase in the joint strength because of the increase in friction, providing enough heat to enable sufficient melting of the polymer. However, the pressure should be controlled because (see Figure 3.9) a low pressure led to a reduction in the frictional heat, meaning the interface temperature was too low to form a strong joint. In contrast, an excessive increase of pressure resulted in a higher frictional heat and thus decomposed the polymers to produce air bubbles on the interface surface, again reduces the joint strength.

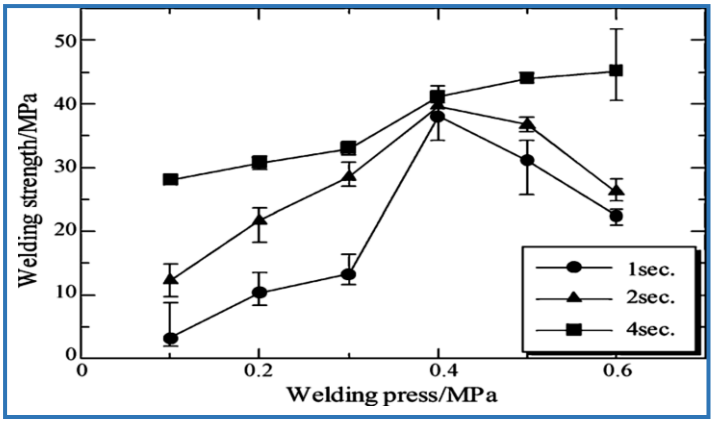

Figure 3.9 Relationship between joining pressure and joining strength between PLA and PMMA at 28KHZ frequency, and different bonding time (1, 2 and 4sec) [62].

- **Metal – Polymer Composite**

The same phenomenon that was shown in the relationship between the joining force and the joint strength in joining similar materials also appeared in the ultrasonic joining of composite materials. This relationship was investigated by Wagner et al. [9], between aluminium alloy (A5754) and fibre reinforced polymers. The average joint strength increased to reach the peak value (31.4 MPa) when the joining force was increased from 120 to 140N. Then, the textile started to damage after the peak value due to the excessive joining force and thus the joint strength was decreased around 11% at 200N (joining force). This behaviour was also confirmed for Al5754-CFRP, and Al1050-CFRP joints by the same authors [79].

It can therefore be summarised Section 3.2.3 that the joining pressure has a significant effect on the joint strength during the ultrasonic joining. Whilst the relevant values of bonding force will depend on the materials to be bonded, the trend of increasing strength until a critical level of force is reached can be seen across all the relevant literature. This behaviour appeared during the ultrasonic joining of polymers, metals, and composite materials, hence, it is necessary to study the relationship between joining force and the joint strength between metals and polymers in the current thesis.

3.2.4 Effects of Vibration Amplitude

Vibration amplitude is a longitudinal displacement (peak to peak) at the horn face. This amplitude is one of the important joining factors that can have an influence on the quality and strength of the joint because it is related to the power of the ultrasonic system. Therefore, the amplitude can control the power level because it has a significant impact on the dissipated energy that converts to heat [105].

- **Metal - Metal**

Elangovan et al. [94] demonstrated the significant impact of amplitude on the joint strength. A design of experiments approach was adopted to find the influence of amplitude on copper-copper joints. The results showed an increase in the average of joint strength by about 15% when the amplitude was increased from 40 to 50μm. The reason for this increase was to enhance the joining area by increasing the vibration and therefore increasing the joint strength. Elangovan [101] used a similar experimental approach to investigate the effect of vibration amplitude on the joint strength for Al–Al joints. The strength of these joints was increased around 50% through increasing the amplitude from 30 to 50μm. The increase in vibration amplitude gave an increased area for friction action between the metal surfaces, thus the joint strength increased.

- **Polymer - Polymer**

Van Wijk et al. [106] observed the behaviour between vibration amplitude and the joint strength in thermoplastic polymer (ABS) samples. When the vibration amplitude increases, the temperature in the joining interface is increased and thus the flow of the molten polymers, which cause a high quality joint, can be at a higher rate [107]. In contrast, a high amplitude reduction can create a non-uniform fusible initiation [14]. The effects of joining parameters, including vibration amplitude, on the joint strength were investigated by adopting design of experiments. The joint strength of ABS polymers increased linearly with vibration amplitude until the amplitude reached 30μm. The energy dissipated

at the interface increases vibration amplitude and therefore the bond developed with increasing the dissipated energy that converts to heat was increased. The measurement of vibration amplitude in Van Wijk's study was inaccurate, where the measurement variation of the vibration amplitude about ±9% which produced variation in the joint strength about ±10%. Therefore, the accuracy of parameters measurement in this thesis should be taken into consideration.

Moreover, the joint strength improved as the vibration amplitude was increased, as observed by Liu et al. [61]. The results showed that the joint strength of polypropylene and polystyrene improved by increasing the amplitude. Energy dissipation that converts to the heat is proportional to the square of the vibration amplitude. Thus, increasing the vibration amplitude leads to significantly increasing the input energy, thereby increasing the joint strength.

- **Metal – Polymer Composite**

In addition to polymer-polymer and metal-metal joints that have been explained previously, the effects of oscillation amplitude on the joint strength of metals (AA5754) and thermoplastic composites (CF-PA66) joints was studied by Wagner et al. [9]. The average tensile shear strength of these joints increased from 29.3 MPa to reach the peak value (about 31.5 MPa) when the amplitude was increased from 38 to 40.5µm because better contact between fibre and metal sheet was created. However, excessive increase of oscillation amplitude led to a decrease in the joint strength because it damages the textile of composite materials. This was also found by Balle and Eifler [79].

It is clear in Section 3.2.4 that the vibration amplitude has a significant effect on the joint strength of metal-metal, polymer-polymer, or metal-composite polymers joints through improving the joining energy. Thus, it is necessary to study vibration amplitude in the current thesis as one of the main ultrasonic factors in metal-polymer joining.

3.2.5 Effects of Holding Time

Holding time is the period that comes after joining time when the bonded samples are still under the static joining force between anvil and sonotrode [14]. Figure 3.10 shows the joining cycle during the ultrasonic joining process. Holding time has been used in the ultrasonic joining of polymers only, as there is no melting state in ultrasonic joining of metals and therefore it does not require re-solidification time.

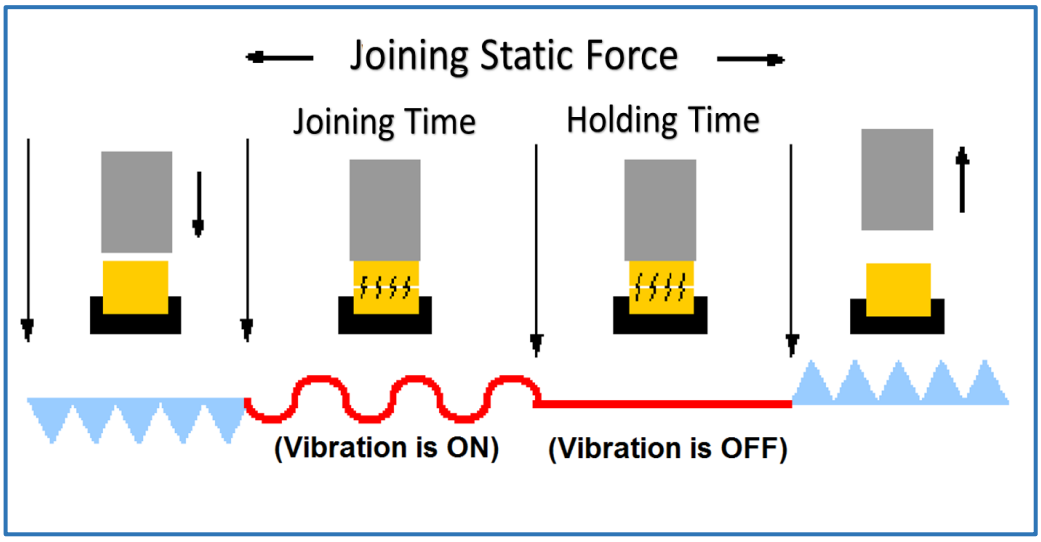

Figure 3.10 Ultrasonic joining cycle, adapted from [108].

Although the hold time or cooling process helps the melted energy director to spread evenly to produce a good bond in thermoplastic joining, most of the previous research has considered the holding time as a minor joining parameter because it does not significantly influence the joint strength [33]. These previous studies conducted tests for range values of holding time to investigate its effects, such as 0.5-2.5 sec for ABS polymer, and 0.5-2.5 sec (HDPE) [50], 0.5-2.5 sec (ABS) and 0.5-2.5 sec (PE) [33], and 0.15-0.45 sec (PP) [48]. While, other research kept the hold time constant during the joint, such as 3 sec for PP, 0.2 sec (ABS) [30], and 5 sec (PMMA) [53].

From the above, Liu et al. [61] showed the effects of hold time on the joint strength of polypropylene joints. The optimum value of hold time of PP joints was 0.2 sec. According to the authors of this study, this effect was due to polypropylene (semi-crystalline polymers) tending to recrystallise during the

cooling time. Thus, the molecular chains might penetrate and entangle with the other side of the interface, thereby improving the joint strength.

Therefore, the effect of hold time will be examined in the current research to observe whether it has a significant effect on the joint strength.

3.3 Effects of Workpiece Conditions

The conditions of workpieces, such as the surface roughness of the metal samples, and the sample geometry may have important influences on the joint strength. Therefore, the effects of these conditions are discussed here:

3.3.1 Surface Roughness

- **Metal - Metal**

The topography of the workpiece surface is a very important factor, which affects the joint strength quality because it increases the interface friction [9]. Thus, this parameter is only adopted during ultrasonic joining of metals.

When the roughness of metal samples becomes too low, the workpieces slip on each other and the joining area cannot be developed. Whereas, too high an increase of surface roughness produces a heat concentration which causes thermo-shock provoked fractures especially for brittle materials due to an excessive temperature [9].

There are many methods to create the roughness on the surface of samples, such as mechanical methods including grinding, polishing, grit blasting, abrasive and emery paper. Chemical treatments have been also used to create a rough surface and include chemical etching and anodising as electrochemical treatment.

Emery papers were used mechanically to create a rough surface of magnesium alloy (AZ31-H24) samples before joining, by Patel et al. [23]. The rough surface helped to increase the interface friction between the samples thereby increasing the heat generated at the interface. This leads to increasing joining temperature and therefore producing a good bond.

Siddiq et al. [8] showed the importance of increasing the friction coefficient on the joining temperature. The generated heat affects the strain deformation and flowing metals for joint formation. The friction coefficient depends on the surface roughness. Elangovan et al. [109] illustrated the relationship between the coefficient of friction and bonding temperature, as shown in Figure 3.11. The results showed that increasing the coefficient of friction increases the bonding temperature which leads to an increase in the plastic deformation and therefore in contact area.

It can be concluded that the surface roughness plays an important role during the ultrasonic joining of metals because the heat generated at the interface between the samples is increased, which leads to an increase the contact area by increasing the local plastic deformation.

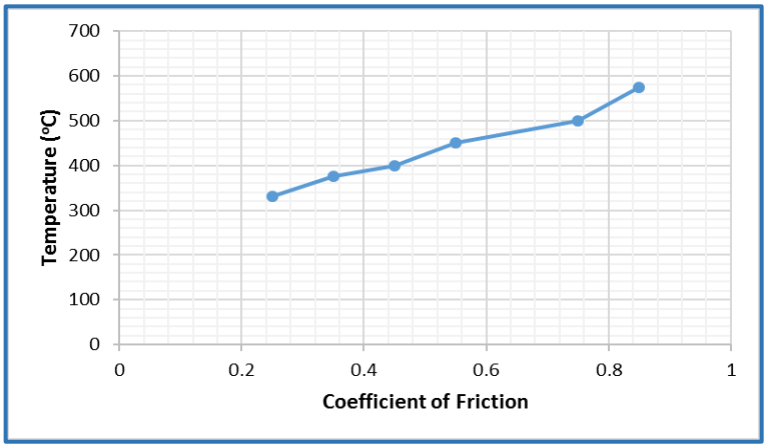

Figure 3.11 Variation of temperature in aluminium sheet (1mm thickness) with coefficient of friction during the ultrasonic process at 20KH, adopted from [109].

- **Metal – Polymer Composite**

Although there is a little literature on the ultrasonic joining between metals and fibre thermoplastic composites, the creation of surface roughness was very important and necessary to form the joint as it enhanced the mechanical interlocking between the metal surface and melted polymer.

The mechanism of joining metal with composites using the ultrasonic technique depends on creating microstructural surface roughness on the metal surface, which allows it to interlock mechanically with the molten

polymers and produces a physical bonding between polymer and the oxide layer of the metallic surface. The physics of melting polymers is based on the intermolecular friction, as explained in detail in Section 2.1.2, whilst the surface roughness of metallic materials may be created using mechanical pre-treatment, such as emery paper or chemical pre-treatment, such as an anodising technique.

Mechanical (corundum blasting) and chemical (acidic etching) pretreatments of AA5754 samples were conducted to establish a rough surface on the samples prior to being ultrasonically bonded AA5754/CFRP by Balle et al. [59]. The results of high resolution (HR) analysis and energy dispersive x-ray analysis showed that chemical pre-treatment creates a filigree structured and cavernous oxide layer (roughness average Ra is about 0.3 µm) on A5754 surface that was filled by molten thermoplastic matrix (PA66). When the corundum blasting was applied, the tensile shear strength increased about 50%, compared with non-pretreated sample joints (30MPa). The average roughness was increased by corundum blasting from 0.3µm (initial state) to 3µm, and the average joint strength reached more than 50MPa when the chemical pretreatment was undertaken. Although, the acidic pickling did not significantly improve the average roughness, it produced a filigree cavernous structure of the oxide layer of aluminium. While the corundum blasting created a thin and closed oxide layer. The tensile shear strength of this joint was investigated by the same authors [9]. Initial states of as 'rolled' (R), 'acid pickling' (AP), 'corundum blasting' (CB) and combined pretreatments (corundum+acid pickling (CB+AP)) were studied. Figure 3.12 shows a comparison between different surface conditions and tensile shear strength. These authors observed that an intensive increase of the average roughness (R_a) for the "CB" surface compared with the "R" condition where "R_a" increased from 0.3 to 3µm with a 41% increase for tensile strength. The tensile strength of the "AP" and (CB+AP) was increased with 52% and 54% respectively compared with "R" condition when the average roughness for AP was 0.3µm and for (AP+CB) was 2.5µm.

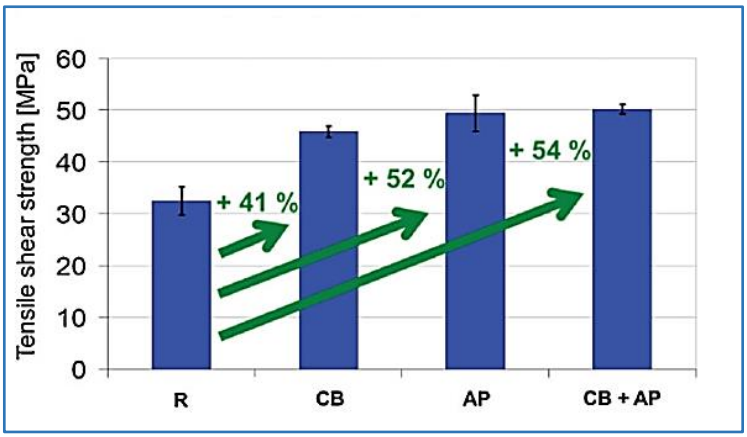

Figure 3.12 Relationship between tensile shear strength of AA5754/CFRP joints (via the ultrasonic joining) and pre-treated type of AA5754 sheets: a) initial state, as rolled (R), b) corundum blasting (CB), c) acid pickled (AP), d) combined pre-treated, CB and AP [9].

Balle et al. [110] investigated the importance of surface roughness on the tensile shear strength of aluminium alloys and fibre thermoplastic composites joints. The joint strength was increased when the aluminium alloy samples were pre-treated with nitric acid before joining, compared with joining of non-treated samples. This increase in the joint strength occurred through the creation of microstructural surface roughness, thereby allowing mechanical interlocking with the polymer matrix surface. The surface roughness of aluminium alloy (AA2024) was increased from average roughness (R_a) 0.2 µm to 1.1µm after pre-treatment.

In the adhesion technique, creating a rough surface is also a very necessary factor to promote the interfacial bonding between metal and polymer composites, as investigated by Ochoa-Putman and Vaidya [111]. The shear lap bond strength of interfacial adhesion between metal and polymer composites was increased by increasing the surface roughness. The bond strength between steel and PPMA was increased to about 50% higher than the steel without coating. Plasma treatment was conducted on the steel surface in this research. Figure 3.13 compares the joint strength of steel and different polymers, such as polypropylene (PP), thermoplastic polyurethane (TPU), carbon-nanotube epoxy (CNT) and poly (propyl methacrylate) (PPMA) polymers. It is clear that increasing the surface roughness produced strong bond strength by increasing the friction coefficient and therefore the melting

polymer was able to fill the cavernous surface and create a strong mechanical bond. Although the previous study is not about ultrasonic joining, it clearly demonstrates the effect of surface roughness on the bond strength between a polymer and a metal.

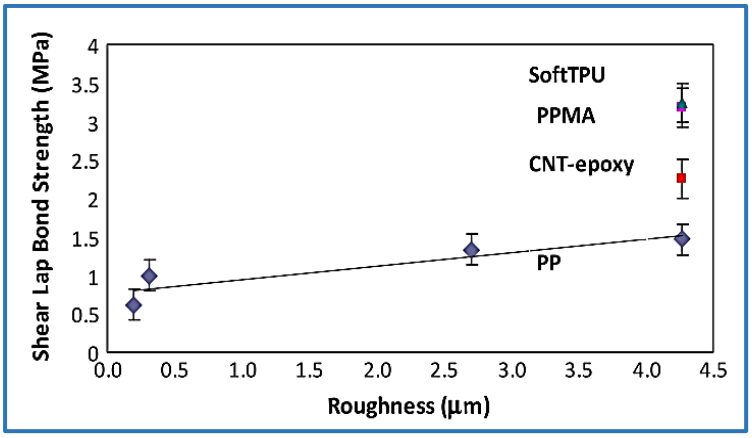

Figure 3.13 Effect of surface roughness on the bond strength (via adhesion technique) of steel and different types of polymers [111].

Budhe et al. [112] determined the optimum surface roughness value to produce the highest bond strength using adhesion technique. The optimum average roughness (R_a) of Al6061 samples that obtained in this study was 1.68 ±0.14µm, as shown in Figure 3.14. This value of roughness was produced by using grinding P-120 (mechanical treatment). This increasing in surface roughness led to a significant increase in joint strength (about 26.7%) compared to a surface without mechanical pre-treatment (0.54 ±0.15µm) due to increase the mechanical locking adhesive between the samples. The authors observed that the higher surface roughness had insufficient wetting which might lead to decrease the bonding strength after R_a = 2µm.

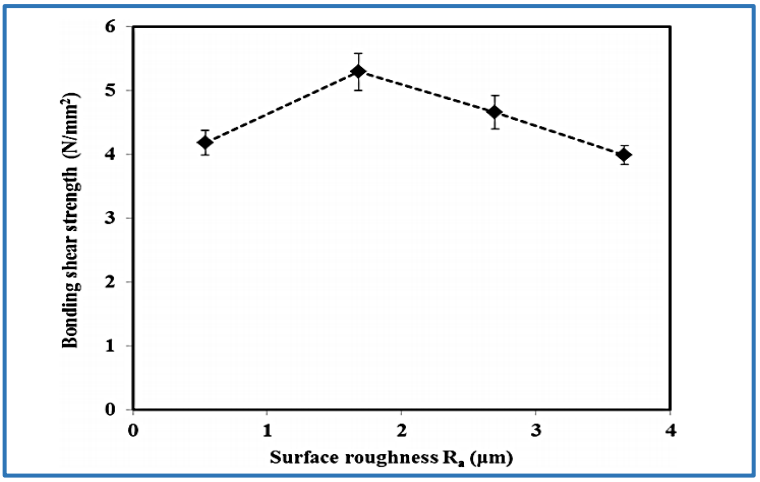

Figure 3.14 Relationship between the joint strength (by adhesion process) and surface roughness of Al6061 joints [112].

- **Polymer - Polymer**

As shown above in the sections of metal and dissimilar materials, the surface roughness has an important factor to enhance the joint strength. In metal materials, the surface roughness used to increase the friction at the interface and therefore increase the heat generation at the bond zone. Whilst, in dissimilar materials, the melting polymer flows inside the cavities on the metal surface to create the mechanical interlocks.

In case of polymer materials, the roughness would not be expected to play an important role because the ultrasonic joining of polymers depends on intermolecular friction which causes melting the polymers at the interface and their chains engage across the interface to create the joints.

In conclusion, this section (Section 3.3.1) has shown that the surface roughness is necessary, and has significant effects on the joint strength when a metal is one of the samples to be bonded. Therefore, the pre-treatment of metals is important in the current thesis to create microstructural pores on the surface of the metal allowing it to be filled by molten polymer and create a strong joint. In addition, the chemical pre-treatment of metal can produce a higher joint strength compared to mechanical pre-treatment.

3.3.2 Sample Geometry

The geometry of the sample to be bonded, such as shape and dimensions are also important and have a significant effect on the joint strength of ultrasonic joining. It can be considered that the dominant parameter is the thickness of the samples, as investigated by Al-Saraaf [12], and Daniels [26]. The ultrasound waves pass through the upper sample to propagate at the interface area; as such internal frictions occur which generate the joining heat [113]. There is a relationship between the thickness of the upper sample (it is valid up to 1 mm thick for metals) and the required joining energy, as it was measured in Equation (3.1) [114].

$$E = 63(Ht)^{3/2} \tag{3.1}$$

Where,

E Energy (watt.sec(J))

H Vickers hardness No.

t material thickness (mm)

The sample is very difficult to join ultrasonically if it has a thickness of more than 3mm due to poor heat generation at the joint interface. Elangovan et al. [109] investigated the effect of upper sample thickness (aluminium) on the heat generation at the interface. This author inferred that the interface temperature decreased around 43.8% when the upper sample thickness increased from 0.5 to 3mm due to the deficiency in heat generation at the interface.

Therefore, most previous works used thin samples during the ultrasonic metal joining process, such as 0.15mm [115], 0.2mm [94], 0.3mm [104], [43], and [75] 0.3 – 0.4mm [101], 0.8mm [97], 0.92mm [42], and 1mm and 1.5 [116], while, the influence of near- and far-field joining on the ultrasonic joining of thermoplastics was explained in Section 2.2.1.1.

Therefore, it is necessary to investigate the affect of the sample thickness during ultrasonic assisted joining metals with polymers in this research.

3.4 Summary

Although many studies have attempted to explain the effect of bonding parameters on the lap shear strength, they are not included all relevant parameters and their interaction. Most research has used a constant sample thickness, and the effect of joining temperature, ultrasonic energy, parameter interaction, and bond features have not been accurately investigated in previous studies.

Therefore, a crucial part of this study will be the development of a detailed understanding of the significance of joining parameters, such as vibration amplitude, bonding force, bonding time, holding time, pretreatment of metal materials, energy director shape, bonding temperature, sample thickness, ultrasonic energy and bond features and variable interactions.

Since ultrasonic assisted joining of metal-polymer has not been performed in the literature, the range of parameters' levels have not been identified. The presented work identified the initial parameters' space. The selection of the minimum and maximum levels will be based on the combined ranges of the ultrasonic parameters used for joining the polymers and the metals, as shown in Figure 3.1.

Chapter 4 METHODOLOGY AND EXPERIMENTAL WORK

This chapter provides an initial investigation of the parameter space within which the US technique can work selection of materials and parameters is presented, as are the relevant test procedures.

4.1 Material Selection

4.1.1 Choice of Metal and Polymer

- **Metal Part**

In the existing literature, aluminium alloy sheet has been one of the most often used metal materials in the ultrasonic joining process, due to its high thermal conductivity and having good properties including corrosion resistance, excellent electrical conductivity, recyclability, non-toxicity, and high strength to weight ratios [117]. One of these aluminium alloy series, which has good properties, is Al 6XXX. This series is promising for today's transportation industries, and light-weight construction applications [118]. In addition, it has been shown to bond effectively using ultrasonic bonding [42], and [75]

Based on the above, the metal used in this research was Al6082, supplied in sheet form from Wilsons Metals Co., with the chemical composition that is shown in Table 4.1. The properties of Al6082 are presented in Table 4.2.

Table 4.1 The composition of Al6082.

Alloying element	Composition %
Manganese (Mn)	1
Iron (Fe)	0.50
Magnesium (Mg)	1.20
Silicon (Si)	1.30
Copper (Cu)	0.10
Zinc (Zn)	0.20

Titanium (Ti)	0.20
Chromium (Cr)	0.25
Nickel (Nl)	0.10
Aluminium (Al)	Balance

The provided sheets of Al6082 were heat treated prior to delivers, followed by artificial ageing (Temper 6) to increase the strength levels [110].

Table 4.2 The properties of A6082-T6.

Modulus of Elasticity (GPa)	69
Shear Modulus (GPa)	34
Tensile Strength, Ultimate (MPa)	295
Thermal Conductivity (W/m-K)	154 - 188
Melting Temperature (C^o)	555

- **Polymer Part**

In the literature review (Chapter 2), amorphous thermoplastic polymers showed high quality performance during the ultrasonic process. One of the most common polymers in ultrasonic bonding and engineering applications is Acrylonitrile Butadiene Styrene (ABS). This is a thermoplastic amorphous polymer and it has many properties such as being a relatively low-cost material, having high impact resistance, toughness, superior chemical resistance, and heat resistance. Additionally, it has very good jointability during the ultrasonic joining process. ABS has many applications including casings for power tools, telephones, computers, and medical equipment [30].

ABS is composed from acrylonitrile that gives a chemical resistance and heat stability, butadiene that gives the impact strength and toughness, and styrene that provides the rigidity [55].

ABS -750SW polymer was supplied from Korea Kumho Petrochemical Co., Ltd, with the properties shown in Table 4.3.

Table 4.3 The properties of ABS 750SW

Modulus of Elasticity (GPa)	1.9
Shear Modulus (GPa)	0.95
Tensile Strength, Ultimate (MPa)	40
Thermal Conductivity (W/m-K)	0.23
Glass Transition Temperature (C^o)	108
Melting Temperature (C^o)	Not Applicable because it is an amorphous polymer.
Melt Flow Index (g/10 mins)	0.92 @ 200 ^{0}C

4.1.2 Compatibility of Selected Materials

There are many expected challenges that may be faced with the ultrasonic assisted joining between ABS and Al6082-T6 sheets. These include the difference in bonding nature between polymers (this depends on the polymer melting) and metals (a solid state without melting) during the joining. Moreover, the physical and chemical properties are also different between ABS and Al6082-T6, as previously given in Table 4.2, and Table 4.3. Given all these differences, challenges in joining dissimilar materials (polymer and metal) are expected to occur in the current research.

However, amorphous polymers have previously been joined ultrasonically at the glass transition temperature, as explained previously in Section 2.1.2. Thus, ABS can be joined at 108 °C (T_g of ABS is approximately 108 °C). During similar joining of aluminium, the measured temperatures at the interface bonding area of aluminium alloy varied between 85-125 °C [104]. Therefore, it should be possible to achieve the desired temperature, which is the most significant factor for successful bonding.

4.2 Determination of Bonding Parameters

According to the literature review (Chapter 3), some parameters can be considered crucial in all types of ultrasonic joining, which will be assessed here.

In the absence of standard levels of bonding parameters and no information in the literature about the range of levels to join polymer and metal ultrasonically, the range of levels of bonding parameters that will be used in the current research was determined experimentally. In order to identify a suitable range of parameters with which to start, the literature on both metal-metal and polymer-polymer was combined to give the maximum range suitable for either material. This range was then narrowed down for this specific material combination by initial experimentations.

4.2.1 Vibration Frequency and Amplitude

According to the literature on ultrasonic bonding processes (Section 3.2.1), the most common frequency of vibration is 20 KHz for bonding similar polymers or metals. This value was therefore selected for this work.

The current ultrasonic generator has only four levels of vibration amplitude that can be studied in terms of their influence; these are 14.7, 16.8, 18.9, and 21 µm. Although the values of vibration amplitude were restricted, these levels fit with previous research [30] for a similar polymer (ABS), and they are within the typical values of vibration amplitude for metals from 0.01 to 0.1mm [119] and [7], as shown in Figure 4.1. These levels are set manually to 70%, 80%, 90% and 100% of 21µm. Therefore, all these values were examined in these preliminary trials.

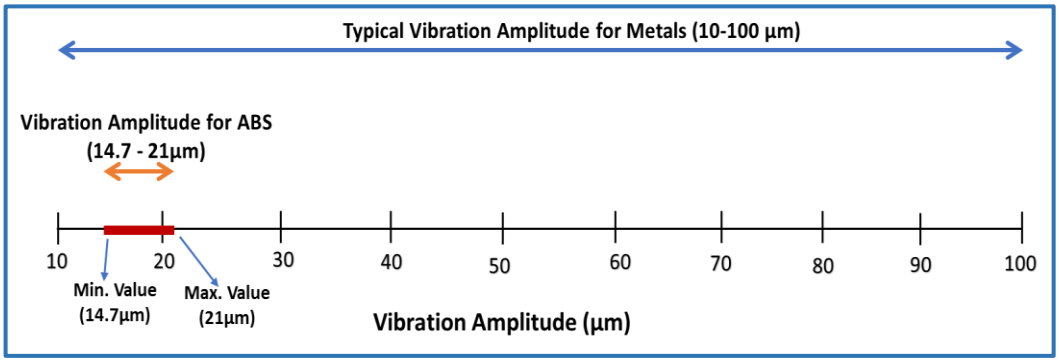

Figure 4.1 the initial range of vibration amplitude for ABS/Al6082 joints.

4.2.2 Bonding Time

It is very important to select the correct bonding time to obtain the joint. The initial range of bonding time used in the initial experimentations of the current study is between 0.2 and 3 sec with an equal interval of 0.4 sec. This range of levels resulted from combining ranges of ABS [30] and [105], and Al alloy [97] in the existing literature, as shown in Figure 4.2.

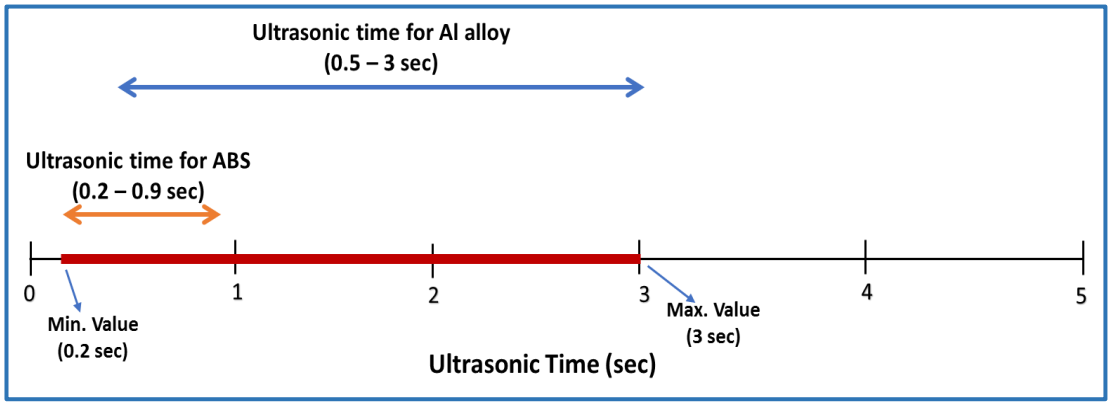

Figure 4.2 The initial range of bonding time for ABS/Al6082 joints.

4.2.3 Bonding Force

Bonding force is a static force and it is necessary to bring the joining horn in to contact with the surface of the top sample, so the vibration may be introduced into the samples. Therefore, the determination of suitable force is essential for good joining. The selection of the initial range of ultrasonic force was determined by the same method as in Section 4.2.2. Therefore, the initial range of ultrasonic force's levels in the current research starts from 500 to 1500N with an interval of 100 N to cover the range used for ABS polymer [30] and Al alloys [97] in the literature, as shown in Figure 4.3.

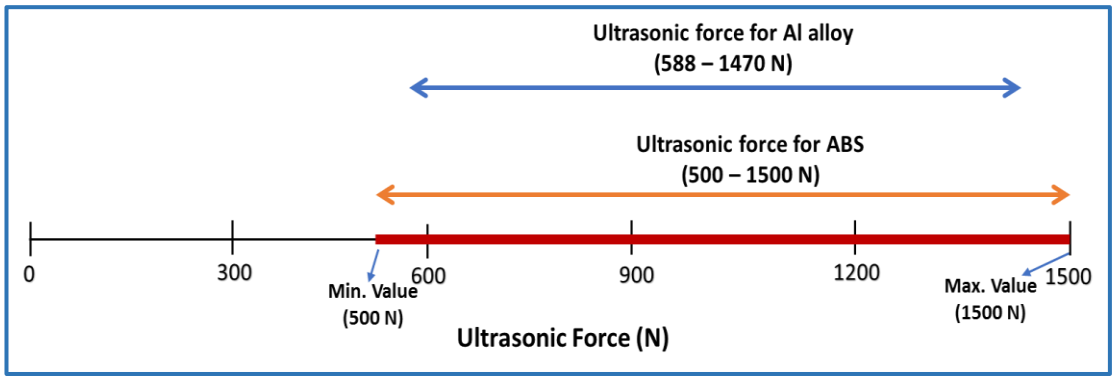

Figure 4.3 The initial range of ultrasonic force for ABS/Al6082 joints.

4.2.4 Hold Time

The period during which the bonded samples are still under the static bonding force between the anvil and the horn without vibration is called hold time. The initial range of holding time was determined as 0.5 to 1 sec with an interval of 0.25 sec, agreement with the literature [120] for thermoplastic polymers, such as ABS (hold time is not required for metals). Modification of this variable has not been investigated for joining similar metals or metals/fibre reinforced polymers. However, as stated previously, the polymer may be affected through this parameter and therefore it has been taken into consideration.

4.2.5 Sample Position

The type of joint in the current ultrasonic bonding is a lap joint, as shown in Figure 4.4.

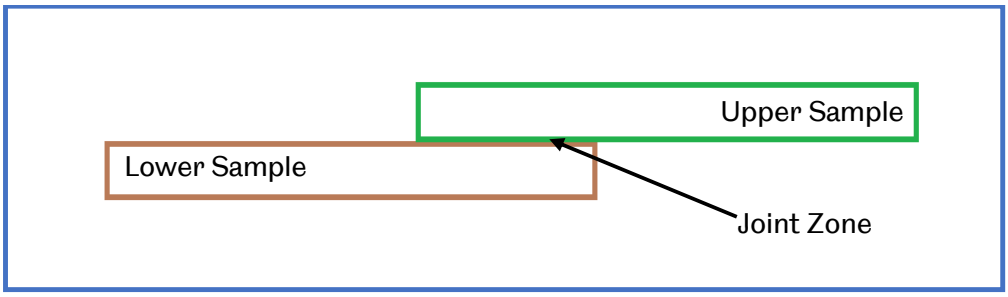

Figure 4.4 Schematic of lap joint.

Since there are two different materials in this research (ABS and Al6082-T6), there are two options in experimental work about the sample position. The upper sample may be either ABS polymer or Al6082-T6. The upper sample has an important role in passing the bonding energy through the upper part (horn side) to transmit into the joining zone [24]. Therefore, the initial experimental tests used both options of sample position to identify the best position.

4.2.6 Sample Thickness

As illustrated previously in Section 3.3.2, the thickness of samples is the dominant parameter that influences the joint strength. Changing the thicknesses of the upper and lower samples was investigated in the initial

experimentation to examine the effect of the thickness on the output results. In the existing literature, near-field joining (the distance between sonotrode and joint zone within 6.3mm) is most appropriate for polymers because the intensity of vibration at the interface joint is similar at the ultrasonic horn, as explained previously in Section 2.2.1.1. Whereas, the thickness of metal has been correlated as inverse relationship with the joint strength due to reducing the heat generation at the joint zone, as illustrated previously in Section 3.3.2. Therefore, three different thicknesses for each sample were used in the initial tests to ensure the effects of samples thickness on the joint strength. Since there is no standard that governed the selection of the thickness of the sample, it was decided to choose thicknesses of 1, 1.5, and 2 mm. These levels are within the allowable range of thickness for ABS polymer (near-field joining) and metals (Al alloy) [59], [119] and [116], as shown in Figure 4.5.

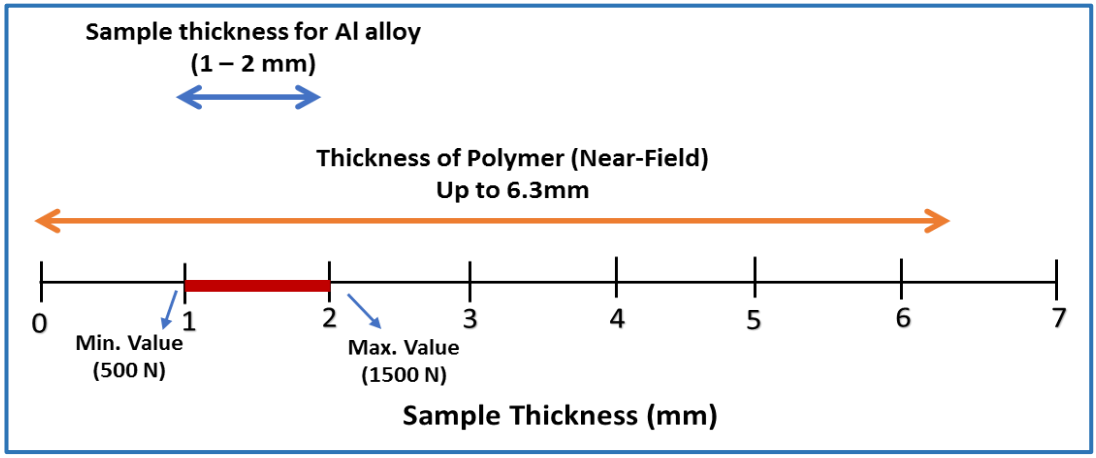

Figure 4.5 the initial range of sample thickness.

4.2.7 Energy Director (ED)

From the literature (Section 2.1.2.1), the energy director is necessary for polymers, to concentrate and focus the joining energy at the joining zone, which leads to melting and flowing of the polymer to create the physical join. Therefore, it can be expected that use of an energy director will be required in the current thesis. The importance of the energy director in the current research was examined in the initial experimentations. In the literature, three shapes of ED were used (triangular, semi-circular, and rectangular). Initial experimentations, one shape was used to explore the importance of its

presence only. The shape selected was a triangle as it is the most frequently used in previous research. Dimensions matched those in the literature [30], as shown in Figure 4.6.

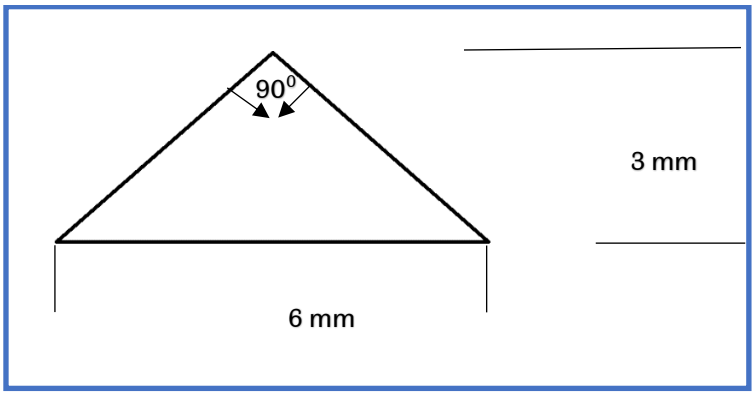

Figure 4.6 Geometry of ED.

4.2.8 Surface Treatment

As explained in the existing literature (Section 3.3.1), the roughness of the metal substrate will have an effect on the level of bonding achieved. There are a variety of methods by which roughness might be introduced, with each method having an effect on the type of roughness induced. Within each method itself, the chosen parameters will also influence the resultant roughness. To study these methods in detail would require a major study in its own right.

The current thesis will focus on the effect of any of the relevant ultrasonic parameters and their interaction on the joint strength rather than focusing on the methods of roughness production. This is because there is currently minimal literature regarding the effects of the ultrasonic parameters on the joints of dissimilar materials.

It was therefore decided to use a single, industry-standard, pre-treatment in order to provide a rough surface to promote good bonding. A more in-depth study of the relevant significance of the mechanism by which roughness is achieved, the exact form of this roughness, and the influence of roughening parameters would form an interesting and novel area for further investigation as future work.

The importance of the surface treatment of metal samples was examined in the initial tests, whereby Al6082-T6 was bonded with ABS, both with and without treatment. The treatment of Al6082-T6 samples involved cleaning and etching the samples, acid pickling, and phosphoric anodizing, following cleaning with isopropyl alcohol. The pre-treatment standard used was ASTM D3933–98 (Reapproved 2010). This type of treatment had previously been shown to be effective when joining aluminium and polymer samples through adhesion [121].

4.3 Production of Samples

4.3.1 Sample Dimensions

In the absence of the standard dimensions of ultrasonic assisted joining of dissimilar materials (metal–polymer), the samples were made to a rectangular shape because this shape is suitable for lap shear testing. The sample thickness is the dominant dimension in the ultrasonic technique because the ultrasound waves pass vertically through the thickness to reach the interface zone [122] and [15]. Hence, the sample size was selected as there was already an appropriately-sized mould for it. The overlap length is 39 mm because the horn tip diameter is 39 mm, while the width is 22 mm to ensure most of the overlap area is covered by the horn tip, as shown in Figure 4.7. The sample dimensions are shown in Table 4.4. In addition, the ED is positioned at the centre of the overlap.

Table 4.4 The sample dimensions.

Materials	Width (mm)	Length (mm)	Thickness (mm)
ABS-750SW	22	59	1, 1.5, and 2
Al6082-T6	22	59	1, 1.5, and 2

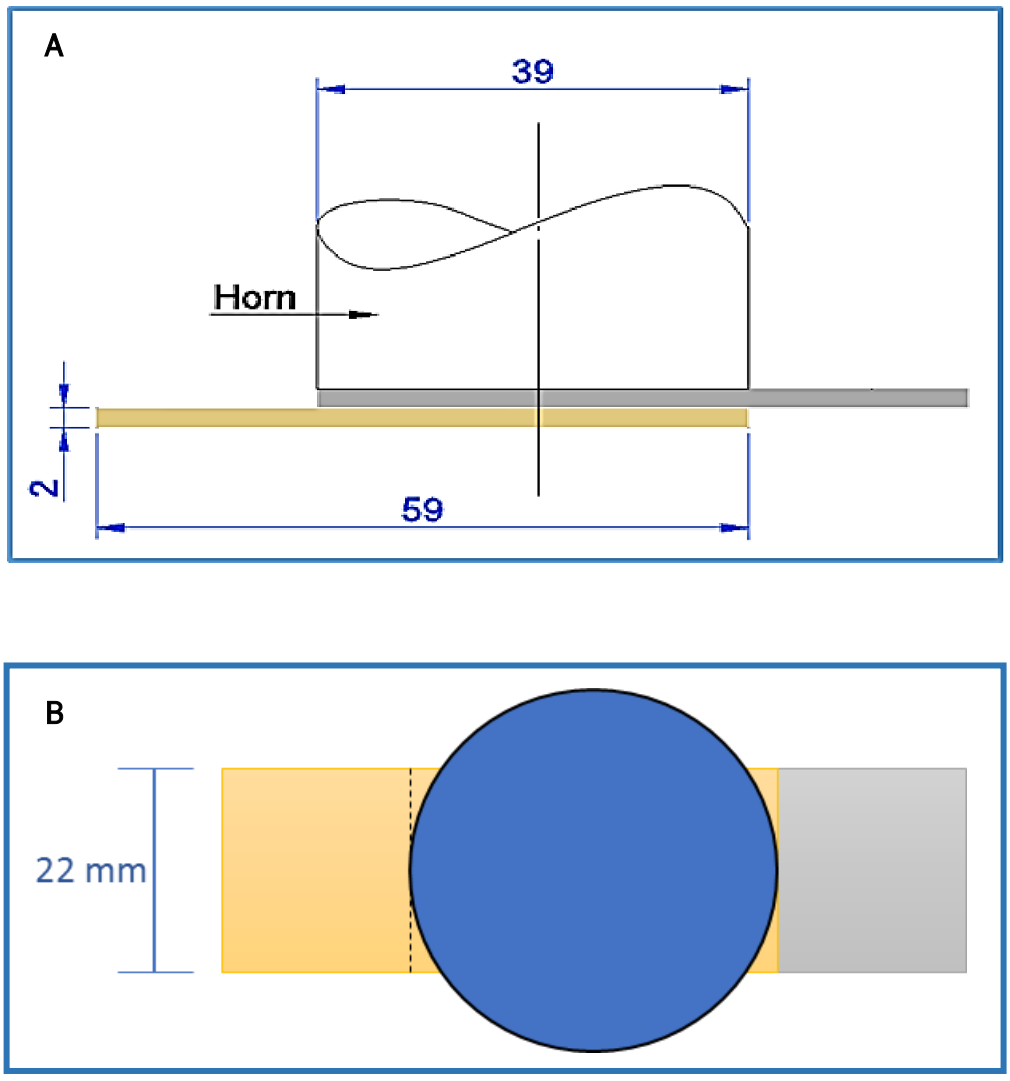

Figure 4.7 Lap joint of dissimilar materials A) side veiw, B) top veiw.

4.3.2 Polymer Sample Preparation

According to the British Plastics Federation (BPF), injection moulding is one of the main methods for producing thermoplastic polymer (such as ABS) articles because it is considered a fast process and can produce high precision samples. Therefore, the injection moulding technique was applied to produce ABS 750SW samples based on the dimensions given above (Table 4.4).

In the current study, the TRAVIN Mini Moulder (TP1) device was used during the process of polymer sample production, as shown in Figure 4.8 (A).

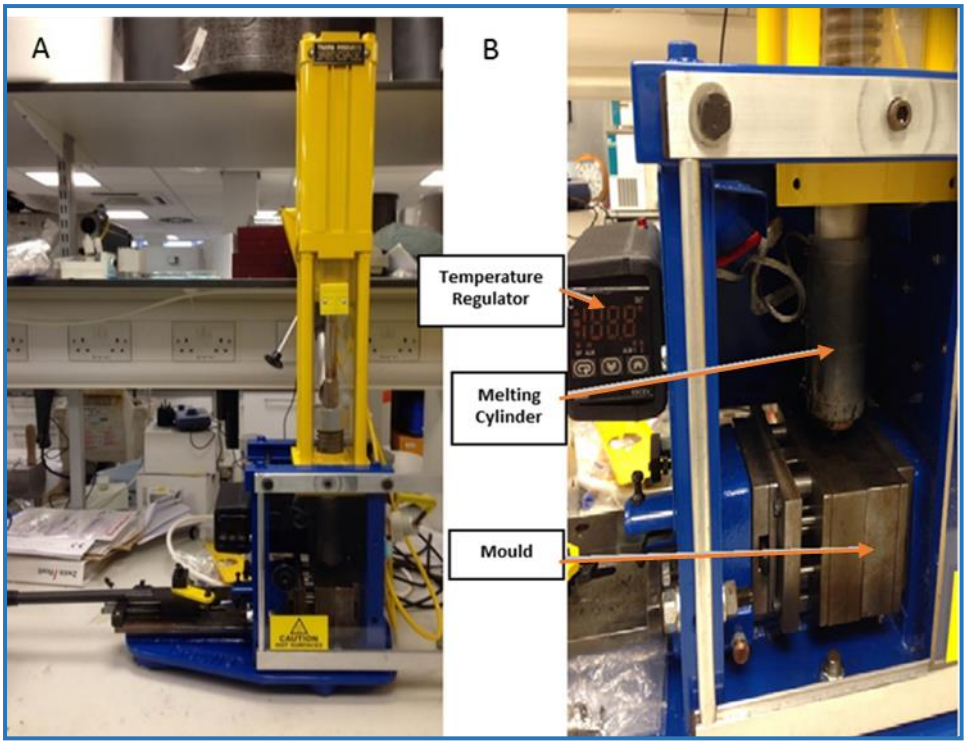

Figure 4.8 Injection Moulding Device.

In this technique, the procedure to prepare ABS samples, and design and manufacture the mould followed the British Standard EN ISO 294-1:1998, as shown in Figure 4.9.

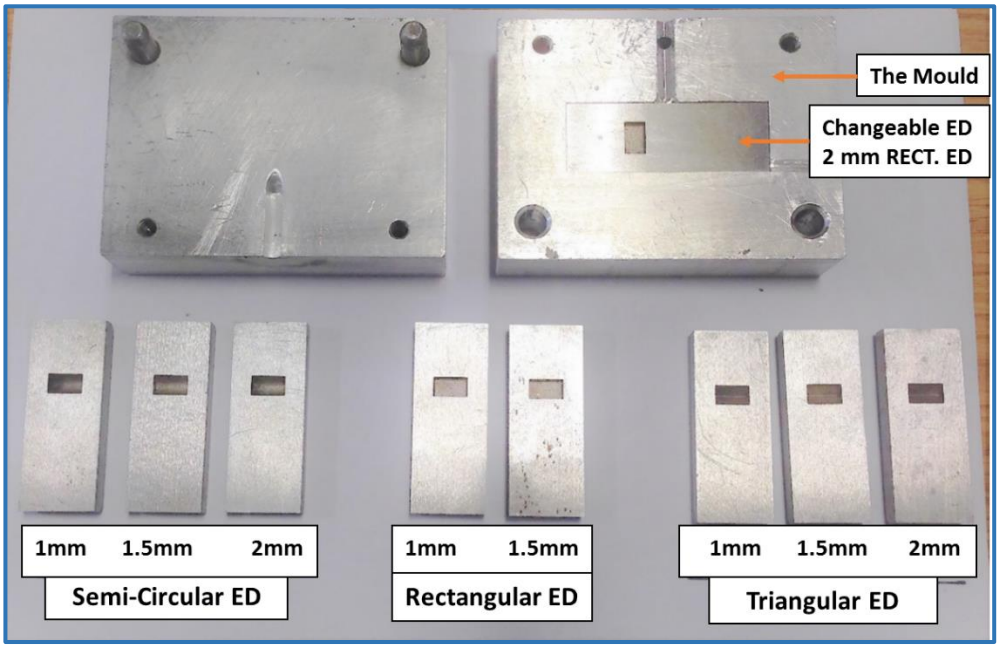

Figure 4.9 Mould with changeable cavities of ED.

Three shapes of energy directors were manufactured on the polymer samples. The mould consists of two frames. The outer frame was made from Aluminium, with changeable inserts fixed to the outer frame and an energy director cavity. The changeable insert was made from hardened steel because the hardened steel can hold sharp edges and it has a long lifespan. The mould (outer frame and changeable inserts) was produced by Travin Plastic Injection Mouldings Co., UK. Figure 4.10 shows the specimens that were produced.

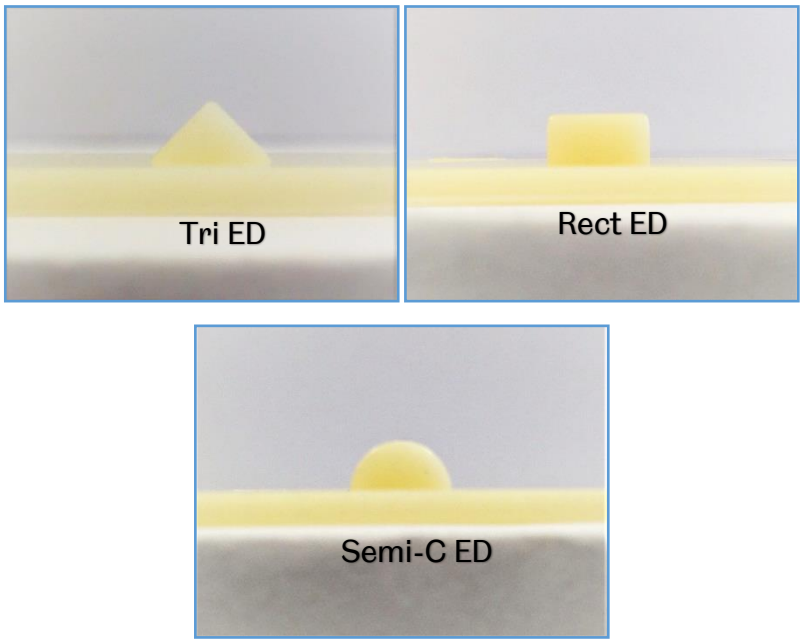

Figure 4.10 ABS 750SW specimens (different ED shape).

The following steps were used to produce ABS samples:

- Dry ABS polymer at 80 °C in the oven for 2 hours to remove the moisture because ABS polymer is a hygroscopic polymer, meaning it can absorb the moisture from the atmosphere.
- Put 10g of the polymer inside the melting cylinder to melt at 200°C.
- A steel piston was used to press the molten polymer into the mould, as illustrated in Figure 4.8 (B).
- There are two types of pressure applied: injection pressure is used to inject the majority of molten polymer into the mould for seconds (pressing time). Then post press or hold pressure is applied to complete filling the mould by packing the molecules together during the holding time. In other words, the polymer will cool down in the mould, thus thermal shrinkage will be

exhibited. Therefore, the post pressure purpose is to replace the volume lost during the solidification and cooling down of the polymer and normally the hold pressure is less than, or equal to, the injection pressure. The air-line pressure of the injection moulder device is from a standard 80 psi.

- The time of melting ABS in the device cylinder before injection into the mould should be enough to facilitate filling the mould.

The parameters used during the injection moulding process, are tabulated in Table 4.5.

Table 4.5 The injection moulding parameters.

Cylinder Temperature (C^o)	Mould Temperature (C^o)	Melting time (min)	Pressing Time (sec)	Holding Time (sec)
200	40	2-3	5	5

4.3.3 Metal Sample Preparation

Al6082-T6 samples were cut by wire EDM at the University of Sheffield workshop, based on the dimensions that were shown in Table 4.4. Then, the Al6082 samples were treated following the standard ASTM D3933–98 (Reapproved 2010). The importance of pre-treatment depends on modifying the surface of the aluminium alloy, so it becomes a format to bond with the polymer by:

- Cleaning the surface, degreasing, and etching the specimens and reducing or removing surface scratches and surface contaminants such as weak oxide layers. These weak layers are formed by heat treatment, humidity or airborne contamination [123].
- Creating a microstructural surface roughness and forming a thick and hard porous oxide film on the aluminium surface, thus the mechanical interlocking with the polymer surface is allowed, as shown in Figure 4.11 [110].
- Increasing the corrosion resistance of pre-treated specimens.

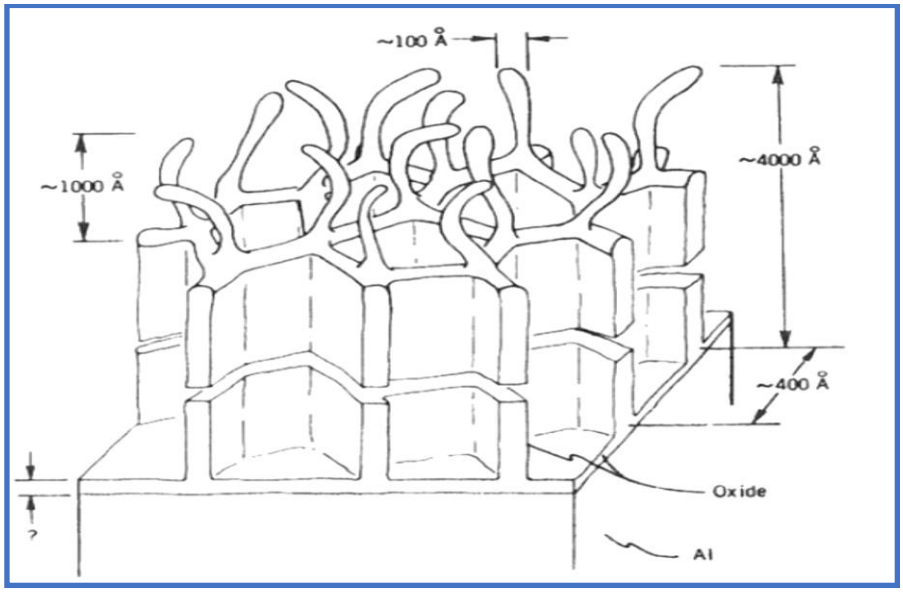

Figure 4.11 The oxide layer after anodising [110].

Figure 4.12 shows the phosphoric anodising step of the Al6082-T6 pre-treatment.

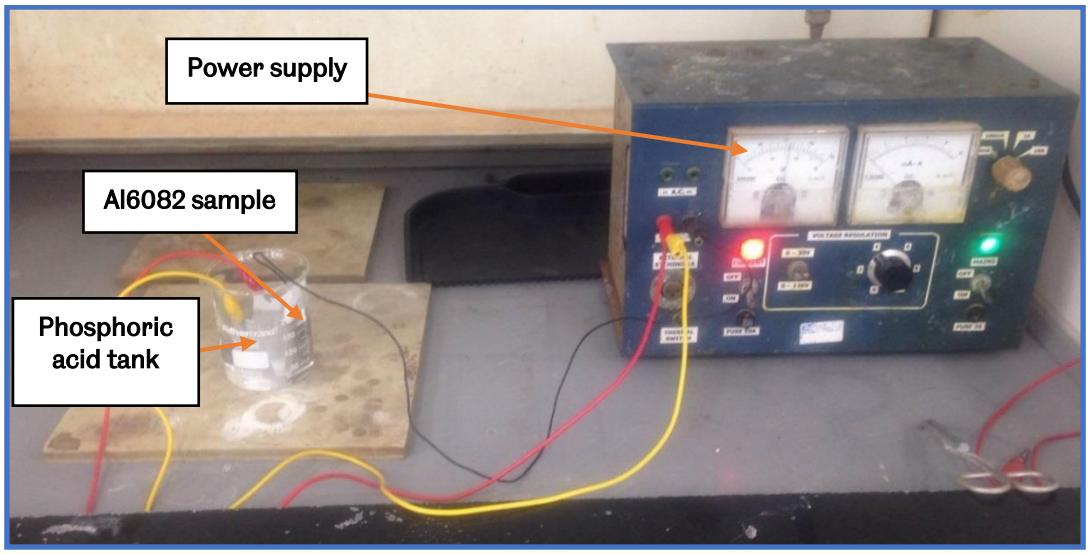

Figure 4.12 Phosphoric anodising of Al6082.

To ensure increasing the surface roughness of Al6082-T6 and to produce a porous surface, the surface roughness was measured before and after the pre-treatment, as explained in the next Section 4.3.3.1. In addition, the microscopic images were captured, as shown in Figure 4.13.

The microscopic images show a microscopically fissured surface, parallel to the rolling direction before the pre-treatment, while the rough and porous surface was produced after chemical pre-treatment of A6082-T6.

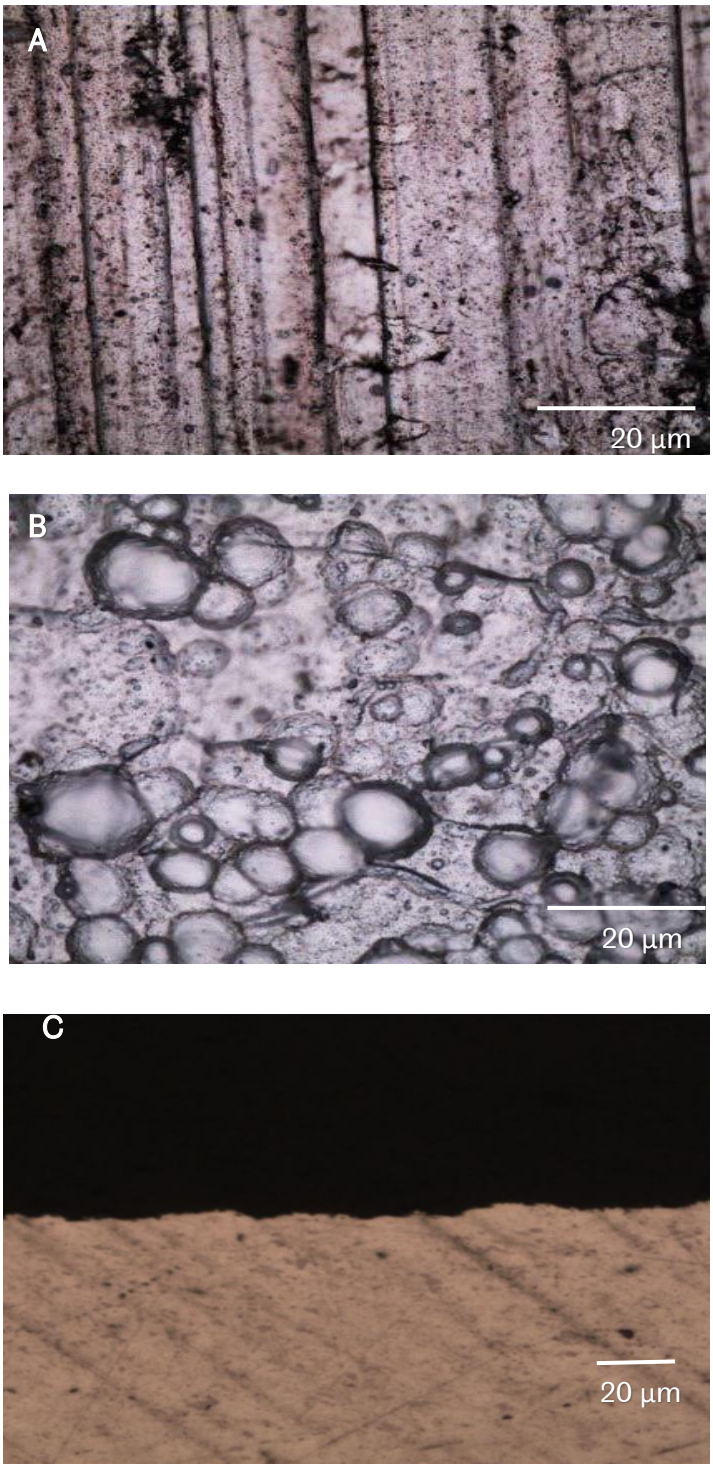

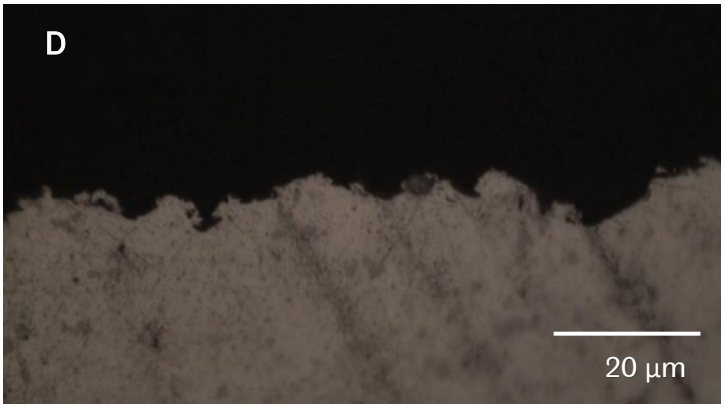

Figure 4.13 Microstructure images of Al6082-T6 surface, a) before pre-treatment (top view), b) after pre-treatment (top view), c) before pre-treatment (side view), d) after pre-treatment (side view).

4.3.3.1 Surface Roughness

In this study, the surface roughness of Al6082-T6 specimens were measured with a Veeco Dektak 150 surface profiler, because the surface roughness is considered one of the critical factors to affect the joint strength. The Dektak 150 can be measured x-y stage, when the stylus is moved over the specimen surface (length of moving (L) is 3 mm). The digital format displayed on a screen is an electrical signal conversion corresponding to the dimensions of the test specimen and this signal is converted from the stylus vertical displacement. The instrument adopted in this study, is shown in Figure 4.14. During the experiments, five samples for each thickness of Al6082-T6 and four tests per sample have been performed. The average roughness R_a was measured and can be calculated by Equation (4.1), as shown in Figure 4.15 [12].

$$R_a = \frac{1}{L}\int_0^L |y| dx \tag{4.1}$$

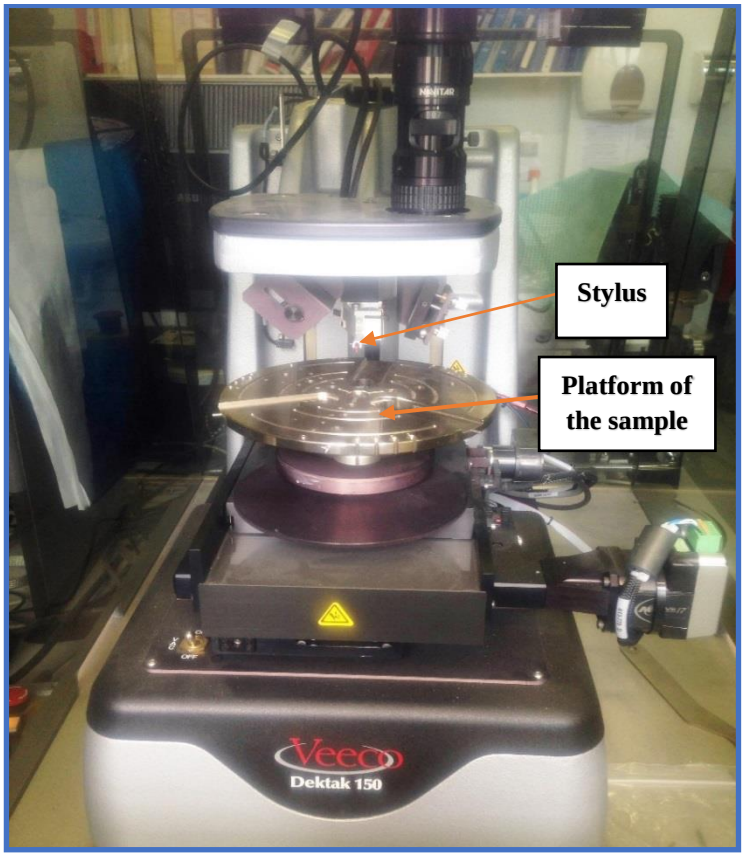

Figure 4.14 The Veeco Dektak 150 instrument.

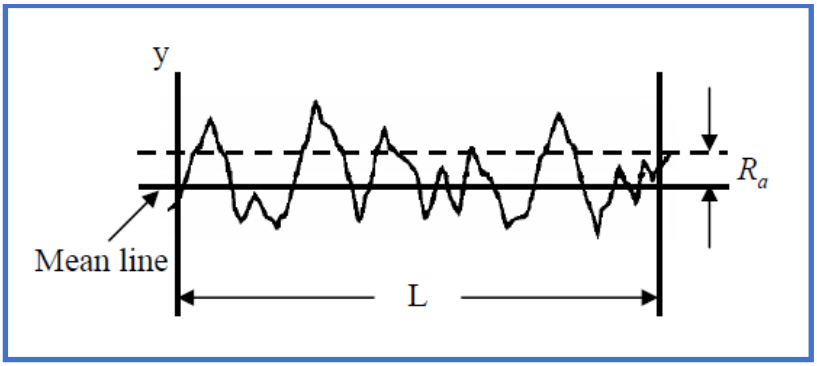

Figure 4.15 Scan surface roughness profile [12].

Beside the average roughness (R_a), ten-point mean roughness, or the mean roughness depth (R_z), was measured as a secondary output parameter because there are different structures that may have the same R_a and therefore these roughness measurements can have a more accurate description of the surface roughness. The calculation of R_z depends on the mean value of five individual roughnesses, as shown in Equation (4.2) and Figure 4.16.

$$R_z = \frac{1}{5}(R_{z1} + R_{z2} + R_{z3} + R_{z4} + R_{z5}) \quad (4.2)$$

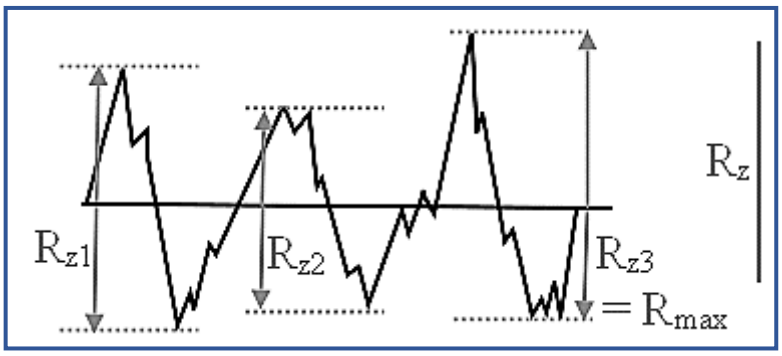

Figure 4.16 Scan surface profile of the mean roughness depth [124]

The resulting side profile before and after the pre-treatment was shown in Figure 4.17. The effect of pre-treatment on the surface roughness is clearly shown. The surface roughness was increased due to the anodising process by creating a rough surface. The peaks and valleys of asperity after pre-treatment become higher than before pre-treatment. Additionally, these asperities, created after pre-treatment, are very dense. While, the surface profile of Al6082 sample without pre-treatment was formed as a wave due to the rolling direction during manufacturing, as previously shown in Figure 4.13a. In practice term that means that the mean line of surface roughness after treatment is higher than before pre-treatment.

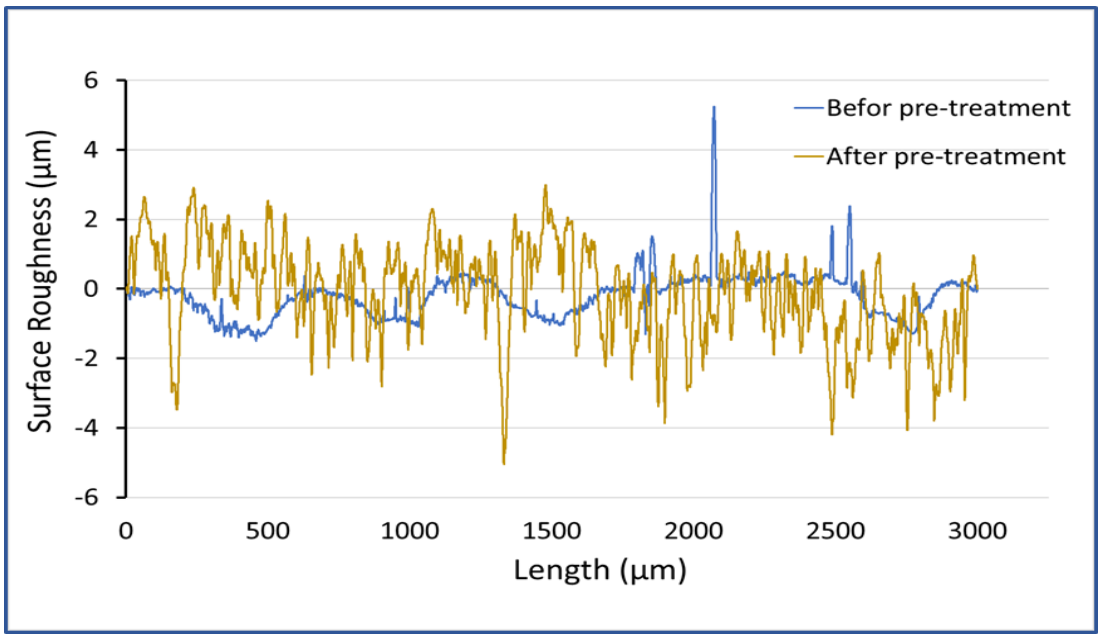

Figure 4.17 Side profile of roughness before and after pre-treatment.

Several steps were followed in order to ensure the consistency of the produced surface roughness. Based on Sections 8.2.3.3 and 8.2.4 in ASTM D3933-98(2010), a fresh tank of solutions was used every five samples during the anodising process to avoid any contamination which may cause changes in the solution's properties. The surface roughness of these five samples was measured to ensure consistency. In addition, the measurements of surface roughness in different batches were repeated five times during the overall joining time to check for any different values and found to be within ±0.07μm of each other. The polymer ABS were joined with the treated sheets of Al6082 within 72 hours after the anodising process to avoid the possibility of inadvertent contamination (Section 7.7 in ASTM D3933-98 (2010)). Therefore, the values of the surface roughness are guaranteed not to have changed before experimental runs.

The results of surface roughness for Al6082-T6 are tabulated in Table 4.6, whereas the full results of the experiments are given in Appendix (B). The results showed that the surface roughness after treatment is fairly consistent because the results of the surface roughness after pre-treatment is approximately very close. In addition, the results observed that the consistency of roughness on the treated samples appears to be unaffected by the roughness before treatment.

Table 4.6 The surface roughness of Al6082-T6.

Thickness (mm)	Before pre-treatment (μm)		After pre-treatment (μm)	
	R_a	R_z	R_a	R_z
1	0.487 ±0.03	2.27 ±0.15	0.94 ±0.05	4.37 ±0.22
1.5	0.33 ±0.09	1.54 ±0.39	1.042 ±0.06	4.84 ±0.28
2	0.37 ±0.08	1.72 ±0.37	1.007 ±0.04	4.68 ±0.1

4.4 Ultrasonic Joining Procedure

The ultrasonic joining machine used in this work is shown in Figure 4.18. The USW system is comprised of a US generator (Telsonic Ultrasonics - Model SG-22-5000-3), a US transducer or convertor (Telsonic Ultrasonics - Model SE

2050 A), a booster (Telsonic Ultrasonics – Model 1.5QC), a bonding horn or sonotrode (circular end tip 39mm diameter, made from Titanium), a moving anvil, an air compressor (Bambi - Model MD 150/500) with pneumatics circuit, and fixing tools.

Power is supplied to the transducer by the US generator and this electrical signal is converted into mechanical vibration by the US transducer. The operating frequency is 20 KHz and the amplitude is between 14 -21 μm. This range of vibration amplitude was achieved and amplified by the booster and the vibration was then taken to the samples by the sonotrode. The air compressor moves up and down the anvil, thus the bonding force (static force) can be measured by this movement. This compressor supplies a static force between 450 - 2350 N. This force can be controlled by the pressure regulator and the pressure sensor in the programmable logic controller (PLC) displays the values. The PC is connected to the PLC by a specific cable. The bonding and holding time were controlled by computer. The start button for the joining is on the PLC programme and when it is pressed, the ultrasonic joining was operated at the selected bonding force, bonding time, and hold time.

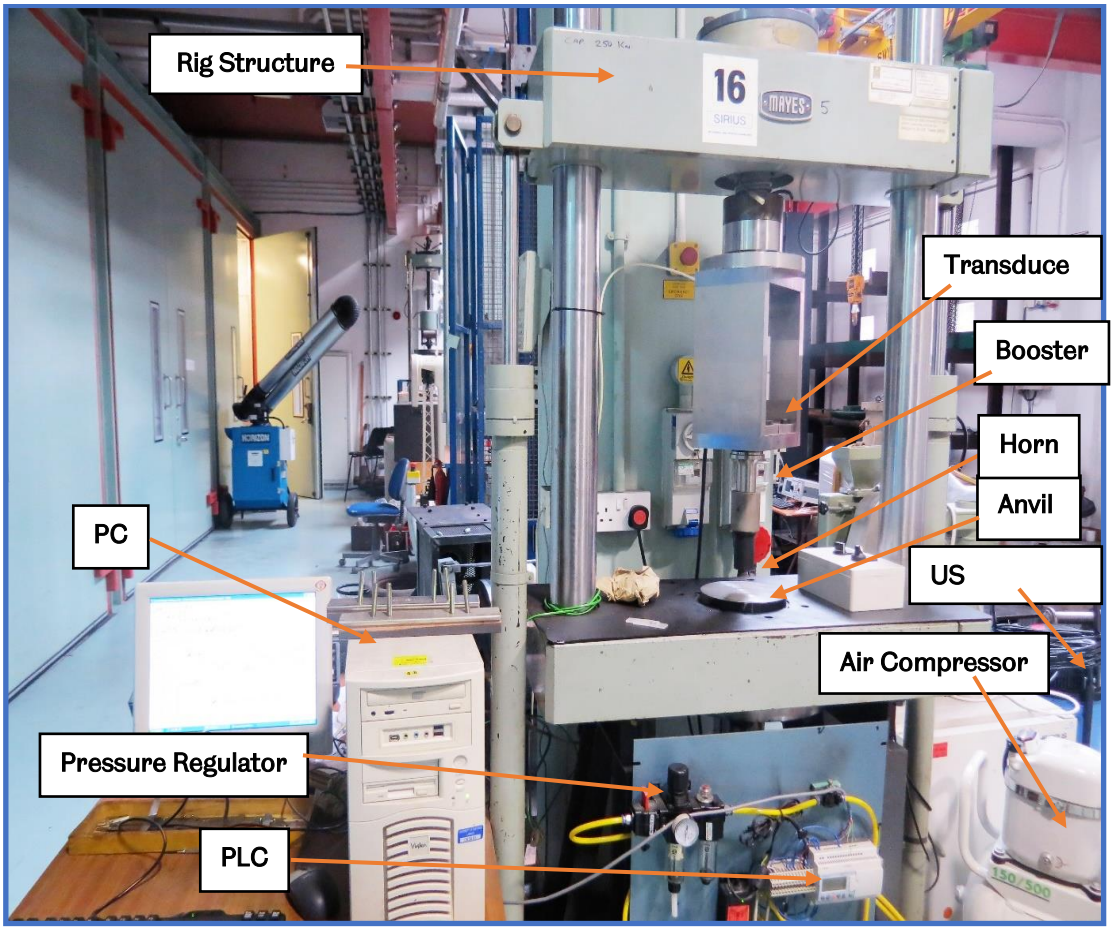

Figure 4.18 The ultrasonic joining device.

A fixing tool was designed and manufactured to align the specimens during the joining. The fixing tool is shown schematically in Figure 4.19. The specimens were placed between two fixtures and these fixtures were placed in a slot located in an aluminium block, with this block fixed to the anvil. The centre of the block was positioned in the centre of the anvil in the same position as the horn tip's centre. Therefore, any horizontal plane movement of the specimens was avoided.

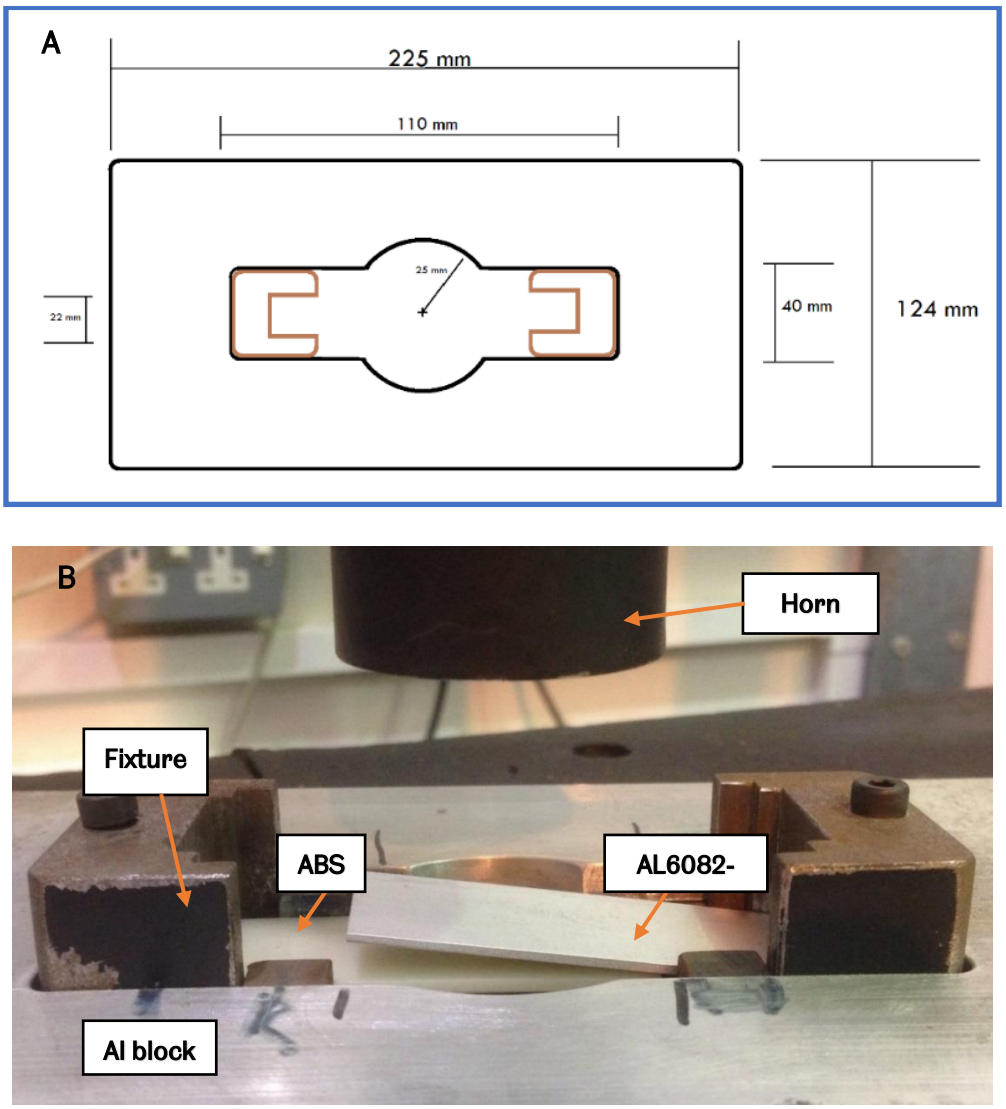

Figure 4.19 Fixing tool system A) dimensions of the tools, thickness of block is 6 mm, B) installation of the tools.

4.4.1 USW Rig Validation

To ensure the reliability of results, the ultrasonic joining machine was validated. It is important to collect accurate measurements of machine parameters, such as vibration amplitude, bonding force, bonding time and hold time because they give an impression on the reliability of results.

The values of vibration amplitude are stabilised by the manufacturer to ±2%. Although there is variation of amplitude measurement, this value of variation is very low compared with ±9% in literature by Van Wijk [106].

The bonding force that is supplied by the compressor is controlled by the pressure regulator and the pressure sensor in the programmable logic controller (PLC) displays the values. Load measurement was conducted by the manufacturer various times before starting to use the rig to check the accuracy of the PLC's pressure sensor. Therefore, the measured load has stabilised to ±1%. There is a table to convert the values that are shown in the PLC into force meter in Newton, as shown in Appendix (C).

The control of bonding time and holding time was computerised with the help of a PLC programme. As its programming language, the PLC system includes a timer block with basic unit 10ms and therefore these blocks were used to measure the ultrasonic time and hold time in the present research. The accuracy of the timer block is similar to the scan of the program. The PLC operates by continually scanning programs and repeating this procedure many times per millisecond to check the input and output status. Therefore, the measurement of time in the current research has a high level of precision. Table 4.7 summaries the accuracy of every bonding parameter.

Table 4.7 The accuracy of the parameters' measurements.

Bonding Parameter	The Percentage of Variation
Vibration Amplitude	±2%
Bonding Force	±1%
Bonding and Hold Time	±Millisecond

As a further check, the validation of the USW rig has been carried out by comparing the results from the current rig with the existing literature.

The literature [105] was used to compare its results with the current rig validation. Near-field ultrasonic bonding of thermoplastic materials (ABS polymer) was used in [105]. The bonding parameters used in the validation process are tabulated in Table 4.8.

Table 4.8 Bonding parameters of calibration.

	Material	Frequency (KHz)	Bonding Time (sec)	Vibration Amplitude (μm)	Boding Pressure (bar)	Hold Time (sec)	ED Shape
Referenced Factors	ABS	20	0.3	24	3.45	0.5	Triangular
Current Factors	ABS	20	0.3	21	3.45	0.5	Triangular

According to the above parameters (Table 4.8), there is a difference value of vibration amplitude level because the current generator can provide vibration amplitude 21 μm as the maximum value.

The validation results showed a slight different in the joint strength between the literature and the current bonding, as illustrated in Table 4.9.

Table 4.9 The calibration results.

	The Literature [105]	The Current Research
LSS (MPa)	9.135	7.974

The difference in the joint strength was about 12.7%, and this value is probably because the vibration amplitude affects the LSS (the percentage of difference in the vibration amplitude is 14.29%). In the literature [105], when the amplitude increased linearly around 15%, the joint strength increased by about 9%.

Therefore, these results provide some confidence that the current rig can be adopted in the current study that results can be expected to be comparable with those discussed in other literature.

4.5 Experimental Testing

4.5.1 Measurement of LSS

The lap shear strength (LSS) was determined by using a tensile / shear strength test method for the bond. This test depends on applying a tensile force parallel to the bond zone plane.

In this study, a Tinius Olsen H5KS device with a laser extensometer (500L) was used to test the strength of the bonded specimens This device consisted of a computer control for data logging, acquisition and calculations, load cells (5KN), dumbbell and roller grips. The specimen was physically fastened to the load cell using grips, and all tests were carried out under ambient conditions.

ISO527-1:1996 provides a standard for this type of testing but does not specify a value for crosshead speed. Based on technical advice provided for the machine used, low speeds were deemed most appropriate due to a relatively high phase mobility of the amorphous polymer and therefore less potential for damaging the polymer itself. Low speeds of 1, 2, and 5mm/min were therefore selected. These speeds were tested to identify the sensitivity of the process, as shown in Figure 4.20, and showed approximately identical breaking force. This ensured that any fluctuations in machine speed should not affect the results obtained.

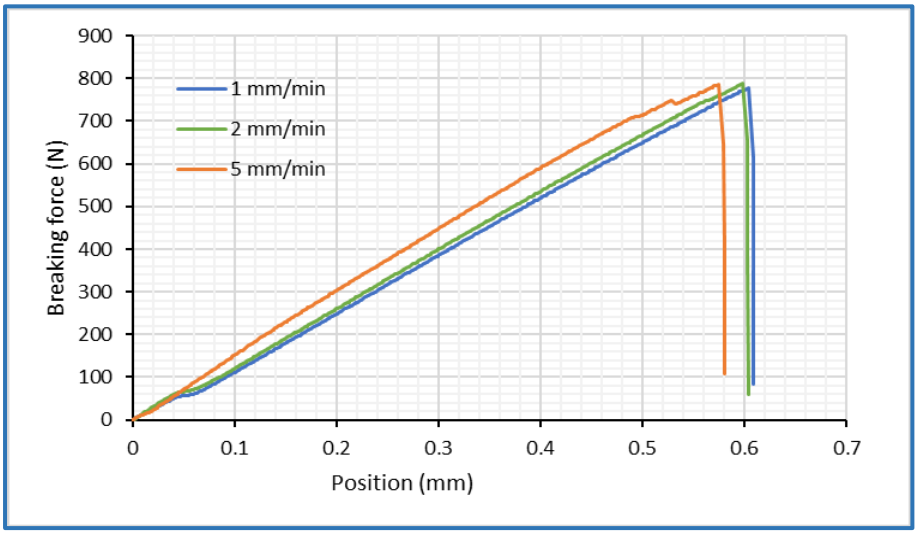

Figure 4.20 Effect of crosshead speed on breaking force.

As shown in Figure 4.20, there is a drop-in force at the initial stage of tensile test. This slight decrease is likely result from the joint failing in small areas at the interface due to low-density bonding in these areas (e.g. due to incomplete filling of the rough metal surface by the melted polymer).

As shown in Figure 4.21-A, the standard grips of the device are at the standard alignment position. Due to the non-symmetric nature of the samples, testing in this manner would mean both tension and bending forces would act on the samples, rather than simply tension. To account for this, grips designed in a previous research study [30] were used to ensure the line of tensile force action would pass through the joint area (Figure 4.21-B).

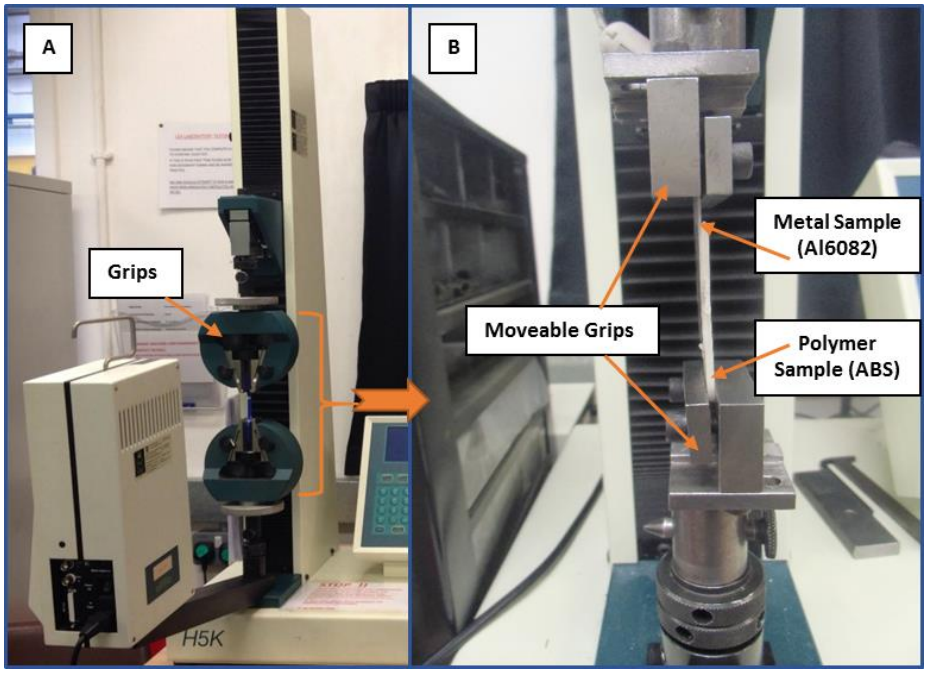

Figure 4.21 Motility grips for lap joint.

After testing, the LSS of the bond was calculated by dividing the shear force required to break the joint by the approximate area measured using Vernier callipers. This technique was used previously to measure the fractured joining area during the ultrasonic process [30].

4.5.2 Temperature Measurement

During the joining process, the temperature in the bonding region was measured to determine the effects of bonding temperature on the quality of joints. Achieving the required joining temperature is important to produce a

bond because the polymer phase changes depend on this temperature. Moreover, the joining temperature is an indication of the energy that reaches the bonding zone.

The temperature generated in the bond region may have an effect on the quality of the joint and bond strength. In this work, the temperature at the bonding region during the bonding process was measured to study the effects of the bonding temperature on the LSS.

The data acquisition system that was utilised consisted of thermocouples (type K (CHAL-005) from OMEGA), a printed circuit board (PCB) with an amplifier (AD595 with cold junction compensation CJC) and a low pass filter, a data acquisition card (DAQ card NI USB-6008 from National Instruments), and analysing software (LabView). The block diagram of the DAQ system is shown in Figure 4.22, and the experimental setup of the temperature measurement system is illustrated in Figure 4.23.

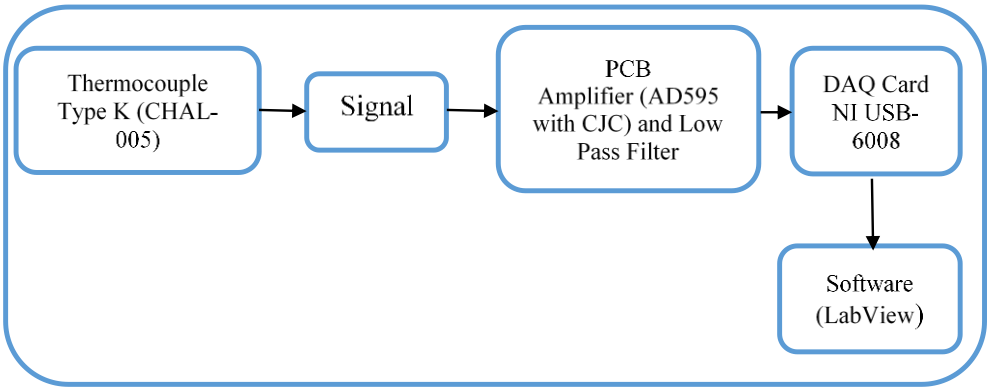

Figure 4.22 Data acquisition system.

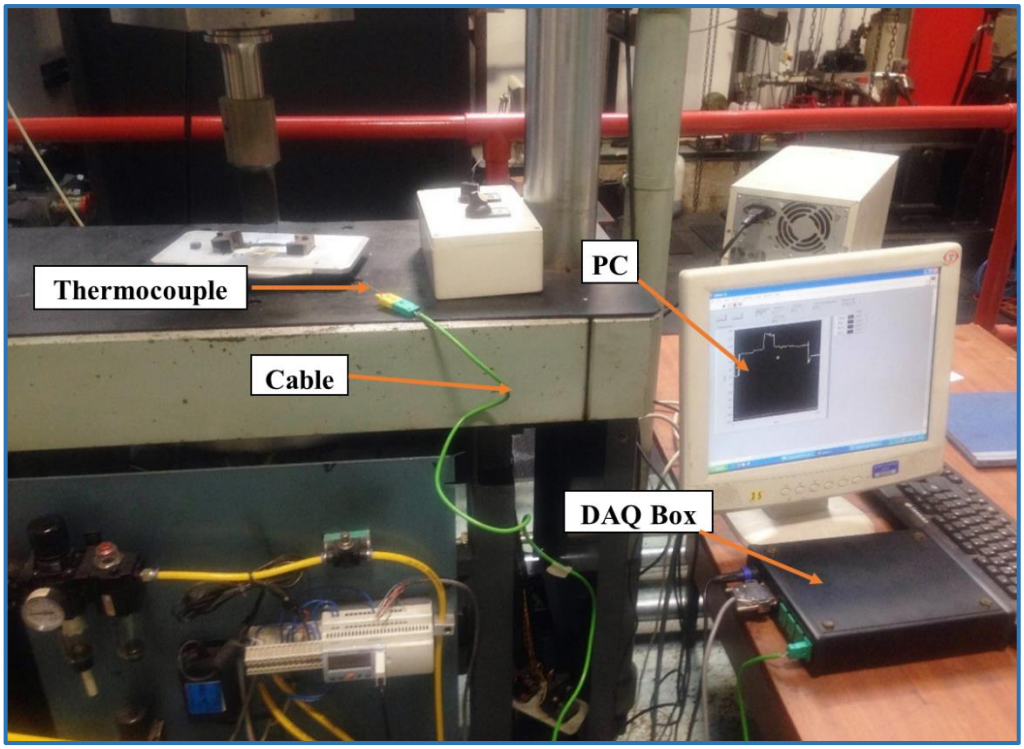

Figure 4.23 Experimental setup of temperature measurement system.

All the thermocouples (18 thermocouples) used in this research were calibrated using a few basic instructions as follows:

1- Put ice in a container to have the freezing point of water 0 ^{0}C.
2- Measure the ice point by the thermocouples and an accurate reference thermocouple (the reference thermocouple is calibrated and checked periodically).
3- Heat the water in the container and measure the temperature by thermocouples and an accurate reference thermocouple for each approximately 10 ^{0}C increase to 100 ^{0}C.
4- Measure the deviation error for the differences between thermocouples and reference thermocouple measurements.
5- Adjust the read out by adjusting the offset to match or compensate for the error.

The results of thermocouples' calibration show the deviation of the Type-K thermocouple was 0.65±0.02 ^{0}C more than the reference thermocouple (the results of calibration are shown in Appendix (D). In other words, all the

temperature values that were measured in this work will be decreased by 0.65 ^{0}C.

After each thermocouple was calibrated, it was positioned at the interface of the flat surface of the Al6082 sample and energy director of the ABS sample, as shown in Figure 4.24. The thermocouple measured the temperature during the bonding process and transmitted it as a signal to the DAQ box by the cable. During the temperature measurements, the thermocouples were not damaged in the ultrasonic joining operation.

Since the thermocouple is a mini Type-K, the amplifier AD595 was utilised to amplify the electrical signal and then filtered by the low pass filter. The signal was then fed into the DAQ card (NI USB-6008) and transmitted to the PC by USB cable. The software (LabView) was used to obtain the temperature during the bonding process.

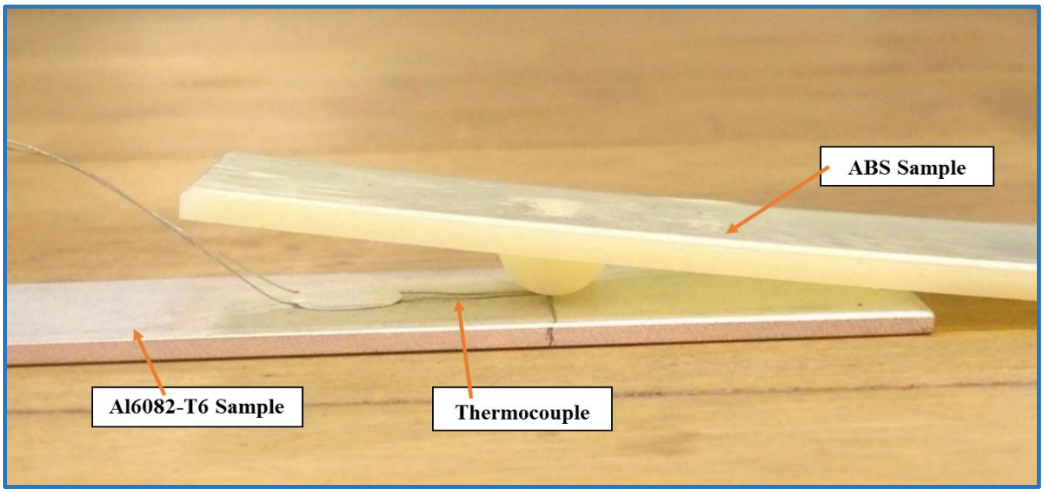

Figure 4.24 Thermocouple position on flat surface.

4.5.3 Microscopic Analysis

Generally, the microscopic analysis of joints is highly significant in examining the relationship between the joint performance and physical joint characteristics, such as bond density. Gaps and deformation in the interfacial joints have a negative impact on the bond quality. Microstructural analysis can therefore show effects of parameters on the interfacial bonds area of dissimilar materials in the joining zone.

In the current study, microscopic analysis, by optical microscope and SEM, was utilised to examine the cross section of the ABS-Al6082 joint before and after breaking the bond. Additionally, it was used to study the fractured surface, and the topography of Al6082 samples before and after the pre-treatment. This was done to clarify the effect of pre-treatment on the Al6082 sample surface, as shown previously in Section 4.3.3.

The model of optical microscope used in this study is a NIKON - Eclipse LV150. Each sample was put on the microscope stage and the appropriate objective lenses were selected. The objective lenses are five (5x, 10x, 20x, 50x, and 100x magnifications) and these are presented graphically as 500µm, 200µm, 100µm, 50µm, and 20µm respectively.

The SEM device used was a table-top HITACHI TM3030 PLUS with a premium SE detector as a high sensitivity detector. In addition, it can be operated effectively under low vacuum conditions and without sample preparation, such as sample coating. The magnification of this device is up to 120,000x with digital zoom.

Each sample was placed in the SEM chamber and fixed on to the sample platform using double sided tape. The suitable magnification and brightness were adjusted until the sample was in focus after closing the sample chamber and pressing the vacuum bottom to conduct the evacuation process.

To examine the samples in the microstructure examination the following process was undertaken:

- The first step was cutting the specimens perpendicular to the bonding interface using a Secotom-15/-50 table-top cut-off machine.
- Cold mounting of the sectioned piece used an epoxy system. This system involved using EpoxiCure2 (epoxy resin), and EpoxiCure2 (epoxy hardener). The resin and hardener were mixed and cured according to the products' directions.
- Grinding and polishing were carried out to prepare the cross section. This step was used to eliminate the damage from the sectioned area

and obtain a highly reflective surface. The steps for this point had to be in line with the laboratory standards for polymer and aluminium alloys' preparation matching.

The next step of this study is how the results were analysed to deduce meaningful information and identify the significance of the parameters and their interactions.

4.6 Initial Experimentations

Based on Section 4.2, the levels of the bonding parameters that are used in the initial experiments are shown in Table 4.10.

Table 4.10 Bonding parameters of initial experimentations.

Parameter	Unit	Initial Range	Parameter interval
Vibration Frequency	KHz	20	Constant
Vibration amplitude	μm	14.7 to 21	2.1
Ultrasonic Time	sec	0.2 to 3	0.4
Ultrasonic Force	N	500 to 1500	100
Hold Time	sec	0.5 to 1	0.25
Sample Thickness	mm	1 to 2	0.5
Energy Director (Polymer)	/	With and without	/
Surface Treatment (Metal)	/	With and without	/
Sample Position	/	Upper sample (polymer or metal)	/

The following procedure was adopted to identify the best conditions with which to achieve a joint between the Al6082-T6 and ABS samples, and to select a suitable range of bonding parameters for subsequent testing:

- The samples were bonded at the extreme conditions (the highest and lowest levels of all parameters) to identify the initial suitable ultrasonic energy range.
- Within the range identified, each parameter was varied one at a time, with all others remaining constant.

- The importance of the presence or absence of an energy director on the ABS sample, and of surface treatment of the Al6082-T6 sample was also assessed.
- The position (top or bottom) of the samples was varied in order to establish the optimum arrangement of the samples.

The order of experiments was randomised, and each set of parameters was repeated three times to check repeatability, as shown in Table 4.11.

Table 4.11 The structure of Initial Experimentations

No.	Amplitude (μm)	Bonding force (N)	Bonding time (sec)	Al6082 thickness (mm)	ABS thickness (mm)	ED (ABS) presence	Al 6082 Pre-treated	Time Holding (sec)	Sample position
1	14.7	500	0.2	1	1	no	no	0.5	ABS upper
2	14.7	500	0.2	1	1	yes	yes	0.5	Al upper
3	21	1500	3	2	2	no	no	1	ABS upper
4	21	1500	3	2	2	yes	yes	1	Al upper
5	18.9	1000	1.4	1.5	1.5	no	no	0.75	ABS upper
6	18.9	1000	1.4	1.5	1.5	yes	yes	0.75	ABS upper
7	18.9	1000	1.4	1.5	1.5	yes	yes	0.75	Al upper
8	18.9	1000	1.4	1.5	1	yes	yes	0.75	Al upper
9	18.9	1000	1.4	1.5	2	yes	yes	0.75	Al upper
10	18.9	1000	1.4	1.5	2	yes	yes	1	Al upper
11	18.9	1000	1.4	1.5	2	yes	yes	0.5	Al upper
12	18.9	1000	1.4	1	2	yes	yes	1	Al upper
13	18.9	1000	1.4	1.5	2	yes	yes	1	Al upper
14	18.9	1000	1.4	2	2	yes	yes	1	Al upper
15	14.7	1000	1.4	1.5	2	yes	yes	1	Al upper
16	16.8	1000	1.4	1.5	2	yes	yes	1	Al upper

17	18.9	1000	1.4	1.5	2	yes	yes	1	Al upper
18	21	1000	1.4	1.5	2	yes	yes	1	Al upper
19	18.9	500	1.4	1.5	2	yes	yes	1	Al upper
20	18.9	600	1.4	1.5	2	yes	yes	1	Al upper
21	18.9	700	1.4	1.5	2	yes	yes	1	Al upper
22	18.9	800	1.4	1.5	2	yes	yes	1	Al upper
23	18.9	900	1.4	1.5	2	yes	yes	1	Al upper
24	18.9	1000	1.4	1.5	2	yes	yes	1	Al upper
25	18.9	1100	1.4	1.5	2	yes	yes	1	Al upper
26	18.9	1200	1.4	1.5	2	yes	yes	1	Al upper
27	18.9	1300	1.4	1.5	2	yes	yes	1	Al upper
28	18.9	1400	1.4	1.5	2	yes	yes	1	Al upper
29	18.9	1500	1.4	1.5	2	yes	yes	1	Al upper
30	18.9	1000	0.2	1.5	2	yes	yes	1	Al upper
31	18.9	1000	0.6	1.5	2	yes	yes	1	Al upper
32	18.9	1000	1	1.5	2	yes	yes	1	Al upper
33	18.9	1000	1.4	1.5	2	yes	yes	1	Al upper
34	18.9	1000	2	1.5	2	yes	yes	1	Al upper
35	18.9	1000	2.2	1.5	2	yes	yes	1	Al upper
36	18.9	1000	2.6	1.5	2	yes	yes	1	Al upper
37	18.9	1000	3	1.5	2	yes	yes	1	Al upper

The results of these initial experimentations were used to inform the required parameters and their levels for using in the DOE experiments

(Section 4.7). The results of initial experimentations are presented in the next chapter (Chapter 5).

4.7 Experimental Structure

After selecting both the experimental design type and the parameters to be used in the investigation, the data collection matrix was created. Statistical software Minitab 17 was adopted to create the data collection by using the central composite design (CCD), as explained previously in Section 2.3. According to Section 4.6, the affected parameters in this study are vibration amplitude, bonding time, bonding force, Al6082 thickness, and energy director shape. These parameters are continuous or quantitative variables, except for the energy director shape, which is a categorical variable. The response of a continuous variable can be estimated at any point between the low to high level of variability. However, the response of a categorical variable is determined only at the selected level, i.e. it is not possible to estimate the response at a point between a triangular and a rectangular energy director shape because the shapes are fixed. In addition, experimental runs were repeated three times to reduce the effect of 'noise'.

Based on the CCD (Section 2.3.5), the number of levels for all parameters should be an odd number and equal for all used parameters. Since the shape of the energy director has three levels, all other parameters must also have three levels.

- **Vibration amplitude:**

Based on the screening results (Section 5.1), the space of vibration amplitude was between 14.7 and 21µm. While the lowest level of 14.7µm would be feasible, the aim of this work is to focus on achieving high levels of bond strength and therefore the higher end of the possible range was selected. Therefore, the three equally-spaced values for vibration amplitude 16.8, 18.9 and 21µm.

- **Bonding time:**

The range identified in the screening results (Section 5.1) indicated a parameter space between 1 and 2 sec, and this was therefore divided into three equally-spaced values of 1, 1.5 and 2 sec.

- **Bonding Force**

During the initial experimentation to determine parameter space, a range of levels between 800N and 1100N was selected (Section 5.1), in order to cover the maximum range of potentially suitable parameters, as shown in Figure 4.25. During this experimentation it was found that these values were on the borderline between good and under/over-bonding. As the following experiments would rely on being able to achieve a good bond at a range of other parameters, it was decided to move slightly away from these borderline values and therefore 850, 950 and 1050N were selected to take forward.

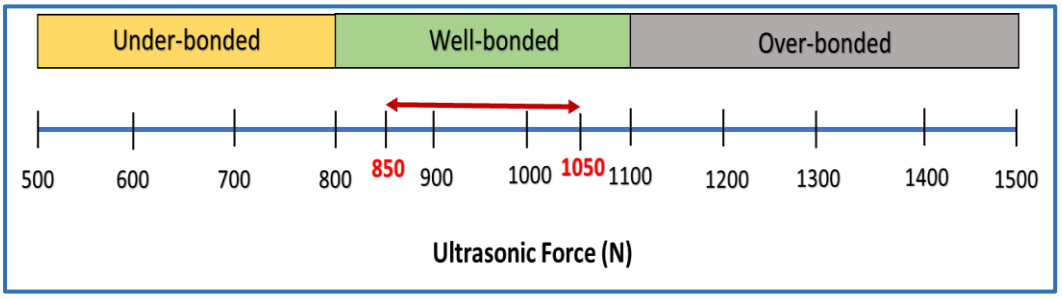

Figure 4.25 Selection of the level of ultrasonic force.

- **Al6082 Thickness**

The range identified in the screening results (Section 5.1) indicated the space of Al6082 thickness between 1 and 2 mm, and this was therefore divided into three equally-spaced values of 1, 1.5 and 2 mm.

- **Energy Director (ED)**

The importance of the presence of the energy director was identified in the screening results (Section 5.1) and therefore the shapes selected to use in this research are; triangular, rectangular and semi-circular.

According to Section 2.1.2.1, the energy director is a very important parameter on the joint strength. In addition, the importance of the presence of the energy director was investigated in the initial experimentations (Section 4.6) and showed it had a significant effect on the LSS. Thus, the current research studies the effects of the energy director on the joint strength. There are no standard dimensions for the energy director, with different dimensions having been used in existing research that has studied the energy director's effect on the LSS.

For example, the height of ED is (W/8) in [52], and [125], where (W) equals the total width of the polymer sample; the height is between 0.25-0.5mm in [14]. While the energy director height is 1.732mm in [40], or 3mm in [30], there are other dimensions of height in the literature. All these height dimensions are for a triangular shape. Thus, this study uses three of the most common shapes of energy director and these shapes have the same the height and base, as shown in Figure 4.26.

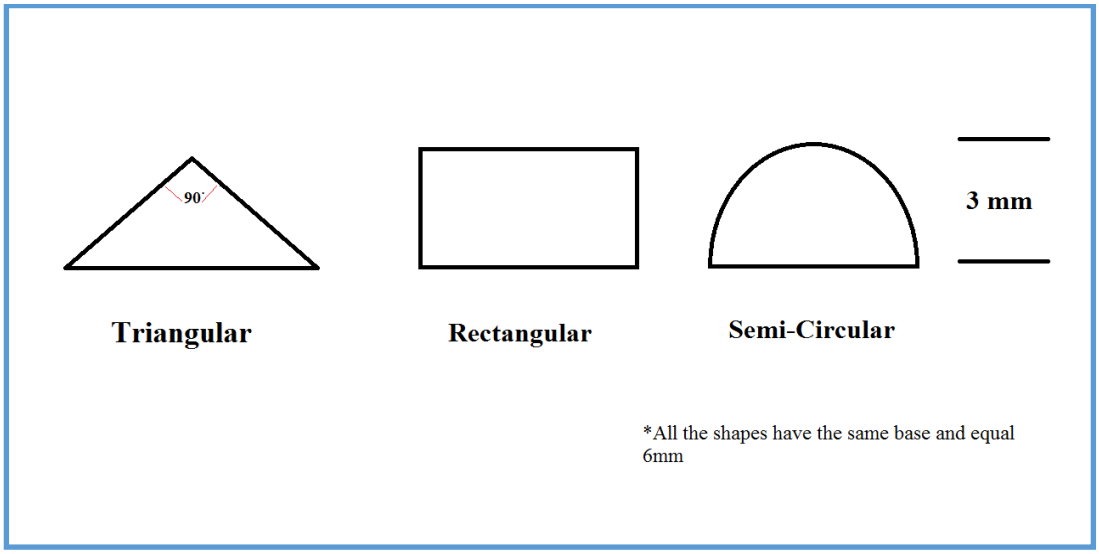

Figure 4.26 Shapes of energy directors.

As shown in Figure 4.26, the dimensions in the current study are larger than most of the dimensions in the literature since this will give a large amount of molten polymer, thereby improving the joint strength between metal and polymer by achieving the greatest joining area to get the highest LSS. The direction of EDs is transverse to the sample to reduce the flash and gain peeling resistance [17].

Therefore, Table 4.12 shows the levels of parameters used in the DOE experiments. The CCD created the data matrix for each energy director shape, as per Table 4.13.

Table 4.12 Parameter levels for the DOE experiments.

	Level 1	level 2	level 3
Vibration Amplitude (µm)	21	18.9	16.8
Bonding Time (sec)	1	1.5	2
Bonding Force (N)	850	950	1050
Al6082 Thickness (mm)	1	1.5	2
Energy Director Shape	Triangular	Rectangular	Semi-Circular

Table 4.13 The DOE Experimental structure.

Exp. run No.	Vibration Amplitude (µm)	Bonding Time (sec)	Bonding Force (N)	Al6082 Thickness (mm)
1	16.8	1.0	850	1.0
2	21.0	1.0	850	1.0
3	16.8	2.0	850	1.0
4	21.0	2.0	850	1.0
5	16.8	1.0	1050	1.0
6	21.0	1.0	1050	1.0
7	16.8	2.0	1050	1.0
8	21.0	2.0	1050	1.0
9	16.8	1.0	850	2.0
10	21.0	1.0	850	2.0
11	16.8	2.0	850	2.0
12	21.0	2.0	850	2.0
13	16.8	1.0	1050	2.0
14	21.0	1.0	1050	2.0
15	16.8	2.0	1050	2.0
16	21.0	2.0	1050	2.0
17	16.8	1.5	950	1.5
18	21.0	1.5	950	1.5

19	18.9	1.0	950	1.5
20	18.9	2.0	950	1.5
21	18.9	1.5	850	1.5
22	18.9	1.5	1050	1.5
23	18.9	1.5	950	1.0
24	18.9	1.5	950	2.0
25	18.9	1.5	950	1.5
26	18.9	1.5	950	1.5
27	18.9	1.5	950	1.5
28	18.9	1.5	950	1.5
29	18.9	1.5	950	1.5
30	18.9	1.5	950	1.5
31	18.9	1.5	950	1.5

The experimental runs in Table 4.13 were repeated for each shape of the energy director to study the effect of shape on the lap joint strength. Thus, the number of experimental runs for each trial was 31 runs $(31 = 2^4 + 2\,(4) + 7)$. In addition, each experimental run was repeated three times in order to reduce experimental errors. Therefore, the total number of experimental runs in this study is 279 runs (31 * 3 ED shapes * 3 trials). Based on Table 4.13, and Section 2.3, the experimental runs from serial number 1 to 16 are called the two-level factorial points. From serial number 17 to 24 are axial or star points, and from 25 to 31 are the centre point replications.

4.8 Summary

This chapter has identified materials, testing methods and parameters. The suitable range of bonding parameters' levels determined by the initial experimentations. These levels were used as a starting point in the experimental work of the current research (DOE experiments) to study the effect of bonding parameters on the lap shear strength and find the best levels of parameters that achieve the highest joint strength.

Chapter 5 INITIAL AND DOE EXPERIMENTS RESULTS

This chapter presents the initial and DOE experiments results. Additionally, the bond characterisation of ABS/Al6082 joints is explained in the current chapter.

5.1 Initial Experimentations Results

As explained in Section 4.6, the screening experiments were performed to identify the parameters for DOE experiments. The screening results were split into three categories; over-bonded joints, well bonded and under-bonded joints. The visual observations of the bonded samples were used to check whether any bond occurred. In addition, the sample was counted as too week if it was unable to be handled. The majority of parameter levels were determined to be acceptable based on having a 'well-bonded' joint. However, influence of hold time and ABS thickness was inconclusive so there were subjected to LSS tests, as shown in Section 6.1. The three phenomena are described briefly before discussing the results of the initial experimentation tests as follow:

- **Over-bonded Joints**

Over-bonded joints are produced due to the input of too much bonding energy that is transmitted to the joining zone [43]. The ultrasonic parameters, such as vibration amplitude, bonding force, bonding time and frequency can control the input ultrasonic energy, as previously shown in the literature review (Equation (2.10)). This extreme energy generated leads a drop-in viscosity and polymer being forced out of the joining zone, as shown in Figure 5.1. Thus, over-bonded joints can be avoided by reducing the levels of ultrasonic parameters.

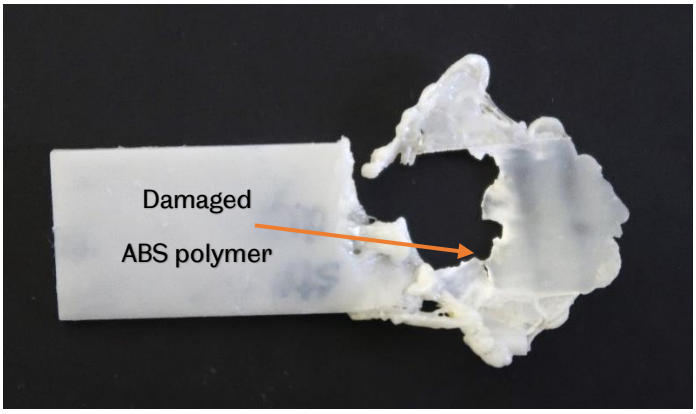

Figure 5.1 Over-bonded joint.

- **Well-Bonded**

Well-bonded joints are achieved when the input ultrasonic energy (Equation (2.10)) and the average dissipated energy that converts to heat (Equation (2.6)) are moderated through moderate levels of ultrasonic parameters. These joints featured dense interfacial bonds without gaps and high lap shear strength. Visual and manual inspection were used to identify this range where the bonds were enough to resist manual handling and not breaking easily, unlike in under-bonded joints. Additionally, the samples were not destroyed as in over-bonded, especially ABS polymers as shown in Figure 5.2.

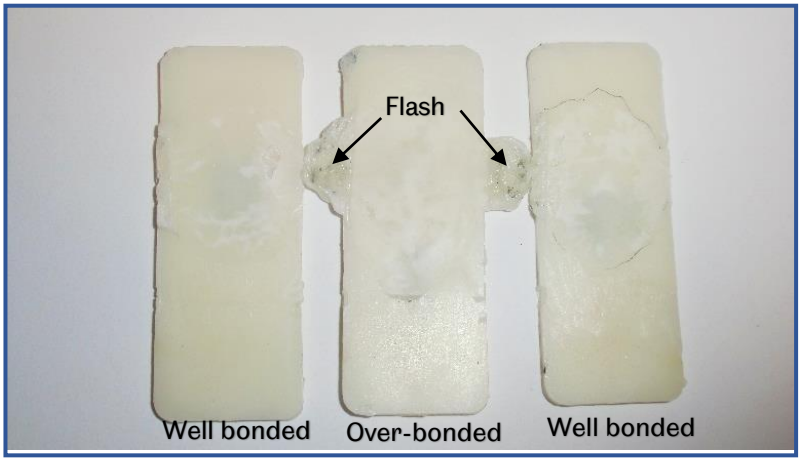

Figure 5.2 Comparison between well bonded and over-bonded joints.

- **Under-bonded Joints**

Under bonded joints between ABS and Al6082 occurred when insufficient energy was transmitted into the joint zone. This issue can be as a result of insufficient bonding time, bonding force or/and vibration amplitude. Insufficient ultrasonic energy generates low heat at the interface and this heat

was not enough to melt large amounts of the energy director (ED) of ABS samples because it did not reach the glass transition temperature of ABS polymer, as shown in Figure 5.3. Therefore, the produced joints were very weak, and in some cases no joints were created between ABS and Al6082.

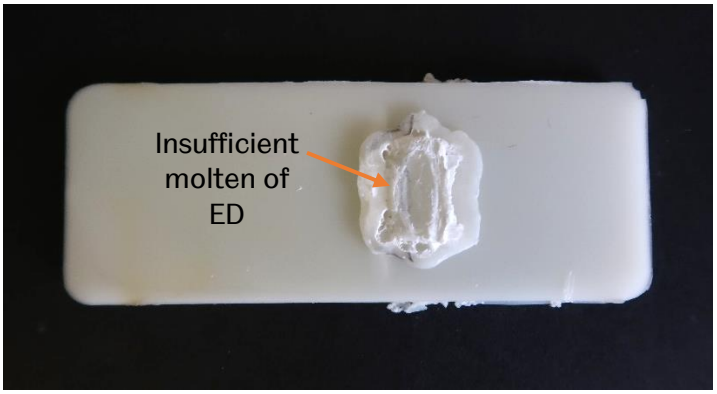

Figure 5.3 Under-bonded joint.

The results obtained from initial experimentations showed the following:

- **Vibration Amplitude**

The initial experimentations tested four levels of the vibration amplitude and showed that the highest three levels achieved well-bonded joints, as shown in Figure 5.4. The initial results were discussed in detail in Section 6.1.

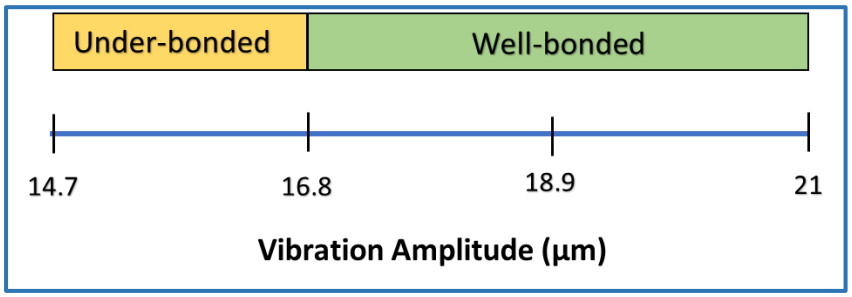

Figure 5.4 The initial results of the quality of ABS/AL6082 joints vs. the vibration amplitude.

- **Ultrasonic Time**

The initial range of the ultrasonic time was between 0.2 and 3 sec, as tabulated previously Table 4.10. The initial results observed that the range from 1 to 2 sec produced well-bonded, while below and above this range achieved under- and over-bonded respectively, as shown in Figure 5.5. The initial results were discussed in detail in Section 6.1.

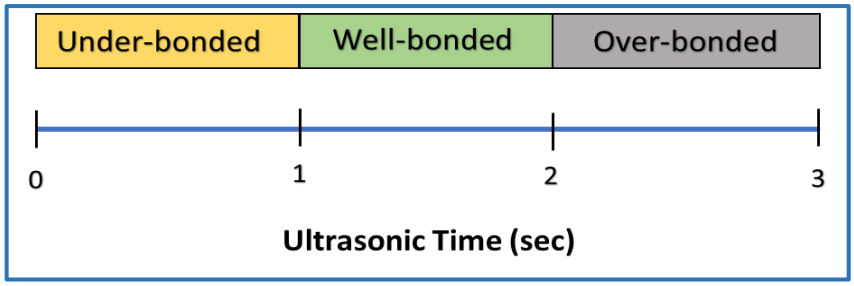

Figure 5.5 The initial results of the quality of ABS/AL6082 joints vs. the ultrasonic time.

- **Ultrasonic Force**

As tabulated in Table 4.10, the initial range of the ultrasonic force was between 500 and 1500 N. The initial results observed that the range from 800 to 1100 N produced well-bonded, while below and above this range achieved under- and over-bonded respectively, as shown in Figure 5.6. These results were discussed in detail in Section 6.1.

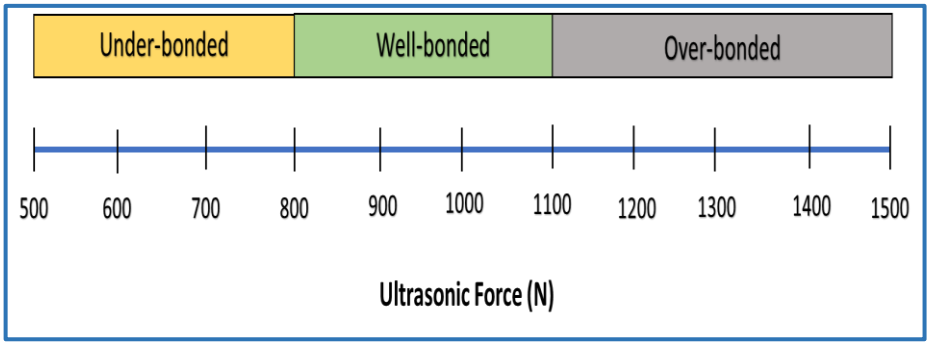

Figure 5.6 The initial results of the quality of ABS/AL6082 joints vs. the ultrasonic force.

- **Hold Time**

As tabulated in Table 4.10, the initial range of hold time was between 0.5 and 1 sec. The results observed that the bond strength was not affected by changing hold time, as shown in Figure 5.7. More discussions about this finding are explained in detail in Section 6.1.

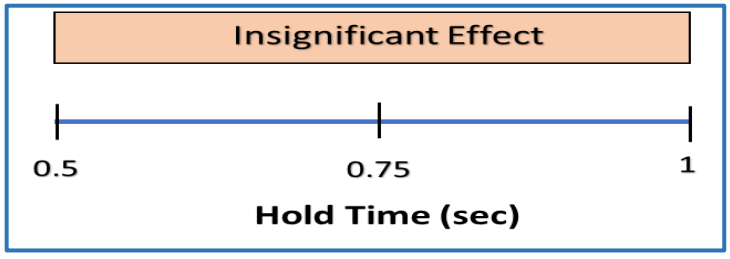

Figure 5.7 The initial results of the quality of ABS/AL6082 joints vs. hold time.

- **Sample Position**

As tabulated in Table 4.10, the initial range was tested two positions of the samples to be bonded. The upper sample was either metal, or polymer. The initial results observed that the well-bonded joint was achieved when the metal was the upper sample, more discussions about this finding are explained in Section 6.1.

- **Al6082 Thickness**

As tabulated in Table 4.10, the initial range of Al6082 thickness was between 1 and 2 mm. The initial results observed that the all range produced well-bonded, as shown in Figure 5.8.

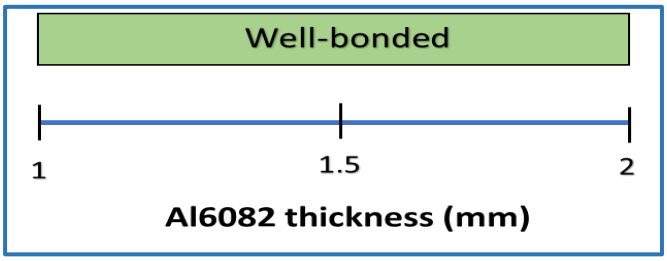

Figure 5.8 The initial results of the quality of ABS/AL6082 joints vs. Al6082 thickness.

- **ABS Thickness**

As tabulated in Table 4.10, the initial range of ABS thickness was between 1 and 2 mm. The results observed that the bond strength was not affected by changing ABS thickness, as shown in Figure 5.9. More discussions about this finding are explained in detail in Section 6.1.

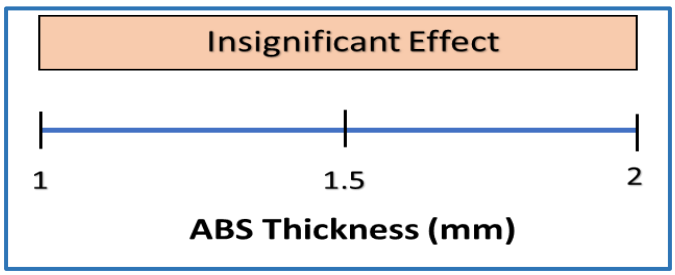

Figure 5.9 The initial results of the quality of ABS/AL6082 joints vs. ABS thickness.

- **The Presence of ED and Surface treatment**

As tabulated in Table 4.10, the initial experimentations examined the importance of using the energy director (ABS polymer), and pre-treatment of Al6082 samples. The results observed that the presence of ED and pre-

treatment was necessary to obtain well-bonded joints. More discussions about this finding are explained in Section 6.1.

5.2 Lap Shear Strength (LSS)

As discussed previously, a manual method of measuring area was chosen for this work, based on previous research [28]. In order to confirm the accuracy of this approach, a selection of samples was also measured using image analysis software. The ImageJ software was used as an alternative technique. This software is very useful because the most common productive joining areas were irregular in shape, as shown in Figure 5.10.

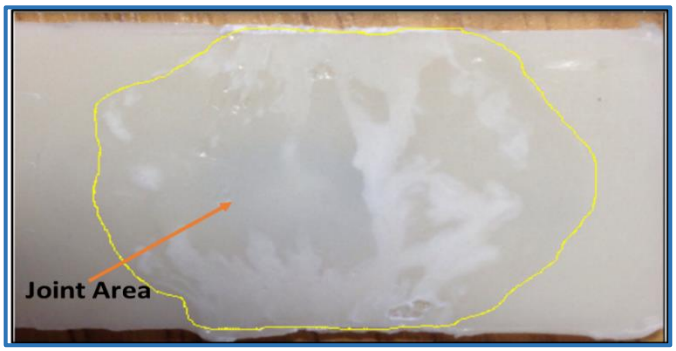

Figure 5.10 The irregular shape of the joint area.

A high-resolution camera (NIKON D3200) was used to capture the joint areas. These images were open using ImageJ software. At the beginning, the scale of photos should be set with known distance because the unit of distance in ImageJ is pixels. Therefore, the scale of distance in ImageJ software is 48 pixels/mm, as shown in Figure 5.11.

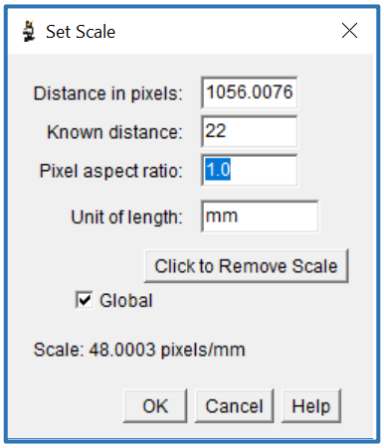

Figure 5.11 The set scale of distance in ImageJ software.

The images were adjusted using brightness/contrast and threshold options to make the joint areas clearer to select it, as shown in Figure 5.12. The default option of threshold method was selected to identify the joint area.

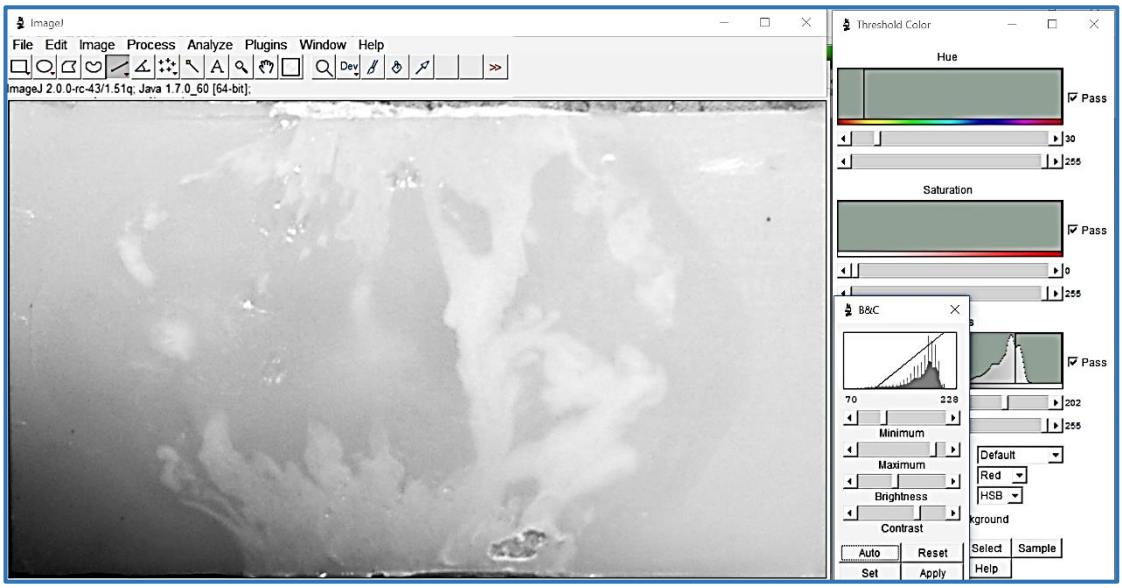

Figure 5.12 The adjustment of images.

Finally, the joint area was selected by drawing a line around the joint area and measured these areas by using measure option in the ImageJ software. Whereas, the manual method to measure the joint area depends on using Vernier and assume that the joint area is performed as oval shape, as shown in Figure 5.13.

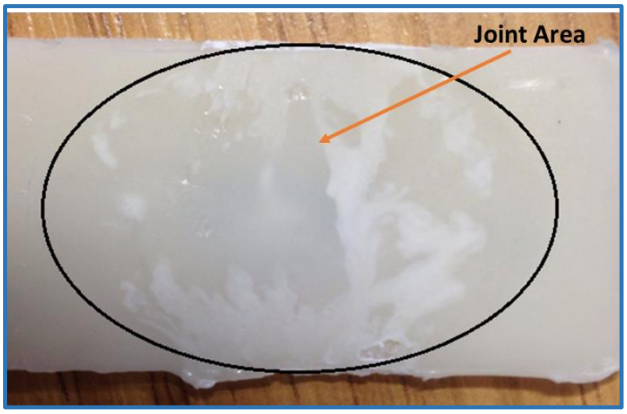

Figure 5.13 The joint area using the manual method.

Figure 5.14 shows the comparison in the joint area and LSS between using the manual method and ImageJ for different samples.

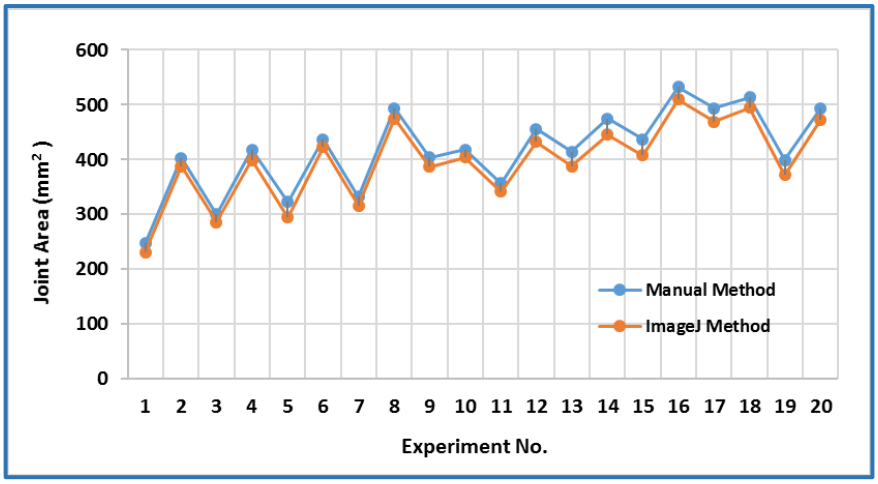

Figure 5.14 Comparison between manual and ImageJ methods for finding the joint area.

The results in Figure 5.14 show that the percentage difference between the two areas was varied 6.1 ± 2.8%. The joint areas that were measured by ImageJ were lower than those measured by Vernier (manual method) because the manual method depends on calculating the area by assuming it is an oval shape, while ImageJ takes into considerations any change in the shape. Therefore, the percentage difference between LSS (manual area) and LSS (ImageJ area) was varied between 3.4 - 9.77% based on the change of area joint with constant breaking force. Thus, the results were considered more reliable because there was little difference between the methods of measuring the joint area.

5.3 Effects of Main Parameters

The next step of this chapter is to show the results briefly together with the relationships between the parameters and the LSS. Thereafter, the results are discussed, and the relationships are explained in detail in a separate chapter (Section 6.2). The results section is divided into two parts. The first shows the results for the main parameters, while the results of parameter interactions form the second part. The full results of DOE experiments are shown in Appendix (E).

5.3.1 Vibration Amplitude

Vibration amplitude was found to have a linear effect on the LSS as shown in Figure 5.15. The mean of LSS increased by approximately 48% when the

vibration amplitude increased from 16.8 to 21μm. This relationship will be explained in detail in the discussion section (Section6.2.1).

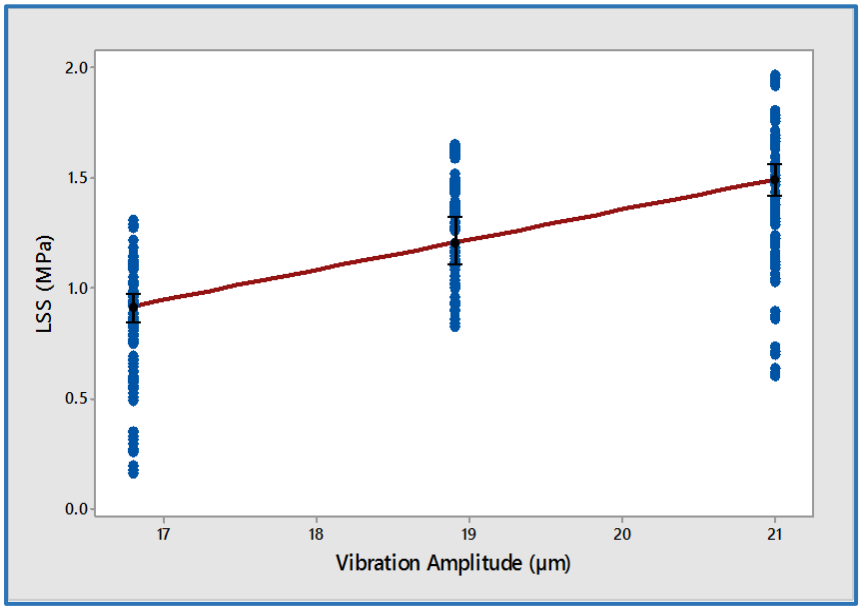

Figure 5.15 Relationship between vibration amplitude and mean of LSS. The all data points of DOE experiments are distributed at three levels of vibration amplitude. Each experimental run was repeated three times.

5.3.2 Bonding Force

The relationship between the bonding force and the mean of LSS is non-linear (curvy). As shown in Figure 5.16, the LSS increased about 11%, when the bonding force was increased from 850 to 910N by the sonotrode tip. The mean of LSS decreased by 44% when the bonding force was increased from 930N to 1050N.

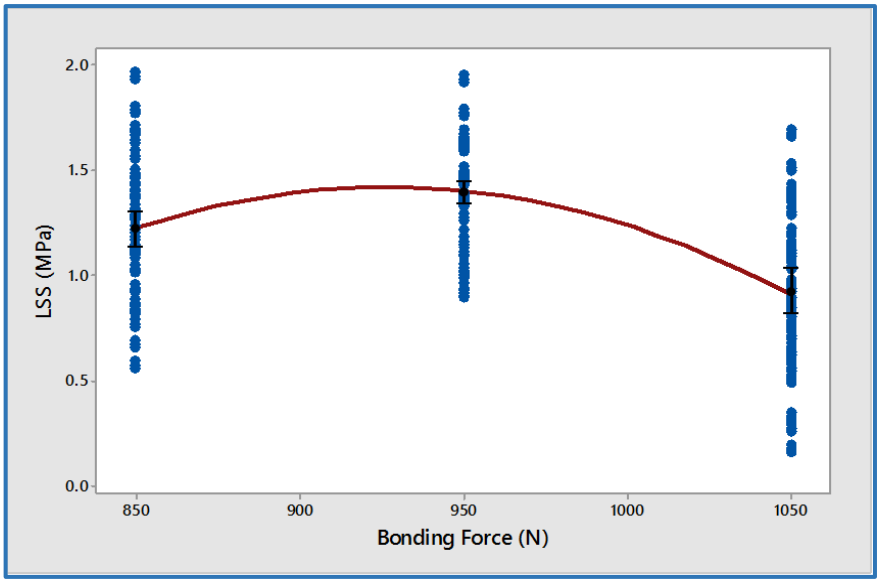

Figure 5.16 Relationship between bonding force and mean of LSS. The all data points of DOE experiments are distributed at three levels of bonding force. Each experimental run was repeated three times.

5.3.3 Bonding Time

As with the bonding force, the bonding time was found to have a non-linear effect on the mean of LSS, as illustrated in Figure 5.17. By increasing the bonding time, the joint strength increased about 12%, reaching the maximum value at 1.3 sec. However, the mean of LSS decreased by about 28% at 2 sec.

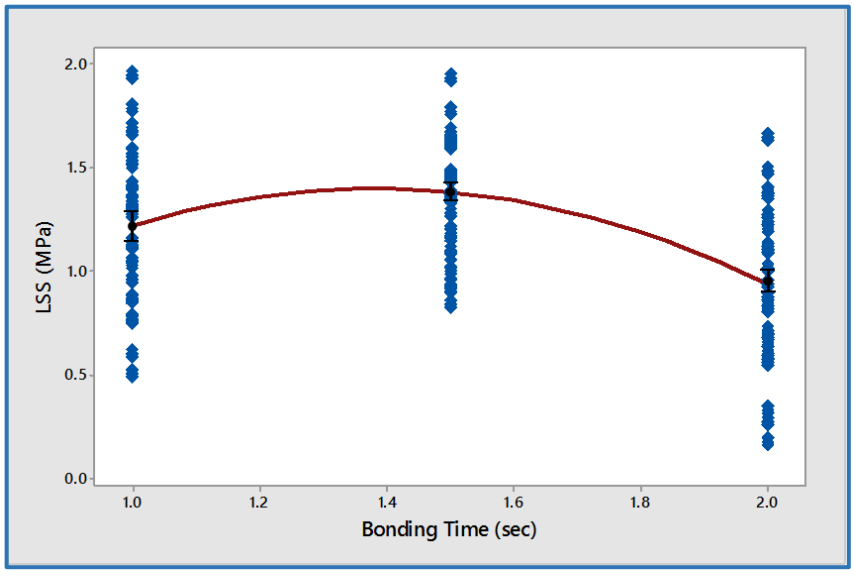

Figure 5.17 Relationship between bonding time and mean of LSS. The all data points of DOE experiments are distributed at three levels of bonding time. Each experimental run was repeated three times.

5.3.4 Al6082-T6 Thickness

According to Figure 5.18, the relationship between the mean of LSS and Al6082-T6 thickness (upper sample) is inverse, i.e. when the thickness increased, the mean of LSS decreased. In this study, the mean of LSS decreased by around 25% when the thickness of Al6082-T6 was increased from 1 to 2mm.

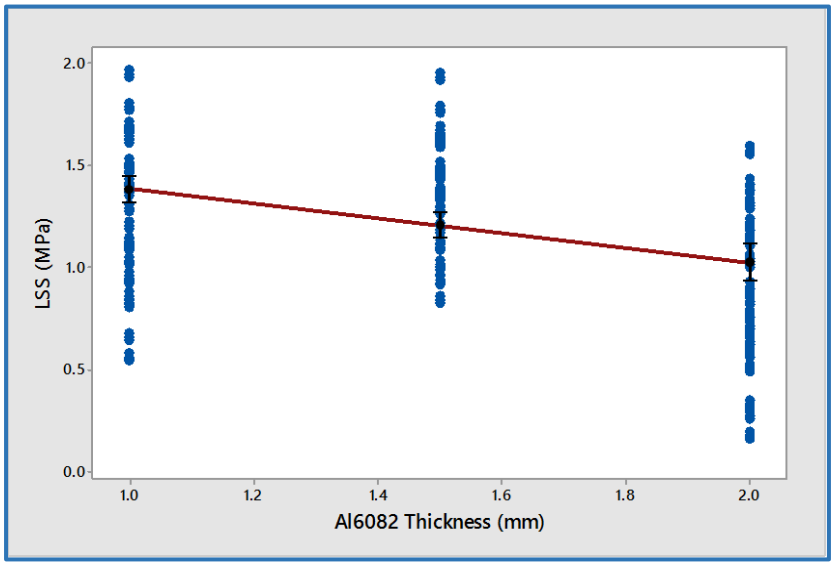

Figure 5.18 Relationship between Al6082 thickness and mean of LSS. The all data points of DOE experiments are distributed at three levels of Al6082 thickness. Each experimental runs was repeated three times.

5.3.5 Energy Director Shape (ED)

The energy director is important during the ultrasonic joining process as the energy concentrator used for polymer samples only (ABS 750SW). Figure 5.19 shows the effect of the shape of the energy director on the mean of LSS. The results show the triangular shaped energy director has a higher bonding strength compared with semi-circular and rectangular shapes under the same conditions. The rectangular shape had the lowest joint strength. The joint strength increased by approximately 20% when the triangular shape was used, compared with using the rectangular shape.

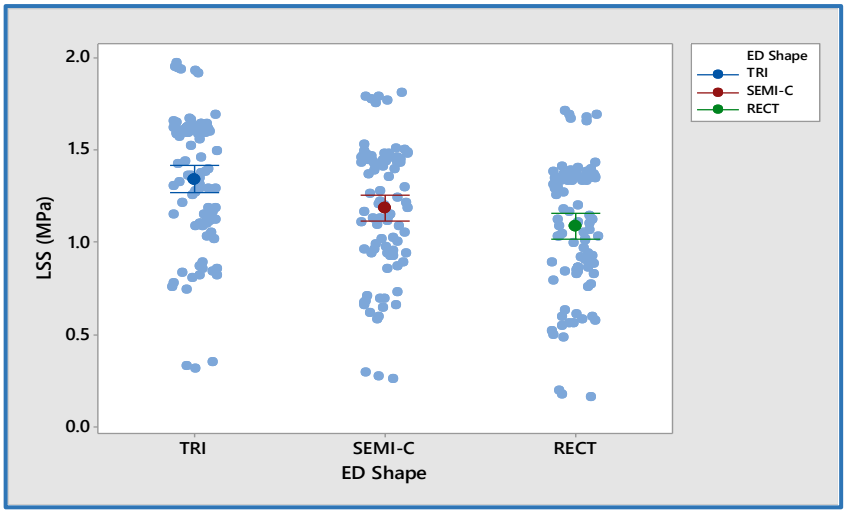

Figure 5.19 Relationship between ED shape and mean of LSS. The all data points of DOE experiments are distributed at three levels of ED shape. Each experimental run was repeated three times.

Based on Section 5.3, the optimum levels of parameters are shown in Table 5.1.

Table 5.1 The optimum levels of parameters.

Vibration Amplitude (μm)	Bonding time (sec)	Bonding force (N)	Al6082-T6 Thickness (mm)	ED Shape
21	1.2	931	1	Tri

The experimental test at these optimum levels of parameters was run for three trials. The LSS was found when the optimum levels of parameters were used, and it was 2.312±0.07 MPa.

5.4 Effects of Parameter Interactions

The explanation of parameter interactions was illustrated in Section 2.3.2. Six two-way interactions between the continuous parameters (vibration amplitude, bonding time, bonding force, and Al6082-T6 thickness) have an effect on LSS.

Furthermore, the energy director shape (categorical variable) had four two-way interaction effects with continuous variables (amplitude, bonding time, bonding force, and Al6082-T6 thickness). Therefore, the total number of parameter interactions was 10 two-way interactions that were investigated. Based on the ANOVA results (Table 6.3) Section6.3.1, most parameter

interactions had a significant effect on the LSS. Three interactions between parameters did not show a significant effect on the LSS: energy director interactions with bonding time, bonding force and Al6082-T6 thickness.

In general, the interaction of parameters becomes practically significant when the lines (the relationship between input and output variables) meet at a point within, or close to the given range of levels, as explained previously in Section 2.3.2. This can occur when the range of parameter is large enough to show the practical consequence of the parameter interactions [81]. For example, the vibration amplitude in the current thesis can only work between 16.8 and 21 µm, the variation in LSS during the interaction with other parameters over that range is around 45%, and it is therefore not show the practical significant of the interactions. Whilst the interaction becomes statistically significant when the lines converge without meeting, it can also be indicated when its P-Value is less than 0.05 (significance level), as explained previously in Section 2.4.2.6. Therefore, the statistical significance itself doesn't imply that the results have the practical consequence [126].

The profile plots of significant parameters' interactions will be shown and discussed in the next Chapter.

5.5 Bond Characterisation

According to the literature (Chapter 2), there are other aspects of the bonding process that may have affected the LSS, for example the hardness distribution around the joint area, the effect of ED collapse, and pit size (this is one aspect of fracture surface) on the LSS. This section will examine these effects in detail.

5.5.1 Al6082-T6 Samples

The melting temperature of Al6082-T6 is 555 ^{0}C (provided by company supplier (Wilsons Ltd)), while the maximum bonding temperature in the current research was 128 ^{0}C meaning the maximum bonding temperature was just 23% of the melting temperature of the base metal (Al6082-T6). Based on the literature [118] that investigated the changes in the microstructure of

Al6082-T6 between 25 to 250 ^{0}C by micrographs, the microstructure of Al6082 alloy should not be not affected up to 250 ^{0}C. Therefore, the maximum resultant bonding temperature (128^{0}C) should not have made any changes to the Al6082-T6 microstructure. To evidence this finding, the microstructure of Al6082 alloy was examined using a micro-hardness test in the cross section of Al6082-T6 at the bonding zone in this study.

5.5.1.1 Hardness Test

Hardness is the material's resistance to plastic deformation when another harder material applies a compressive load. The primary aim of the hardness test is to define the suitability of a material, or the particular treatment to which the material has been submitted. There are many types of hardness test, classified into two main groups depending on measuring style. Rockwell and Ball indentation hardness tests measure the depth of indenter penetration, while, the Vickers, Knoop, and Brinell hardness test measure the size of an impression left by the indenter.

In bonding, the hardness test is often used to check the quality of the bonded samples by measuring the hardness at various places across the sample especially around the heat affected zone.

In the current research, a micro hardness test was utilised to investigate whether the ultrasonic joining process has an effect on the microstructure of Al6082 alloy at the joint zone, which helped to understand if the Al6082-T6 samples had lost their properties and thus affected the joint quality. The device used in the measurement of hardness was Struers-DuraScan and its Vickers hardness test. The load test used was HV 0.05, corresponding to 0.4903N on the standard Vickers scale BS EN ISO 6507-1:2005 (BS 427: Part 1:1961). Four lines in the cross-section of the centre of bonding area were measured in terms of hardness and the distance between the lines was 0.5mm, as illustrated in Figure 5.20. In addition, each line had seven points with the first point starting from the bonding side to the other side of the material. The objective lens utilised in the hardness measurements was 40x.

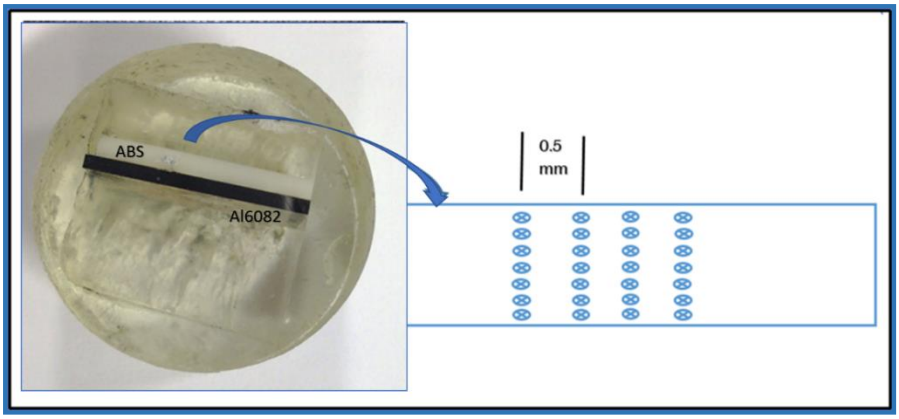

Figure 5.20 Hardness test sample.

Two samples were selected as having been subjected to the highest interface bonding temperature (Section 6.2.7), as tabulated in Table 5.2. Thus, if there had been any changes in hardness, they would have appeared in these samples.

Table 5.2 Hardness test samples.

No.	Vibration Amplitude (μm)	Bonding time (sec)	Bonding force (N)	Al6082 Thickness (mm)	ED shape	Temperature (°C)
1	21	2	1050	1	TRI	128
2	21	2	850	1	TRI	126

The results of the hardness test for the Al6082-T6 samples are shown in Figure 5.21. The figure shows the change in the hardness of the sample between its two sides (from the bonded side (interface) to the un-bonded side). The Al6082-T6 (base metal) hardness based on the micro hardness test was about 120 HV. The percentage increase in hardness at the bonded side was approximately 2.5%, and this percentage is very small and insignificant. The hammering which is the vibration of ultrasonic horn on the metal surface might be likely to cause a change in hardness [127], but there was no evidence of strain hardening. In addition, T6 (heat-treated) aluminium is very hard to dislocate or displace and that resulted in the high hardening (120HV) compared with O-conditions (annealed treatment).

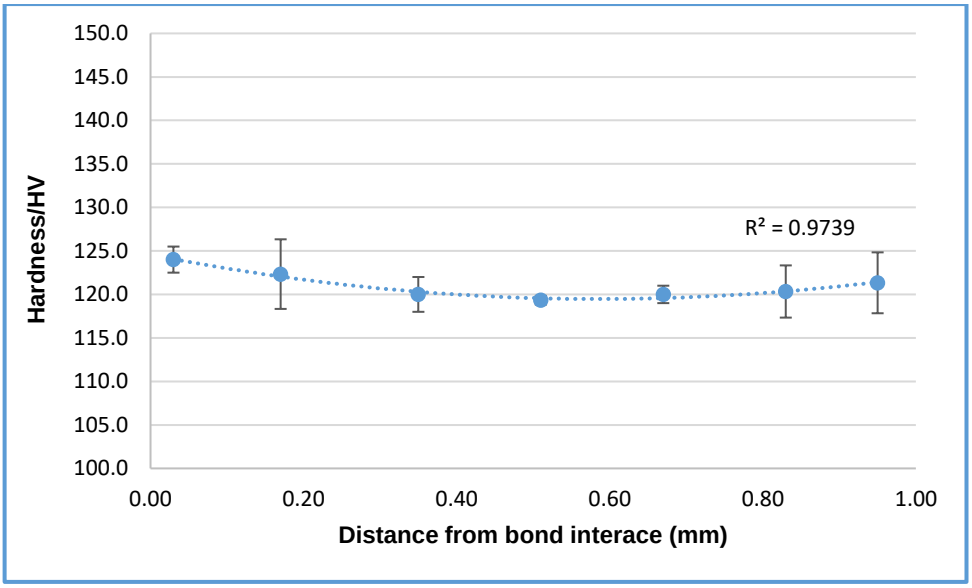

Figure 5.21 Micro hardness distribution along the cross section of Al6082.

Therefore, the results in Figure 5.21 indicate that there was no microstructure changing in the Al6082-T6 bonded sample because there was no significant change in the hardness even at the maximum temperature recorded in the samples.

5.5.2 ABS Samples

5.5.2.1 Effect of ED Collapse

The effect of ED collapse on LSS was investigated through examination of the final gap between the Al6082-T6 and ABS samples. A larger gap suggests less complete melting of the energy director (ED), which would be likely to result in a lower LSS. As explained in the existing literature, this gap is produced due to the collapse of the ED because of the joining process which produced a heat at the interface that leads to reach ABS to its glass transition temperature. The ABS polymer starts to melt after reaches its the transition temperature [39]. In the ultrasonic process, a portion of the ED melts and joins to the second sample, as shown in Figure 5.22.

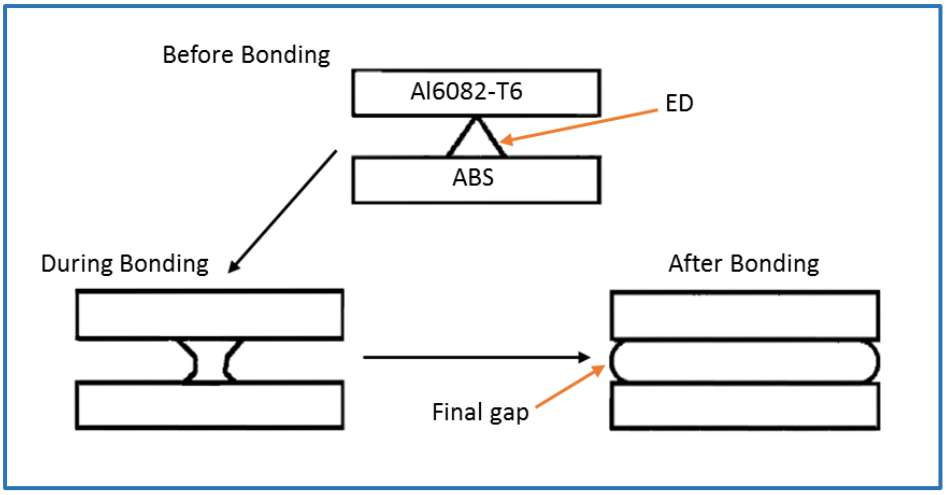

Figure 5.22 ED collapse during ultrasonic joining process.

The final gap is considered to be the melt thickness of the ED, as shown in Figure 5.23. The wanted final gap should be a small, but not zero-gap. This is because the zero-gap means that all molten polymer is pushed out of the joint area.

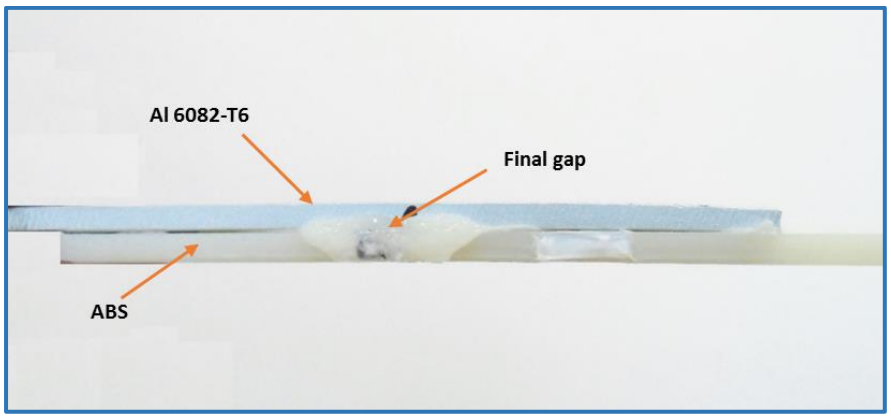

Figure 5.23 ED collapse of ABS sample.

To examine and measure the ED collapse (ED collapse = ED length – final gap), a Vernier calliper and microscopic analysis were used. The samples used to investigate the relationship between ED collapse and LSS are tabulated in Table 5.3. These samples have been selected because each parameter has one degree of freedom in level. In other words, each bonding parameter has two levels.

Table 5.3 ED collapse for different parameters.

No.	Amplitude (μm)	Bonding time (sec)	Bonding force (N)	Al6082-T6 thickness (mm)	ED shape	ED collapse (μm)	LSS (MPa)
1	21	1.5	950	1	Tri	2956.5	1.925
2	18.9	1.5	950	1	Tri	2849	1.609
3	18.9	1	950	1	Tri	2798	1.645
4	18.9	1.5	950	1.5	Tri	2689	1.515
5	18.9	1.5	850	1	Tri	2590	1.504
6	18.9	1.5	950	1.5	Semi-C	2383	1.454
7	18.9	1.5	950	1.5	Rect	2189	1.337

Therefore, the relationship between ED collapse and LSS is shown in Figure 5.24.

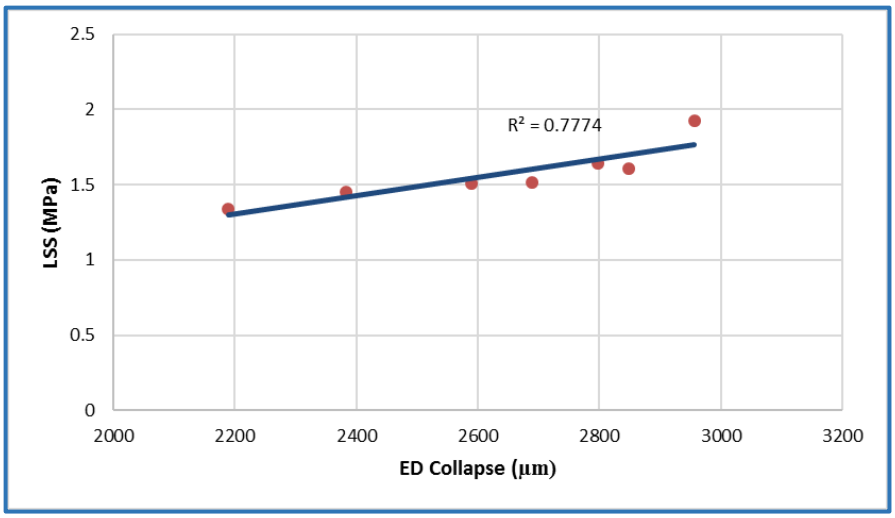

Figure 5.24 Relationship between ED collapse and LSS.

Figure 5.24 shows an increase in LSS of approximately 44% when the ED collapse increases from 2189 to 2956.5 μm. The increase of ED collapse

produced a bigger contact area between the upper and lower samples, thus increasing the LSS. An example of ED collapse under SEM is shown in Figure 5.25. The possible reasons for producing higher ED collapse are utilization of high level of ultrasonic parameters and higher loss modulus for ABS [30]. Therefore, the increase of vibration amplitude, bonding time and bonding force led to achieve higher ED collapse, as shown previously in Table 5.3.

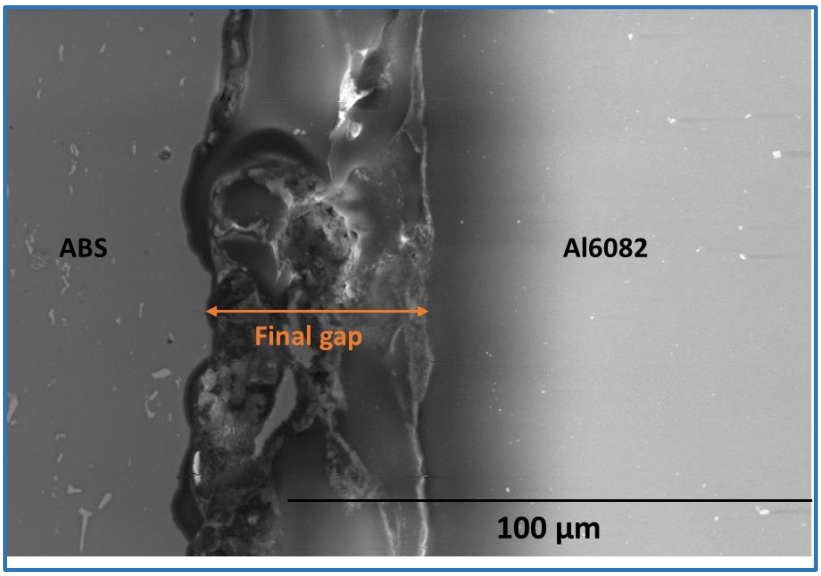

Figure 5.25 ED collapse for serial number 1 in Table 5.3 (21µm vibration amplitude, 1.5sec bonding time, 950N bonding force, 1mm Al6082 thickness, and triangular shape of ED).

In addition, the collapse of the triangular shape was greater when compared with the rectangular and semi-circular shapes, as shown in Figure 5.26. The volume of the triangular energy director (90mm^3) is the lowest compared with the rectangular (180mm^3) and semi-circular (141.37mm^3) EDs, meaning the triangular ED melts quickly and starts to flow inside the pores of the Al6082 surface.

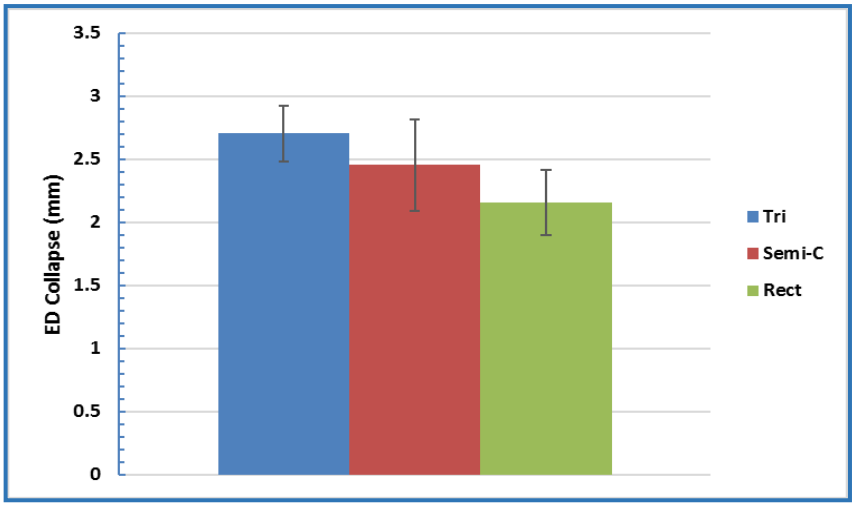

Figure 5.26 ED collapse at 18.9 µm, 950N, 1.5 sec, and 1.5mm thickness of Al6082.

The collapse of ED results due to material flow at the interface and the excess of molten polymer flows outside the joining zone to produce the flash, as explained previously in the existing literature. It is possible that there may be some thermal decomposition of the polymer during melting, which may also cause an effect on LSS. This is investigated in the subsequent sections, through DSC and TGA measurements

- **Differential Scanning Calorimeter (DSC)**

The DSC was adopted to measure the thermal characteristics of the polymer, such as glass transition temperature (T_g), melting temperature, specific heat, and decomposition of the polymer. In addition, the DSC provides quantitative and qualitative information about physical and chemical changes in a material that involves endothermic and exothermic processes. The DSC has many advantages, for example, its quick analysis time (about 30 minutes), easy preparation of material, used with both solids and liquids, and its wide range of temperature applicability.

In this research, the DSC was utilised for bonded and un-bonded polymers (ABS) to observe the glass transition temperature and if there were any changes in the properties between bonded and un-bonded samples.

DSC 8500 PerkinElmer was used in the current study. The device consists of the DSC chamber, sample pan with its cover (made from aluminium), and nitrogen cylinder and intercooler. The sample is put inside the pan, which is

then closed tightly. Each sample was weighed before being put in the DSC chamber. Pyris software was used to write the DSC program, such as heating and cooling rates, heating range, sample weight, and holding time at a certain temperature. The DSC program that was used for ABS is tabulated in Table 5.4, and it was tested according to standard laboratory procedures.

Table 5.4 DSC program for ABS

Program Factors	Set Values
Sample weight (mg)	6.8
Heating Range (C^0)	20 – 220
Heating Rate (C^0/min)	10
Cooling Rate (C^0/min)	10
Hold Time at 220 C^0 (min)	1

In the current study, the heat flow rate curves of ABS before and after the ultrasonic process were measured, as illustrated in Figure 5.27.

The glass transition temperature (T_g) for an ABS polymer was 108 ^{0}C, as per Figure 5.27. It appears as a step in the baseline of the DSC signal. No changes occur in the polymer's formal phase at T_g, it is just a change in the heat capacity of the ABS. The bonded sample used in this test was tabulated in Table 5.5 because it had the maximum bonding temperature (more details about the bonding temperature in Section 6.2.7).

Table 5.5 DSC sample.

Type	Vibration Amplitude (μm)	Bonding time (sec)	Bonding force (N)	Al6082 Thickness (mm)	ED shape	Bonding Temperature (°C)
Bonded	21	2	1050	1	TRI	128

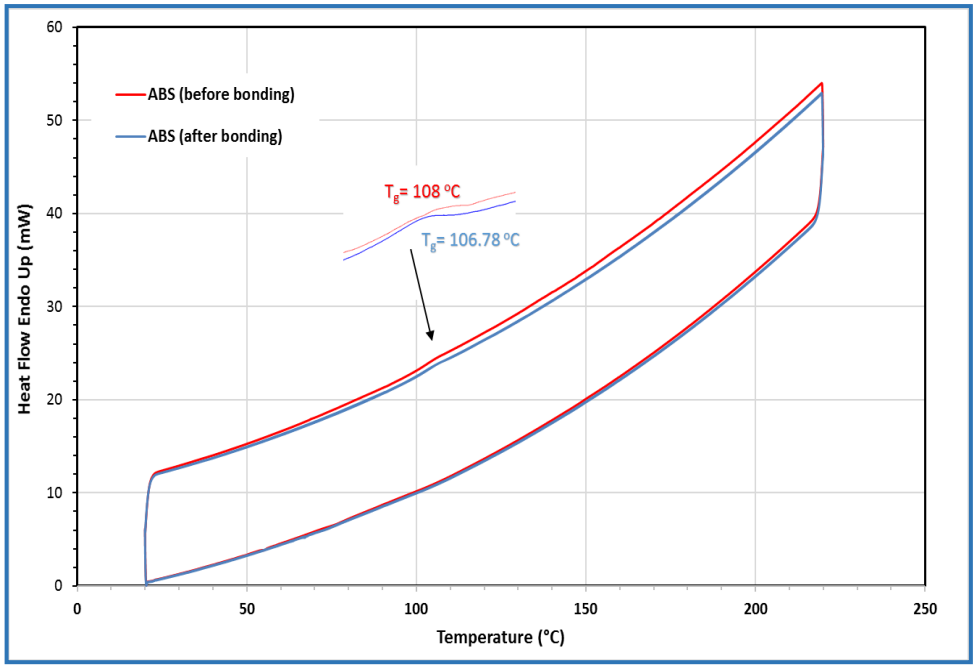

Figure 5.27 Characteristic curves of bonded and un-bonded ABS.

As shown in Figure 5.27, both curves of bonded and un-bonded ABS were almost identical. The difference between T_g before joining (108 °C) and after joining (106.78 °C) is around 1%. Thus, the ultrasonic assisted joining of dissimilar materials between Al6082-T6 and ABS did not have a significant effect on the critical values of ABS temperatures.

- **Thermo-gravimetric Analysis (TGA)**

TGA is a thermal analysis method that measures the physical and chemical properties of polymeric materials by increasing the temperature. The examples of physical properties provided by TGA are vaporisation, sublimation, and absorption, while the chemical properties are decomposition, dehydration, and solid-gas reactions.

In this work, TGA was used to determine the chemical changes of polymer (ABS) properties during the increase of temperature. In addition, TGA was utilised to find out selected properties of ABS that exhibited either mass loss or gain because of the decomposition, oxidation, or loss of volatiles such as gases or moisture.

The TGA device utilised in the current study was TGA 4000, supplied by PerkinElmer. The sample of ABS from the energy director position was put inside an aluminium pan, which was then closed tightly with a pan cover. The sample was then heated to 500 ^{0}C. The TGA device was connected to the specialist gas analysis system (HPR-20 QIC R&D) to monitor the evolved gases and vapours. Pyris software was utilised to write the TGA program, such as heating rate, heating range and sample weight. The program adopted in the TGA of ABS is shown in Table 5.6, and it is based on standard laboratory procedures.

Table 5.6 TGA program for ABS.

Program Factors	Set Values
Sample weight (mg)	13.7
Heating Range (C^0)	20 - 500
Heating Rate (C^0/min)	20

The bonded sample used in the TGA test was the same as that used in the DSC test and it had the parameters as per Table 5.5 because it had the highest joining temperature of 128 ^{0}C (Section 6.2.7).

The results of the investigation by Thermo-gravimetric (TG) combined with mass spectroscopy (MS) can determine the thermal properties such as the decomposition temperature of the ABS polymer before and after ultrasonic bonding is shown in Figure 5.28. The figure shows the comparison of TGA results between bonded and un-bonded ABS.

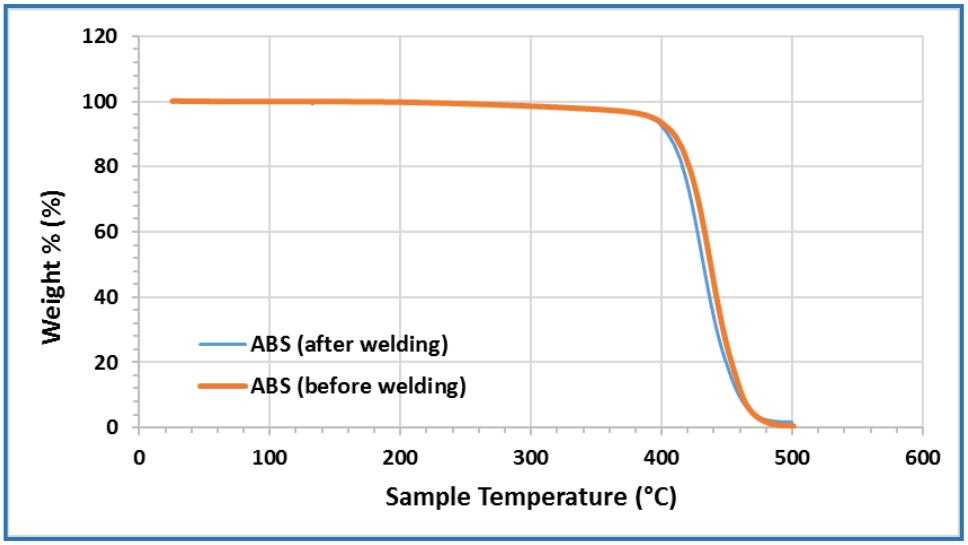

Figure 5.28 TGA comparison between before and after bonding for ABS samples.

As shown in the above figure, decomposition of the ABS sample started from around 350 ^{0}C for both curves when its weight was decreased. In addition, both curves (bonded and un-bonded) were approximately the same (the percentage difference is around 1%). Therefore, The ABS sample was not lost its properties and not decomposed during the ultrasonic joining.

In addition, air bubbles were noticed during the microscopic investigation on the joint zone, as shown in Figure 5.29.

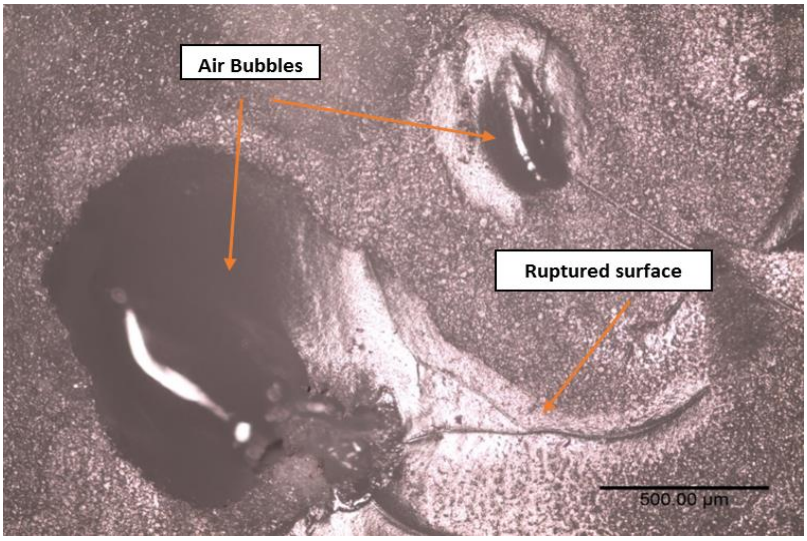

Figure 5.29 Air bubbles on ABS surface after bonding.

Air bubbles appeared on the joint interface (polymer surface side) because the ABS polymer is considered a hygroscopic polymer. In other words, these bubbles were not produced because of the decomposition or degradation of

the ABS during the bonding process; rather the gases were released because of moisture. Although, the ABS samples were dried before the bonding process, a small percentage of moisture is likely to have remained, and this may appear as bubbles after both the bonding time and force reached higher levels. The moisture negatively affects joinability [128], and [100]. This is because the water trapped within the polymer itself evaporates and boils off when the temperature increases to reach the boiling point. Therefore, air bubbles appear at the interface that makes it difficult to produce a high bond density [129]. The increase of temperature that leads to appear these air bubbles can be produced when the levels of ultrasonic time or force are excessive [63], as explained previously in Sections 3.2.2 and 3.2.3. In addition, the bubbles can be produced due to the interaction the molten polymer with atmosphere air during the joining process [30].

To prove the moisture content, the moisture analyser (OHAUS MB45) was used to measure this content for ABS samples before bonding. Standard laboratory procedures were adopted in this test, as shown in Table 5.7.

Table 5.7 Moisture analyser program for ABS.

Program Factors	Set Values
Sample weight (g)	2.935
Drying Temp. (C^0)	80
Elapsed Time in analyser (min)	5

Although the ABS polymer was dried before manufacturing, the results showed the moisture percentage to be 0.14%. Therefore, it is feasible to attribute the air bubbles to the moisture content being released at an increased temperature during the bonding process.

Furthermore, these bubbles may possibly be produced from the gas trapping inside the pores of Al6082 samples [7]. As shown in Figure 5.30, different shapes of pores or pockets were formed on the surface after the pre-treatment of Al6082 samples. The air inside these pockets may have been pushed out when the melted polymer (ABS) flow filled these pores during the

joining process. Thus, this is another possible reason for the appearance of air bubbles at the interface.

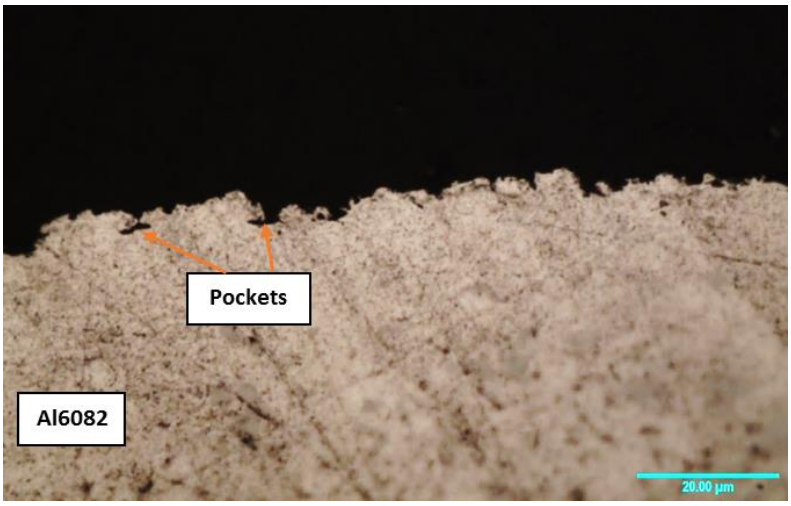

Figure 5.30 Side-view of Al6082 sample after pre-treatment.

5.5.2.2 Pit Size Effect

As mentioned in the existing literature, the surface fracture was observed during the ultrasonic joining of similar thermoplastics [30], and dissimilar materials (metal-thermoplastic composite) [3]. The surface fracture produced after single lap shear test when parts of polymer stayed on the surface of the second sample, either polymer or metal.

In polymer/metal joints, two types of failure can occur; adhesive (interfacial) and cohesive failure [130]. The adhesive failure happened when the fracture occurred at the interface between polymer and metal materials. Whereas, the cohesive failure occurred in polymer because the cohesive strength of polymer is greater than the polymer-metal interfacial strength [130]. Therefore, some patches of polymer remain on the metal surface.

In the current thesis, the surface fracture was observed on the ABS and Al6082 surfaces. These were called pit and patch, as shown in Figure 5.31.

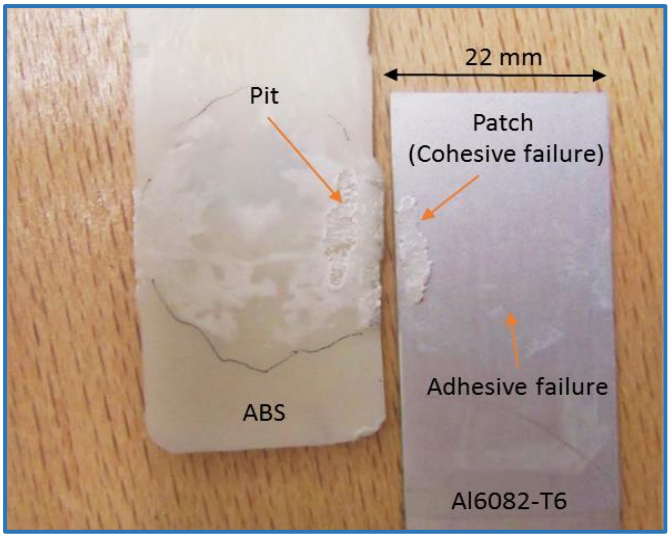

Figure 5.31 Pits on the ABS samples.

Based on Figure 5.31, a mixed failure mode occurred in this study means adhesive and cohesive failure. Al6082 surface is microscopically rough. When the energy director (ED) melted and applied to a rough surface, it conformed to the rough surface and filled up the irregularities of the metal surface, such as holes, or dips. Therefore, the adhesive failure first occurs at the flat area because the interfacial adhesion was relatively weak and therefore the crack propagates along the interface. The interfacial crack may be deflected into the ABS material because the driving force at the crack tip changes due to changes in the stress concentration. In other words, the adhesive failure occurs quickly and therefore overload was concentrated in the regions which have not completely failed. This gave a mixed of failure mode, as shown in Figure 5.32. This figure (Figure 5.32) shows the deviation of the crack path away from the interface into the bulk polymer (ABS). The fact that this occurs in the bulk layer of polymers rather than at the interface between the two samples, indicates that cohesive failure rather than adhesive failure is occurring.

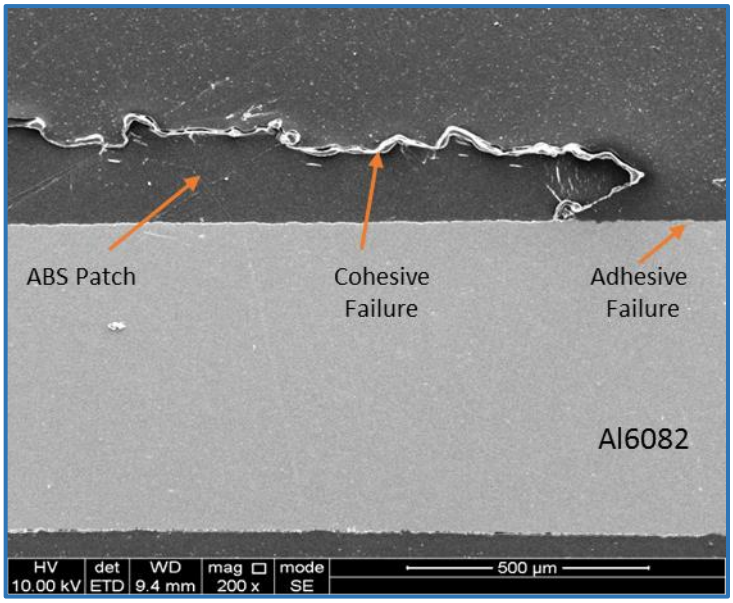

Figure 5.32 Scanning electron micrographs of profile of ABS pit on Al6082 surface.

In case of the cohesive failure, the adhesive bonding is equal or greater than the boundary layer strength and the failure due to the shear force occurs in the ABS layers rather than at the interface between ABS and Al6082, as shown in Figure 5.33. Figure 5.33 shows the surface of ABS patch that illustrates the failure at the intermolecular layers of ABS due to the shear force.

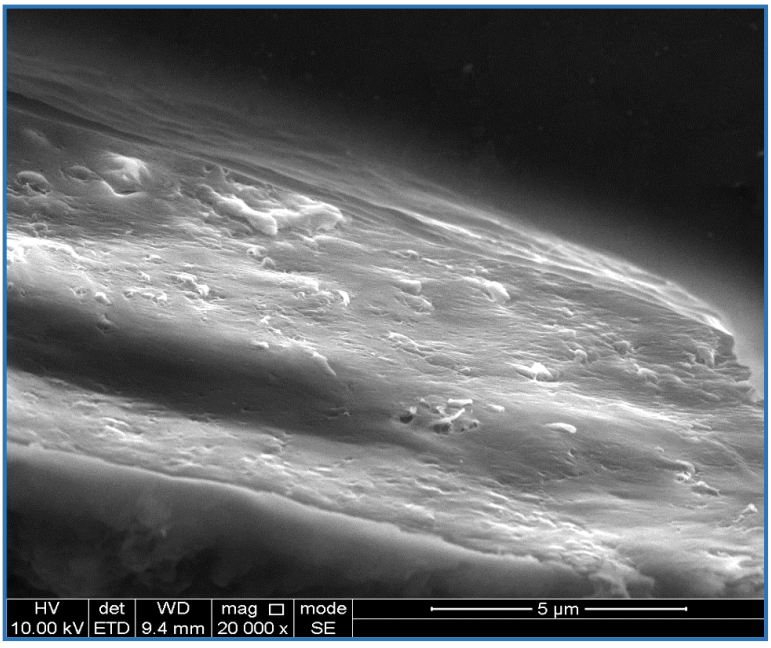

Figure 5.33 Scanning electron micrographs of the surface of ABS patch due to the shear force.

In the current research, the effect of pit size on the lap shear joint strength was investigated since it was observed that there were a variety of pit sizes

which might have had an effect on the LSS. Vernier calliper and microscopic analysis measured these pit sizes, which were approximated to an ellipse shape as a surface area of a pit, multiplied by the depth of the pits.

Ten samples were used to investigate the effects of pit size on LSS. These samples were characterised by a variety of sizes and bonding parameters, as tabulated in Table 5.8.

Table 5.8 Bond parameters and pit size.

No.	Amplitude (μm)	Bonding time (sec)	Bonding force (N)	Al6082-T6 thickness (mm)	ED shape	Pit Size (mm^3)	LSS (MPa)
1	21	2	1050	1	Tri	5.846	1.349
2	18.9	1.5	1050	1.5	SEMI-C	2.79	0.924
3	21	1.5	950	1.5	TRI	15.67	1.945
4	18.9	1.5	950	1.5	TRI	12.42	1.614
5	18.9	1.5	950	1.5	SEMI-C	9.16	1.489
6	21	2	850	2	SEMI-C	5.26	1.239
7	16.8	1	1050	1	TRI	4.4	1.105
8	18.9	1.5	1050	1.5	SEMI-C	3.7	0.959
9	21	2	1050	2	SEMI-C	0.92	0.711
10	16.8	2	1050	2	TRI	0	0.315

The pit size has been found to have a direct relationship with the joint strength, as shown in Figure 5.34.

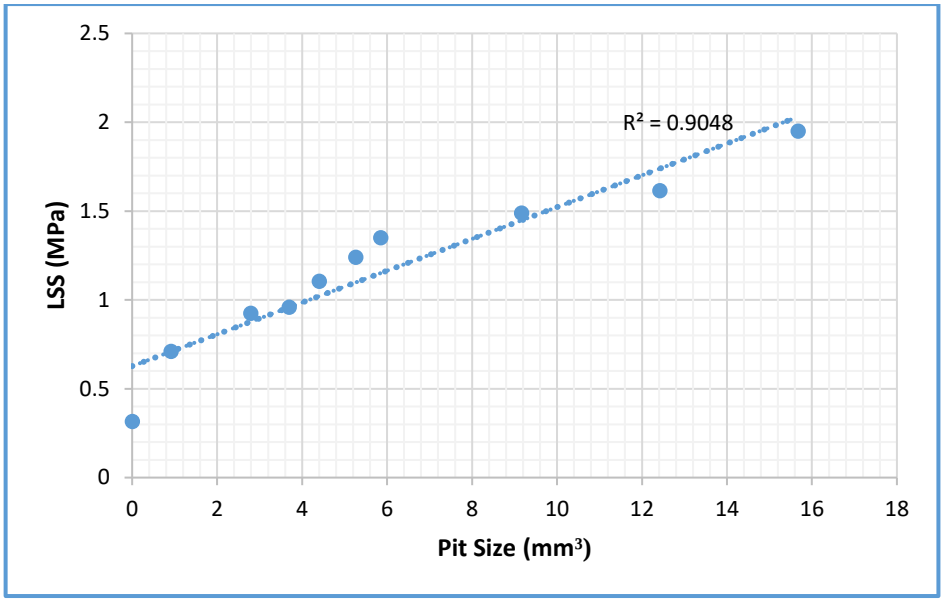

Figure 5.34 Relationship between pit size and LSS

The biggest pit size can produce the maximum LSS, while, the minimum LSS happened in the bonding without a pit (no fracture). The LSS increased about 517.4% when the pit size increased from 0 to 15.6 mm^3. The presence of patches on Al6082 surface means that the resistance against the fracture of the joint zone during the tensile shear testing is higher than the joints without patches because the joints at these points were the strongest and thus the fracture occurred at the ABS sample itself rather that at the interface. The possibility reason of creating these patches is the form of pores on Al6082 surface, some pores were as pockets, tubes or flat as shown in Figure 5.35. Thus, this variation in forms may have contributed to the variation of the joint strength at the interface between ABS and AL6082.

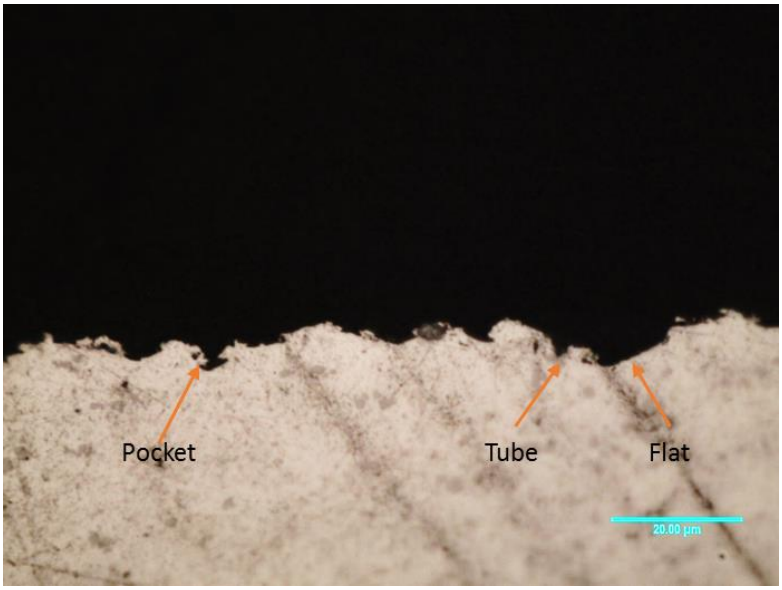

Figure 5.35 Form of pores on Al6082 surface.

Figure 5.36 shows the interface between the small region of ABS (patch) that remained on the Al6082 sample after fracture. The bond density was shown clearly at the interface which produced a stronger joint between ABS and Al6082.

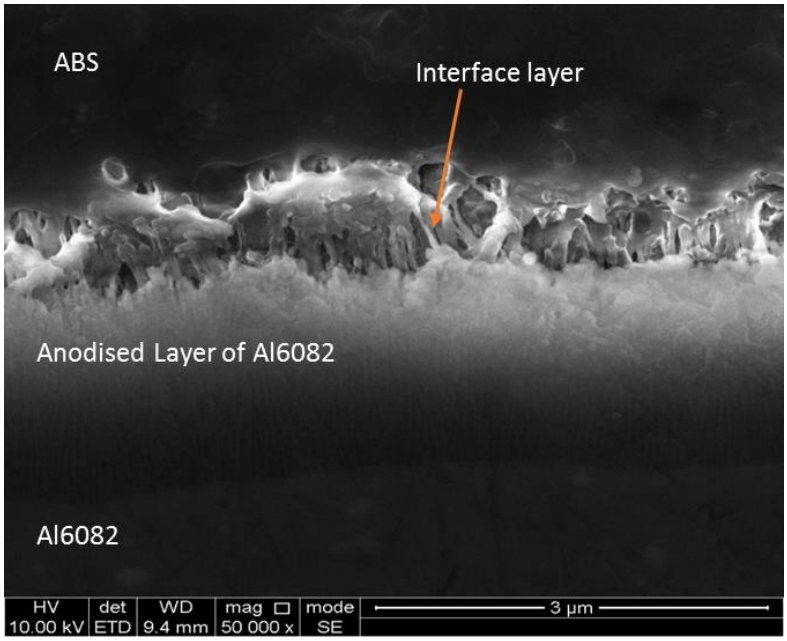

Figure 5.36 Scanning electron micrographs of ABS-Al6082 interface.

5.6 Summary

This chapter has presented the initial and DOE experimental results of ultrasonic bonding between Al6082-T6 and ABS.

The findings indicate that the parameters (vibration amplitude, bonding time, bonding force, Al6082 thickness, and energy director shape) have significant effects on the joint strength.

Bonding time, and bonding force had a non-linear effect. In practical terms, this means that these factors must be moderate values to obtain the highest lap shear strength (LSS). The excessive increase of these factors led to decreased joint strength.

Vibration amplitude has a direct relationship with LSS, while Al6082 thickness has an inverse one. In other words, the highest LSS can be achieved by increasing the amplitude or decreasing the thickness.

The findings observed that there was no change in the microhardness in the Al6082-T6 side because the bonding temperature was not enough to change its microstructure. However, ED collapse due to the polymer melting was explained in the ABS side as the difference between ED length and final gap between Al6082-T6 and ABS after melting or collapsing the energy director (ED). The highest ED collapse (lowest final gap) resulted in the maximum LSS.

Furthermore, the presence of pit sizes indicates strong joints. The highest LSS was obtained at the biggest size.

Chapter 6 Discussion

This chapter is divided into two main parts. Firstly, it discusses the initial experimentations results which informs the required parameters for the DOE experiments. The results of experimental works are discussed to study the effects of parameters on the joint strength in the second part.

6.1 Discussion of Initial Experimentations

The results obtained from initial experimentations (Section 5.1) to select the range levels of each bonding parameters for the DOE experiments showed the following:

- Serial No. 1 and 2 from the structure of initial experimentations (Table 4.11) were tested at the lowest levels of ultrasonic parameters and with/without the presence of the energy director and pre-treatment. Under-bonded joints were produced due to insufficient bonding energy (Equation (2.10)) that was generated at the interface where the energy director was not melted enough to interlock with Al surface, as shown previously in Figure 5.3. Whilst, the highest levels of parameters were used in serial No.3 and 4 (Table 4.11), which produced a huge energy that caused damage to the ABS samples (over-bonded joints), especially when the ABS sample is the upper one. This happened because the ABS was placed between the horn tip and Al sample and therefore the ABS sample squeezed due to the compression forces from the horn tip that pushed the samples down and the Al samples resist this force and thus the ABS sample was destroyed, as shown previously in Figure 5.1.
    - ❖ It can be concluded from the above point that both sets of levels (the lowest and the highest) are not suitable because they generated huge or insufficient energy to produce good bonds between ABS and Al6082. In addition, the position of the samples was a critical parameter. The ABS samples were damaged when it

became the upper position because it did not endure the high levels of bonding force or time. There was no joint when the bonding force or time was decreased. Therefore, the suitable sets of levels are between these extreme conditions, and Al6082 samples are placed at the upper.

- Importance of presence of ED on ABS sample and pre-treatment of Al6082 sample were examined by Serial No. 5, 6 and 7 (Table 4.11). The other parameters, such as vibration amplitude, ultrasonic force, time, hold time and thicknesses of samples were at the mid values of the initial range. The initial experimentations proved the importance of presence for both the energy director of ABS and pre-treatment of Al6082 to obtain a joint, because without using these parameters there was either no joint between ABS and Al6082-T6 or the joint was very weak. The contact surface of ABS (the overlap area) was melted leading to a decrease in the thickness of polymer when ED of ABS was not used, as shown in Figure 6.1.
    - ❖ The findings of this point are important in using the energy director on ABS surface and pre-treating Al6082 samples. These factors enhance the bond between ABS and Al6082 by using the ultrasonic technique through creating the mechanical interlocking at the interface.

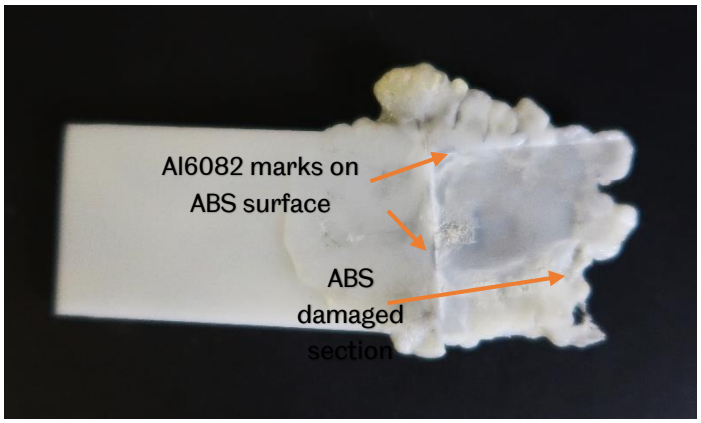

Figure 6.1 Effect of the presence of energy director of ABS.

- According to the initial test results (Serial No. 7, 8 and 9 (Table 4.11)), the thickness of the ABS sample did not impact on the lap shear strength results, as shown in Figure 6.2. Each experimental run was repeated three times to obtain accurate and reliable results.

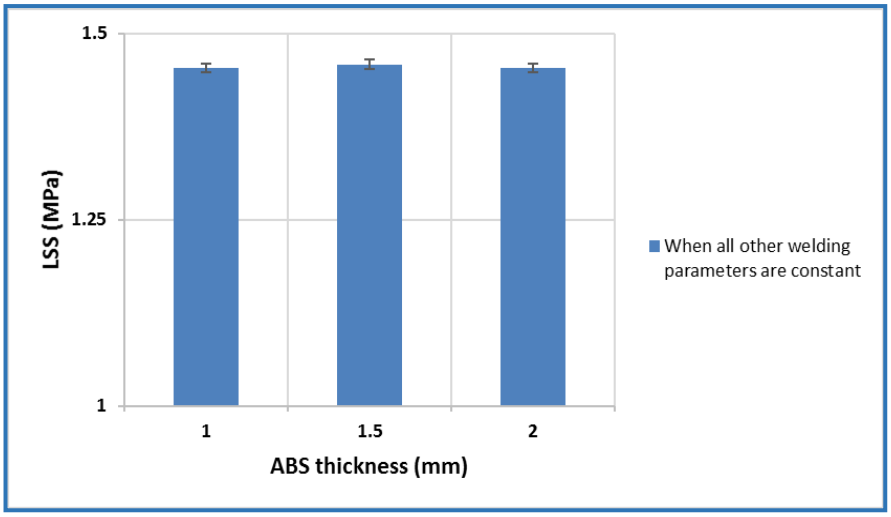

Figure 6.2 Relationship between ABS thickness and LSS at constant other parameters. Each test repeated three times.

It is clear that the LSS value is approximately similar at different thicknesses of ABS material. In other words, the ABS thickness does not have an effect on the LSS, which corresponds with previous work [12] and [113]. This is due to the input bonding energy having been passed through the upper sample (Al6082) to propagate at the interface, and most of this energy being dissipated to heat due to friction between the two samples. This in turn means that relatively small amounts of energy were passing through the ABS material to reach the anvil. Thus, the energy was reflected from the anvil into the bonding zone and was not found to be significant in increasing the heat at the interface to promote the bonding [113].

- ❖ Based on this, the thickness of ABS samples was set to be constant for the remainder of the thesis at 2mm, which is consistent with a previous study [30].

- The effects of hold time on the joint strength were illustrated in Serial No. 9, 10 and 11 (Table 4.11). The results showed no effect on the LSS, as shown in Figure 6.3.

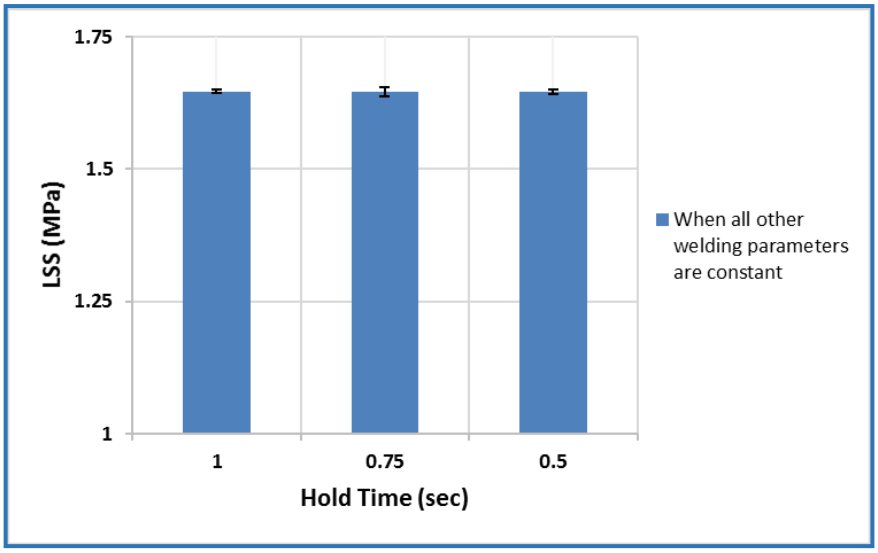

Figure 6.3 Relationship between hold time and the joint strength at constant other parameters. Each test repeated three times.

The hold time does not change the bond strength, which implies that it is not a critical parameter because it does not affect the bonding energy and it is used as a cooling period after the bonding stage. This finding is agreed with the existing literature (Section 3.2.5).

- ❖ As the hold time does not have an influential effect on the joint strength, a one second hold time was maintained throughout the remainder of the current research, which is consistent with a previous study [33].

- The level range of thickness of the upper sample (Al6082) and vibration amplitude were checked in Serial No. from 12 to 18 (Table 4.11). Three initial levels for Al6082 thickness and 4 levels for vibration amplitude were conducted in the initial experimentations. The results observed that all levels of both vibration amplitude and Al6082 thickness produced "well bonded" joints. The manual inspection and visual observation were used to check the quality of joint in the initial experimentations. All bonded joints by those experimental runs (Sr. No. 12-18 (Table 4.11)) had a good external shape without damaging samples, either ABS or Al6082. In addition, there were varying strengths in manual testing in these tests. Therefore, all levels of both Al6082 thickness and vibration amplitude are suitable in the current research.

- ❖ It can be concluded from this point that the range of levels used (Al6082 thickness and vibration amplitude) produced "well bonded" joints based on the visual observation and manual inspection. Hence, all these levels are suitable to conduct the current research.

- The suitable range of levels for bonding force and time were examined in Serial No. from 19 to 37 (Table 4.11). These tests showed that both bonding force and time produced insufficient joining energy (under-bonded joints) at low levels. The input ultrasonic energy depends on bonding force and time (Equation (2.10)) and therefore the lower levels of these parameters leads to the low energy that was not enough to melt the energy director and separate it on the overlap area, as shown previously in Figure 5.3. Hence, very weak bonds between ABS and Al6082 were produced at this range of levels and these bonds broke easily manually. When the range of levels was increased, the bonds between ABS and Al6082 became stronger (well bonded) because the sufficient energy generated at the interface melted ABS polymer and allowed them to flow inside the pores on Al6082 surface and achieve a mechanical interlocking. However, the excessive increase in the levels of bonding force and time generated too much ultrasonic energy at the interface and produced over-bonded joints which were characterised by melting a large amount of ABS and producing a large flash (molten polymer that is pushed out of the joining zone), as shown in Figure 6.4.
  - ❖ In this research, the levels that produced "well bonded" joints based on the manual testing are used; bonding force (800 – 1100N) and bonding time (1 -2 sec).

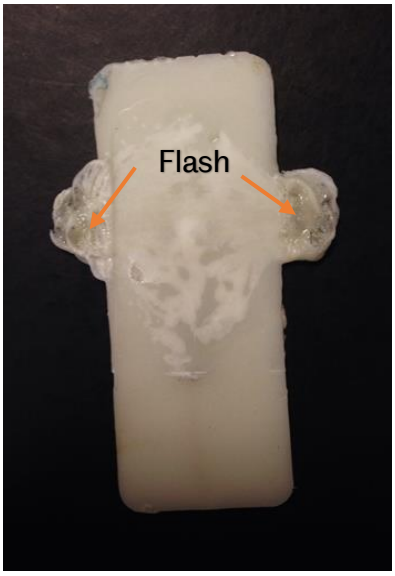

Figure 6.4 Over-bonded joint.

6.2 Discussion of DOE Experiments

The relationships between the main parameters and their two-way parameter interactions were identified in the results section, and will now be discussed and explained in detail. This discussion will be divided into seven sections. The first section represents the effect of vibration amplitude and its interactions. The effect of bonding time and its interactions will be discussed in the second section. The third will explain the effect of bonding force and its interactions. The effects of the energy director and input energy on the LSS will be discussed in sections four and five respectively.

The effects of the input ultrasonic energy and bonding temperature on the LSS will be discussed in sections six and seven respectively.

6.2.1 Effect of Vibration Amplitude and Interactions

The effect of vibration amplitude on LSS as a main bonding parameter is discussed and interpreted, followed by its significant interactions with other bonding parameters. From the literature in Section 3.2.4, vibration amplitude had a significant impact on the joint strength. In practical terms, this means the amplitude is directly proportional to the LSS in polymer-polymer, metal-metal, and metal-composite joints.

The vibration amplitude in the current research has been found to have a linear relationship with the mean of LSS (previously shown in Figure 5.15), indicating that the relationship identified in the literature are also true in the current case. This relationship results from the viscoelastic heating and interfacial friction induced by the perpendicular ultrasonic vibrations of the ultrasonic horn which is pressed on the overlapping area of the samples to be bonded. An increase in vibration amplitude leads to activation of the molecular segments of ABS. Thus, the elastic modulus decreases towards the glass transition temperature of ABS due to a drop-in viscosity, whereas the loss modulus reaches a maximum at the transition region of polymer, as shown previously in Figure 2.4. The heating rate in the polymer increases when the loss modulus increases and this energy is dissipated to the heat at the interface, as shown in Equation (2.6). Therefore, when the vibration amplitude was increased from 16.8 to 21 μm, the dissipated energy increased dramatically. This allows the ABS polymer to flow more easily and flow fully over the Al6082 surface when the vibration amplitude increased, leading to increased joint strength.

In the current thesis, the LSS was seen to increase by 48% when the vibration amplitude increased 25% (from 16.8 to 21 μm). This percentage is significant compared with the existing literature. For example, the LSS was increased 15% in [94] when the vibration amplitude increased 25% (from 40 to 50 μm), while the LSS in [9] was increased about 7% when the amplitude increased around 8% (from 38 to 40.5 μm). This is because the range of vibration amplitude in the current thesis was lower than in the existing literature. At low levels of the vibration amplitude, the joint strength increases significantly compared with the high levels due to develop the heat dissipation at the interface. The high levels of vibration amplitude generates an excessive heat generation which causes the vescocity of polymer to drop [9]. Therefore, the rate of increasing the joint strength at the high levels begin to reduce until reaches a certain value and then the joint strength decreases with continuous increase in the vibration amplitude.

This behaviour and the significance of vibration amplitude in the ultrasonic bonding process correspond with previous studies (polymer-polymer joining [30], and [61]), or (metal-metal joining [13]).

The effect of interaction vibration amplitude and bonding time on the LSS is discussed in this section. An increase in bonding time decreases the joint strength along with a continous increase in the vibration amplitude. Thus, the highest LSS was achieved at the highest vibration amplitude and the lowest bonding time, as shown in Figure 6.5 and Figure 6.6.

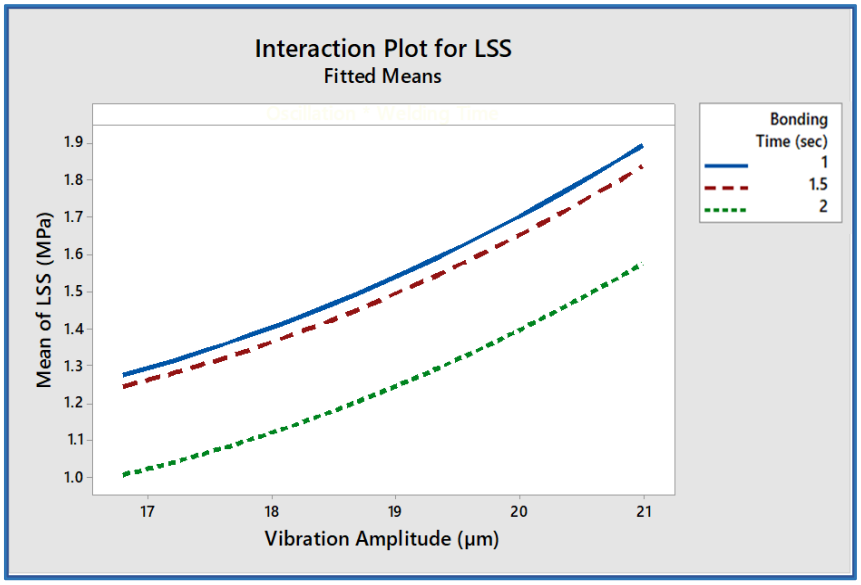

Figure 6.5 Effect of vibration amplitude- bonding time interaction on LSS.

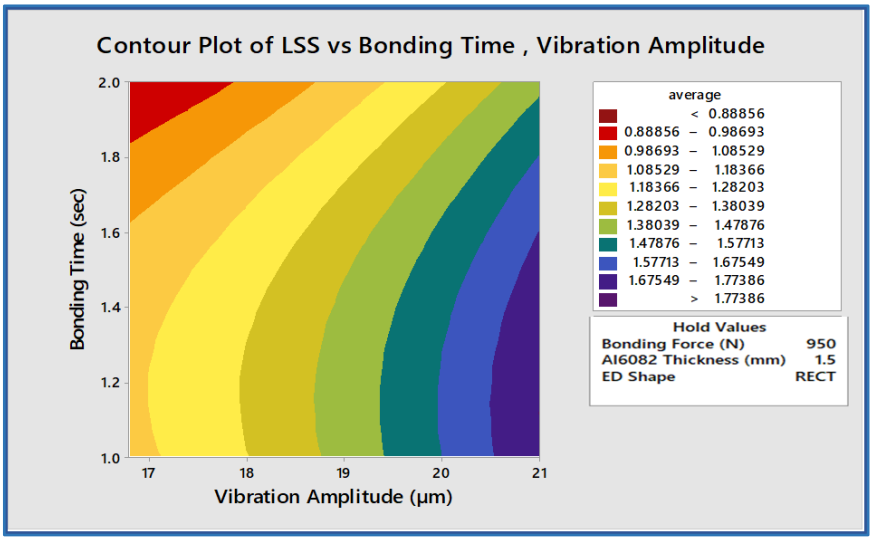

Figure 6.6 Contour plot of LSS vs. bonding time, vibration amplitude.

Data from the ANOVA analysis (Table 6.3) showed a statistically significant effect of interaction between vibration amplitude and bonding time. However, this does not have any practical significance within the range of parameters within which ultrasonic joining of these materials is possible. It can therefore be concluded that there is no interaction between these two parameters that will have an influence on the strength of joint produced.

The same trend occurred with the effect of interaction between vibration amplitude and bonding force. Although this interaction is statistically significant, in practice it is not (the difference between statistical and practical significance was explained previously in Section 5.4), as shown in Figure 6.7 and Figure 6.8.

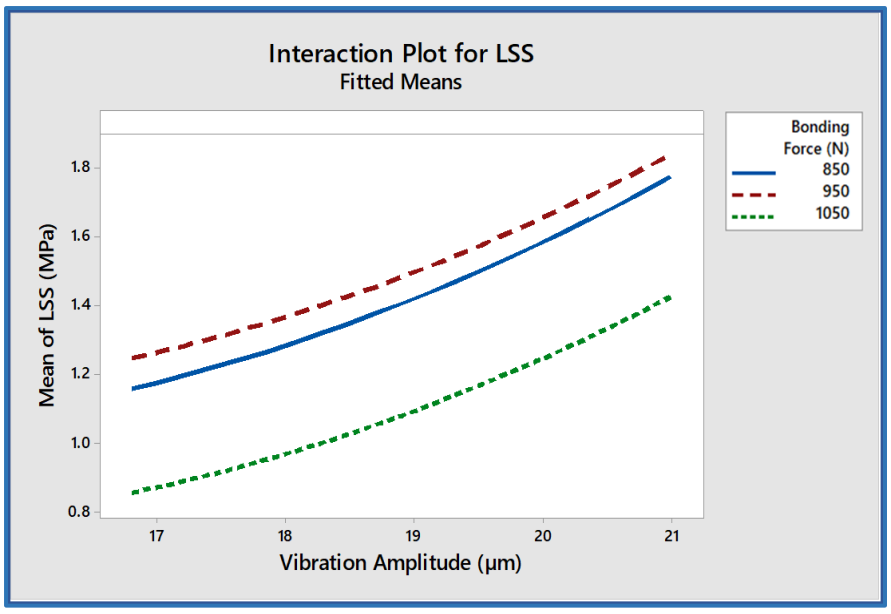

Figure 6.7 Effect of vibration amplitude- bonding force interaction on LSS.

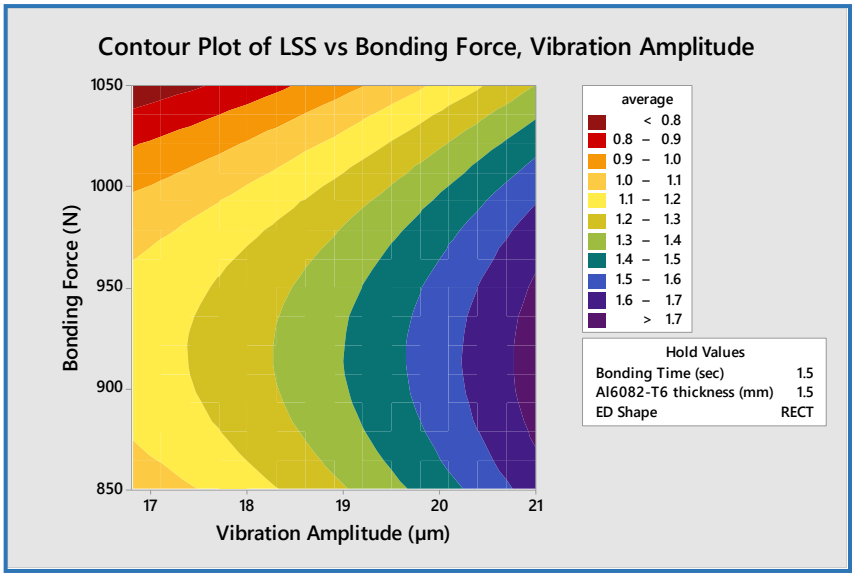

Figure 6.8 Contour plot of LSS vs. bonding force, vibration amplitude.

Increasing the bonding force from 850 to 950 N resulted in increasing the LSS in conjunction with increasing the vibration amplitude, but continuing to increase the bonding force to 1050N caused a 20% decrease in the joint strength. The reasons for that trend are likely to be due to the increase in amplitude that promotes the strength of the joint through increasing the dissipated energy. This energy causes the energy director to melt, while the applied bonding force allows the molten energy director (ABS polymer) to spread and flow on the joining zone, thus increasing the contact area between Al6082-T6 and ABS. When the applied bonding force was too high, a large amount of molten energy director was pushed out of the bonding region, leading to only a thin layer of contact material (the squeezing flow of molten polymer (ABS) is related to the bonding force, as shown previously in Equation (2.7)). Thus, a large amount of melted ABS was pushed out of the interface, as illustrated in Figure 6.9.

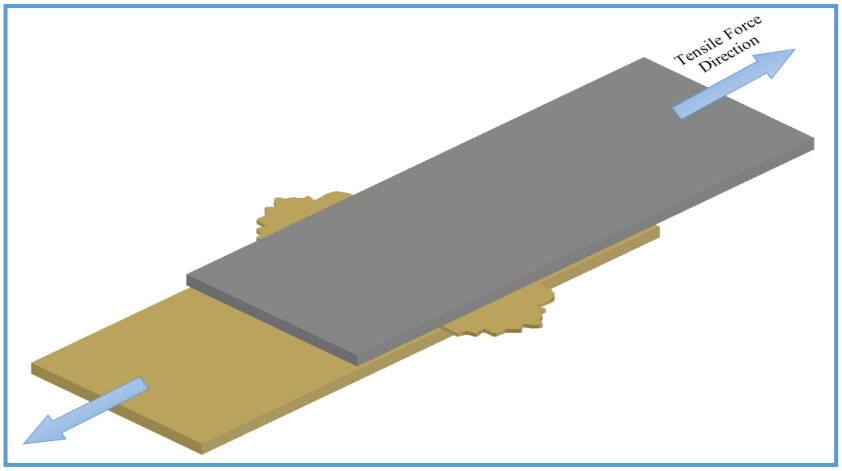

Figure 6.9 Direction of molten polymer.

Furthermore, the interaction between amplitude and Al6082-T6 thickness and the effect on the mean of LSS was investigated in the current research. The findings also showed that this interaction is statistically significant but not practically so within an applicable parameter space, as shown in Figure 6.10 and Figure 6.11.

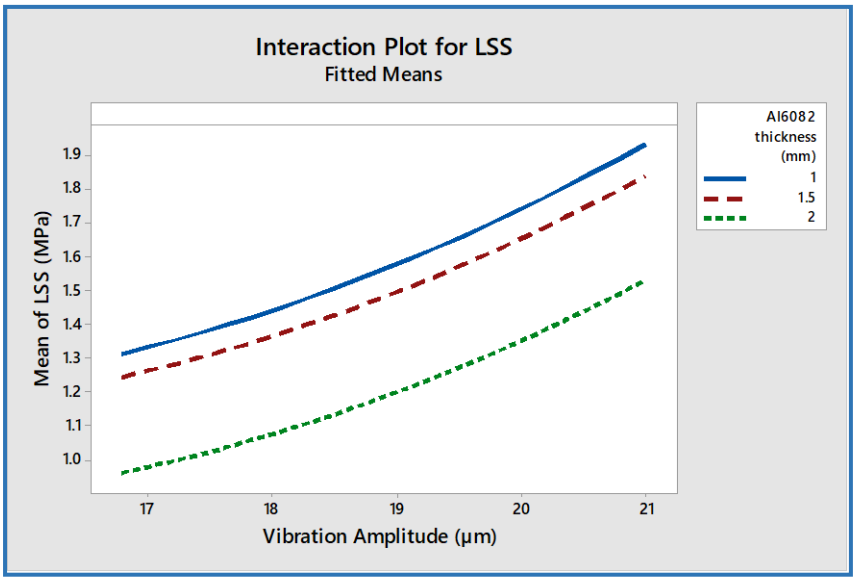

Figure 6.10 Effect of vibration amplitude- Al6082-T6 thickness interaction on LSS.

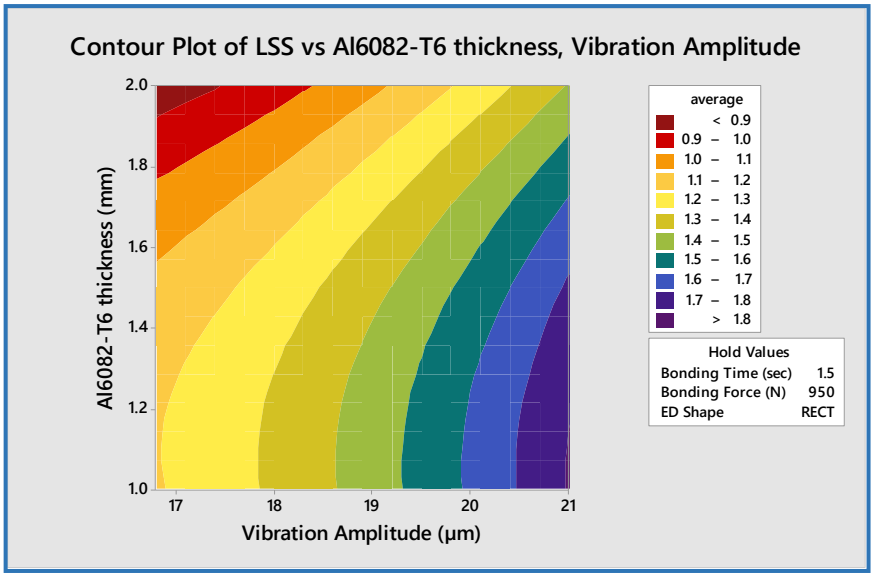

Figure 6.11 Contour plot of LSS vs. Al6082-T6 thickness, vibration amplitude.

Decreasing the thickness of Al6082-T6 when increasing the vibration amplitude produced the highest LSS because of the large amount of energy that travelled through the thickness of the top sample (Al6082-T6). In other words, to achieve a suitable bonding energy for a thicker sample, it is necessary to increase the dissipated energy, which implies increasing the vibration amplitude. Therefore, the highest value of the mean of LSS has been found at the highest level of vibration amplitude and with the thinner Al6082-T6.

Moreover, there was one other statistically significant interaction between vibration amplitude and the shape of the energy director, as shown in Figure 6.12. This is not practically significant when considered over a reasonable range of parameters, although it cannot be comprehensively stated that there would be no interaction with a different shaped ED.

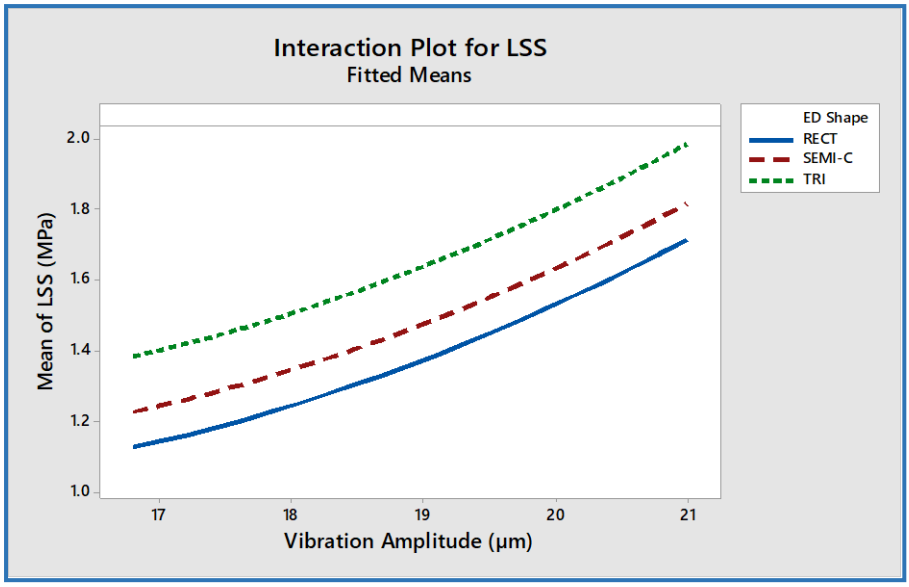

Figure 6.12 Effect of vibration amplitude- ED shape interaction on LSS.

As mentioned before, increasing the vibration amplitude produced a large amount of dissipated energy that becomes heat and melts the energy director. The shape of energy director promoted the heat when the triangular shape was utilised, which will be discussed later (Section 6.2.5).

6.2.2 Effect of Bonding Time and its Interactions

As mentioned in the existing literature (Section 3.2.2), bonding time has a significant effect on the dissipated energy meaning that the joint strength is increased when the bonding time is increased [10]. However, the strength did not improve when the time continued increasing but rather this decreased the strength of the joint.

In the current research, the non-linear relationship between bonding time and the joint strength was previously shown in Section 5.3.3. At the beginning, the joint strength was increased as the bonding time increased. This lead to an increase in energy dissipation at the interface and is expected to increase the joint strength (as discussed in the previous section (6.2.1)). The maximum mean of LSS was about 1.4MPa at 1.3 sec (the best level of the ultrasonic time).

However, the excessive increase in duration of vibrations (more than 1.3 sec) leads to an increase in heat dissipation and therefore to overheating of the polymer in the joining region. In other words, the temperature at the interface

area becomes much higher than the glass transition temperature of ABS (approximately 108°C). This causes the viscosity of the ABS to drop, allowing flow of molten material. Once this begins to occur, the molten polymer can be squeezed out of the bonding area with a high bonding force, leading to movement of the samples even though fixing tools had been put in place to prevent this movement, as shown in Figure 6.13.

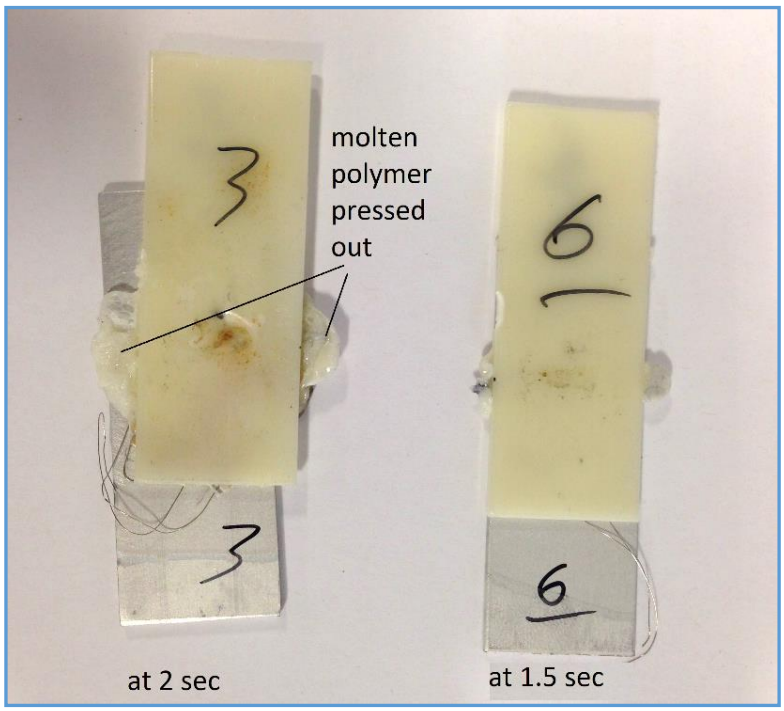

Figure 6.13 Comparison between two different bonding times when other parameters are constant.

Therefore, it can be clearly seen that the mean of LSS decreased with the extended bonding time after the flow occurred. The non-linear trend in the current thesis agrees with the behaviour observed in the existing literature [97], [62] and [63], where by the LSS decreased after reacheing a certain value, as a result of excessive dissipation energy at the interface (as explained previously in Section 3.2.2). Some of the existing literature observed a linear behaviour that means the LSS trend increased when the joining time was increased, such as in [30] where the optimal LSS (1.58MPa) was attained when high level of joining time (1.7 sec) was set for bonding similar PP. This is because the loss modulus is related to the energy dissipated as heat when ultrasonic vibrations are applied to the samples. Therefore, the highest value

in the used range of the joining time achieved the best heat at the interface to produce the strong joint between similar polymers (PP).

During this extended period of bonding time, the joint strength decreased much more when the bonding force was 950N compared with 850N and it was very close at bonding time of 2 sec, as shown in Figure 6.14.

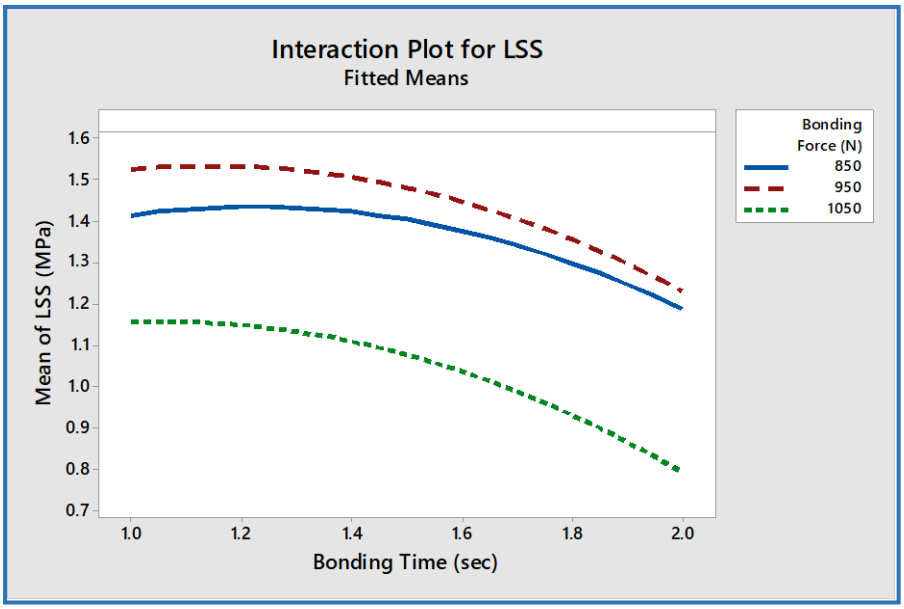

Figure 6.14 Effect of bonding time- bonding force interaction on LSS.

The figure shows that the joint strength increased firstly with increasing both ultrasonic time and force because the force is necessary to spread the molten polymer at the interface. Therefore, the molten polymer had enough time to flow fully over the Al6082 surface and produce mechanical interlocking. However, an excessive increase of ultrasonic force with an increase in bonding time led to drop-in the LSS, as molten polymer became forced out of the joint region before filling all the pores at the interface. In addition, the surface of the ABS 750SW ruptured at the longer ultrasonic vibration and under pressure from the upper part (Al6082-T6) associated with a higher bonding force. Furthermore, air bubbles were found at the highest level of both the bonding time and bonding force, as discussed in Section5.5. The interaction between bonding time and bonding force showed both statistical and practical effects on the joint strength. It means that the effect of bonding force on the joint strength is different for different values of bonding time.

In contrast, the interaction between bonding time and Al6082-T6 thickness showed no practical significance to the LSS. It was only statistically significant, as shown in Figure 6.15, where the joint strength decreased when the bonding time was increased at different thickness of Al6082-T6 samples. This is because the amount of travelled energy from the vibrated horn to the joint zone was decreased by increasing the distance between the horn and the interface, as explained previously in Section 3.3.2. As before, the range of parameters at which this would have any practical effect are outside of the parameter set at which.

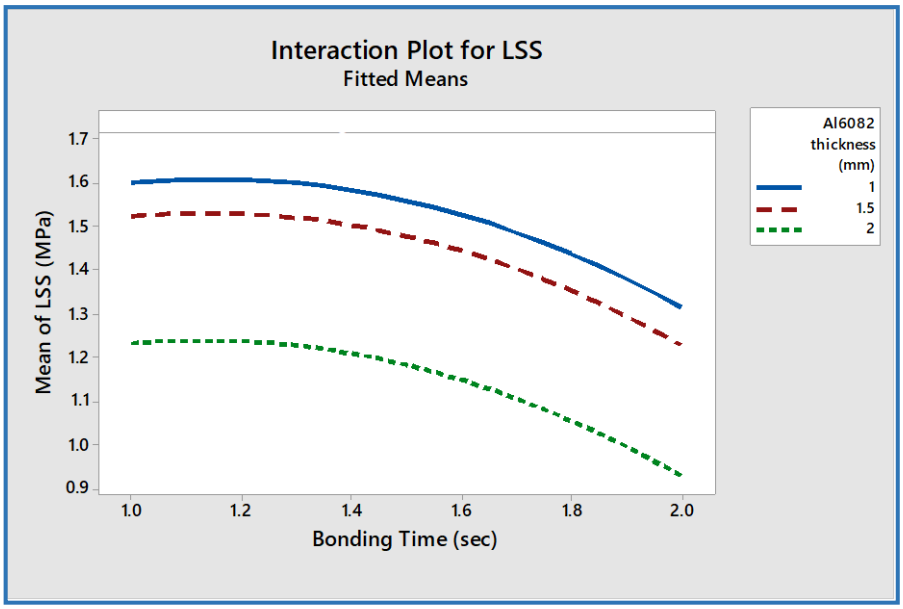

Figure 6.15 Effect of bonding time- Al6082-T6 thickness interaction on LSS.

6.2.3 Effect of Bonding Force and its Interactions

As shown in Figure 5.16, and expected from the existing literature (Section 3.2.3), a non-linear relationship between bonding force and the mean of LSS was identified in the current research. This behaviour occurred because the bonding force is an important factor in transmitting the energy from the USW machine to the interface surface (the surface to be joined) through the upper part (Al6082-T6). The applied force was used to clamp the samples in the interface onto each other by exerting this pressure onto the ultrasonic horn. In addition, the bonding force has an effect on the input ultrasonic energy and therefore a subsequnt influence on the dissipation energy, as shown previously in Equation (2.10). The increased the input energy and friction heat dissipation

was a result of increased joining force. This results in a faster melting of the entire joining interface. Once the energy director was molten and flow was possible, a high joining force resulted in faster flow of the molten polymer. Due to the high joining force (after 930N), the molten polymer was squeezed out the interface that produced reduction in the mean of LSS from around 1.5MPa to 0.9MPa at 1050N (ultrasonic force).

The non-linear behaviour in the current thesis between the joining force and the LSS was also shown in the existing literature for polymers and metals' joints, as investigated in [63] and [97] respectively. These studies observed that excessive ultrasonic force led to excessive dissipation energy at the interface. Thus, the joint strength decreased as molten polymer was forced out the joint region [63], or through cracking of the metal surface [97]. Some of the existing literature, such as in [41], observed a direct relationship between the force and the LSS because the highest level of joining pressure (2 bar) in this previous work achieved optimum joint strength.

There is a statistical significant interaction effect between the bonding force and Al6082-T6 thickness, as shown in Figure 6.16.

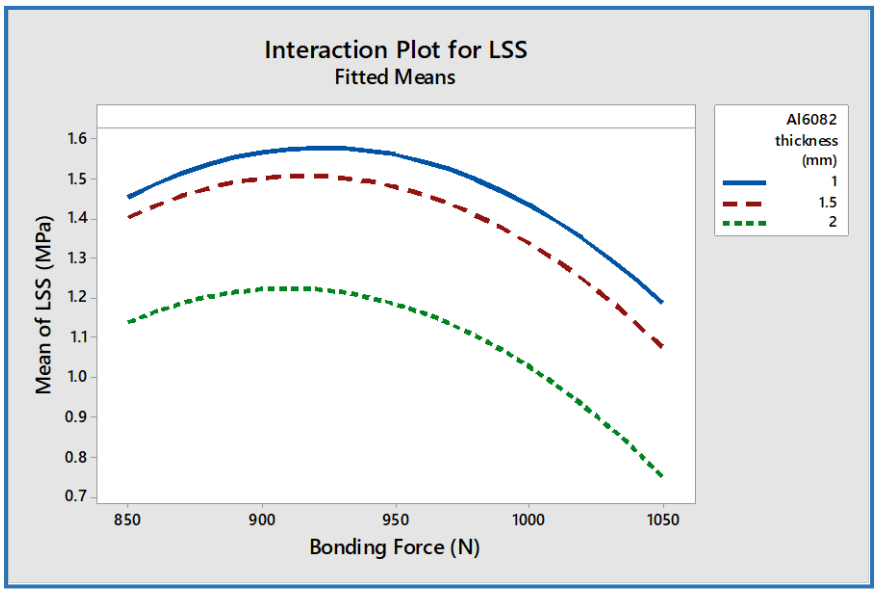

Figure 6.16 Effect of bonding force- Al6082-T6 thickness interaction on LSS.

As explained early in this section, the ultrasonic force has a direct impact on the input energy and therefore this energy reduced when the distance from

the ultrasonic horn and the joint zone increased. Thus, the highest mean of LSS (about 1.6MPa) was achieved in the thinner thickness of Al6082-T6 and moderate bonding force (around 930 N).

6.2.4 Effect of Al6082-T6 Thickness and its Interactions

As expected from the existing literature, the results showed a direct relationship between Al6082-T6 thickness and mean LSS, as previously shown in Figure 5.18. The highest joint strength (around 1.4 MPa) was achieved at the lowest level of thickness (1mm). This behaviour happens because the required energy for the bonding decreased when the thickness of the upper sample (Al6082-T6) was increased. In the literature, this relationship was studied and the findings concluded that the required energy increased when the sample thickness was increased [131]. Additionally, this relationship was broadly explained in conjunction with its equation in Section 3.3.2.

The ultrasonic energy coming from the sonotrode, was passed through the top sample (Al6082-T6) to propagate at the interface area between ABS and Al6082-T6 as heat. The generated heat was then conducted and rapidly dispersed in the Al6082-T6 sample volume, due to the high conductivity of the Al6082-T6. Therefore, the amount of molten ABS able to interlock inside the pores of the thick Al6082-T6 was less than at the thin Al6082-T6, culminating in a weaker joint strength. To produce a strong bond for a thicker material, the ultrasonic bonding energy should be increased, as the input energy is a function of bonding time, bonding force, and vibration amplitude so the input energy increases when these parameters are increased. However, excessive increasing of parameters (bonding time and bonding force) led to a decrease in the joint strength, as discussed above (Sections 6.2.2, and 6.2.3 respectively). Therefore, the selection of the optimum levels of parameters to achieve the highest strength must be precise.

6.2.5 Effect of Energy Director Shape

The results obtained from the data analysis in respect of the effect of the energy director shape on the joint strength showed that the triangular shaped

energy director has the highest mean of LSS (1.35MPa) compared with semi-circular (1.2MPa) and rectangular shapes (1.1MPa), as previously shown in Figure 5.19.

The greatest concentration of ultrasonic bonding energy occurs at the smallest contact surface and smallest volume. The volumes of triangular, semi-circular, and rectangular ED are 90, 141.38, and 180 mm^3 respectively. Therefore, the triangular shaped energy director melted quicker than the semi-circular and rectangular shapes because it reaches above its glass transition temperature (108 °C) quickly and starts to flow due to the ABS viscosity drop. After melting a portion of the energy director, the molten polymer, pressed by static bonding force, spreads through the joint area. Hence, the high level of bonding force pushes the molten polymer outside the joint zone, thereby reducing the joint strength. The findings of the current thesis are agreed with the existing literature [48], and [30] (Section 2.1.2.1). However, there was another literature which found that the semi-circular shape produced the highest joint strength when joining similar polymers compared with other shapes (triangular and rectangular) [33]. This was because the greatest contact area was produced when the shape of energy director was the semi-circular. The energy transfers through the top polymer sample at a different rate, and the temperatures would be reached at a more similar time, meaning the contact area is more important.

6.2.6 Effect of Input Energy

The total input bonding energy has an important effect on the joint strength and it represents the values of bonding parameters that contribute to the bonding process. Therefore, the input energy can be considered a dependent variable. For example, Table 6.1 shows the importance of choosing suitable levels of parameters and how these levels could produce an approximate value of input energy but a different value of LSS.

In the current study, the relationship between the input bonding energy and the mean of LSS is shown in Figure 6.17. The input energy was governed by

physical principles of ultrasonic technology, as shown previously in Equation (2.10) [30], and [41].

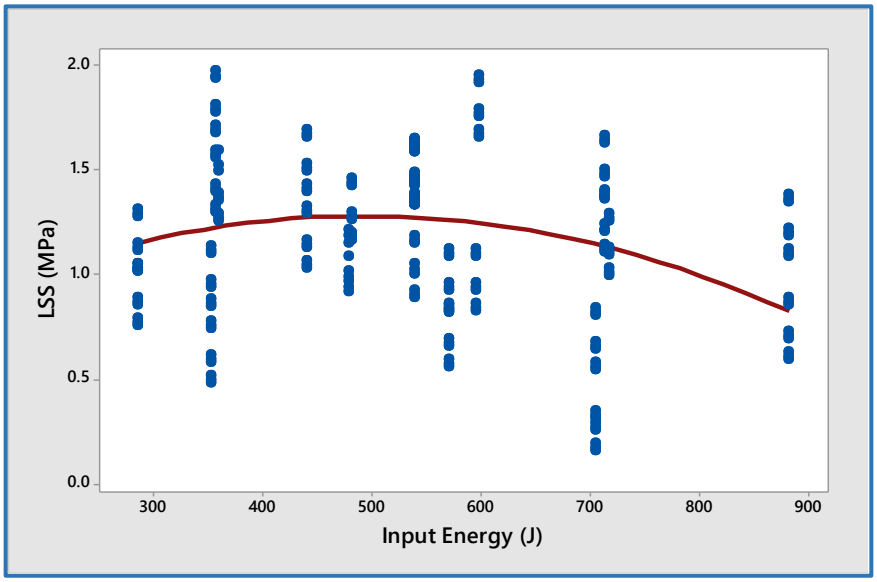

Figure 6.17 Relationship between input energy and mean of LSS.

The joint formation was developed during low input energy usage until a plateau was reached, which was expected due to an increase in the main bonding parameters that are a function of input energy (vibration amplitude, bonding force, and bonding time). With higher input energy (500J), the bond flash became quite extensive and caused a decrease in the bond strength due to the excessive increase of bonding parameters. The effect of excessive increase of the parameters, such as bonding time and force on the LSS were discussed in Sections 6.2.2, and 6.2.3 respectively. This highlights the importance of precise selection of the values of bonding parameters. This behaviour between input energy and LSS concurs with previous research [106], that investigated the process optimisation of a thermoplastic polymer (ABS).

Table 6.1 The effect of parameters on input energy and LSS.

No.	Vibration Amplitude (µm)	Bonding time (sec)	Bonding force (N)	Input Energy (J)	LSS (MPa)
1	16.8	1.5	950	478	1.15
2	18.9	1.5	850	482	1.43
3	21	1.5	950	600	1.915

It is clear that the LSS changed significantly (~67%) when the levels of bonding parameters changed i.e. when the input energy was changed by ~ 25%, as illustrated in serial No. 1 and 3 as per Table 6.1.

Therefore, Figure 6.17 shows that the medium energy range produced the best LSS. An increase in the input energy results from an increase in one parameter level or more of a parameter, thus the excessive increase in multiple parameter levels leads to the LSS decreasing as explained in previous sections.

6.2.7 Effect of Bonding Temperature

From the literature, the recommendation is to join the amorphous polymer ultrasonically around its glass transition temperature (T_g) because the chain mobility increases above T_g in the region of joining. The increase of chain mobility allows for their diffusion across the joint interface and to become entangled with chains on the other side of the joint interface [132]. In the case of joining a polymer with a metal, the polymer can flow across the rough surface of the metal to create a physical bond.

In the current research, the temperature generated in the bonding region was measured, as previously explained in Section 4.5.2. The temperature profiles of measured samples were shown in Appendix (F). From these profiles, the maximum bonding temperatures that were produced during ultrasonic joining have been tabulated in Table 6.2.

The relationship between the bonding temperature (at the interface) and LSS is shown in Figure 6.18. The samples that were tested to measure the interface temperature during the bonding were 18 experimental runs at the triangular energy director shape (see Table 6.2).

Table 6.2 The effect of bonding temperature on the joint strength.

No.	Vibration Amplitude (μm)	Bonding Time (sec)	Bonding Force (N)	Al6082 Thickness (mm)	LSS (MPa)	Temperature (°C)	Input Energy (J)
1	16.8	1	850	1	1.29	113	285.6
2	16.8	2	850	1	1.1	114.5	571.2

3	16.8	1	1050	1	1.14	112	352.8
4	16.8	1	850	2	1.03	109.5	285.6
5	16.8	2	850	2	0.84	110	571.2
6	16.8	1	1050	2	0.77	109	352.8
7	16.8	1.5	950	1.5	1.18	113.5	478.8
8	18.9	2	950	1.5	1.27	119	718.2
9	18.9	1.5	850	1.5	1.44	118.2	481.95
10	18.9	1.5	950	1	1.62	121	538.65
11	21	1	850	1	1.95	121	357
12	21	2	850	1	1.64	126	714
13	21	1	1050	1	1.68	124.5	441
14	21	2	1050	1	1.36	128	882
15	21	1	850	2	1.58	120.5	357
16	21	2	850	2	1.385	120.2	714
17	21	1	1050	2	1.3	118.4	441
18	21	1.5	950	1.5	1.935	124	598.5

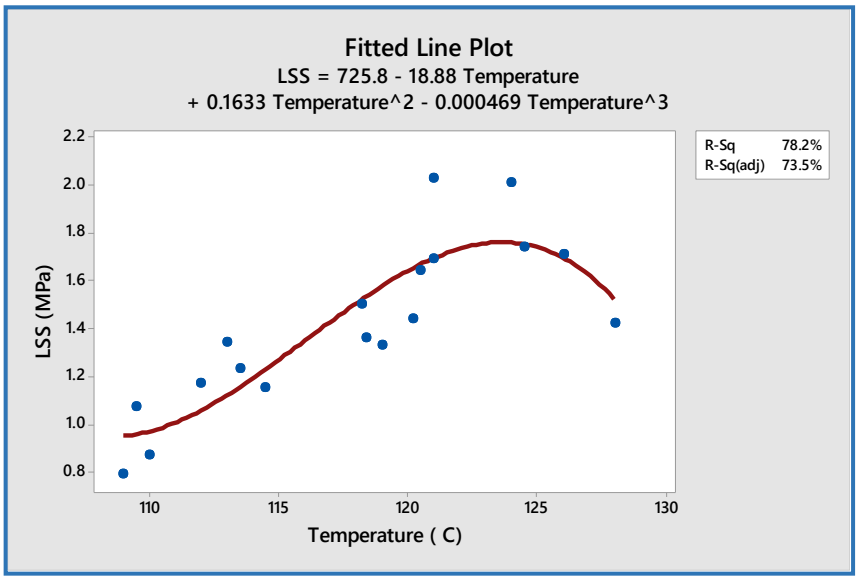

Figure 6.18 Effect of bonding temperature on LSS.

Figure 6.18 shows that the joining between Al6082-T6 and ABS began at just above the T_g of ABS polymer (about 108 °C) because the maximum loss

modulus of polymer occurs at the transition region, as previously shown in Figure 2.4. The LSS increased when the temperature in the interface region was increased. The LSS was decreased after the bond temperature excessed 125 °C because the viscosity of ABS dropped, and the majority of the melted polymer was forced out of the bond zone.

The relationship between bonding temperature and bonding parameters is shown as follows:

- **Bonding Force**

The bonding force has a limited influence on the bonding temperature (see Figure 6.19) because the heat generation at the interface depends mainly on the frequency, strain amplitude and loss modulus, as illustrated previously in Equation (2.6). For example, Figure 6.20 showed the effect of using different bonding forces on the bonding temperature. The bonding temperature rises very rapidly to the peak value when the ultrasonic vibration turned on, and then remains at the approximately same level for the period of joining before cooling.

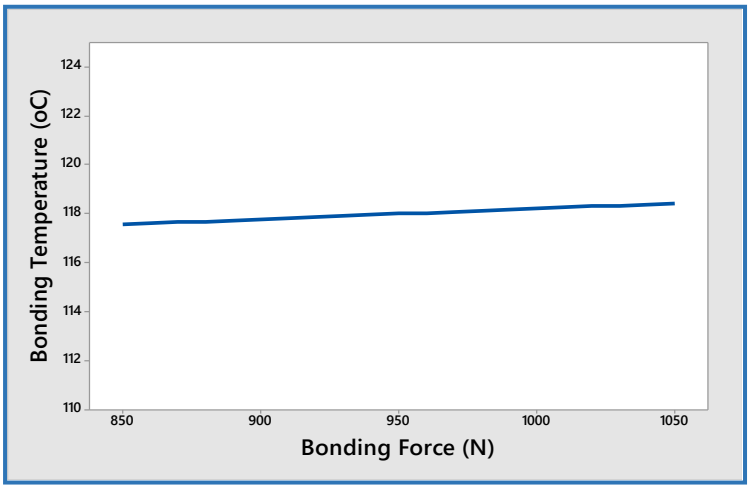

Figure 6.19 Relationship between bonding temperature and bonding force.

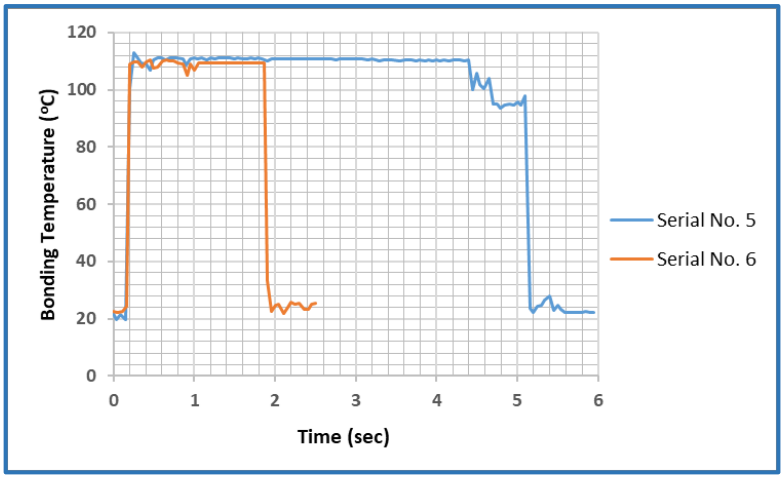

Figure 6.20 Comparison between Serial No. 5 in Table 6.2(16.8μm amplitude, 2sec bonding time, 850N bonding force and 2mm Al6082 thickness), and Serial No. 6 (16.8μm amplitude, 1sec bonding time, 1050N bonding force and 2mm Al6082 thickness).

However, bonding force had a significant effect on the joint strength, due to its role in transmitting the ultrasonic energy from the ultrasonic horn to bonded samples, as explained previously in Section 3.2.3.

- **Bonding Time**

The bonding time also showed a limited effect on the bonding temperature, as shown in Figure 6.21. The mean of the bonding temperature was increased around 4% when the bonding time increased from 1 to 2 sec. The bonding time was the period to subject the bonded sample by ultrasonic vibration and therefore this was a little change in bonding temperature, but the influence of bonding time was significant on the bond strength, as previously explained in Section 6.2.2. An increase in bonding time meant this temperature was maintained for a longer period, but did not continue to increase, as shown in Figure 6.22.

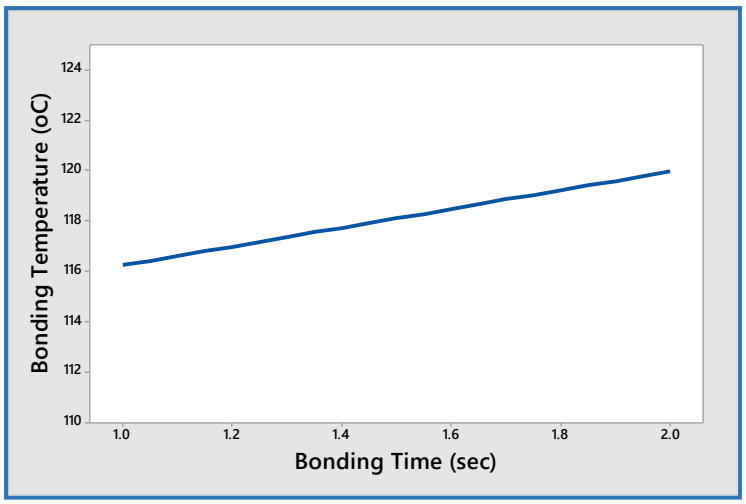

Figure 6.21 Relationship between bonding temperature and bonding time.

Figure 6.22 observed that the average bonding temperature at 2 sec bonding time (128 ^{0}C) was higher than at 1 sec bonding time (124.5 ^{0}C). This is because the longer period of vibration amplitude applied on the samples which caused drop-in viscosity and then decreased in the joint strength.

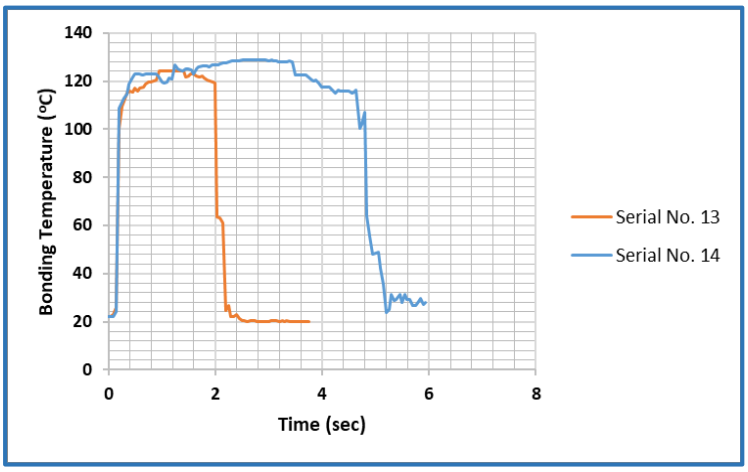

Figure 6.22 Comparison between Serial No. 13 in Table 6.2 (21µm amplitude, 1sec bonding time, 1050N bonding force and 1mm Al6082 thickness), and Serial No. 14 (21µm amplitude, 2sec bonding time, 1050N bonding force and 1mm Al6082 thickness).

- **Al6082-T6 Thickness**

An inverse relationship was seen between bonding temperature and Al6082 thickness, as shown in Figure 6.23. The mean of the bonding temperature was decreased around 5% when the Al6082-T6 thickness increased from 1 to 2mm. This is because the ultrasonic energy is passing through the Al6082 thickness

to reach the interface and therefore an increase of energy path leads to a reduction in the temperature at the interface [109].

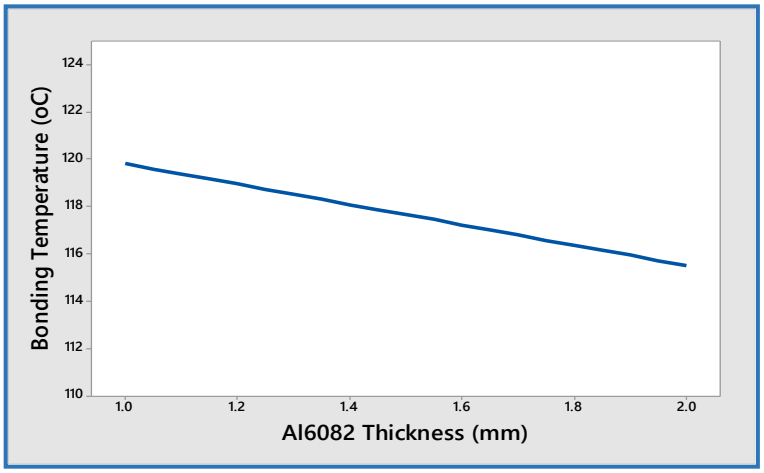

Figure 6.23 Relationship between bonding temperature and Al6082 thickness.

Figure 6.24 illustrated the effects of Al6082 thickness on the bonding temperature. The use of thinner Al6082 thickness produced a higher temperature at the interface compared with thicker thickness, as discussed previously in Section 6.2.4. The temperature increased rapidly as soon as the vibration started due to an increase the energy dissipation at the interface, and continued during the bonding time.

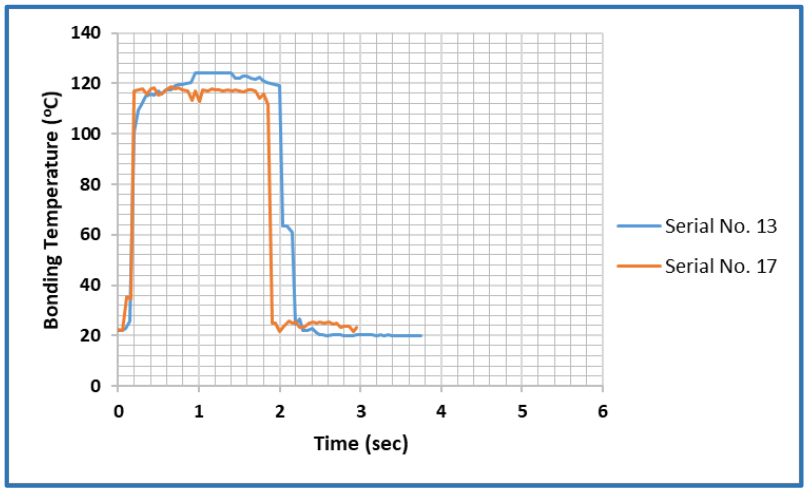

Figure 6.24 Comparison between Serial No. 13 in Table 6.2 (21µm amplitude, 1sec bonding time, 1050N bonding force and 1mm Al6082 thickness), and Serial No. 17 (21µm amplitude, 1sec bonding time, 1050N bonding force and 2mm Al6082 thickness).

- **Vibration Amplitude**

The most influential parameter on the bonding temperature is the vibration amplitude, as shown in Figure 6.25. The mean of the bonding temperature was

increased by approximately 12% when the vibration amplitude increased from 16.8 to 21 µm.

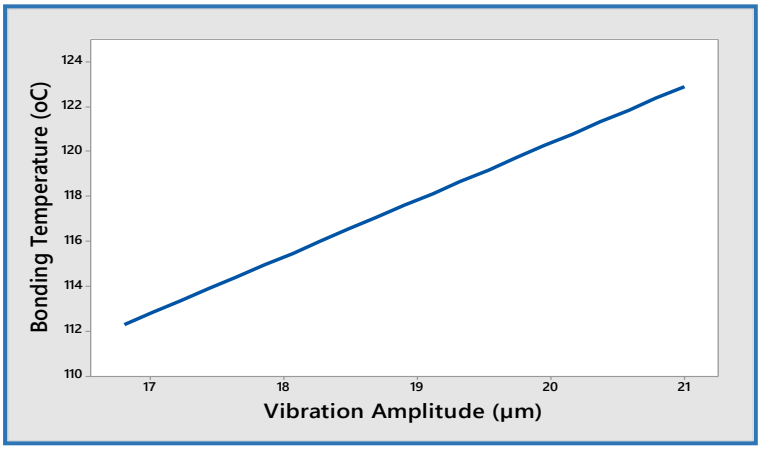

Figure 6.25 Relationship between bonding temperature and vibration amplitude.

In Table 6.2 (from serial No.1 to 7), the vibration amplitude of 16.8µm produced a range of bonding temperature between 109 and 114.5 °C at different bonding parameters. As shown in the temperature profile Figure 6.26, the bonding temperature developed at a vibration amplitude of 21 µm is higher than that produced at 16.8 µm. In addition, the temperature increased rapidly when the ultrasonic process started to reach its peak value until the vibration was stopped.

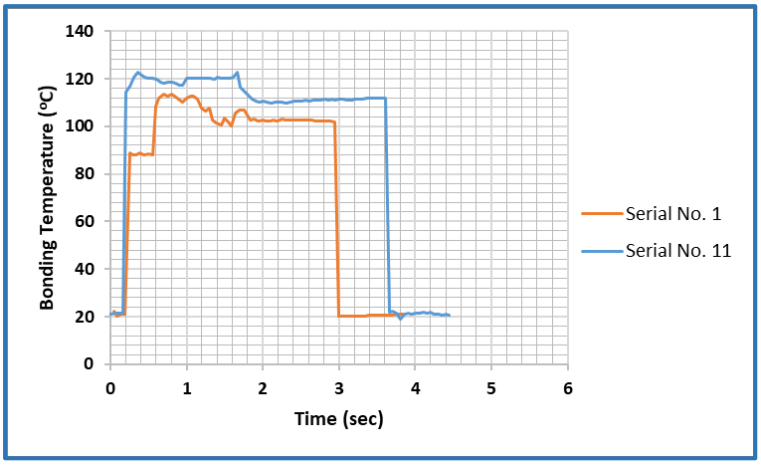

Figure 6.26 Comparison between Serial No. 1 in Table 6.2 (16.8µm amplitude, 1sec bonding time, 850N bonding force and 1mm Al6082 thickness), and Serial No. 11 (21µm amplitude, 1sec bonding time, 850N bonding force and 1mm Al6082 thickness).

As shown in Equation (2.6), the dissipated energy converted to heat at the interface relates to the squared vibration amplitude. This heat was very

necessary to melt the energy director and thus allow it to spread and flow by the bonding force action on the rough surface of Al6082. A joint was produced between ABS and Al6082 when the bonding temperature reached the glass transition temperature of ABS (108 °C). The increase of temperature caused the energy director (ABS) to melt and thus to interlock with the roughened surface of Al6082-T6. This amount of generated heat produced a bond strength variation of 0.77- 1.29 MPa. The range of joint strength increased when the bonding temperature was increased, as shown in Figure 6.18 and Table 6.2.

In Table 6.2 (Serial No. 8 to 10), vibration amplitude of 18.9 µm produced bonding temperatures from 118.2 to 121 °C. Increasing vibration amplitude enhanced the joint strength by increasing the dissipated energy and thus a larger amount of energy director was melted, and a larger joining area was produced, as shown in Figure 6.27.

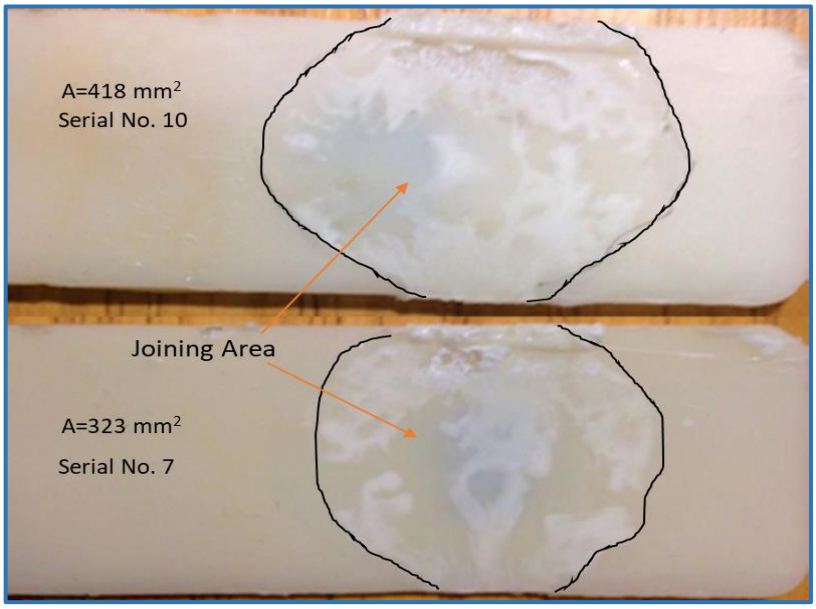

Figure 6.27 Joining area at different bonding temperature.

In Table 6.2 (serial No. 11 to 18), the highest range of bonding temperature was generated at vibration amplitude 21µm, where temperature ranged from 117.4 to 128 °C. At this range of bonding temperature, the mean of the joint strength increased and then decreased at 128 °C. The excessive temperature at the joining area melted much more of the energy director (ABS) and holding at this excessive temperature caused the viscosity of the ABS to drop; this in turn

allowed the polymer to flow and squeeze out of the joining area. When the bonding force was at the maximum (1050N) this force pressed the bonded samples (ABS and Al6082) together to push out the majority of the melted ABS.

- **Input Energy**

The relationship between the input energy and bonding temperature is shown in Figure 6.28. The effects of excessive increasing of bonding parameters (bonding time, and bonding force), and input energy on the LSS were discussed previously in Sections 6.2.2, 6.2.3 and 6.2.6 respectively.
As expected, an increase in input energy led to an increase in the generated temperature at the interface.

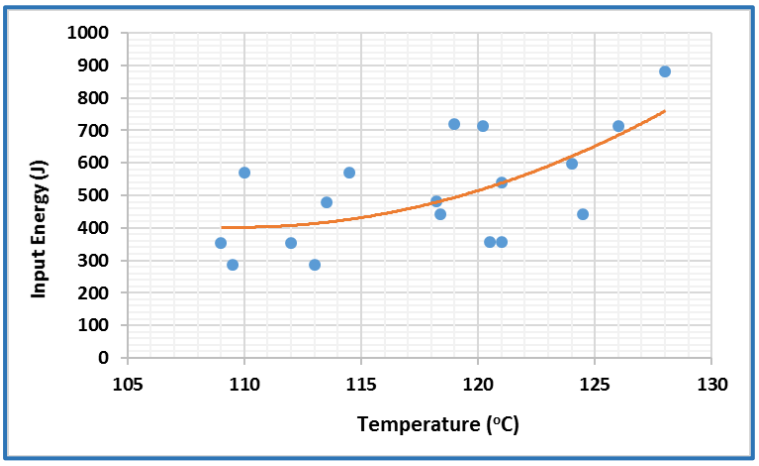

Figure 6.28 Relationship between the input energy and interface temperature.

The possible errors in the measurements of ultrasonic parameters might cause the scatter points in the correlation between the bonding temperature and the input energy, as previously explained in Section 4.4.1. Although the percentage of variation for parameters was small, it could affect the relationship, especially as the input energy and bonding temperature are a function of the bonding parameters. In addition, the input energy was calculated theoretically (Equation 2.10), meaning the same values of input energy could come from different values of parameters. These differences in the parameters values had an effect on the bonding temperature, as explained previously in Section 6.2.7. In other words, it is not just the input energy that is important, but also the way in which the input energy is achieved.

6.3 Results of Statistical Analysis

6.3.1 Analysis of Variance (ANOVA) Results

As explained in Section 2.4.2, the analysis of variance (ANOVA) used to evaluate the results statistically within the scope of it.

In the present work, the importance and significance of the bonding parameters and their interactions were studied using the analysis of variance ANOVA, as shown in Table 6.3. Based on Section 2.4.2.6, the significance level is 0.05, thereby the main parameters or/and its interactions are significant factors when their P-value is less than 0.05.

Table 6.3 ANOVA results.

Source	DF	Adj SS	Adj MS	F-value	P-value	Sig.
Model	24	9.63	0.40	659.72	0.000	Yes
Liner	6	7.3	1.22	2000.97	0.000	Yes
Vibration Amplitude	1	3.24	3.24	6321.30	0.000	Yes
Bonding time	1	0.88	0.88	1442.63	0.000	Yes
Bonding force	1	1.11	1.11	1818.64	0.000	Yes
Al6082-T6 Thickness	1	1.4	1.4	2302.29	0.000	Yes
ED shape	2	0.68	0.34	560.49	0.000	Yes
Square	4	2.1	0.52	862.78	0.000	Yes
Vibration Amplitude* Vibration Amplitude	1	0.0045	0.0045	7.32	0.007	Yes
Bonding time *Bonding time	1	0.05	0.05	79.68	0.000	Yes
Bonding force* Bonding force	1	0.3	0.3	446.48	0.000	Yes
Al6082-T6 Thickness* Al6082-T6 Thickness	1	0.06	0.06	97.74	0.000	Yes
2-way Interaction	14	0.23	0.016	26.89	0.000	Yes
Vibration Amplitude* Bonding time	1	0.005	0.005	7.67	0.006	Yes

Vibration Amplitude* Bonding force	1	0.01	0.01	13.25	0.000	Yes
Vibration Amplitude* Al6082-T6 Thickness	1	0.09	0.09	14.60	0.000	Yes
Vibration Amplitude* ED Shape	2	0.006	0.003	4.53	0.012	Yes
Bonding time* Bonding force	1	0.09	0.09	145.66	0.000	Yes
Bonding time* Al6082-T6 Thickness	1	0.02	0.02	32.26	0.000	Yes
Bonding time* ED Shape	2	0.0013	0.0007	1.08	0.342	No
Bonding force* Al6082-T6 Thickness	1	0.09	0.09	144.39	0.000	Yes
Bonding force* ED Shape	2	0.002	0.001	1.61	0.202	No
Al6082-T6 Thickness* ED Shape	2	0.0025	0.00125	2.06	0.130	No
Error	254	0.154	0.00061			
Lack-of-Fit	50	0.137	0.003	31.47	0.000	
Pure Error	204	0.02	0.0001			
Total	278	9.78				
Model Summary S R-sq R-sq(adj) R-sq(pred) 0.025 98.42% 98.27% 98.11%						

The ANOVA analysis has shown that all main parameters and most of their interactions have significant effects on the LSS results. According to the model summary in Table 6.3, the chosen model of the LSS shows a high percentage of R-squared, Adj R-squared, and predicted R-squared, equalling 98.42, 98.27, and 98.11% respectively. These high percentages indicates that most of the response data (LSS) is around its means, thereby indicating the high quality of the chosen model and it being precise in predicting the value of the response [133]. In addition, the standard deviation of the model is small (0.025) indicating

that the average distance between the observed values of experimental runs are very close to the fitted line of the model. Thus, the model can be trusted and is reliable.

From the ANOVA results, it was observed that the vibration amplitude and Al6082 thickness are the most significant parameters affecting the joint strength. This is because these parameters had the largest Adj SS which means have the highest percentage contribution that affect the joint strength, as explained previously in Section 2.4.2.3. The percentage contribution of the vibration amplitude and Al6082 thickness were 33.1% and 14.31% respectively. This is because the vibration amplitude is the main parameter for the heat generation at the interface, as explained previously in Section 6.2.1. This finding is agreed with the existing literature, such as [96], and [134], where the percentage contribution of vibration amplitude was 26% and 32.32% respectively. Whilst, the energy director shape had the lowest percentage contribution 7%.

Based on Table 6.3, the most two-way parameter interactions have a significant effect on the joint strength and these parameter interactions were discussed previously in Section 6.2. To summarise effect of the two-way parameter interactions on the mean of LSS, Table 6.4 distinguishes between the statistical significant interactions and insignificant (no interaction) effects.

Table 6.4 Bonding parameters interactions.

	Vibration Amplitude	Bonding Time	Bonding Force	Al6082-T6 Thickness	Energy director Shape
Vibration Amplitude	/	Significant	Significant	Significant	Significant
Bonding time	Significant	/	Significant	Significant	Insignificant
Bonding force	Significant	Significant	/	Significant	Insignificant
Al6082-T6 Thickness	Significant	Significant	Significant	/	Insignificant
Energy director Shape	Significant	Insignificant	Insignificant	Insignificant	/

6.4 Summary

This chapter has discussed and analysed the initial and experimental results of ultrasonic bonding between Al6082-T6 and ABS.

The findings indicate that all investigated parameters and most of the two-way parameter interactions had significant effects on the joint strength. Additionally, input energy and bonding temperature which result from parameter selection also had a significant influence on the LSS.

The levels of parameters chosen due to the pre-investigation have been shown to be appropriate because the highest joint strength happened at approximately the mid or central values, especially the bonding time and bonding force.

Based on ANOVA results, the vibration amplitude and Al6082 thickness are the most significant parameters affecting the joint strength.

Chapter 7 CONCLUSIONS AND FUTURE WORK RECOMMENDATIONS

7.1 Conclusions

This research has provided a novel understanding of the ultrasonic assisted joining of lightweight dissimilar materials. Despite the importance of this type of joining in industries and engineering applications, only very limited studies have been carried out in this field.

In this work, the ultrasonic joining of ABS (amorphous polymer) and Al6082-T6 (metal) has been achieved successfully. The maximum lap shear strength obtained is about 2.312 MPa (1.156 KN shear force).

Key specific findings are as follows:

Sample Preparation

- Pre-treatment of Al is crucial to obtain joining because it creates a microstructural surface roughness and it allowed the mechanical interlocking between ABS and Al surfaces. However, very weak joints or no joints formed when Al samples were not pre-treated due to the molten polymer sllipping outside the joining zone. Therefore, the joint with pre-treatment is stronger than the joint without pre-treatment of Al samples.
- The metal sample should be the upper sample because the polymer sample became damaged when it was on top. Polymer samples cannot endure the high levels of bonding force or time. Furthermore, very weak joints or no joint were produced by decreasing these parameters.
- The thickness of the top sample is an important factor. As it becomes thicker, the LSS reduces due to lack of heat generation at the joint interface, However, the thickness of the lower sample is likely to be unimportant.
- Energy director shape: whilst all the tested geometries provided a joint, the triangular geometry was found to be best at concentrating the US energy most efficiently.

Bonding Parameters

- The most significant parameters are vibration amplitude, metal thickness, and bonding force.
- Hold time, whilst mentioned in literature, was not important here.
- The joint strength was increased when bonding time, bonding force and oscillation amplitude increased, and Al6082-T6 decreased. However, the excessive increase of bonding time, and bonding force led to decreased LSS. This indicates an optimum level.
- The most 2-way parameter interactions had a significant effect on the joint strength, except three interactions between parameters did not show a significant effect on the joint strength: energy director interactions with bonding time, bonding force and Al6082-T6 thickness.

Bond Structure

- There were no physical changes in base properties. Additionally, there was no heat affected zone in the Al6082-T6 side because the bonding temperature was insignificant to alter its microstructure. The effect of the final gap between the Al6082-T6 and ABS samples on the LSS was investigated. The highest ED collapse resulted in the maximum LSS.
- The biggest pit size can produce the maximum joint strength, while, the minimum joint strength occurred in the bonding without a pit (no fracture).

Overall the current research has delivered substantial progress in developing a comprehensive understanding about ultrasonic joining for lightweight dissimilar materials. This process for polymer/metal hybrid joints is still in the developmental stages. Hence, further study is required to effectively understand the feasibility and durability of the ultrasonic joining of polymer/metal.

7.2 Future Work Recommendations

The present study has provided considerable improvements in understanding the ultrasonic joining of lightweight materials (metal-polymer). Despite the success of the joining between Al6082-T6 (metal) and ABS (thermoplastic amorphous polymer), there are several further investigations that would be interesting in the future, which are recommended as follows:

- This research can be expanded to study the feasibility of ultrasonically joining other amorphous polymers to identify any commonalities.
- The combinations of metals with semi crystalline polymers, such as PP, PEEK, PA. may be further investigated. This would offer the opportunity to compare the results established in this research with amorphous polymers, and to introduce new polymers for use in this technique.
- The metal choice may be expanded to study its effects on the joint strength and to compare it with aluminium.
- The surface roughness of metal may be further studied to develop a relationship between the pre-treatment of metal (anodising) and the joint strength. The effect of process parameters (such as current, voltage, time, and acids concentration) on the surface roughness should be examined so that the effect on the joint strength can be determined.

References

[1] W. Miller, L. Zhuang, J. Bottema, A. Wittebrood, P. De Smet, A. Haszler, and A. Vieregge, "Recent development in aluminium alloys for the automotive industry," *Mater. Sci. Eng. A*, vol. 280, no. 1, pp. 37–49, 2000.

[2] K. Szeteiová, "Automotive materials plastics in automotive markets today," *Inst. Prod. Technol. Mach. Technol. Mater. Fac. Mater. Sci. Technol. Trnava, Slovak Univ. Technol. Bratislava*, pp. 27–33, 2010.

[3] S. Bolt, "Ultrasonic Plastic Welding of Carbon Fiber Reinforced Polyamide 6 to Aluminium and Steel," Delft University of Technology, 2014.

[4] D. Stavrov and H. E. N. Bersee, "Resistance welding of thermoplastic composites-an overview," *Compos. Part A Appl. Sci. Manuf.*, vol. 36, no. 1, pp. 39–54, 2005.

[5] R. D. Adams, J. Comyn, and W. Charles, *Structural Adhesive Joints in Engineering*, 2nd ed. Springer Science & Business Media, 1997.

[6] S. Hartshorn, Ed., *Structural adhesives: chemistry and technology*. 2012.

[7] D. Ensminger and L. J. Bond, *Ultrasonics: fundamentals, technology and applications*, 3rd Editio. Taylor & Francis, 2011.

[8] A. Siddiq and E. Ghassemieh, "Thermomechanical analyses of ultrasonic welding process using thermal and acoustic softening effects," *Mech. Mater.*, vol. 40, no. 12, pp. 982–1000, 2008.

[9] G. Wagner, F. Balle, and D. Eifler, "Ultrasonic welding of aluminum alloys to fiber reinforced polymers," *Adv. Eng. Mater.*, vol. 15, no. 9, pp. 792–803, 2013.

[10] "Overview of Ultrasonic Welding." [Online]. Available: https://www.bakersgas.com/weldmyworld/2011/02/08/overview-of-ultrasonic-welding/. [Accessed: 01-Sep-2017].

[11] S. Lee, "Process and Quality Characterization for Ultrasonic Welding of LIthium-Ion Batteries," University of Michigan, 2013.

[12] Z. S. Al-Sarraf, “A Study of Ultrasonic Metal Welding,” University of Glasgow, 2013.

[13] M. Ganesh and P. R. R, “Experimental Study on Ultrasonic Welding of Aluminum Sheet To Copper Sheet,” *Int. J. Res. Eng. Technol.*, vol. 2, no. 12, pp. 161–166, 2013.

[14] M. J. Troughton, *Handbook of Plastics Joining - A Practical Guide (2nd Edition)*. William Andrew Publishing, 2008.

[15] F. Balle, G. Wagner, and D. Eifler, “Ultrasonic metal welding of aluminium sheets to carbon fibre reinforced thermoplastic composites,” *Adv. Eng. Mater.*, vol. 11, no. 1, pp. 35–39, 2009.

[16] “No Title.” [Online]. Available: http://www.ewf.be/media/documentosDocs/doc_73_technical_sheet_-ultrasonic_welding_.pdf. [Accessed: 06-Nov-2013].

[17] J. Michael, *Handbook of Plastics Joining*. William Andrew, Inc., 1997.

[18] V. G. Gutnik, N. V. Gorbach, and a. V. Dashkov, “Some characteristics of ultrasonic welding of polymers,” *Fibre Chem.*, vol. 34, no. 6, pp. 426–432, 2002.

[19] I. F. Villegas, L. Moser, A. Yousefpour, P. Mitschang, and H. E. N. Bersee, “Process and performance evaluation of ultrasonic , induction and resistance welding of advanced thermoplastic composites,” *J. Thermoplast. Compos. Mater.*, vol. 26, no. 8, pp. 1007–1024, 2012.

[20] “Ultrasonic Welding.” [Online]. Available: http://en.wikipedia.org/wiki/Ultrasonic_welding. [Accessed: 06-Nov-2013].

[21] L. Brown, “Copper Development Association Cost-Effective Manufacturing : Joining of Copper and Copper Alloys,” *CDA Publ.*, no. 98, 1994.

[22] S. S. Machinery, “Understanding Ultrasonic Welding Process,” 2012.

[23] V. K. Patel, S. D. Bhole, and D. L. Chen, “Influence of ultrasonic spot welding on microstructure in a magnesium alloy,” *Scr. Mater.*, vol. 65, no.

10, pp. 911–914, 2011.

[24] G. Wagner, F. Balle, and D. Eifler, “Ultrasonic welding of hybrid joints,” *Jom*, vol. 64, no. 3, pp. 401–406, 2012.

[25] W. Michaeli, E. Haberstroh, and W. Hoffmann, “Ultrasonic welding of micro plastic parts,” *Multi-material micro Manuf. Cardiff Univ. Cardiff, UK Google Sch.*, 2008.

[26] H. Daniels, “Ultrasonic Welding,” *Ultrasonics*, vol. 3, no. 4, pp. 190–196, 1965.

[27] “No Title.” [Online]. Available: http://www.kaer-welder.com/techcenter/viewtechcenter50f0f3838dfe8.html. [Accessed: 11-Nov-2013].

[28] “Ultrasonic Welding Packaging.” [Online]. Available: https://www.dukane.com/us/AP_Pack.htm. [Accessed: 28-Mar-2016].

[29] H. S. Mukeshbhai, M. M. Dipakkumar, A. B. Vikramsinh, and V. B. Patel, “Modeling and Optimization of Ultrasonic Welding Process for Low Density Polymer : A Review,” *IJRITCC*, vol. 4, no. 3, pp. 155–158, 2016.

[30] S. F. Raza, “Ultrasonic welding of thermoplastics,” Sheffield, 2015.

[31] “Thermoplastics and Liquid Silicone Rubber (LSR).” [Online]. Available: https://www.simtec-silicone.com/thermoplastics-and-liquid-silicone-rubber-lsr/. [Accessed: 26-Aug-2015].

[32] “Polymer Viscosity.” [Online]. Available: http://www.injectionmoldingonline.com/Molding101/PolymerViscosity.aspx. [Accessed: 06-Sep-2017].

[33] Y. K. Chuah, L. H. Chien, B. C. Chang, and S. J. Liu, “Effects of the shape of the energy director on far-field ultrasonic welding of thermoplastics,” *Polym. Eng. Sci.*, vol. 40, no. 1, pp. 157–167, 2000.

[34] S. Thomas, “A Comprehensive Guide to Mechanical Fastener Options.” [Online]. Available: https://www.fictiv.com/blog/posts/from-snap-fits-to-adhesives-a-comprehensive-guide-to-mechanical-fastener-options. [Accessed: 02-Mar-2018].

[35] A. Benatar, “Ultrasonic welding of Advanced Thermoplastic Composites,” Massachusetts Institute of Technology, 1987.

[36] F. Lionetto and A. Maffezzoli, “Polymer Characterization by Ultrasonic Wave Propagation,” *Adv. Polym. Technol.*, vol. 27, no. 2, pp. 63–73, 2009.

[37] “Thermoset Characterization Part 16: Applications of Dynamic Mechanical Analysis (DMA).” [Online]. Available: https://polymerinnovationblog.com/thermoset-characterization-part-16-applications-dynamic-mechanical-analysis-dma/. [Accessed: 06-Sep-2017].

[38] “Polymer Chemistry.” [Online]. Available: http://faculty.uscupstate.edu/llever/polymer resources/glasstrans.htm. [Accessed: 18-Nov-2013].

[39] M. R. Rani, K. Prakasan, and R. Rudramoorthly, “Study of Different Joints for Ultrasonic Welding of Semicrystalline Polymers,” *Exp. Tech.*, no. August, pp. 43–51, 2009.

[40] C. J. Nonhof and G. a Luiten, “Estimates for process conditions during the ultrasonic welding of thermoplastics,” *Polym. Eng. Sci.*, vol. 36, no. 9, pp. 1177–1183, 1996.

[41] S. Sharma and K. Anand, “Parametric optimization of ultrasonic welding process for ABS material using Taguchi method,” *Discovery*, vol. 52, no. April, pp. 1381–1388, 2016.

[42] D. Bakavos and P. B. Prangnell, “Mechanisms of joint and microstructure formation in high power ultrasonic spot welding 6111 aluminium automotive sheet,” *Mater. Sci. Eng. A*, vol. 527, no. 23, pp. 6320–6334, 2010.

[43] M. Shakil, N. H. Tariq, M. Ahmad, M. a. Choudhary, J. I. Akhter, and S. S. Babu, “Effect of ultrasonic welding parameters on microstructure and mechanical properties of dissimilar joints,” *Mater. Des.*, vol. 55, pp. 263–273, 2014.

[44] N. Amanat, N. L. James, and D. R. McKenzie, “Welding methods for joining

thermoplastic polymers for the hermetic enclosure of medical devices," *Med. Eng. Phys.*, vol. 32, no. 7, pp. 690–699, 2010.

[45] A. L. Buxton, "Welding Technologies for Polymers and Composites." [Online]. Available: https://www.twi-global.com/technical-knowledge/published-papers/welding-technologies-for-polymers-and-composites/. [Accessed: 15-Apr-2018].

[46] R. Rashiqah, A. B. Elmi, and K. Shahrul, "Determination of ultrasonic welding optimal parameters for thermoplastic material of manufacturing products," *Sci. Eng.*, vol. 64, no. 1, pp. 19–24, 2013.

[47] K. S. Suresh, M. R. Rani, K. Prakasan, and R. Rudramoorthy, "Modeling of temperature distribution in ultrasonic welding of thermoplastics for various joint designs," *J. Mater. Process. Technol.*, vol. 186, no. 1–3, pp. 138–146, 2007.

[48] S. J. Liu, I. T. Chang, and S. W. Hung, "Factors affecting the joint strength of ultrasonically welded polypropylene composites," *Polym. Compos.*, vol. 22, no. 1, pp. 132–141, 2001.

[49] I. F. Villegas and H. E. N. Bersee, "Ultrasonic Welding of Advanced Thermoplastic Composites: An Investigation on Energy-Directing Surfaces IRENE," *Adv. Polym. Technol.*, vol. 29, no. 2, pp. 112–121, 2010.

[50] R. M. Rani, K. S. Suresh, K. Prakasan, and R. Rudramoorthy, "A statistical study of parameters in ultrasonic welding of plastics," *Exp. Tech.*, vol. 31, no. 5, pp. 53–58, 2007.

[51] J. Devine, "Ultrasonic Plastics Welding Basics," *Weld. J.*, vol. 80, no. 1, pp. 29–33, 2001.

[52] "Ultrasonic Plastic Joining," Branson Ultrasonics Corporation, 2013.

[53] Y. Luo, Z. Zhang, X. Wang, and Y. Zheng, "Ultrasonic bonding for thermoplastic microfluidic devices without energy director," *Microelectron. Eng.*, vol. 87, no. 11, pp. 2429–2436, 2010.

[54] T. H. Ramarathnam, G.; Libertucci, M.; Sadowski, M. M.; North, "Joining of Polymers to Metal," *Weld. Res. Suppl.*, no. 2, pp. 483–490, 1992.

[55] E. Faes, “Acrylonitrile-Butadiene-Styrene (ABS),” *Plastics Europe*. [Online]. Available: http://www.plasticseurope.org/what-is-plastic/types-of-plastics-11148/engineering-plastics/abs.aspx. [Accessed: 22-May-2014].

[56] S. M. Darwish, “Analysis of weld-bonded dissimilar materials,” *Int. J. Adhes. Adhes.*, vol. 24, no. 4, pp. 347–354, 2004.

[57] J. Gresham, W. Cantwell, M. J. Cardew-Hall, P. Compston, and S. Kalyanasundaram, “Drawing behaviour of metal–composite sandwich structures,” *Compos. Struct.*, vol. 75, no. 1–4, pp. 305–312, 2006.

[58] C. Hopmann, S. Kreimeier, J. Keseberg, and C. Wenzlau, “Joining of Metal-Plastics-Hybrid Structures Using Laser Radiation by Considering the Surface Structure of the Metal,” *J. Polym.*, vol. 2016, pp. 1–10, 2016.

[59] F. Balle, S. Emrich, G. Wagner, D. Eifler, A. Brodyanski, and M. Kopnarski, “Improvement of ultrasonically welded aluminum/carbon fiber reinforced polymer-joints by surface technology and high resolution analysis,” *Adv. Eng. Mater.*, vol. 15, no. 9, pp. 814–820, 2013.

[60] V. N. Khmelev, A. N. Slivin, A. D. Abramov, and S. V. Levin, “Weld strength test of thermoplastics obtained by ultrasonic welding,” *Int. Work. Tutorials Electron Devices Mater. EDM - Proc.*, pp. 227–230, 2008.

[61] S. J. Liu, W. F. Lin, B. C. Chang, G. M. Wu, and S. W. Hung, “Optimizing the joint strength of ultrasonically welded thermoplastics,” *Adv. Polym. Technol.*, vol. 18, no. 2, pp. 125–135, 1999.

[62] G. Zhang, J. Qiu, L. Shao, M. Liu, M. Zhang, and Y. Wu, “Ultrasonic weld properties of heterogeneous polymers: Polylactide and poly (methyl methacrylate),” *J. Mater. Process. Technol.*, vol. 211, no. 8, pp. 1358–1363, 2011.

[63] J. Qiu, G. Zhang, M. Asao, M. Zhang, H. Feng, and Y. Wu, “Study on the novel ultrasonic weld properties of heterogeneous polymers between PC and PMMA,” *Int. J. Adhes. Adhes.*, vol. 30, no. 8, pp. 729–734, 2010.

[64] K. Hargou, K. Pingkarawat, a. P. Mouritz, and C. H. Wang, “Ultrasonic

activation of mendable polymer for self-healing carbon-epoxy laminates," *Compos. Part B Eng.*, vol. 45, no. 1, pp. 1031–1039, 2013.

[65] D. Grewell and A. Benatar, "Welding of plastics: Fundamentals and new developments," *Int. Polym. Process.*, vol. 22, no. 1, pp. 43–60, 2007.

[66] "Near welding and far welding." [Online]. Available: http://www.sonic-machine.com/en/News-140.html. [Accessed: 01-Sep-2017].

[67] A. Benatar, R. V. Eswaran, and S. K. Nayar, "Ultrasonic welding of thermoplastics in the near-field," *Polym. Eng. Sci.*, vol. 29, no. 23, pp. 1689–1698, 1989.

[68] A. Benatar and Z. Cheng, "Ultrasonic Welding of Thermoplastics in The Far Field," *Polym. Eng. Sci.*, vol. 29, no. 23, pp. 1699–1704, 1989.

[69] J. L. Harthoorn, *Ultrasonic metal welding*. 1978.

[70] E. A. Neppiras, "Ultrasonic welding of metals," *Ultrasonics*, vol. 3, no. 3, pp. 128–135, 1965.

[71] S. K. Ginzburg and Y. G. Nosov, "Characteristics of diffusion processes in commercial iron during ultrasonic welding," *Met. Sci. Heat Treat.*, vol. 9, no. 4, pp. 306–308, 1967.

[72] W. J. Lewis, J. N. Antonevich, R. E. Monroe, and P. J. Rieppel, *Fundametal Studies on the Mechnism of Ultrasonic Welding*. 1960.

[73] T. Watanabe, A. Yanagisawa, and S. Konuma, "Ultrasonic Welding of Al-Cu and Study on the Ultrasonic Welding of Dissimilar Metals.," *Weld. Int.*, vol. 13, no. 11, pp. 875–886, 1999.

[74] M. Bloss and K. Graff, "Ultrasonic Metal Welding of Advanced Alloys: The Weldability of Stainless Steel, Titanium, and Nickel-Based Superalloys," *Proc. 8th Int. Conf. Trends Weld. Res.*, pp. 348–353, 2009.

[75] Z. Zhu, K. Y. Lee, and X. Wang, "Ultrasonic welding of dissimilar metals, AA6061 and Ti6Al4V," *Int. J. Adv. Manuf. Technol.*, vol. 59, no. 5–8, pp. 569–574, 2012.

[76] A. Babkin and E. A. Gladkov, "Identification of Welding Parameters for

Quality Welds in GMAW," *Weld. Res.*, vol. 95, no. January, pp. 37–46, 2016.

[77] V. PATEL, "Ultrasonic Spot Welding of Lightweight Alloys," Ryerson University, 2014.

[78] Z. Zhang, X. Wang, Y. Luo, Z. Zhang, and L. Wang, "Study on Heating Process of Ultrasonic Welding for Thermoplastics," *J. Thermoplast. Compos. Mater.*, vol. 23, no. 5, pp. 647–664, 2010.

[79] F. Balle and D. Eifler, "Statistical test planning for ultrasonic welding of dissimilar materials using the example of aluminum-carbon fiber reinforced polymers (CFRP) joints," *Materwiss. Werksttech.*, vol. 43, no. 4, pp. 286–292, 2012.

[80] R. L. Mason, R. F. Gunst, and J. L. Hess, *Statistical Design and Analysis of Experiments*. 2003.

[81] P. G. Mathews, *Design of Experiments with MINITAB*. ASQ Quality Press, 2005.

[82] T. Nam, "Introduction to Design of Experiments." [Online]. Available: https://www.slideshare.net/TeckNamAng/introduction-to-design-of-experiments-by-teck-nam-ang-university-of-malaya. [Accessed: 03-Sep-2017].

[83] D. P. Raykundaliya and A. Shanubhogue, "Comparison Study: Taguchi Methodology vis.-a-vis. Response Surface Methodology Through a Case Study of Accelerated Failure in Spin-on-Filter," *Iarjset*, vol. 2, no. 3, pp. 1–5, 2015.

[84] R. K. Roy, *Design of experiments using the Taguchi approach: 16 steps to product and process improvement.* John Wiley & Sons, 2001.

[85] N. Bradley, "The Response Surface Methodology," *Indiana Univ. South Bend*, p. 73, 2007.

[86] A. Asghar, A. A. Abdul Raman, and W. M. A. W. Daud, "A comparison of central composite design and Taguchi method for optimizing Fenton process.," *ScientificWorldJournal.*, vol. 2014, p. 869120, 2014.

[87] A. I. Khuri and S. Mukhopadhyay, "Response surface methodology," *Wiley*

Interdiscip. Rev. Comput. Stat., vol. 2, no. 2, pp. 128–149, 2010.

[88] R. H. Myers and D. C. Montgmery, *Response Surface Methodology: Process and Product Optimization Using Designed Experments*, 4th ed. John Wiley & Sons, 2016.

[89] S. Ferreira, R. E. Bruns, H. S. Ferreira, G. D. Matos, J. M. David, G. C. Brandão, E. G. P. da Silva, L. a. Portugal, P. S. dos Reis, a. S. Souza, and W. N. L. dos Santos, "Box-Behnken design: An alternative for the optimization of analytical methods," *Anal. Chim. Acta*, vol. 597, no. 2, pp. 179–186, 2007.

[90] J. Zolgharnein, A. Shahmoradi, and J. B. Ghasemi, "Comparative study of Box-Behnken, central composite, and Doehlert matrix for multivariate optimization of Pb (II) adsorption onto Robinia tree leaves," *J. Chemom.*, vol. 27, no. 1–2, pp. 12–20, 2013.

[91] "5 Simple Steps to Conducting a Non-Normal Capability Analysis in Minitab." [Online]. Available: https://sixsigmadsi.com/non-normal-capability-analysis/. [Accessed: 06-Sep-2017].

[92] "Minitab Express - Simple Linear Regression." [Online]. Available: https://onlinecourses.science.psu.edu/stat200/node/164. [Accessed: 06-Sep-2017].

[93] John H. Mc.Donald, *Handbook of Biological Statistics*, 2nd ed. 2008.

[94] S. Elangovan, K. Prakasan, and V. Jaiganesh, "Optimization of ultrasonic welding parameters for copper to copper joints using design of experiments," *Int. J. Adv. Manuf. Technol.*, vol. 51, no. 1–4, pp. 163–171, 2010.

[95] "Two-way ANOVA using Minitab," *Laerd Statistics*. [Online]. Available: https://statistics.laerd.com/minitab-tutorials/two-way-anova-using-minitab.php. [Accessed: 02-Oct-2015].

[96] B. N. Patel, "Experimental Investigation on Effect of Parameters in Ultrasonic Plastic Welding of Few Thermoplast Materials," Ganpat University, 2014.

[97] T. Watanabe, H. Sakuyama, and A. Yanagisawa, "Ultrasonic welding between mild steel sheet and Al-Mg alloy sheet," *J. Mater. Process. Technol.*, vol. 209, no. 15–16, pp. 5475–5480, 2009.

[98] S. Elangovan, S. Venkateshwaran, and K. Prakasan, "Experimental Investigations on Optimization of Ultrasonic Welding Parameters for Copper To Brass Joints Using Response Surface Method and Genetic Algorithm," *Int. J. Adv. Eng. Res. Stud.*, vol. 1, no. 3, pp. 1–6, 2012.

[99] J. Tsujino, M. Hongoh, M. Yoshikuni, H. Miura, and T. Ueoka, "Frequency Characteristics of Ultrasonic Plastic Welding," *Jsme Int. J.*, vol. 49, no. 5, pp. 634–641, 2006.

[100] A. Shoh, "Welding of thermoplastics by ultrasound," *Ultrasonics*, vol. 14, no. 5, pp. 209–217, 1976.

[101] S. Elangovan, K. Anand, and K. Prakasan, "Parametric optimization of ultrasonic metal welding using response surface methodology and genetic algorithm," *Int. J. Adv. Manuf. Technol.*, vol. 63, no. 5–8, pp. 561–572, 2012.

[102] H. Liu, W. Dai, and Y. Lee, "Moisture effects and acoustic emission characterization on lap shear strength in ultrasonic welded carbon / nylon composites," vol. 5, pp. 3389–3396, 2000.

[103] E. Sancaktar, "Polymer adhesion by ultrasonic welding," *J. Adhes. Sci. Technol.*, vol. 13, no. 2, pp. 179–201, 1999.

[104] S. Elangovan, S. P. John Henry, and P. Kalakkath, "Experimental studies on optimization of process parameters and finite element analysis of temperature and stress distribution on joining of Al–Al and Al–Al2O3 using ultrasonic welding," *Int. J. Adv. Manuf. Technol.*, vol. 55, no. 5–8, pp. 631–640, 2010.

[105] R. Eswaran, "Near Field Ultrasonic Welding Of Thermoplastics," The Ohio State University, 1988.

[106] H. Van Wijk, G. a. Luiten, P. G. Van Engen, and C. J. Nonhof, "Process optimization of ultrasonic welding," *Polym. Eng. Sci.*, vol. 36, no. 9, pp.

1165–1176, 1996.

[107] M. Pop-Calimanu and T. Fleser, “The Increasing of Weld Strength By Parameters Optimization of Ultrasonic Welding for Composite Material Based on Aluminium Using Design of Experiments .,” in *NANOCON*, 2012.

[108] “Dual pressure welding methods for ultrasonic assembly.” [Online]. Available: https://www.dukane.com/us/P_dualpress.htm. [Accessed: 26-Aug-2015].

[109] S. Elangovan, S. Semeer, and K. Prakasan, “Temperature and stress distribution in ultrasonic metal welding-An FEA-based study,” *J. Mater. Process. Technol.*, vol. 209, no. 3, pp. 1143–1150, 2009.

[110] F. Balle, S. Huxhold, S. Emrich, G. Wagner, M. Kopnarski, and D. Eifler, “Influence of Heat Treatments on the Mechanical Properties of Ultrasonic Welded AA 2024/CF-PA66-Joints,” *Adv. Eng. Mater.*, vol. 15, no. 9, pp. 837–845, 2013.

[111] C. Ochoa-Putman and U. K. Vaidya, “Mechanisms of interfacial adhesion in metal-polymer composites - Effect of chemical treatment,” *Compos. Part A Appl. Sci. Manuf.*, vol. 42, no. 8, pp. 906–915, 2011.

[112] S. Budhe, A. Ghumatkar, N. Birajdar, and M. D. Banea, “Effect of surface roughness using different adherend materials on the adhesive bond strength,” *Appl. Adhes. Sci.*, vol. 3, no. 1, p. 20, 2015.

[113] E. de Vries, “Mechanics and Mechanisms of Ultrasonic Metal Welding,” The Ohio State, 2004.

[114] AWS, *Welding Handbook*, Sixth. American Welding Society, 1968.

[115] G. D. Janaki Ram, Y. Yang, and B. E. Stucker, “Effect of process parameters on bond formation during ultrasonic consolidation of aluminum alloy 3003,” *J. Manuf. Syst.*, vol. 25, no. 3, pp. 221–238, 2006.

[116] S. I. Matsuoka and H. Imai, “Direct welding of different metals used ultrasonic vibration,” *J. Mater. Process. Technol.*, vol. 209, no. 2, pp. 954–960, 2009.

[117] “Introduction to Aluminium and its alloys,” *Alaco Metals Ltd.* [Online].

Available: http://www.aalco.co.uk/datasheets/aluminiumalloy_introduction-to-aluminium-and-its-alloys_9.ashx. [Accessed: 23-Dec-2014].

[118] A. Aginagalde, X. Gomez, L. Galdos, and C. García, "Heat Treatment Selection and Forming Strategies for 6082 Aluminum Alloy," *J. Eng. Mater. Technol.*, vol. 131, no. 4, p. 44501, 2009.

[119] M. Kessler, "Ultrasonic welding of aluminum: a practical study in consistency, part marking and control modes," Lowa State University, 2007.

[120] K. S. Suresh, "Studies on Temperature Distribution in Various Joint Designs and Design of Horns for Ultrasonic Welding of Thermoplastics," Anna University, 2007.

[121] C. F. Ebnesajjad, *Surface Treatment of Materials for Adhesion Bonding*, 2nd Editio. USA, 2006.

[122] V. N. Khmelev, A. N. Slivin, and A. D. Abramov, "Model of process and calculation of energy for a heat generation of a welded joint at ultrasonic welding polymeric thermoplastic materials," *2007 8th Annu. Int. Work. Tutorials Electron Devices Mater. EDM'07 - Proc.*, pp. 316–322, 2007.

[123] O. Lunder, "Chromate-free pre-treatment of aluminium for adhesive bonding," Norwegin University, 2003.

[124] "The Home Of Surface Measurement." [Online]. Available: http://www.rubert.co.uk/faqs/roughness-parameters/. [Accessed: 25-Sep-2017].

[125] "ED Design." [Online]. Available: http://www.psgtech.edu/department/production/ultrasonicwelding/html/jointdesigns.html. [Accessed: 04-Jun-2016].

[126] "Statistical and practical significance." [Online]. Available: http://support.minitab.com/en-us/minitab-express/1/help-and-how-to/basic-statistics/inference/supporting-topics/basics/statistical-and-practical-significance/. [Accessed: 04-May-2018].

[127] “Distortion - corrective techniques.” [Online]. Available: https://www.twi-global.com/technical-knowledge/job-knowledge/distortion-corrective-techniques-037/. [Accessed: 04-May-2018].

[128] Dukane Corporation, “Guide to Ultrasonic Plastics Assembly,” *Supplier Des. Guid.*, no. 403, 1995.

[129] P. Cognard, *Handbook of Adhesives and Sealants: Volume 1*, vol. 1. 2005.

[130] Q. Yao and J. Qu, “Interfacial Versus Cohesive Failure on Polymer-Metal Interfaces in Electronic Packaging—Effects of Interface Roughness,” *J. Electron. Packag.*, vol. 124, no. 2, p. 127, 2002.

[131] AWS, *Welding Handbook Vol 1*, vol. 53. 2013.

[132] Y. Zhou, *Microjoining and nanojoining*. England: Woodhead Publishing Limited, 2008.

[133] J. Frost, “Regression Analysis,” *The Minitab Blogs*, 2013. [Online]. Available: http://blog.minitab.com/blog/adventures-in-statistics-2/regression-analysis-how-do-i-interpret-r-squared-and-assess-the-goodness-of-fit. [Accessed: 01-May-2016].

[134] A. Makwana and V. R. Patel, “Influence of Processing Parameters on Ultrasonic welding of Thermoplastic Material Material Using Taguchi Method,” *Int. J. Adv. Eng. Res. Dev.*, vol. 4, no. 10, pp. 43–49, 2017.

Appendices

Appendix A

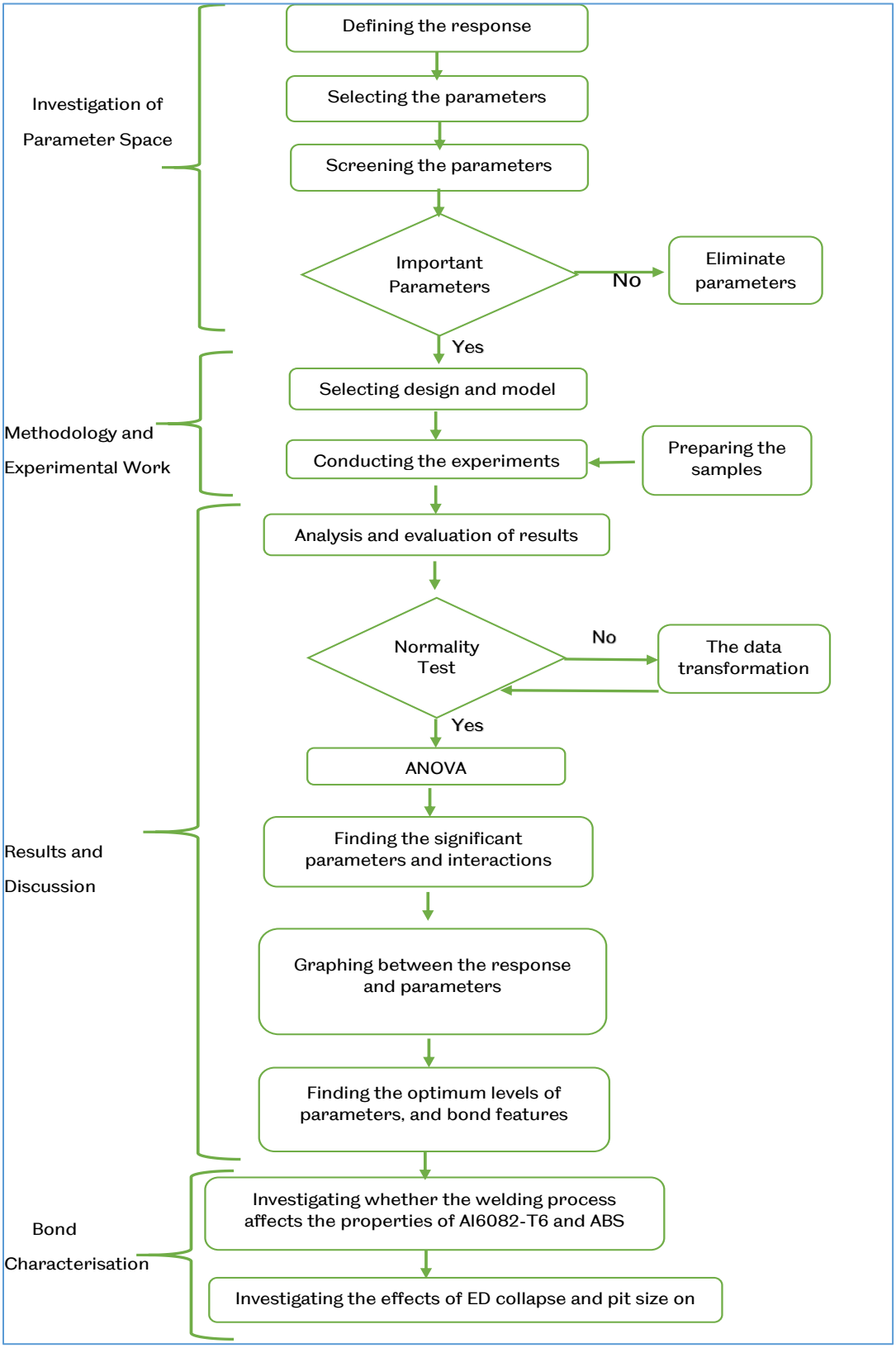

Figure A-1 The current study flow diagram.

Appendix B

Table B-1 Full results of the surface roughness for Al6082-T6 samples.

Sample No.	Thickness (mm)	Before pre-treatment (μm)		After pre-treatment (μm)	
		R_a	R_z	R_a	R_z
1	1	0.4916	2.311	0.887	4.116
		0.37194	1.748	0.863	4.004
		0.45966	2.160	0.976	4.529
		0.45721	2.149	1.020	4.733
2		0.45285	2.128	0.961	4.459
		0.405	1.904	0.87	3.712
		0.485	2.280	0.973	4.515
		0.4846	2.278	0.857	3.512
3		0.64	3.008	1.050	4.872
		0.44	2.068	0.941	4.366
		0.494	2.322	0.91	4.222
		0.54	2.538	1.04	4.826
4		0.53	2.491	0.99	4.594
		0.4	1.880	0.992	4.603
		0.523	2.458	0.98	4.547
		0.4745	2.230	0.842	3.907
5		0.546	2.566	0.9387	4.356
		0.507	2.383	0.922	4.278
		0.528	2.482	0.952	4.417
		0.50348	2.366	0.9341	4.334
1	1.5	0.18075	0.850	1.105	5.127
		0.248	1.166	1.0642	4.938
		0.2862	1.345	1.076	4.993
		0.305	1.434	1.03	4.779
2		0.309	1.452	0.927	4.301
		0.3875	1.821	1.00312	4.654

		0.34168	1.606	1.127	5.229
		0.36752	1.727	1.098	5.095
3		0.28	1.316	1.0598	4.917
		0.32514	1.528	1.229	5.703
		0.31267	1.470	1.1096	5.149
		0.41578	1.954	1.0005	4.642
4		0.336	1.579	0.935	4.338
		0.34221	1.608	0.8367	3.882
		0.372	1.748	1.0093	4.683
		0.36306	1.706	1.0378	4.815
5		0.24246	1.140	1.084	5.030
		0.359	1.687	1.0486	4.866
		0.34552	1.624	1.0534	4.888
		0.38851	1.826	0.9988	4.634
1	2	0.221	1.039	1.07	4.965
		0.288	1.354	1.029	4.775
		0.326	1.532	1.041	4.830
		0.345	1.622	0.995	4.617
2		0.349	1.640	0.892	4.139
		0.428	2.012	0.968	4.492
		0.382	1.795	1.092	5.067
		0.408	1.918	1.063	4.932
3		0.32	1.504	1.025	4.756
		0.365	1.716	1.194	5.540
		0.353	1.659	1.075	4.988
		0.456	2.143	0.966	4.482
4		0.376	1.767	0.9	4.176
		0.382	1.795	0.802	3.721
		0.412	1.936	0.974	4.519
		0.403	1.894	1.003	4.654
5		0.282	1.325	1.049	4.867

		0.399	1.875	1.014	4.705
		0.386	1.814	1.018	4.724
		0.429	2.016	0.964	4.473

Appendix C

Table C-1 PLC–bonding force convert

Sr.No	Load Meter in Newtons	Pressure Sensor from PLC Display
1	450	83
2	460	87
3	474	90
4	521	96
5	527	99
6	542	102
7	575	105
8	597	108
9	607	111
10	620	115
11	654	118
12	665	121
13	681	124
14	706	127
15	720	130
16	740	133
17	761	136
18	770	139
19	795	143
20	817	146
21	844	149
22	854	152
23	874	155
24	894	158
25	917	161
26	934	164
27	951	167
28	969	171
29	987	174
30	1004	177

31	1022	180
32	1047	183
33	1069	186
34	1076	189
35	1089	192
36	1115	195
37	1137	199
38	1156	202
39	1177	205
40	1198	208
41	1218	211
42	1233	214
43	1252	217
44	1268	220
45	1287	223
46	1311	226
47	1327	230
48	1344	233
49	1361	236
50	1378	239
51	1400	242
52	1415	245
53	1438	248
54	1454	251
55	1472	254
56	1494	258
57	1509	261
58	1530	264
59	1550	267
60	1565	270
61	1585	273
62	1601	276
63	1620	279
64	1634	282

65	1656	286
66	1674	289
67	1696	292
68	1710	295
69	1730	298
70	1751	301
71	1764	304
72	1788	307
73	1809	310
74	1825	314
75	1847	317
76	1861	320
77	1879	323
78	1899	326
79	1924	329
80	1941	332
81	1958	335
82	1970	338
83	1992	342
84	2008	345
85	2035	348
86	2052	351
87	2072	354
88	2089	357
89	2102	360
90	2118	363
91	2136	366
92	2168	370
93	2182	373
94	2200	376
95	2215	379
96	2235	382
97	2251	385
98	2269	388

99	2284	391
100	2300	394
101	2315	398
102	2334	401
103	2350	404

Appendix D

Table D.1 Calibration of thermocouples results.

Ref. Thermo-meter Temp. (^{0}C)	Thermocouple Temperature (^{0}C)																	
	No. 1	No. 2	No. 3	No. 4	No. 5	No. 6	No. 7	No. 8	No. 9	No. 10	No. 11	No. 12	No. 13	No. 14	No. 15	No. 16	No. 17	No. 18
0	0.8	0.64	0.5	0.65	0.86	0.93	1.2	0.7	0.88	1.6	1.1	0.86	1.26	0.76	0.55	0.8	0.79	0.7
10	10.5	10.34	10.15	10.35	10.56	10.6	10.9	10.4	10.6	10.9	10.4	10.1	10.5	10.0	9.82	10.1	10.1	9.97
20.9	22.3	22.14	21.95	22.15	22.36	22.4	22.7	22.2	22.4	22.7	22.2	21.9	22.3	21.8	21.7	21.9	21.9	21.8
29.1	29.6	29.44	29.25	29.45	29.66	29.7	30	29.5	29.7	30	29.5	29.2	29.6	29.1	28.9	29.2	29.2	29.1
39	40.1	39.94	39.75	39.95	40.16	40.2	40.6	40	40.2	40.5	39.9	39.8	39.9	39.5	39.3	39.6	39.6	39.5
48.1	49.8	49.54	49.45	49.65	49.86	49.9	50.3	49.7	49.9	50.2	49.7	49.5	49.6	49.2	49.0	49.3	49.3	49.2
62	63.2	62.94	62.85	63.05	63.26	63.3	63.7	63.1	63.2	63.5	63.0	62.9	63.0	62.5	62.4	62.7	62.6	62.5

70.15	72	71.74	71.7	71.89	72.06	72.0	72.4	71.9	72.0	72.3	71.8	71.7	72.0	71.5	71.3	71.7	71.6	71.5
83.3	84.1	83.84	83.8	83.99	84.16	84.1	84.5	84	84.1	84.4	83.9	83.8	84.2	83.6	83.4	83.8	83.7	83.6
90	92.7	92.44	92.4	92.59	92.76	92.7	93.1	92.6	92.7	93.0	92.5	92.3	92.7	92.2	92.0	92.3	92.2	92.1
98	99.6	99.34	99.3	99.49	99.66	99.6	100	99.5	99.6	99.9	99.4	99.2	99.6	99.1	98.9	99.2	99.1	99.0

Appendix E

According to the experimental structure in Section (4.7), each shape of energy director has its data matrix and each experimental run was repeated three times as shown in Table E.1, Table E.2 and Table E.3.

Table E.1 Experimental lap shear strength for Triangular ED.

Exp. run No.	Oscillation Amplitude (μm)	Bonding Time (sec)	Bonding Force (N)	Al6082-T6 thickness (mm)	Experimental Lap Shear Strength LSS (N/mm^2)		
					Trial 1	Trial 2	Trial 3
1	16.8	1	850	1	1.275	1.31	1.289
2	21	1	850	1	1.935	1.97	1.949
3	16.8	2	850	1	1.085	1.12	1.099
4	21	2	850	1	1.628	1.663	1.642
5	16.8	1	1050	1	1.105	1.14	1.119
6	21	1	1050	1	1.659	1.694	1.673
7	16.8	2	1050	1	0.805	0.84	0.819
8	21	2	1050	1	1.349	1.384	1.363
9	16.8	1	850	2	1.015	1.05	1.029
10	21	1	850	2	1.557	1.592	1.571
11	16.8	2	850	2	0.82	0.855	0.834
12	21	2	850	2	1.365	1.4	1.379
13	16.8	1	1050	2	0.745	0.78	0.759
14	21	1	1050	2	1.289	1.324	1.303
15	16.8	2	1050	2	0.315	0.35	0.329

16	21	2	1050	2	0.858	0.893	0.872
17	16.8	1.5	950	1.5	1.15	1.184	1.215
18	21	1.5	950	1.5	1.955	1.97	1.929
19	18.9	1	950	1.5	1.499	1.591	1.521
20	18.9	2	950	1.5	1.258	1.293	1.272
21	18.9	1.5	850	1.5	1.425	1.46	1.439
22	18.9	1.5	1050	1.5	1.085	1.12	1.099
23	18.9	1.5	950	1	1.609	1.644	1.623
24	18.9	1.5	950	2	1.151	1.186	1.164
25	18.9	1.5	950	1.5	1.615	1.65	1.629
26	18.9	1.5	950	1.5	1.595	1.63	1.609
27	18.9	1.5	950	1.5	1.6	1.636	1.614
28	18.9	1.5	950	1.5	1.59	1.625	1.603
29	18.9	1.5	950	1.5	1.592	1.627	1.606
30	18.9	1.5	950	1.5	1.59	1.625	1.604
31	18.9	1.5	950	1.5	1.608	1.643	1.621

Table E.2 Experimental lap shear strength for Semi-Circular ED

Exp. run No.	Oscillation Amplitude (μm)	Bonding Time (sec)	Bonding Force (N)	Al6082-T6 thickness (mm)	Experimental Lap Shear Strength LSS (N/mm^2)		
					Trial 1	Trial 2	Trial 3
1	16.8	1	850	1	1.114	1.149	1.128
2	21	1	850	1	1.774	1.809	1.788

3	16.8	2	850	1	0.913	0.959	0.938
4	21	2	850	1	1.467	1.502	1.481
5	16.8	1	1050	1	0.944	0.979	0.958
6	21	1	1050	1	1.498	1.533	1.512
7	16.8	2	1050	1	0.644	0.679	0.658
8	21	2	1050	1	1.188	1.223	1.202
9	16.8	1	850	2	0.854	0.889	0.87
10	21	1	850	2	1.396	1.431	1.41
11	16.8	2	850	2	0.659	0.694	0.673
12	21	2	850	2	1.204	1.239	1.218
13	16.8	1	1050	2	0.584	0.619	0.598
14	21	1	1050	2	1.128	1.163	1.142
15	16.8	2	1050	2	0.256	0.291	0.27
16	21	2	1050	2	0.697	0.732	0.711
17	16.8	1.5	950	1.5	1.09	0.987	1.015
18	21	1.5	950	1.5	1.754	1.789	1.768
19	18.9	1	950	1.5	1.354	1.389	1.368
20	18.9	2	950	1.5	1.097	1.132	1.111
21	18.9	1.5	850	1.5	1.264	1.299	1.278
22	18.9	1.5	1050	1.5	0.924	0.959	0.938
23	18.9	1.5	950	1	1.448	1.483	1.462
24	18.9	1.5	950	2	1.055	1.025	1.003
25	18.9	1.5	950	1.5	1.454	1.489	1.468

26	18.9	1.5	950	1.5	1.434	1.469	1.448
27	18.9	1.5	950	1.5	1.439	1.475	1.453
28	18.9	1.5	950	1.5	1.429	1.464	1.442
29	18.9	1.5	950	1.5	1.431	1.466	1.445
30	18.9	1.5	950	1.5	1.429	1.464	1.443
31	18.9	1.5	950	1.5	1.447	1.482	1.46

Table E.3 Experimental lap shear strength for Rectangular ED.

Exp. run No.	Oscillation Amplitude (μm)	Bonding Time (sec)	Bonding Force (N)	Al6082-T6 thickness (mm)	Experimental Lap Shear Strength LSS (N/mm^2)		
					Trial 1	Trial 2	Trial 3
1	16.8	1	850	1	1.017	1.052	1.03
2	21	1	850	1	1.677	1.712	1.69
3	16.8	2	850	1	0.827	0.862	0.84
4	21	2	850	1	1.37	1.405	1.383
5	16.8	1	1050	1	0.847	0.882	0.86
6	21	1	1050	1	1.4	1.436	1.414
7	16.8	2	1050	1	0.547	0.582	0.56
8	21	2	1050	1	1.09	1.126	1.104
9	16.8	1	850	2	0.757	0.792	0.77
10	21	1	850	2	1.299	1.334	1.312
11	16.8	2	850	2	0.562	0.597	0.575
12	21	2	850	2	1.107	1.142	1.12

13	16.8	1	1050	2	0.487	0.522	0.5
14	21	1	1050	2	1.031	1.066	1.044
15	16.8	2	1050	2	0.159	0.194	0.172
16	21	2	1050	2	0.6	0.635	0.613
17	16.8	1.5	950	1.5	0.965	0.94	0.919
18	21	1.5	950	1.5	1.657	1.692	1.67
19	18.9	1	950	1.5	1.257	1.292	1.27
20	18.9	2	950	1.5	1	1.035	1.013
21	18.9	1.5	850	1.5	1.167	1.202	1.18
22	18.9	1.5	1050	1.5	0.827	0.862	0.84
23	18.9	1.5	950	1	1.351	1.386	1.364
24	18.9	1.5	950	2	0.892	0.927	0.91
25	18.9	1.5	950	1.5	1.357	1.392	1.37
26	18.9	1.5	950	1.5	1.337	1.372	1.35
27	18.9	1.5	950	1.5	1.342	1.377	1.356
28	18.9	1.5	950	1.5	1.331	1.366	1.345
29	18.9	1.5	950	1.5	1.334	1.369	1.347
30	18.9	1.5	950	1.5	1.332	1.367	1.345
31	18.9	1.5	950	1.5	1.349	1.384	1.363

Appendix F

The temperature profiles of the bonding temperature were explained in Section 6.2.7, and some of these profiles were shown in Section 6.2.7. The findings of all profiles, such as the maximum bonding temperature were tabulated in Table 6.2. The following figures are the remaining profiles :

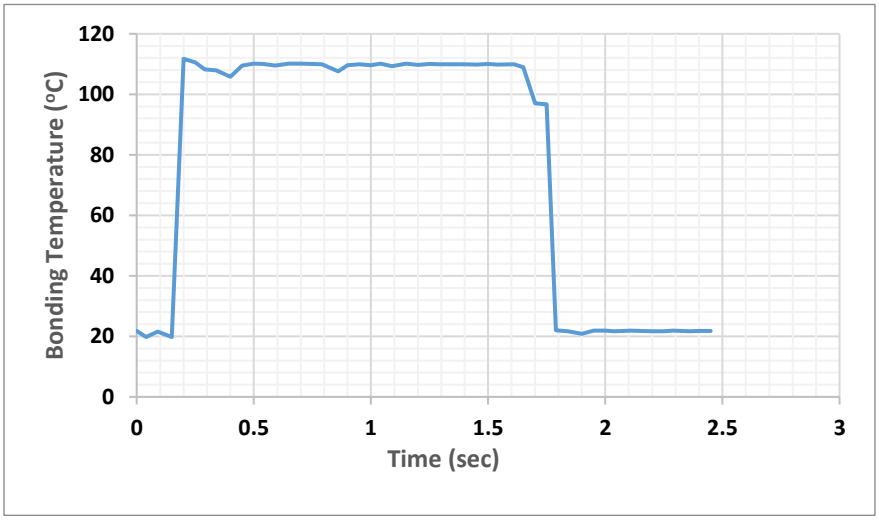

Figure F.1 Temperature profile of serial No.2 (vibration amplitude 16.8 µm, bonding time 2sec, bonding force 850N and Al6082 thickness 1mm).

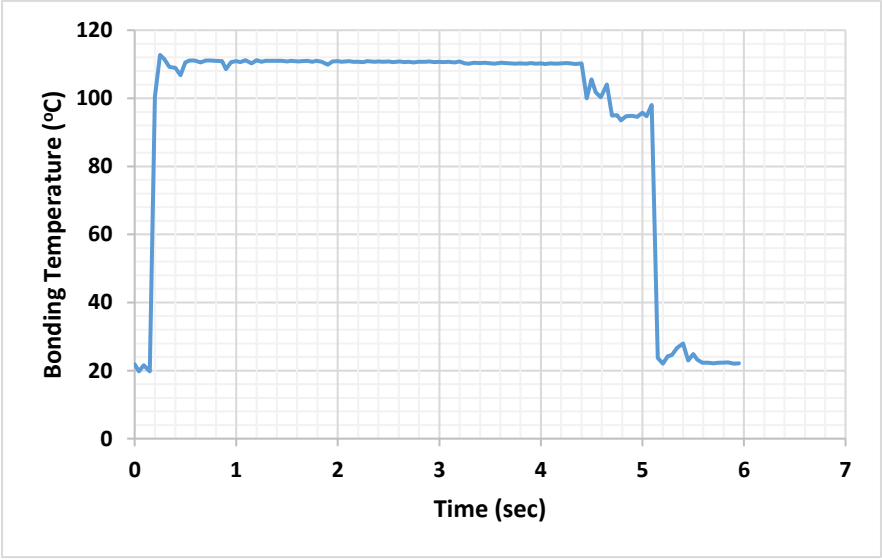

Figure F.2 Temperature profile of serial No.3 (vibration amplitude 16.8 µm, bonding time 1sec, bonding force 1050N and Al6082 thickness 1mm).

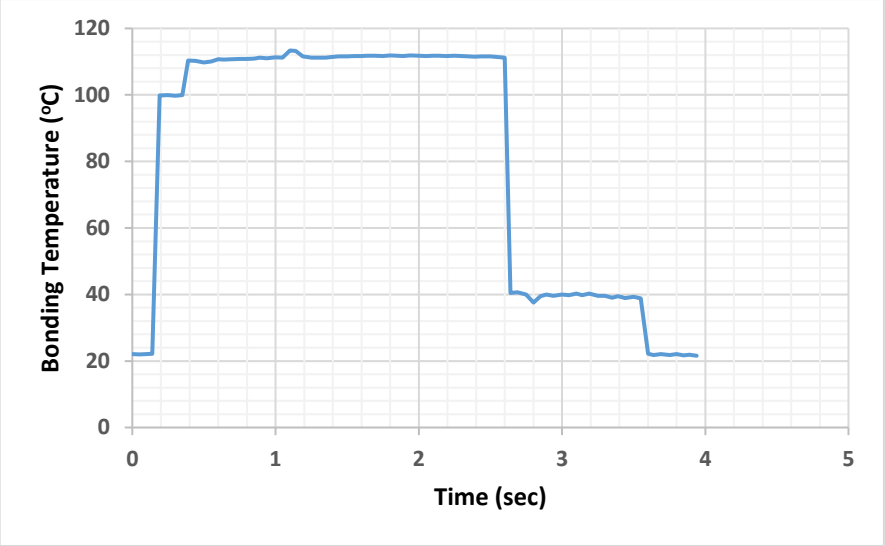

Figure F.3 Temperature profile of serial No.4 (vibration amplitude 16.8 μm, bonding time 1sec, bonding force 850N and Al6082 thickness 2mm).

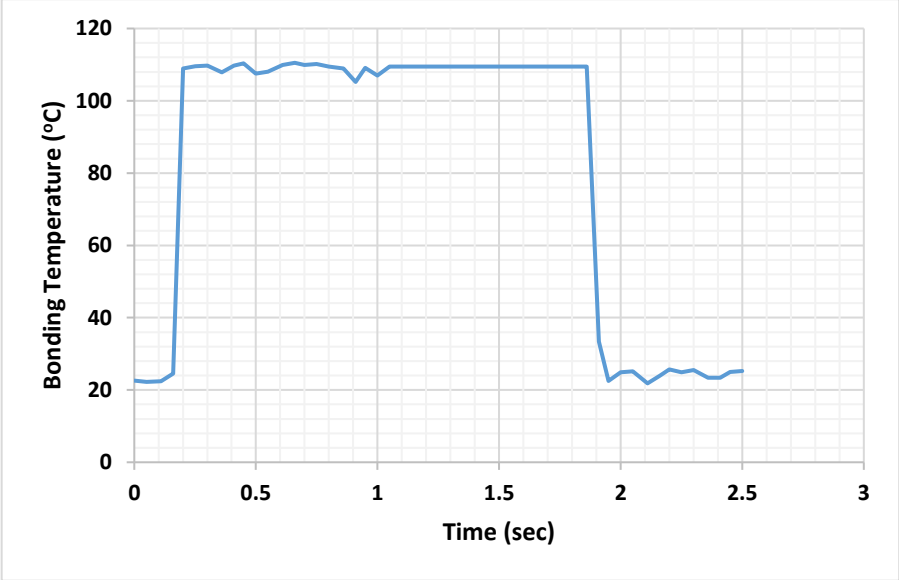

Figure F.4 Temperature profile of serial No.7 (vibration amplitude 16.8 μm, bonding time 1.5sec, bonding force 950N and Al6082 thickness 1.5mm).

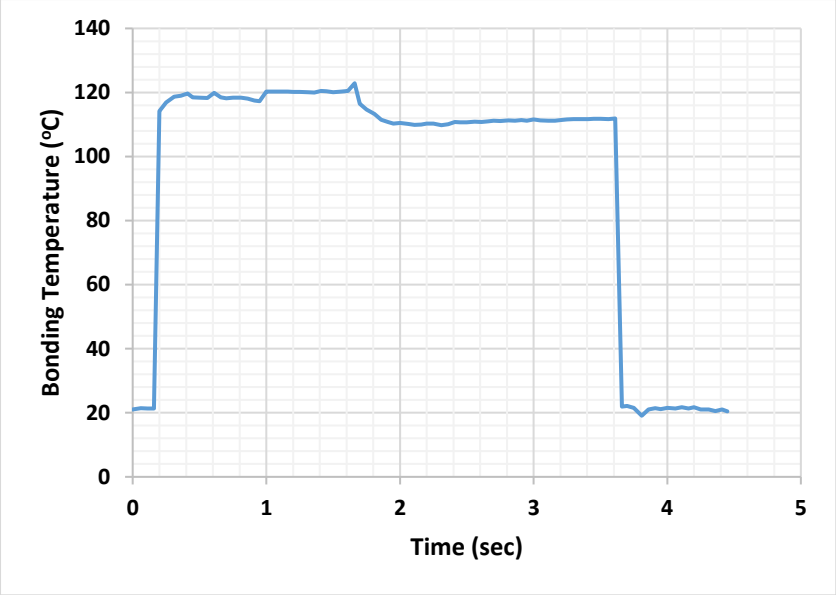

Figure F.5 Temperature profile of serial No.8 (vibration amplitude 18.9 µm, bonding time 2sec, bonding force 950N and Al6082 thickness 1.5mm).

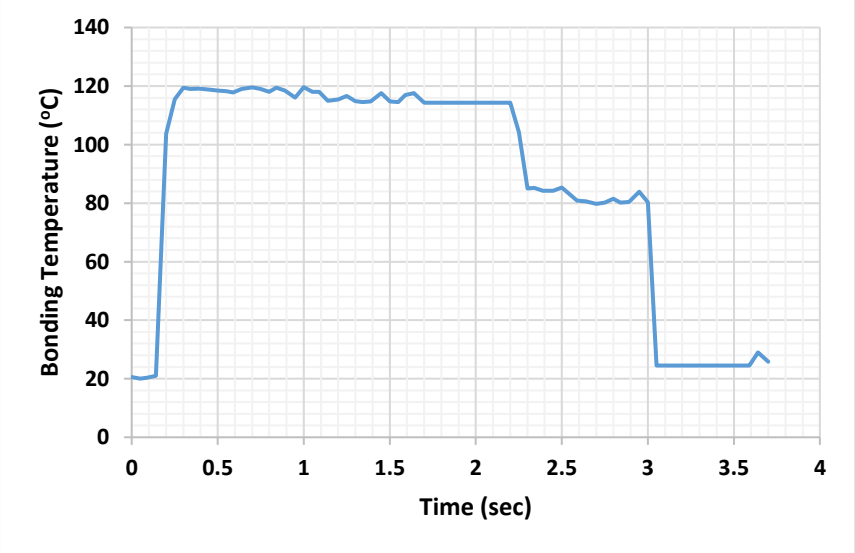

Figure F.6 Temperature profile of serial No.9 (vibration amplitude 18.9 µm, bonding time 1.5sec, bonding force 850N and Al6082 thickness 1.5mm).

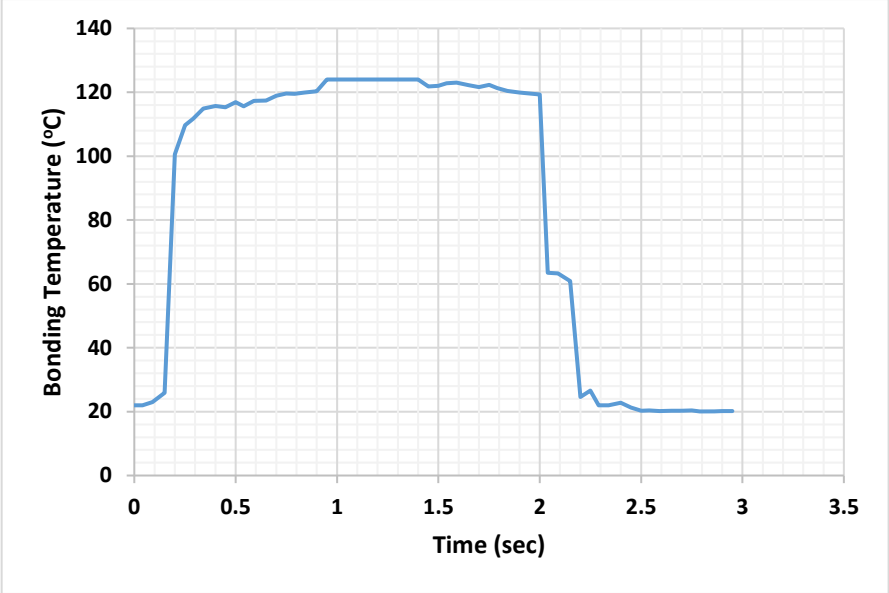

Figure F.7 Temperature profile of serial No.10 (vibration amplitude 18.9 μm, bonding time 1.5sec, bonding force 950N and Al6082 thickness 1mm).

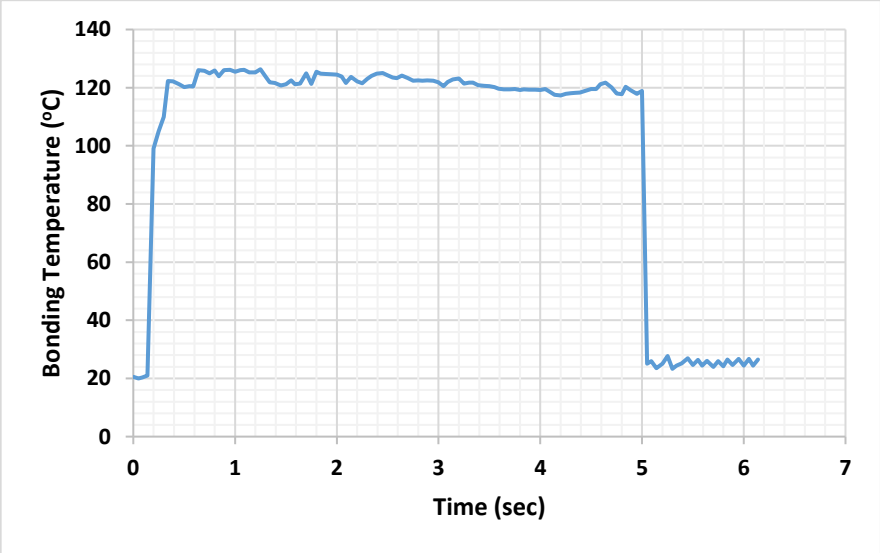

Figure F.8 Temperature profile of serial No.12 (vibration amplitude 21μm, bonding time 2sec, bonding force 850N and Al6082 thickness 1mm).

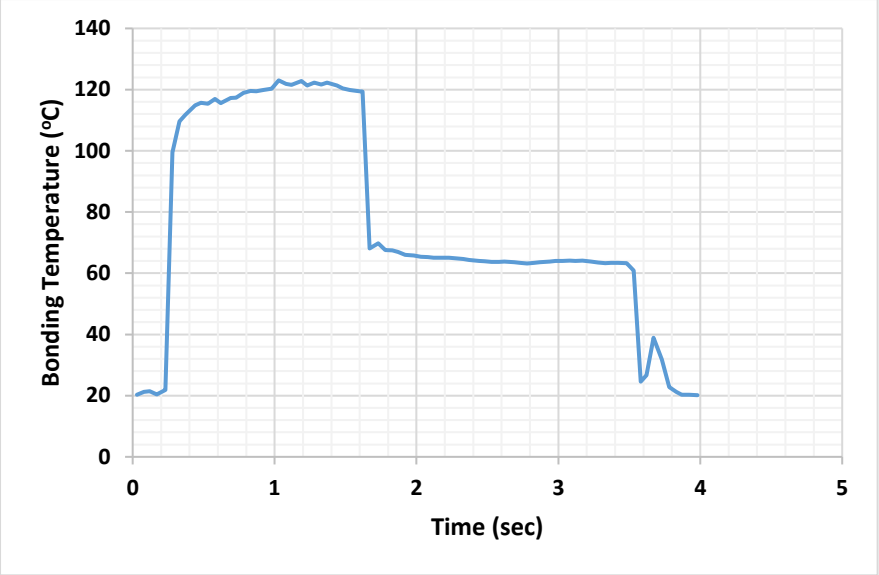

Figure F.9 Temperature profile of serial No.15 (vibration amplitude 21μm, bonding time 1sec, bonding force 850N and Al6082 thickness 2mm).

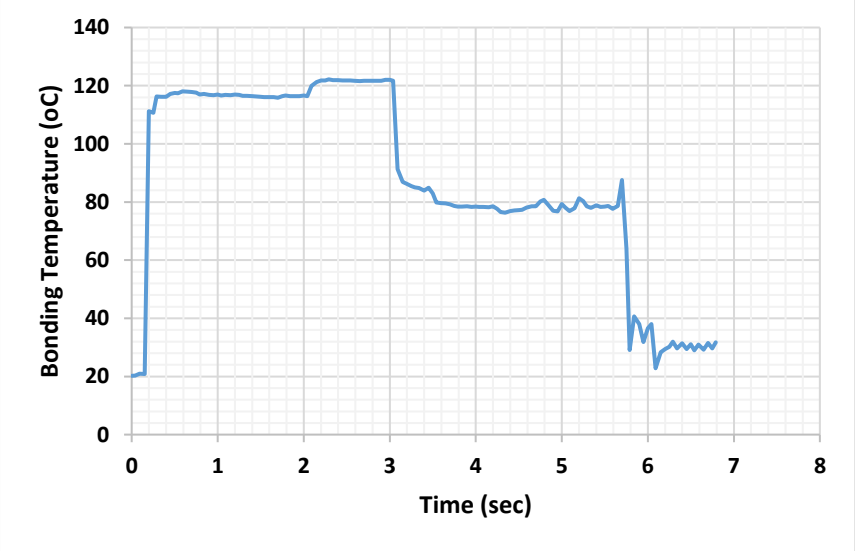

Figure F.10 Temperature profile of serial No.16 (vibration amplitude 21μm, bonding time 2sec, bonding force 850N and Al6082 thickness 2mm).

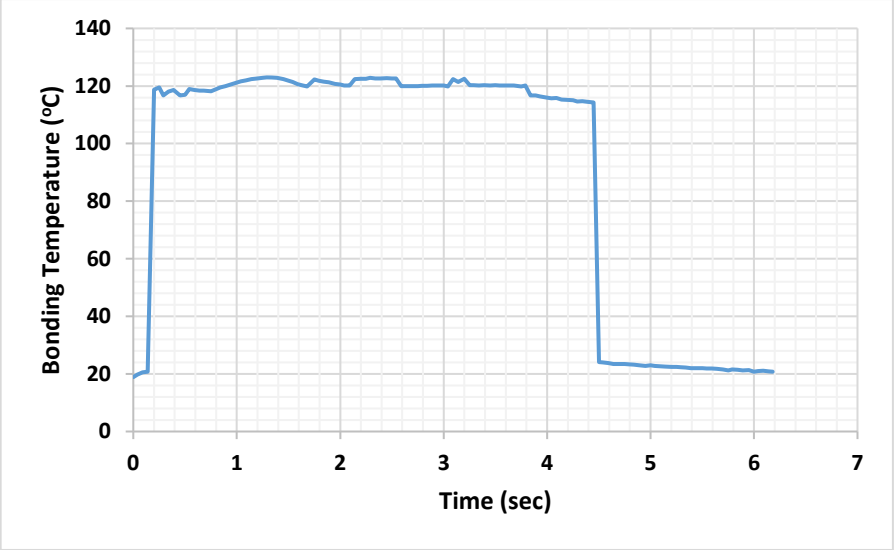

Figure F.11 Temperature profile of serial No.18 (vibration amplitude 21μm, bonding time 1.5sec, bonding force 950N and Al6082 thickness 1.5mm).